AD-A148 467 METHODOLOGY IMPROVEMENT PROGRAM FOR THE SECOND GENERATION MISS DISTANCE R.. (U) GEORGIA INST OF TECH ATLANTA ENGINEERING EXPERIMENT STATION 1/3

UNCLASSIFIED G V MORRIS ET AL. 30 OCT 84 F/G 17/9 NL

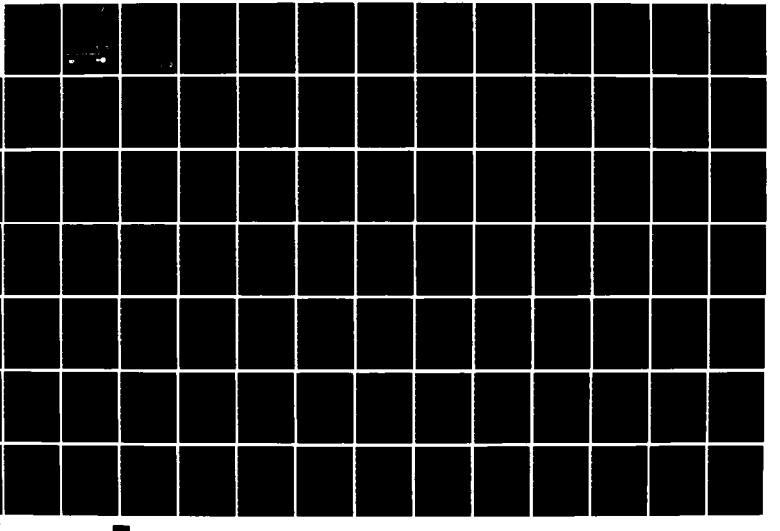

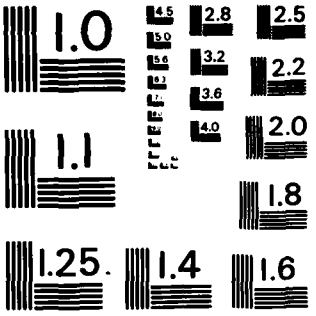

FINAL TECHNICAL REPORT
GT PROJECT A-3812

METHODOLOGY IMPROVEMENT PROGRAM FOR THE SECOND GENERATION MISS DISTANCE RADAR (MIDI II)

By

G. V. Morris, B. Perry, IV, and R. B. Efurd

Prepared for

U.S. ARMY AIR DEFENSE ARTILLERY BOARD
FORT BLISS, TEXAS 79916

Under

Contract No. DABT60-84-C-0040

September 1984

GEORGIA INSTITUTE OF TECHNOLOGY
A Unit of the University System of Georgia
Engineering Experiment Station
Atlanta, Georgia 30332

FINAL TECHNICAL REPORT
GEORGIA TECH PROJECT A-3812

METHODOLOGY IMPROVEMENT PROGRAM FOR THE SECOND GENERATION MISS DISTANCE RADAR (MIDI II)

BY
G. V. MORRIS, B. PERRY IV, AND R. B. EFURD

PREPARED FOR
U. S. ARMY AIR DEFENSE ARTILLERY BOARD
FORT BLISS, TEXAS 79916

UNDER CONTRACT NUMBER
DABT60-84-C-0040

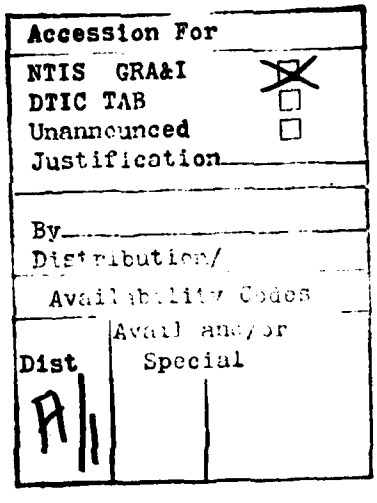

30 SEPTEMBER 1984

Georgia Institute of Technology
A Unit of the University System of Georgia
Georgia Tech Research Institute
Atlanta, Georgia 30332

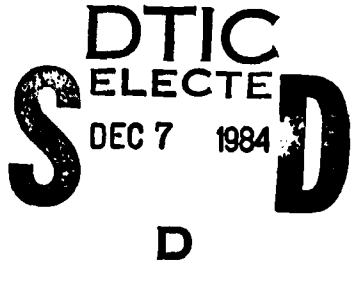

UNCLASSIFIED

SECURITY CLASSIFICATION OF THIS PAGE

REPORT DOCUMENTATION PAGE

1a. REPORT SECURITY CLASSIFICATION UNCLASSIFIED	1b. RESTRICTIVE MARKINGS
2a. SECURITY CLASSIFICATION AUTHORITY	3. DISTRIBUTION/AVAILABILITY OF REPORT Unlimited DISTRIBUTION STATEMENT Approved for public release; Distribution Unlimited
2b. DECLASSIFICATION/DOWNGRADING SCHEDULE	
4. PERFORMING ORGANIZATION REPORT NUMBER(S) A-3812	5. MONITORING ORGANIZATION REPORT NUMBER(S)
6a. NAME OF PERFORMING ORGANIZATION Georgia Tech Research Institute Georgia Institute of Technology 6b. OFFICE SYMBOL (If applicable) RAIL	7a. NAME OF MONITORING ORGANIZATION U.S. Army Air Defense Artillery Board
6c. ADDRESS (City, State and ZIP Code) Atlanta, Georgia 30332	7b. ADDRESS (City, State and ZIP Code) Ft. Bliss, Texas 79916
8a. NAME OF FUNDING/SPONSORING ORGANIZATION U.S. Army TRADOC 8b. OFFICE SYMBOL (If applicable) ATCA	9. PROCUREMENT INSTRUMENT IDENTIFICATION NUMBER DABT60-84-C-0040
8c. ADDRESS (City, State and ZIP Code) Ft. Eustis, Virginia 23504	10. SOURCE OF FUNDING NOS. PROGRAM ELEMENT NO.: 65712A PROJECT NO.: TASK NO.: WORK UNIT NO.:
11. TITLE (Include Security Classification) Methodology Improvement Program for Second Generation Miss Distance Radar	
12. PERSONAL AUTHOR(S) Morris, Gut V.; Perry, Benjamin, IV; Efurd, Raymond B.	
13a. TYPE OF REPORT Final 13b. TIME COVERED FROM 840329 TO 841030	14. DATE OF REPORT (Yr., Mo., Day) 84 10 30 15. PAGE COUNT 187 + v
16. SUPPLEMENTARY NOTATION	

17. COSATI CODES			18. SUBJECT TERMS (Continue on reverse if necessary and identify by block number)
FIELD	GROUP	SUB. GR.	Miss Distance Indicator Radar, Instrumentation
17	09		

19. ABSTRACT (Continue on reverse if necessary and identify by block number)

The present Miss Distance Indicator (MIDI I) Radar tracks a target and measures the vector miss distance of projectiles fired at the target. The major conclusion of this study is that the MIDI I limitation of operating against targets 150 meters or more above ground level can be improved down to 15 meters for gun scoring and 60 meters for missile scoring by applying a combination of radar techniques such as: (1) pulsed Doppler to attenuate the ground clutter; (2) multiple, selectable antenna beamwidths to meet both low altitude operation and scoring volume requirements; and (3) a remote antenna/receiver/transmitter to provide favorable elevation geometry.

20. DISTRIBUTION/AVAILABILITY OF ABSTRACT UNCLASSIFIED/UNLIMITED ☒ SAME AS RPT. ☐ DTIC USERS ☐	21. ABSTRACT SECURITY CLASSIFICATION UNCLASSIFED
22a. NAME OF RESPONSIBLE INDIVIDUAL Javier Montez	22b. TELEPHONE NUMBER (Include Area Code) (915) 568-3355 22c. OFFICE SYMBOL ATZC-DTD

DD FORM 1473, 83 APR EDITION OF 1 JAN 73 IS OBSOLETE.

UNCLASSIFIED

SECURITY CLASSIFICATION OF THIS PAGE

TABLE OF CONTENTS

TABLE OF CONTENTS (continued)

LIST OF FIGURES

LIST OF FIGURES (continued)

LIST OF TABLES

SECTION 1
INTRODUCTION

The present Miss Distance Indicator (MIDI) Radar was developed in 1973 by the U. S. Army Air Defense Board and the Westinghouse Defense and Space Center. MIDI performs an essential role in the development, test, and evaluation of air defense weapons. The MIDI radar tracks a target and measures the vector miss distance (both distance and direction) to the point of closest approach of projectiles fired at the target, as illustrated in Figure 1-1. The MIDI is capable of performing other range instrumentation radar functions such as tracking bullets or missiles to provide trajectory data. Two interchangeable antennas (3 foot diameter and 6 foot diameter) permit either short range, wide field-of-view operation or long range, narrow field-of-view operation. This feature permits scoring of a wide range of projectile types. The mobility of the MIDI allows it to be used wherever needed within the Ft. Bliss or White Sands Missile Range military reservations.

The recent air defense artillery systems have been developed to counter the various low altitude threats such as nap-of-the-earth penetration aircraft and attack helicopters. The U.S. Army Air Defense Artillery Board needs a Miss Distance Indicator Radar that provides tracking and scoring of air defense weapons against simulated low altitude threats. Ideally this upgraded radar should retain all the desirable characteristics of the current system, e.g., accuracy and mobility, but be capable of scoring more closely to the horizon.

Two types of interference -- clutter and multipath -- degrade the tracking accuracy against low altitude targets. Clutter is the backscatter of the radar energy from the ground. Multipath interference is a forward scattering phenomenon in which the radar echo from the target is reflected from the ground, creating a false "image" in addition to the direct return to the radar. Clutter will be strongest and multipath reflection interference will be weakest from rough surfaces. Conversely, for smooth terrain, clutter will be weak and multipath interference will dominate. The terrain roughness

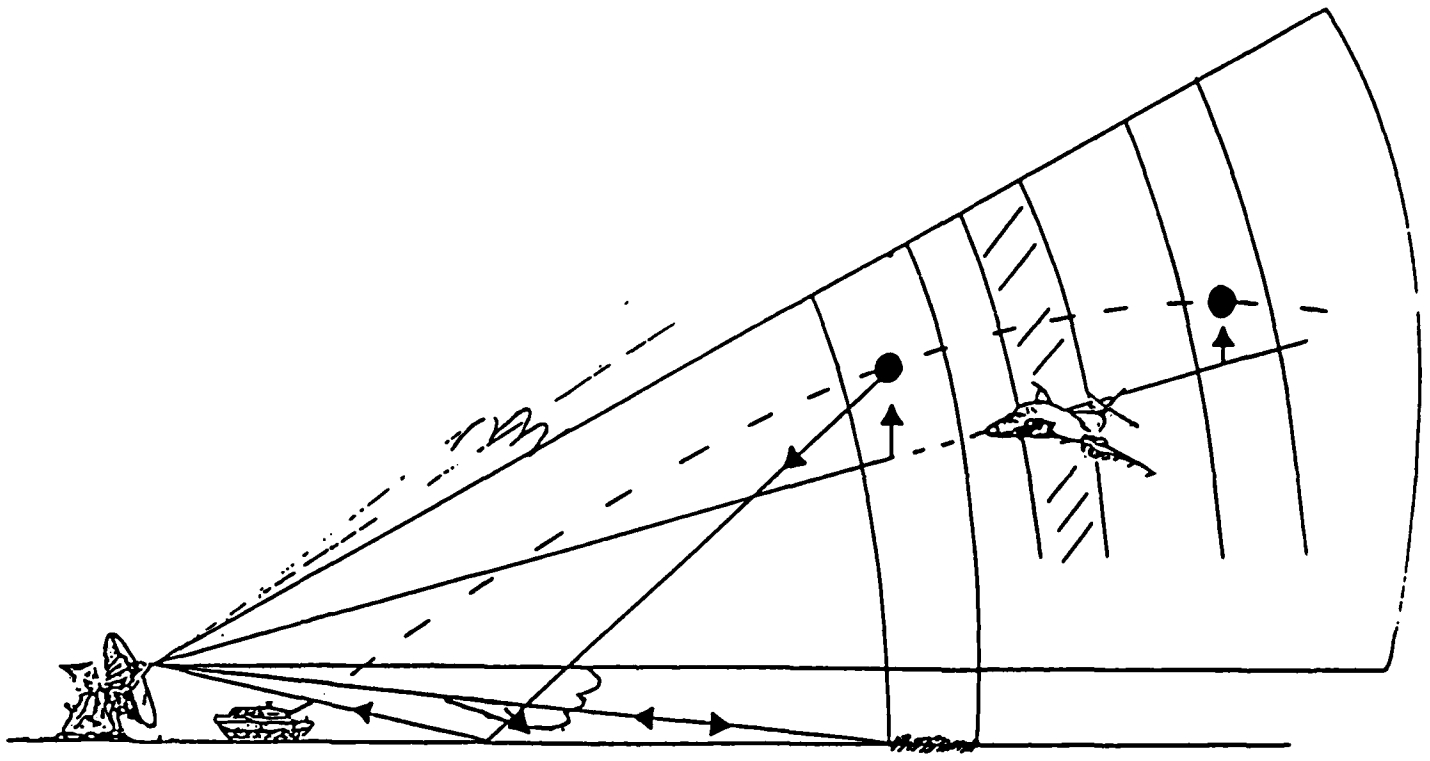

Figure 1-1 Current MIDI concept

from a radar standpoint depends not only upon the physical features but also upon the radar wavelength and grazing angle. All surfaces appear smoother when viewed at small grazing angles.

The U.S. Army Air Defense Board contracted, via the Training and Doctrine Command Contracting Activity at Ft. Eustis, with Georgia Tech for a Methodology Improvement Program to examine techniques and methodologies that will improve low angle elevation tracking and scoring capabilities of a second generation MIDI radar. The major output of this program, as stated in the contract, is a report stating:

1. Conclusions and recommendations concerning the best method or combination of methods to employ for accurate low-elevation tracking and scoring and
2. Minimum achievable elevation angle specified in terms of technological risks as a function of elevation angle.

The general approach was as follows:

1. Become familiar with current and future MIDI requirements. This was achieved through study of several documents provided by the U.S. Army Air Defense Board, visits by Army personnel to Georgia Tech, observing MIDI missions at the North McGregor Test Range, and numerous discussions with Ft. Bliss and White Sands Missile Range personnel.
2. Eliminate the less desirable techniques based upon MIDI operational requirements.
3. Calculate the performance for the most promising methods by varying several radar parameters (e.g., antenna beamwidth, pattern shape, number of Doppler filters), geometric parameters (e.g., radar height and target height) and environmental parameters (e.g., backscatter coefficient and reflection coefficient).
4. Measure the environmental parameters at the North McGregor Test range using MIDI to the extent possible within program constraints such as range time available and weather.

5. Validate the hardware feasibility of achieving the required transmitter power, digital signal processing throughput rates, and storage.

The conclusions and recommendations were presented at a program review in a letter report during August 1984. This final report reiterates these results and provides detailed descriptions of the supporting analyses.

SECTION 2

MAJOR RADAR PERFORMANCE OBJECTIVES

The desired MIDI radar operating modes are summarized in Table 2-1. The primary use of the system is tracking the unmanned targets and measuring vector miss distance during live firing weapon tests. Air defense weapon scoring is desired within the range/altitude envelopes shown in Figures 2-1 and 2-2. No augmentation, passive or active, is permitted on the bullets or missiles. The radar must be capable of tracking an individual bullet or missile to provide trajectory data. Another use is tracking manned aircraft for mission control or range safety. The manned aircraft and the recoverable unmanned targets can be equipped with a radar beacon to improve detection and tracking in clutter. The expendable towed targets will be passively augmented to a radar cross section of one square meter or greater.

Gun 1

Gun 1 fires 20 millimeter projectiles at rates of 3600 per minute. The projectile velocity at the target vicinity may be as high as 1000 meters per second. Firings of intermixed types of ammunition, e.g., tracer rounds, with slightly different ballistics can cause the bullets to bunch or pass. The MIDI should score all ammunition loads properly. The required scoring accuracy for Gun 1 is one milliradian. This translates to a miss distance accuracy of 1 meter at a target range of 1000 meters.

Gun 2

Gun 2 fires 40 millimeter projectiles at rates of less than 1000 per minute. The other requirements are the same as those of Gun 1.

Missiles

The performance envelope boundaries for missile scoring were established for the long range, vehicular-mounted launcher class of air defense missiles. A missile diameter of 15 inches was used in estimating the radar cross section. The required angular scoring accuracy for missiles scoring, is 0.1 milliradian; this translates to a miss distance accuracy of 1 meter at a target range of 10 kilometers.

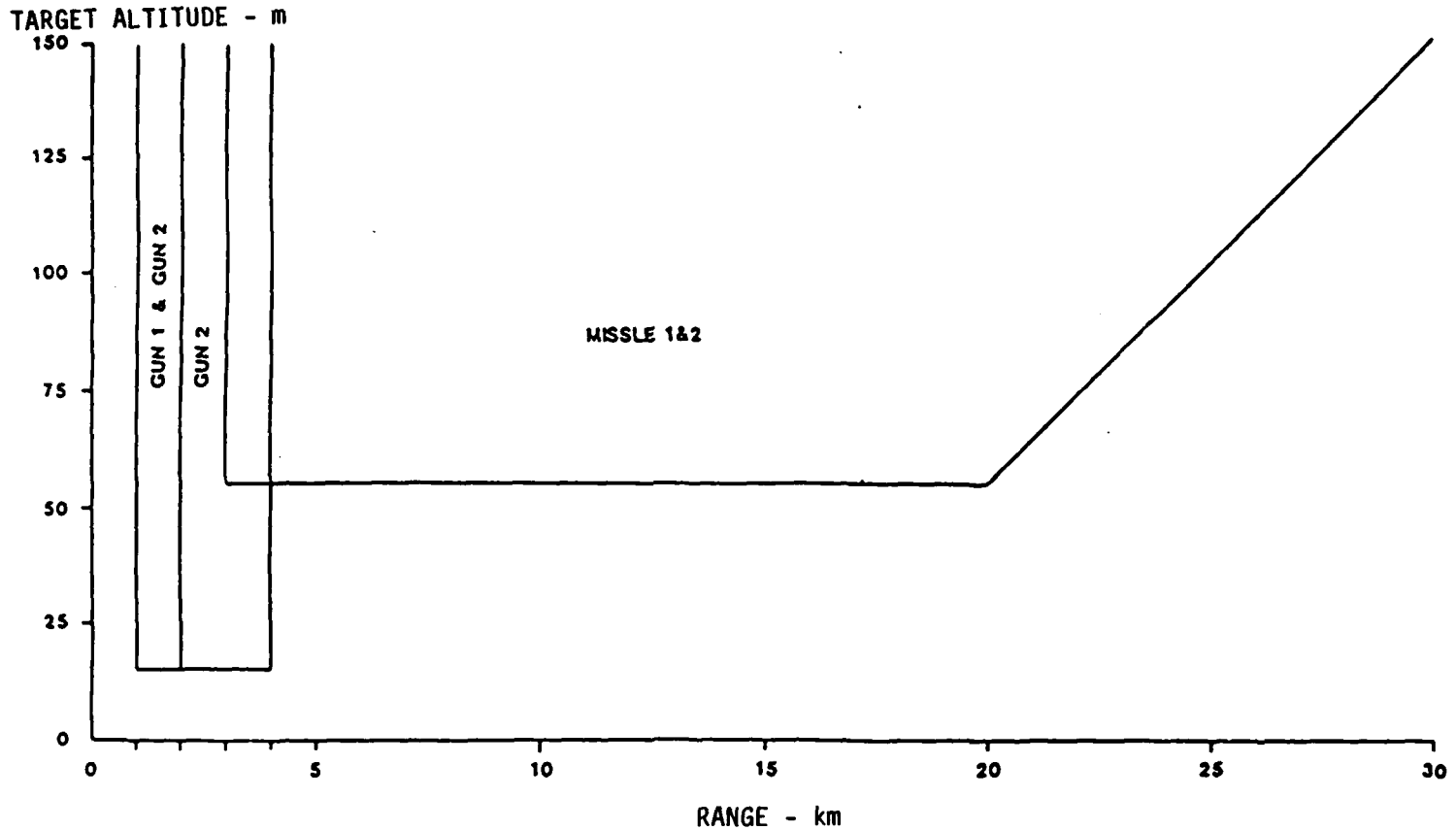

Figure 2-1 Scoring envelopes.

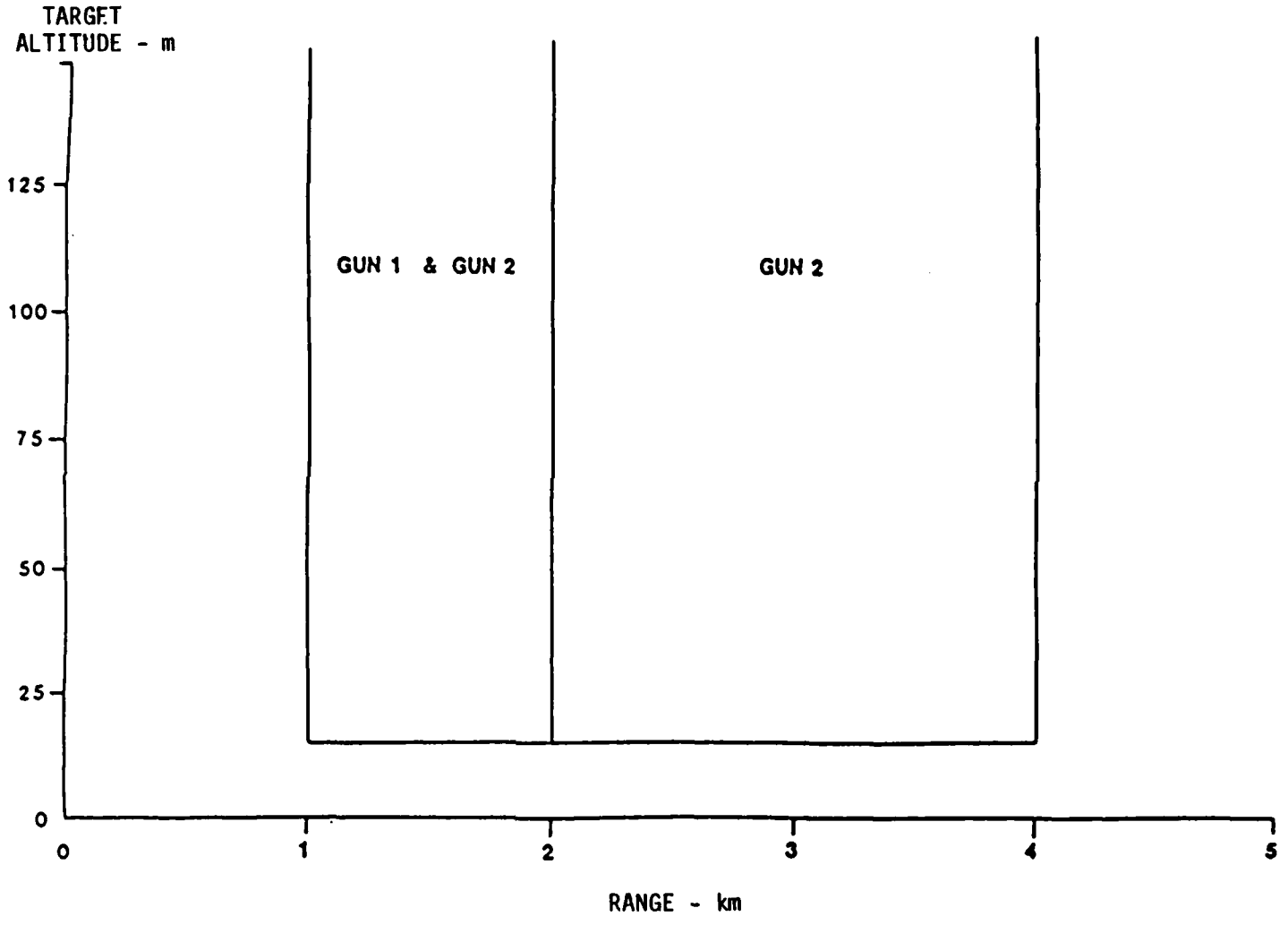

Figure 2-2 Gun Scoring envelopes.

TABLE 2-1. DESIRED MIDI OPERATING MODES

OBJECT TRACKED BY RADAR	BEACON MODE	TRACKING ENVELOPE MAXIMUM RANGE (km)	TRACKING ENVELOPE MINIMUM ALTITUDE (m)	TYPICAL SCORING RANGES BULLET (km)	TYPICAL SCORING RANGES MISSILE (km)
UNMANNED TARGETS					
TOW		30	150	1-4	2-20
HELICOPTER		30	15	1-4	2-20
FIXED WING	YES	30	15	1-4	2-20
MANNED AIRCRAFT	YES	30	15		
BULLETS		6			
MISSILES		30			

SECTION 3
CLUTTER ANALYSIS

The present noncoherent MIDI radar system is designed to operate at elevation angles of 3.5 beamwidths (BW) and above. The system employs no moving target indication (MTI) processing for clutter interference reduction. Instead, the required clutter rejection is achieved by attenuation of the received clutter power through the reduced gain of the antenna elevation sidelobes. At the minimum 3.5 BW elevation angle, the antenna provides a two-way attenuation of greater than 50 dB which is adequate to remove clutter interference as a serious source of tracking error.

The second generation MIDI must operate at elevation angles considerably lower than 3.5 BW. Elevation angles as low as 0.2° are desirable. At these low angles, the received clutter power will be entering the radar through the main beam of the antenna, thus removing the antenna pattern as a mechanism for clutter rejection. Consequently, the required clutter rejection must be achieved by signal processing in the receiver. Because of the large velocity differences between the targets of interest and the clutter background, MTI Doppler processing provides an excellent alternative for clutter reduction. The following section provides a detailed analysis of the nature of the MIDI clutter background, the types of MTI processing that could be employed to reduce clutter interference, and the effects of the residual clutter on the second generation MIDI scoring performance.

3.1 MIDI CLUTTER REFLECTIVITY MEASUREMENTS

During a visit to the present MIDI radar location at the North McGregor Missile Range, New Mexico, Georgia Tech personnel utilized the MIDI system to collect samples of ground clutter video data at four ranges and three elevation angles. Because of instrumentation vans located in the vicinity of the MIDI system, only one azimuthal direction provided an unobstructed view of the desert surface. The resulting set of twelve data runs is, therefore, by no means a definitive description of ground clutter at the MIDI site, but it proved useful in determining reasonable bounds for clutter reflectivity coefficients in a representative MIDI environment.

3.1.1 CLUTTER MEASUREMENT AND ANALYSIS PROCEDURE

The clutter measurement procedure was designed to produce sum channel video clutter data as well as sufficient calibration information to allow reduction of the raw clutter data to equivalent clutter reflectivity (m^2/m^2) information. The calibration procedure consisted of two stages. First, the amplitude response function of the receiver was determined before and after data collection using 10 dB step attenuators built into the MIDI system. The response of the reciver from noise level to 70 dB above noise was determined by boresighting the antenna on a calibration beacon and collecting video samples as receiver attenuation was varied from 0 to 70 dB. This documented the receiver response over the signal range of interest. Second, a reference sample of video data was collected while the antenna was boresighted on a trihedral corner reflector located on a pole 6 km north of the MIDI. This provided a sample of output power for a known radar cross section (RCS) target at a known distance.

Once the calibration was completed, the radar antenna was pointed in the obstruction-free direction and clutter data collection was begun. At each elevation position, the range gate was set to various ranges having a large clutter return and several seconds of video data were collected. Therefore, the samples collected represented a higher clutter power than would have resulted from sampling every range bin. The collected data thus represent a worst case condition. This consideration was included in the analysis of the required clutter rejection.

The reduction of the clutter data to useful reflectivity values involved three steps. Calibration of the received video clutter data with the receiver response function resulted in clutter power values in dB above noise. Normalizing the clutter power data using the range and the reference corner reflector video resulted in clutter RCS (σ) in dBsm. Finally, the clutter RCS was normalized with respect to illuminated area to produce clutter reflectivity (σ^o) values in dB (m^2/m^2).

3.1.2 CLUTTER MEASUREMENT RESULTS

The results of the MIDI clutter measurements are presented in Table 3-1. Four different ranges were sampled, varying from ~ 1,500 m to ~ 25,000 m. Three elevation settings corresponding to horizontal, one beamwidth above horizontal, and one beamwidth below horizontal were used at each range. As can be seen from the table, the reflectivity values do not follow any regular pattern. Raising and lowering the antenna at a given range resulted in as much as 14 dB of variation in the return signal. This was a result of the uneven nature of the terrain surface, particularly at the longer ranges, where the terrain became hilly. In fact, the high reflectivity values at 25 km are discounted because they represent backscatter data from the foothills of a local mountain range. The rest of the data exhibit a reflectivity that varies from -15 dB to -38 dB. The following clutter interference analysis uses values for σ^o of -20 dB and -30 dB which adequately represents the expected average values.

3.2 MIDI SCORING PROJECTILE RCS

The second generation MIDI must perform scoring missions for a large variety of weapons, ranging from the 20 mm Vulcan gun up to the Patriot class missile at ranges from 0.5 km to 30 km. Four basic weapon types were considered: a 20 mm gun, a 40 mm gun, and two air defense missiles. A detailed tracking error analysis requires estimation of the radar cross section of these projectiles.

The MIDI Final Technical Report produced by Westinghouse reports the RCS of a 20 mm projectile to be -30 dBsm.[1] The source of this value was not referenced, but since it was used in designing the original MIDI, the same value was used in our analysis. A means of predicting the X-band RCS of the 40 mm projectile was developed by comparing the nominal -30 dBsm RCS of the 20 mm projectile with theoretical predictions as follows. The RCS Handbook edited by George Ruck was examined for theoretical and experimental RCS values

1. "Mobile Miss Distance Indicator (MIDI) Final Technical Report," Westinghouse Electric Corporation, Data Item A003, Contract DAAD07-72-C-0155, May 1973.

TABLE 3-1. MIDI CLUTTER MEASUREMENTS RESULTS

Range (m)	Elevation (mils)	RCS (m^2)	RCS (dBsm)	Reflectivity (m^2/m^2)	Reflectivity (dB)
25375	-11	78.7090	19.0	.0143	-18.5
25375	0	1028.7295	30.1	.1858	-7.3
25375	11	1785.0685	32.5	.3225	-4.9
15170	-11	6.0778	7.8	.0019	-27.3
15170	0	79.0687	19.0	.0239	-16.2
15170	11	105.4475	20.2	.0319	-15.0
3606	-11	.9686	-.1	.0012	-29.2
3606	0	12.5476	11.0	.0156	-18.1
3686	11	5.9803	7.8	.0074	-21.3
1429	-11	.1235	-9.1	.0004	-34.0
1429	0	.4700	-3.3	.0015	-28.2
1429	11	.0535	-12.7	.0002	-38.2

for objects of the same general shape as bullet projectiles.[2] A bullet is most closely modeled as a flattened ogive; however, the RCS Handbook presents no data for such an object. A short cylinder was considered the next best approximation, but no RCS data existed for a cylinder with both dimensions in the resonant region, which represents 20 mm and 40 mm bullets at X-band. Consequently, the initial approach was to estimate the RCS from a circular flat plate at normal incidence. This was used to represent the RCS of the bullet projectile when viewed from the rear.

Figure 7-24 from the RCS Handbook presents radar cross sections for a disk at normal incidence as a function of wave number k_o and radius a. This graph is reproduced in Figure 3-1. Table 3-2 demonstrates the results of this RCS calculation for the two projectiles of interest:

TABLE 3-2. RCS OF A DISK AT NORMAL INCIDENCE

Projectile	a (m)	$k_o a$	σ (M^2)	σ (dBsm)
20 mm bullet	0.01	2.0	0.003	-25
40 mm bullet	0.02	4.0	0.02	-17

The theoretical estimate of -25 dBsm for the 20 mm projectile is 5 dB higher than the RCS used in the MIDI design. Presumably, this 5 dB accounts for the reduction in RCS at aspect angles off of normal. Applying the same correction factor to the theoretical 40 mm projectile RCS of -17 dBsm results in an average cross section of -22 dBsm. The values of -30 dBsm and -22 dBsm are used in the tracking error analyses that follow.

The radar cross sections of potential missiles to be scored by the MIDI was less easily derived. No data for RCS measurements of advanced air defense missiles was found by Georgia Tech, and any experimental RCS value would almost certainly be classified. Because of the complex shape of missiles,

2. Ruck, G. T., Editor Radar Cross Section Handbook, Plenum Press, 1970.

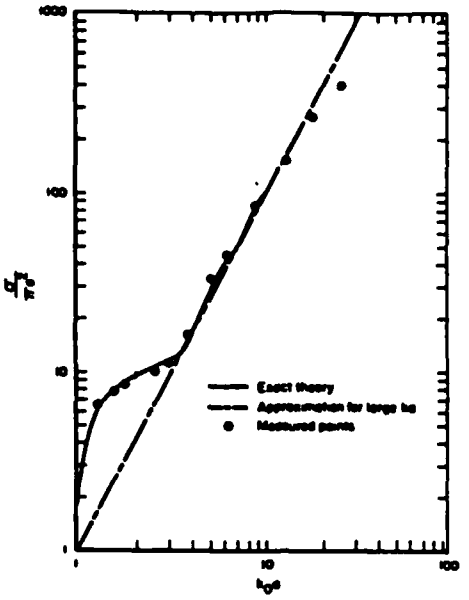

Source: Ruck (1970)

Figure 3-1. Exact and physical-optics backscatter cross sections for a perfectly conducting disc at normal incidence.

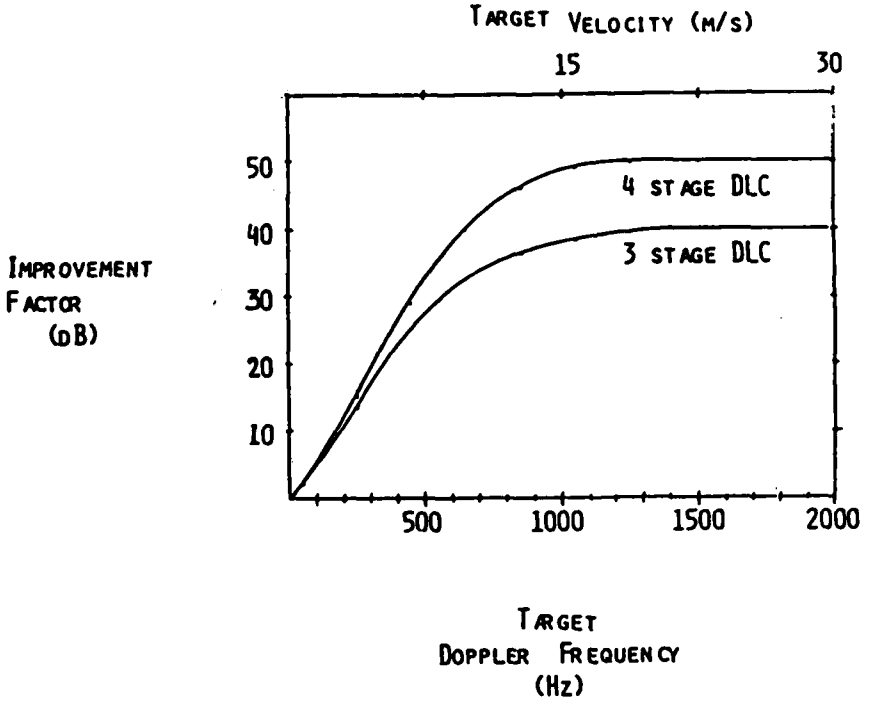

Figure 3-2. Improvement factor of a Butterworth delay line canceller.

including the concave nozzle of the propulsion unit, a simple but accurate theoretical prediction using physical optics was not possible. The source used for missile RCS estimates was the MIDI Final Technical Report[1]. This report stated that the RCS of missiles could range from -17 dBsm to -5 dBsm at X-band. The larger RCS value of -5 dBsm was used to represent the long range air defense missiles.

3.3 CLUTTER REJECTION REQUIREMENTS

The representative clutter reflectivity values of -20 dB and -30 dB were used to predict the amount of clutter power received by the MIDI radar under various configurations. The expected projectile RCS and the required signal-to-clutter ratio (SCR) were used to estimate the necessary MTI improvement factor.

The signal-to-interference ratio (SIR) required for adequate performance of the MIDI tracking radar was derived using procedures described in the Handbook of Radar Measurements by Barton and Ward[3]. In Chapter 8, Barton outlines a method for calculating the required SNR using the desired accuracy and the radar system parameters. The same procedure can be applied to the (SCR) ratio as follows.

The required energy ratio, R, is given by

$$R = \left(\frac{\Theta_3}{\sigma_\theta \, k_m}\right)^2, \qquad 3.1$$

where

Θ_3 = the 3 dB beamwidth,
k_m = the normalized monopulse slope, and
σ_θ = the desired rms tracking error.

From the energy ratio the SIR is computed from the equation

3. Barton, D. K. and Ward, H. R., Handbook of Radar Measurements, Prentiss-Hall, 1969.

$$\frac{S}{I} = \frac{R}{2nL_m} \qquad 3.2$$

where n = the number of pulses on the target and

L_m = the filter mismatch loss.

The 3 dB beamwidth of the present MIDI large antenna is 22 mrad, and the monopulse error slope is approximately 1.8. Instrumentation and mechanical inaccuracies limit the minimum rms tracking error to approximately 0.1 mrad. For these values, Equation 3.1 produces a required energy ratio of 15,000. The number of pulses on a projectile such as a bullet, is limited to approximately 20 by the projectile velocity. If the receiver bandwidth B is matched to the pulse length τ such that $B\tau \approx 1$, then the filter mismatch loss will be 1 dB. For these values, Equation 3.2 predicts a required SIR of 26 dB.

The MTI improvement factor required to produce a 26 dB SCR is given by

$$I = \frac{SCR\ \sigma^o\ A}{\sigma_T}, \qquad 3.3$$

where

A = $R \sin \theta_3 \cdot \frac{c\tau}{2}$ = area illuminated,

σ^o = clutter reflectivity,

σ_T = target RCS, and

SCR = required signal-to-clutter ratio.

Table 3-3 demonstrates the required improvement factor for a variety of scenarios. The MTI improvement values range from a low of 36 dB for missile scoring at 30 km in low clutter to a high of 60 dB for 20 mm bullet scoring at 2 km in high clutter. An improvement factor of 60 dB is difficult to achieve, particularly with as few pulses as are available to the MIDI system. For this reason, the MTI processing analysis that follows concentrates on achieving improvement factors of 40 and 50 dB.

Table 3-3 REQUIRED MTI IMPROVEMENT FACTOR FOR A 26 dB SCR.

Projectile	RCS (dBsm)	Range (km)	BW (deg)	σ^o (dB)	I (dB)
20 mm bullet	-30	2	1.25	-20	60
				-30	50
40 mm bullet	-22	4	1.25	-20	54
				-30	44
Missile	-5	30	1.25	-20	46
				-30	36

3.4 MTI PROCESSING ANALYSIS

The high radial velocity of missiles and bullets to be scored by the MIDI and the stationary arrangement of the radar make an ideal situation for implementation of Doppler processing. The very speed that makes MTI processing attractive, however, induces technical problems that impact the selection and design of candidate MTI systems. This section discusses the nature of the Doppler detection problem, the candidate MTI techniques available, and the types of improvement factors that can be achieved.

3.4.1 PRF SELECTION

The projectiles that the second generation MIDI must score may be travelling at speeds up to 1000 m/s. This velocity corresponds to a required unambiguous Doppler frequency f_d of 64,500 Hz at X-band. Some form of PRF staggering must be employed to extend the unambiguous Doppler frequency f_d to the required range of 64,500 Hz. For a two PRF stagger, the appropriate pulse rates can be determined as follows.

The maximum scoring projectile velocity is 1000 m/s. The sampling time t_o is determined by the time the projectile is within the 5 m range gate. Since the range gates are tracking the drone target, which may have velocities on the order of 200 m/s, the net velocity difference between projectile and range gate could be as great at 1200 m/s. For a 5 m range gate, this correspond to a sampling time of 4.17 ms. The number of pulses on the projectile would then be

$$N = PRF \cdot t_o \qquad 3.4$$
$$= PRF \cdot 4.17 \text{ ms.}$$

For a two PRF stagger, the maximum unambiguous frequency occurs when multiples of each PRF overlap. This occurs at a frequency f_d given by

$$f_d = \frac{PRF_1 \cdot PRF_2}{PRF_2 - PRF_1} . \qquad 3.5$$

By establishing a known relationship between PRF_1 and PRF_2, Equations 3.4 and 3.5 can be used to determine the appropriate PRF values. If a bank of N narrow band filters were employed to provide velocity information, the two PRF's would be chosen such that the first ambiguous frequency of PRF_1 would fall in the middle of the N - 1 filter of PRF_2. This statement corresponds to the following equation:

$$PRF_1 = \left(\frac{N - 1}{N}\right) PRF_2 . \qquad 3.6$$

A quadratic equation for PRF_2 is obtained by combining equations 3.4, 3.5, and 3.6

$$t_o \, PRF_2^2 - PRF_2 - f_d = 0$$

The solution of Equation 3.7 is:

$$PRF_2 = \frac{1 + \sqrt{1 + 4 \, t_o \, f_d}}{2 \, t_o} . \qquad 3.8$$

If t_o 4.17 ms and f_d = 64,500 Hz, Equation 3.8 gives PRF_2 = 4055 Hz. Then by Equation 3.5, PRF_1 = 3815. For a 1000 m/s projectile, these PRF's will provide on the order of 16 pulses on targets. This is a worst case estimate. The average bullet velocity in the scoring region is approximately 680 m/s. At this velocity, 32 pulses could be accumulated. This result is considered in the following MTI analysis.

3.4.2 MTI PROCESSING TECHNIQUES

Two MTI processing techniques considered in this analysis can provide the necessary 1000 m/s coverage in the Doppler domain: a delay line canceller and a coherent FFT. The characteristics of these filters are described in the following sections, and their relative merits as applied to the second generation MIDI radar are considered.

3.4.2.1 Delay Line Canceller

Delay line cancellers (DLCs) are a common technique for achieving a broad passband for detecting moving targets while filtering out a large proportion of the stationary clutter return. Since the DLC can be implemented digitally, a large number of range gates can be accommodated, and good MTI improvement can be achieved with three or four delay stages. Increasing in the number of stages increases the length of time necessary for the canceller to achieve a steady-state condition and places more stringent requirements on transmitter and oscillator stability. But increasing the number of stages results in a sharper slope of the MTI response function and thus increases the clutter cancellation produced by the filter. The response function H(f) of a Butterworth canceller is closely approximated by the equation

$$|H(f)|^2 = \frac{1}{1 + \left(\frac{f_c}{f}\right)^{2m}} \qquad 3.9$$

where f_c = the cutoff frequency and

m = the number of poles or stages in the filter.

The improvement factors for 3-stage and a 4-stage Butterworth DLC as a function of target velocity is presented in Figure 3-2. Both cancellers achieve their maximum improvement at a target velocity of 15 m/s. The improvement of the 3-stage canceller is limited to 40 dB, but the 4-stage filter has a theoretical limit of 50 dB. The 4-stage canceller is considerably more effective in detecting small bullet targets in high background clutter.

The DLC filters discussed so far are for a fixed PRF and have a passband limited to the PRF. For the second generation MIDI to fulfill its scoring mission on high speed projectiles, pulse-to-pulse staggering of the PRF must be employed to extend the blind velocity V_B to the 1000 m/s requirement. At an average PRF of 4000 Hz the first unstaggered blind speed V occurs at

$$\frac{V}{V_B} = \frac{R_1 + R_2 + R_3 + \ldots + R_N}{N} \qquad 3.10$$

where R_1, R_2 ..., R_N are the ratios of the pulse intervals expressed as integers[4]. A typical velocity response curve for a staggered DLC from Skolnik's Radar Handbook is presented in Figure 3-3.[4] The overlap of blind velocities of the individual PRF's causes modulation of the response function in the passband region. The severity of this modulation is reduced as the number of PRF's employed increases. For the second generation MIDI, the ratio of true blind speed to the unstaggered blind speed is $V/V_B = \frac{1000 \text{ m/s}}{62 \text{ m/s}} = 16$. An adequate Doppler coverage could be achieved with a pulse internal ratio of 19:16:17:13.

Staggering the pulse interval has drawbacks as well as advantages. In a nonstaggered multistage DLC, a slowly varying waveform, such as a specular clutter return, will be almost perfectly cancelled. But in a staggered DLC, the time interval between the two samples will vary, resulting in a voltage residue out of the canceller. Skolnik has derived the MTI improvement factor to be

$$I = 20 \log \frac{2.5\, n}{\delta - 1} \ , \qquad 3.10$$

where n = number of pulses on target and
δ = ratio of pulse intervals.[4]

For the staggering choice previously described the maximum improvement factor would be 41 dB. If this improvement were deemed insufficient, a 5 interval PRF stagger might be required.

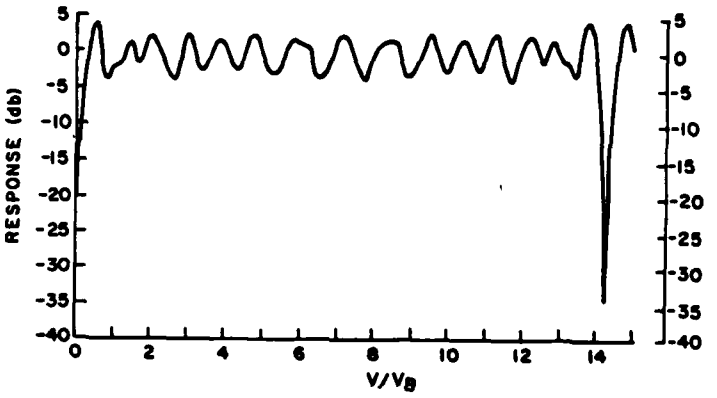

Source: Skolnik (1970)

Figure 3-3. Velocity-response curve: dual canceller, no feedback, 11:16:13:17 pulse-interval ratio.

The previous analysis indicates that a 4-stage delay line canceller (DLC) with 4 or 5 period PRF stagger could achieve the improvement factors required in the MIDI II scenario. Delay line cancellers have a disadvantage which would seriously limit their usefulness in the MIDI scenario. As previously mentioned, DLC filters require a period of several pulses to achieve their optimum steady state condition. This effect is demonstrated in Figure 3-4

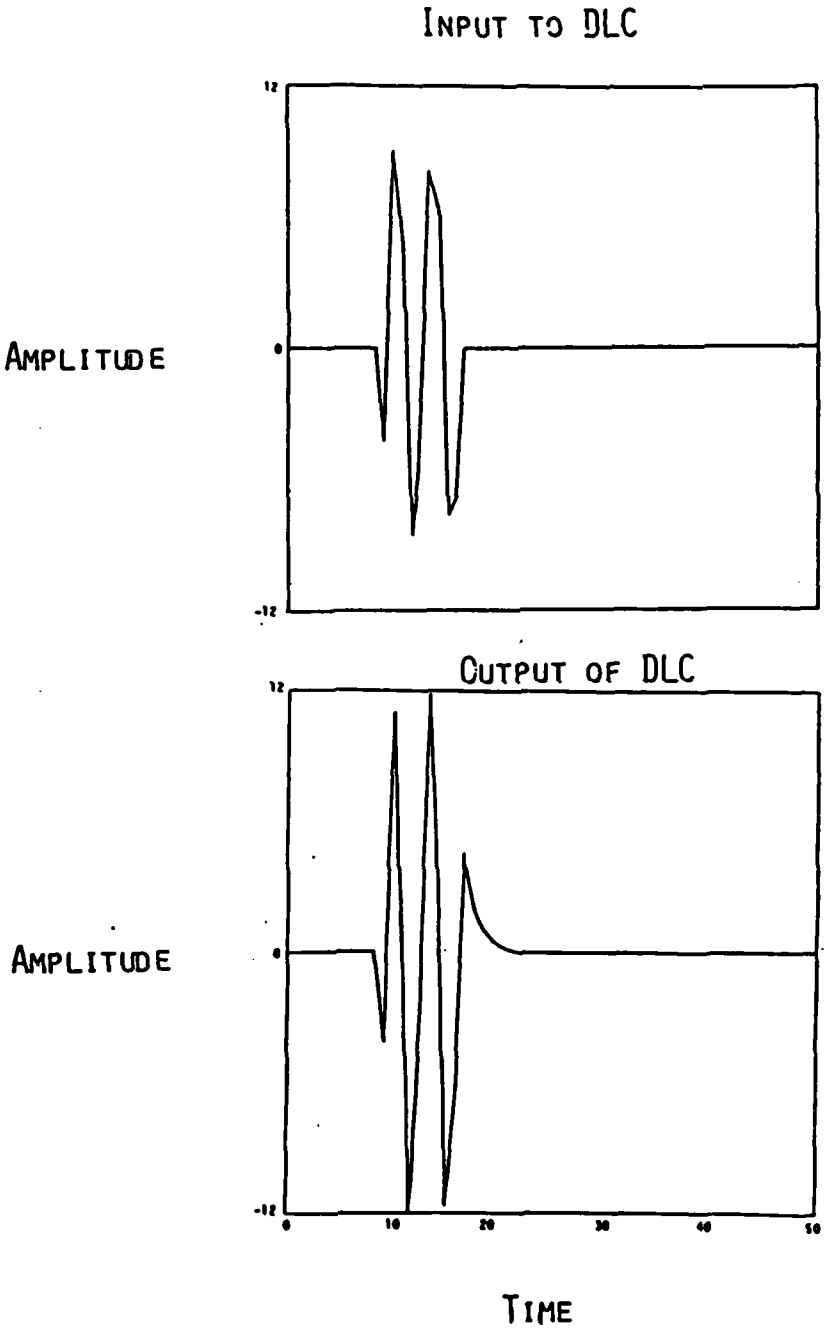

Figure 3-4. Effect of transient target signal on delay line canceller.

which presents the response of a DLC to a transient signal. This response is representative of a bullet passing through a scoring range gate at 600 m/s. The canceller takes 4 or 5 pulses to reach optimum operation, and another 4 or 5 pulses to return to zero once the bullet is gone. This degradation of performance would be acceptable if it were the only source of transient errors. Since the scoring range gates of the MIDI system would track the drone target at speeds up to 200 m/s, large specular clutter sources could suddenly appear within a range gate even if the objects themselves were stationary. Figure 3-5 depicts the canceller response to such a transient clutter signal. While the DLC effectively removes the clutter during steady state operation, the sudden appearance and disapperance of the clutter signal results in strong spikes in the output voltage. Under certain conditions, these transient responses to clutter could greatly increase the number of clutter false alarms. This would seriously affect the MIDI scoring performance. Consequently, the delay line canceller is not recommended as a solution to clutter interference in the second generation MIDI radar system.

3.4.2.2 Coherent Fast Fourier Transform

Recent advances in the speed of digital microprocessors and other hardware have made fast Fourier transforms (FFT) increasingly useful in radar applications where high data rates are an inherent requirement. Like the DLC, the FFT can be implemented digitally, allowing high speed performance at a moderate cost. The FFT, however, possess a number of characteristics that make it superior to a delay line canceller.

One PRF interval of the coherent video spectrum of a moving target in noise and clutter is depicted in Figure 3-6. The bandwidth of the target spectrum (B_s) is primarily determined by the length of the sampling period ($B_s \approx 1/t_o$), whereas the bandwidth of the clutter spectrum is determined by both the sampling time and internal clutter motion. For the MIDI radar, the average sampling time is so short ($\sim$ 5 msec) that it will almost certainly be the limiting factor on clutter spectrum bandwidth as well. The fast Fourier transform essentially acts as a bank of N_F contiguous, narrowband Doppler filters ranging from -PRF/2 to +PRF/2. Optimally, the bandwidth of these

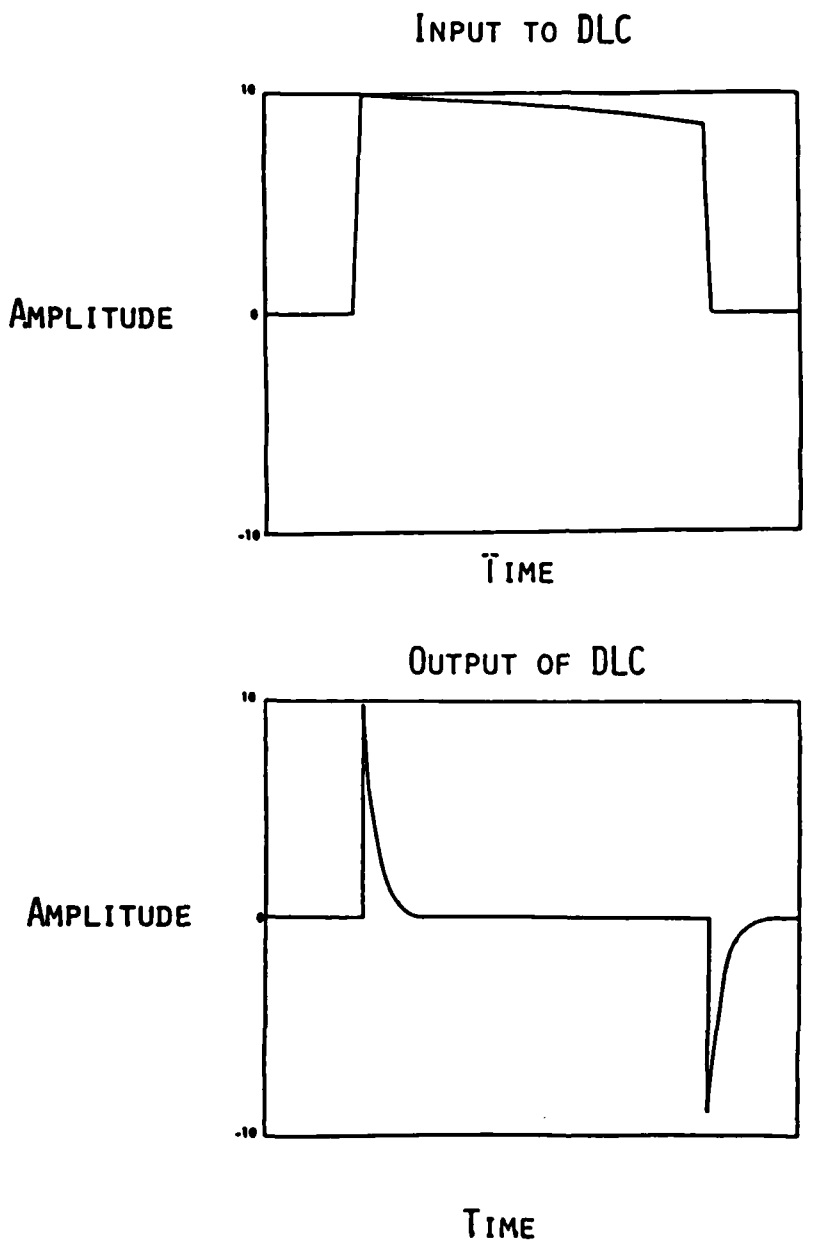

Figure 3-5. Effect of transient clutter signal on delay line canceller.

filters is chosen to equal the target spectrum bandwidth B_s; this choice maximizes the signal-to-noise ratio (SNR) out of each filter. In fact, one of the advantages of the FFT is that the SNR out of the filter is the product of the SNR at the input to the filter and the number of filters. The delay line canceller, on the other hand, passes nearly all of the noise through its wide passband. An additional advantage of the filter bank is that the target's velocity can be determined from the filter in which it was detected. This could be useful in matching projectile trajectories to precomputed ballistic tables.

The FFT has a final advantage over the DLC. Because it is a batch process, rather than a continuous one, the FFT does not display the adverse response to transient clutter and target signals produced by the DLC. The result of a sudden appearance of a strong clutter signal during a batch will be a widening of the clutter spectrum associated with the reduced sampling time. Such a widening could reduce target detectability in the two filters contiguous with the clutter filter, but it will not have the disastrous effect produced by the DLC circuit.

Coherent FFT Improvement Factor

The improvement factor I of the FFT can be computed as follows:

$$I = \frac{S_o}{S_i} \frac{C_i}{C_o}, \qquad 3.11$$

where S_i and C_i are the target and clutter powers into the FFT processor and S_o and C_o are the respective powers out of the processor. The FFT filter bin size was assumed to be matched to the target bandwidth. Signal losses due to filter mismatch as well as to other sources in the processor are considered later.

The frequency response of the FFT for a single frequency bin is pictured in Figure 3-7. The uniform sidelobes are a result of a Dolph-Chebyshev weighting applied to the input time samples. Some form of weighting is necessary in any practical FFT application to reduce the frequency sidelobes; Dolph-Chebyshev weighting is commonly employed because it produces uniform

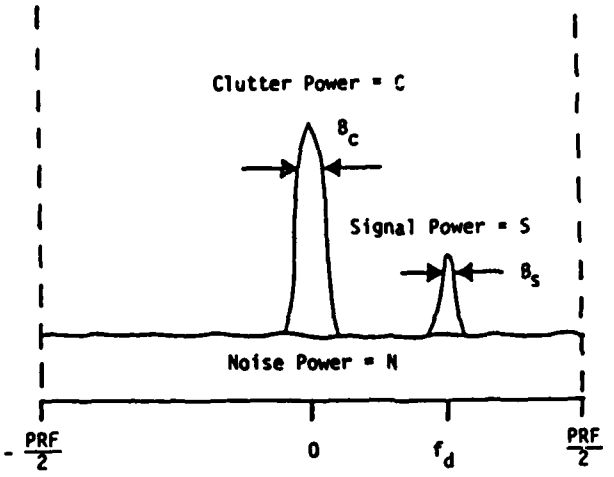

Figure 3-6. One PRF interval of the coherent video spectrum of a moving target in noise and clutter.

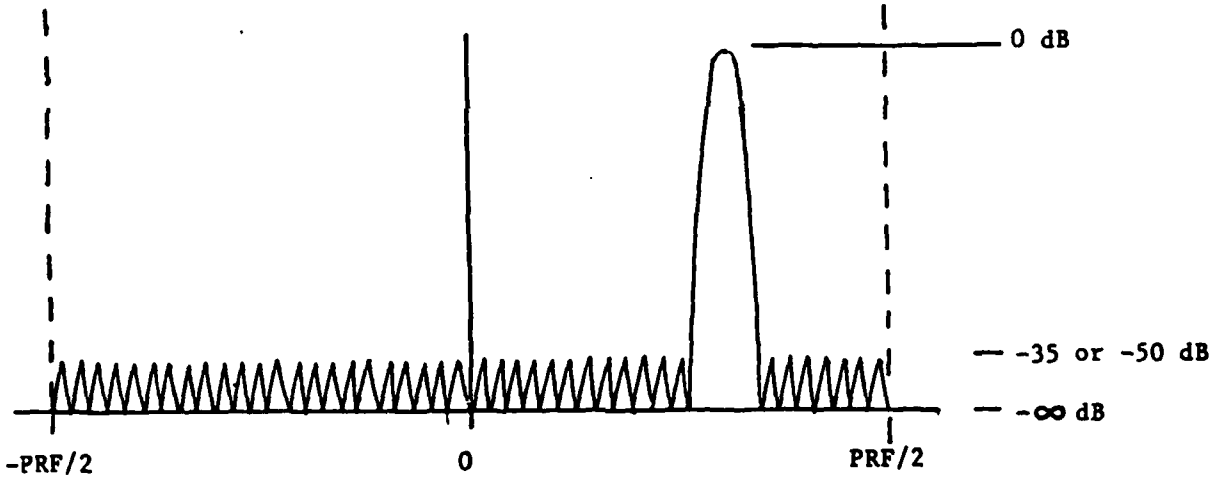

Figure 3-7. Filter response of target frequency bin with Dolph-Chebyshev weighting applied.

height sidelobes. The FFT response was evaluated for two frequency sidelobe levels: -35 dB and -50 dB. The amount of clutter power out of the FFT processor is the sum of the clutter power within the frequency bin of the target plus the residual clutter that is passed through the sidelobes of the filter response.

The improvement factor produced by a coherent FFT is demonstrated in Figure 3-8 for a 16-point and a 32-point FFT. In both cases, the maximum improvement achieved is limited by the frequency sidelobe level (FSL). Since adequate MIDI II tracking performance requires 40 dB to 50 dB of improvement, the frequency sidelobes should be suppressed as much as possible. As can be seen in the figure, the narrower frequency bins of the 32-point FFT result in a more rapid rise to the maximum improvement factor. In adddition, they allow a more accurate estimation of the target velocity, which could prove useful in determining vector miss distance.

Coherent FFT Losses

There are a number of sources of signal loss in the implementation of a fast Fourier Transform. The process of weighting the input signal train to reduce the frequency sidelobe level (FSL) results in a loss in signal power. The lower the desired sidelobe level, the higher the loss associated with it. For the Dolph-Chebyshev weighting described previously, the loss is 0.8 dB for 35 dB sidelobes or 1.4 dB for 50 dB sidelobes.

In addition to the weighting loss, there is a filter mismatch loss that results from target energy extending beyond the bandwidth of the FFT bin in which it resides. The amount of this loss is a function of the FFT bin size and the width of the target spectrum. The FFT bin sizes considered in this analysis were 250 Hz for the 16-point FFT and 125 Hz for the 32-point FFT. For the high speed targets of the MIDI system, the target spectrum bandwidth will be determined by the sampling time t_o; i.e.

$$B_s \approx \frac{1}{t_o} . \qquad 3.12$$

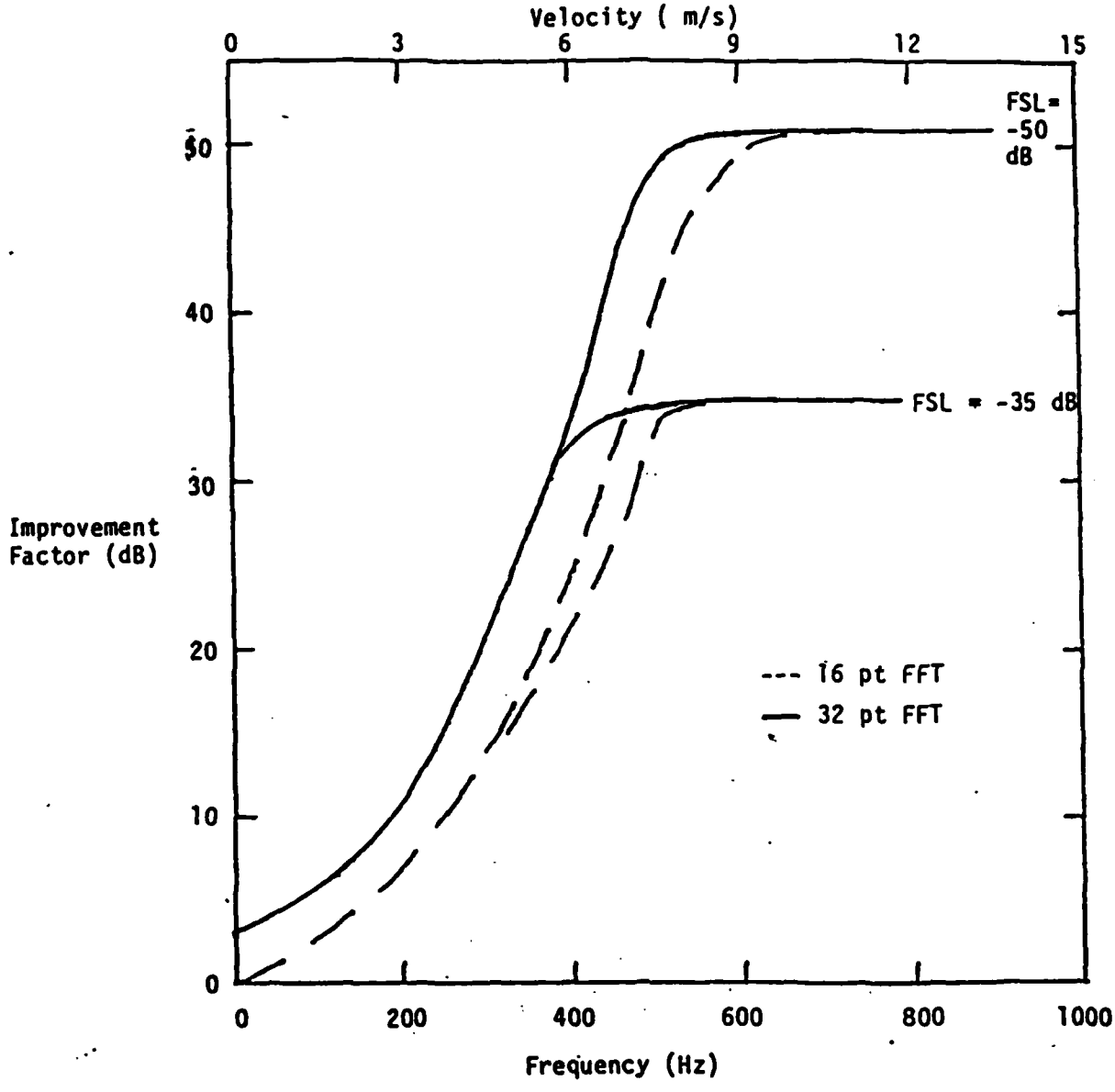

Figure 3-8. Improvement factor of a coherent FFT filter.

This bandwidth could be as high as 240 Hz for 1000 m/s missiles shot at an oncoming drone target. A more representative bandwidth would be 120 Hz, which corresponds to the average velocity of bullets (600 m/s) in the vicinity of the drone aircraft. For a 120 Hz target spectrum bandwidth, the 16-point FFT has a filter mismatch loss of 1.5 dB; i.e., 30% of the power extends beyond the bandwidth of the FFT bin. For the the same target signal, the 32-point FFT has a filter mismatch loss of 4 dB. In this case, more than half of the energy extends beyond the filter. These loss figures assume that the detection threshold is applied to each bin individually. Some of the lost energy could be recovered by integrating over several bins surrounding the target bin. Barring such processing, the total loss associated with the FFT signal processing is summarized in Table 3-4.

TABLE 3-4. COHERENT FFT PROCESSING LOSSES

Source	16-point FFT (dB)		32-point FFT (dB)	
Mismatch loss	1.5	1.5	4.0	4.0
-35 dB FSL	0.8		0.8	
-50 dB FSL		1.4		1.4
Total losses	2.3	2.9	4.8	5.4

In spite of the processing losses associated with FFT processing, it is still the best approach for the second generation MIDI design. The desired 50 dB improvement factor can be achieved with proper weighting to reduce frequency sidelobes. The 1000 m/s unambiguous velocity can be reached with a

two stage, batch staggered PRF of 4055 and 3815 Hz. Because the FFT is a batch process, the undesirable transient response of clutter signals which affects the DLC design is absent. For all these reasons, a coherent FFT is the best MTI processing design for the MIDI II.

3.5 CLUTTER INTERFERENCE TRACKING ERROR ANALYSIS

The low angle scoring coverage desired for the second generation MIDI radar places stringent requirements on the MTI processor. A graphic depiction of the coverage requirements were presented in Figure 2-1. The effect of residual clutter interference on MIDI tracking performance was analyzed for these low angle scenarios. The results were compared to the desired coverage diagram to determine the effectiveness of MTI processing in reaching the low angle goals.

3.5.1 CLUTTER INTERFERENCE MODEL

The effect of clutter interference on MIDI II tracking performance was simulated with a computer model. The physical scenario for the model is shown in Figure 3-9. A drone target is flown toward the radar at a constant altitude h_t. The radar sits on a pedestal at a height of 5 m above the surrounding terrain. The radar is assumed to be boresighted on the drone target, and the scoring target (projectile or missile) flies past the drone at some offset angle θ_T. The clutter power returned from the same range cell as the scoring target enters the antenna at an angle θ_C. The gains associated with these signals are listed in Table 3-5.

TABLE 3-5. TARGET AND CLUTTER ANTENNA GAINS

Object	Sum Channel	Difference Channel
target	$G_\Sigma^2(\theta_T)$	$G_\Sigma(\theta_T)\, G_\Delta(\theta_T)$
clutter	$G_\Sigma^2(\theta_C)$	$G_\Sigma(\theta_C)\, G_\Delta(\theta_C)$

The clutter RCS is computed from the reflectivity σ^o and the illuminated area A:

$$\sigma_C = \sigma^o A \ . \qquad 3.13$$

For the gains previously described, the received signal-to-clutter ratios (SCR) in the sum and difference channels were computed as follows:

$$\left(\frac{S}{C}\right)_{\Sigma in} = \frac{G_\Sigma^2 (\theta_T)\ \sigma_T}{G_\Sigma^2 (\theta_C)\ \sigma_C} \ , \qquad 3.14$$

and

$$\left(\frac{S}{C}\right)_{\Delta in} = \frac{G_\Sigma (\theta_T)\ G_\Delta (\theta_T)\ \sigma_T}{G_\Sigma (\theta_C)\ G_\Delta (\theta_C)\ \sigma_C} \ . \qquad 3.15$$

where σ_T = scoring target RCS. Finally, the MTI processing in the receiver provides an increase in the SCR out of the signal processor such that

$$\left(\frac{S}{C}\right)_{out} = I \left(\frac{S}{C}\right)_{in} \ . \qquad 3.16$$

The modified signal-to-clutter ratios were used in the following computer program to compute the tracking error introduced by the clutter interference.

3.5.2 MTI ANGLE PROCESSING

Unlike conventional monopulse radars, which process sum and difference channels separately, the MIDI monopulse system converts the basic Δ and Σ channels into $(\Sigma/2 + j\Delta\sqrt{2})$ and $(\Sigma/2 - j\Delta/\sqrt{2})$ channels, as illustrated in Figure 4-3. The phase angle between the two channels is computed from

$$\phi_T (\theta) = 2 \arctan \left(\frac{\sqrt{2}\ \Delta (\theta)}{L\ \Sigma (\theta)}\right) \qquad 3.17$$

where $\Delta(\theta)$ = difference voltage at angle θ,

$\Sigma(\theta)$ = sum voltage at angle θ, and

L = loss difference between Δ and Σ channels.

The MIDI system uses a look-up table to compute the off-boresight angle θ_T from the measured phase angle ϕ.

3.5.3 EFFECT OF CLUTTER INTERFERENCE ON MIDI ANGLE PROCESSING

Signals received from clutter or multipath will interfere with an accurate estimate of the off-boresight angle location of scoring targets. Note that an estimate of target location will still be made in the presence of interference, but the result will be erroneous. Since the radar gives no indication that interference is present, it is important that the useful limits of the MIDI II system be determined.

Interfering signals from clutter backscatter will contaminate the true Σ and Δ target signals as depicted in Figure 3-10. The amplitude of the clutter signal will depend on the radar cross of the clutter and the clutter attenuation of the signal processor. The phase of the clutter signal relative to the target signal, δ_c, will vary randomly from 0 to 360°. The contaminated voltage signals will thus be

$$\Sigma' = \Sigma_T + \Sigma_C \cos \delta_C \qquad 3.18$$

and

$$\Delta' = \Delta_T + \Delta_C \cos \delta_C \,, \qquad 3.19$$

where Σ_T = target sum channel voltage,

Δ_T = target difference channel voltage,

Σ_C = clutter sum channel voltage,

Δ_C = clutter difference channel voltage, and

δ_C = relative clutter-to-target phase angle.

These signals can be related to the pure target signal and the clutter-to-signal voltage $(C/S)^V$ ratio by

$$\Sigma' = \Sigma_T(1 + (\frac{C}{S})^V_\Sigma \cos \delta_C) \qquad 3.20$$

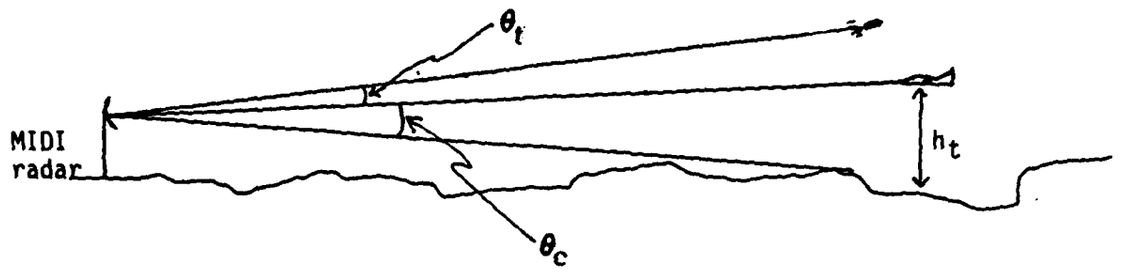

Figure 3-9. Physical scenario for clutter interference model.

RECEIVED SIGNALS FROM TARGET PLUS CLUTTER

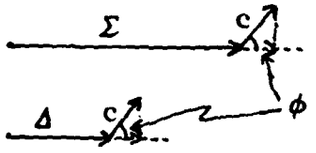

ANGLE PROCESSING

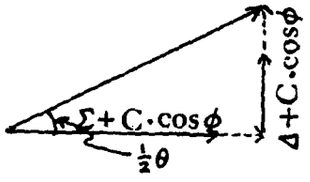

θ = CORRUPTED ANGLE MEASUREMENT

$$\theta = 2 \text{ ATAN } \frac{\sqrt{2}\,(\Sigma + C \cos\phi)}{L_E\,(\Delta + C_\Delta \cos\phi)}$$

Figure 3-10. Effect of clutter interference on MIDI angle processing.

$$\Delta' = \Delta_T(1 + (\frac{C}{S})^V_\Delta \cos \delta_C) \ . \qquad 3.21$$

where $(\frac{C}{S})^V_\Sigma = \frac{1}{\sqrt{(\frac{S}{C})_\Sigma \text{ (power)}}}$ and

$$(\frac{C}{S})^V_\Delta = \frac{1}{\sqrt{(\frac{S}{C})_\Delta \text{ (power)}}} \ .$$

The contaminated phase angle measurement is then

$$\phi_E = 2 \arctan \left(\frac{\sqrt{2}\ \Delta_T}{\Sigma_T} \cdot \frac{1 + (\frac{C}{S})^V_\Delta \cos \delta_C}{1 + (\frac{C}{S})^V_\Sigma \cos \delta_C}\right) \ . \qquad 3.22$$

The MIDI look-up table is used to translate the phase angle ϕ_E to a geometric angle θ_E. The measured angle error induced by clutter interference is then

$$\Delta\theta = \theta_E - \theta_T. \qquad 3.23$$

3.5.4 COMPUTER PROGRAM "CLTERR"

A computer model was generated to compute angle error as a function of range for a varitey of target and environmental characteristics. Table 3-6 lists the input variables used to generate the matrix of performance predictions presented in Appendix D. A clutter reflectivity of -20 dB was used for all cases. This represents a worst case condition for the present MIDI environment.

in detail in Section 3.4.6. The complete set of output plots is included in Appendix D.

3.5.5 CLUTTER TRACKING ERROR RESULTS

The output of the clutter interference tracking error model consisted of plots of rms tracking error in mils as a function of range. Figure 3-11 depicts an example of this output for the case of an X-band MIDI with 40 dB MTI improvement scoring a 20 mm projectile fired at a drone target at 50 m altitude. As can be seen in the figure, good tracking accuracy is achieved out to a range of 1700 m, where the rms error is less than 0.5 mils. Beyond this range, the tracking error increases exponentially and exceeds 1 mils at a range of 2000 m. The sharp rise in tracking error is the result of illumination of the clutter area by the difference antenna pattern. While the low gain portion of the pattern is on the ground, the effect of clutter interference changes slowly. As the illuminating point approaches the 3 dB point on the difference pattern, the influence of clutter increases rapidly.

A significant improvement in tracking error performance can be achieved by increasing the MTI improvement to 50 dB, as shown in Figure 3-12. The shape of the curve is unchanged, but because of the increased improvement, the rms tracking error at 2000 m is less than 0.35 mils.

The tracking performance for each weapon was summarized as a function of target height and range to present the results of the tracking error analysis in a form more useful to a radar system performance evaluation. A total rms error of 1 mil was chosen as an appropriate design specification. For statistically independent error sources, this error allowance would be equivalent to four errors of 0.5 mil each. This limit of 0.5 mil was applied to both the multipath and clutter interference analyses.

Figure 3-13 presents the MIDI II 20 mm bullet scoring performance for a tracking error of 0.5 mil. The performance limits for a second generation MIDI with 40 dB and 50 dB of MTI improvement are compared to the coverage goal. For comparison, the operating limit of the present MIDI system is also shown. Clearly, the very low angle coverage of 0.4^{o} is not achievable even with 50 dB of MTI improvement. The addition of MTI processing, however, does provide a great improvement over the present MIDI capabilities.

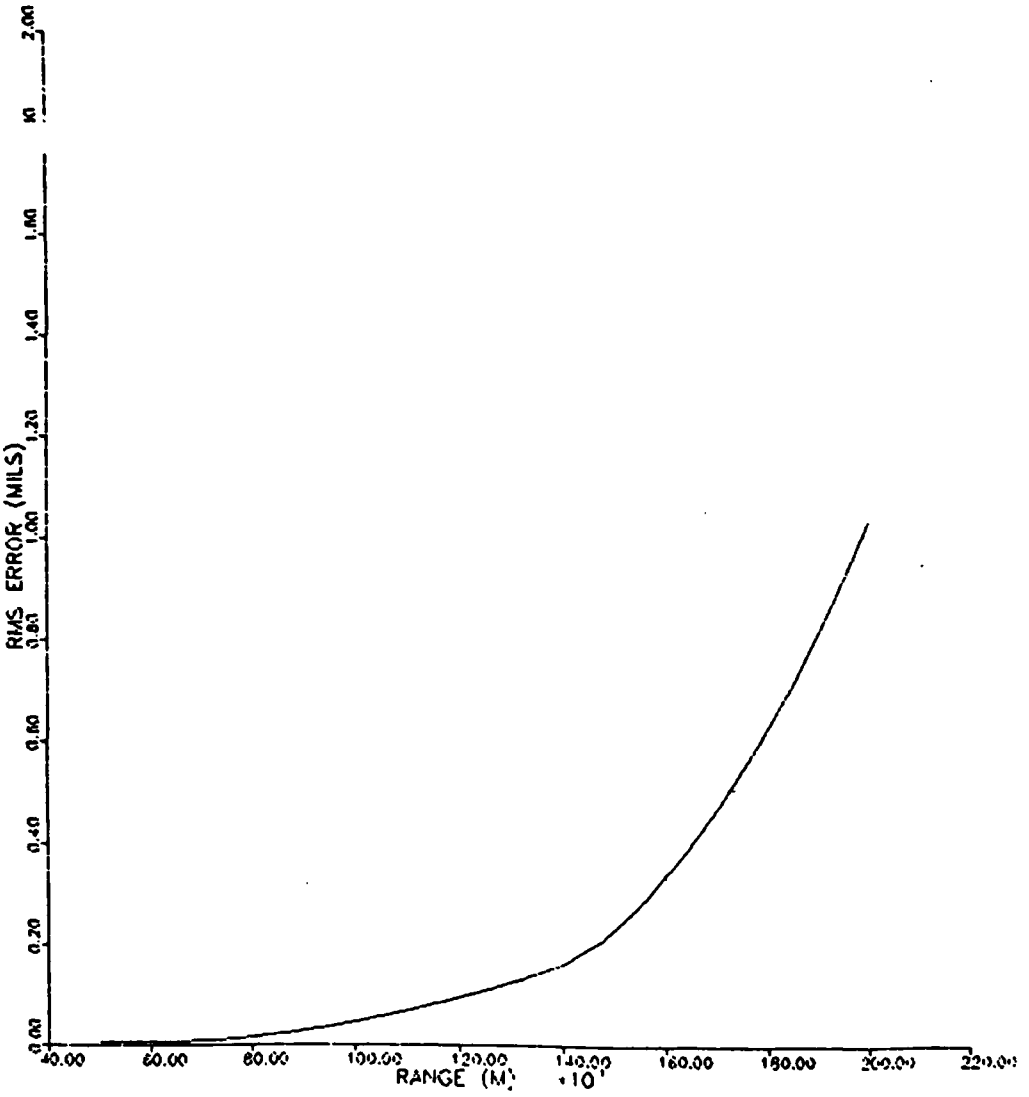

Figure 3-11. MIDI tracking error for 20 mm bullet scoring; X-band; 40 dB MTI improvement; 50 m target height.

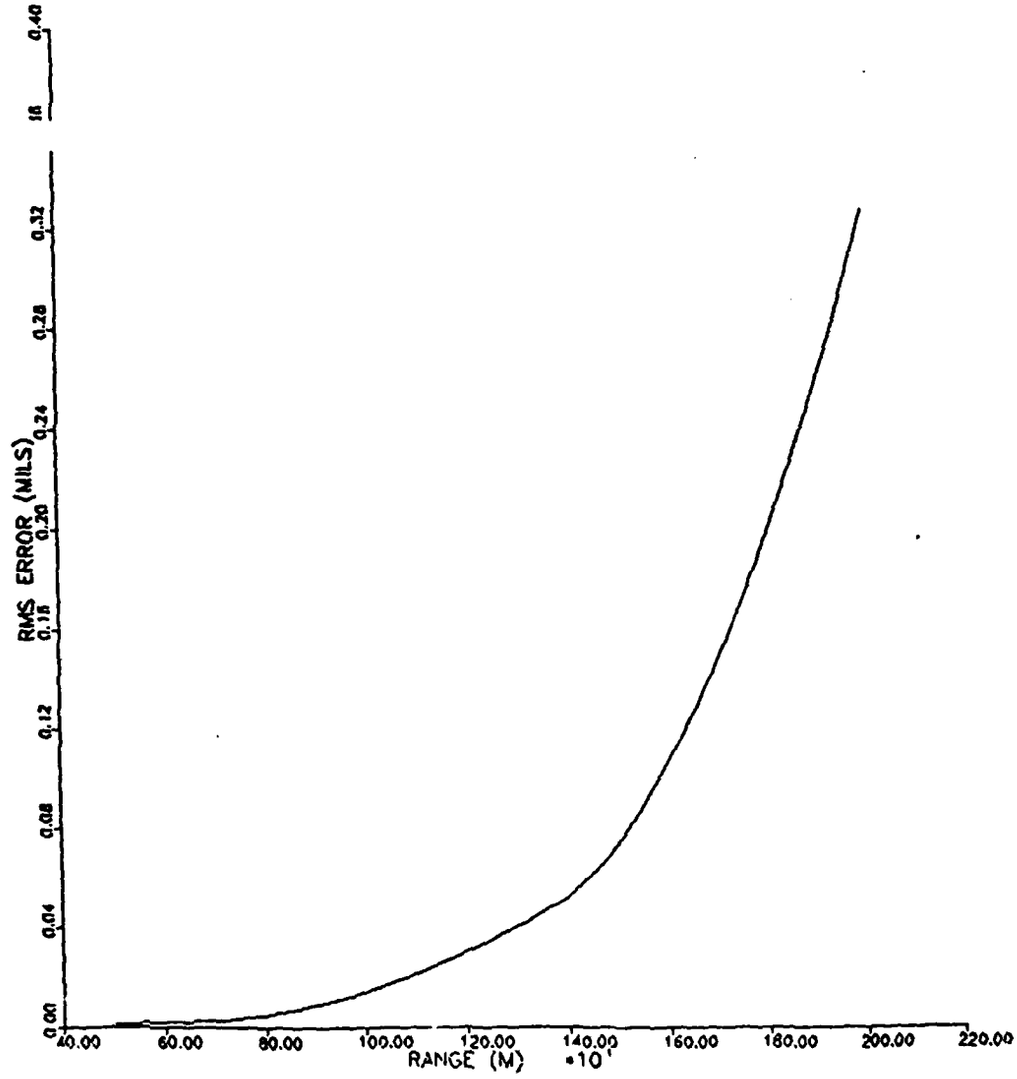

Figure 3-12. MIDI tracking error for 20 mm bullet scoring: X-band; 40 dB MTI improvement; 50 m target height.

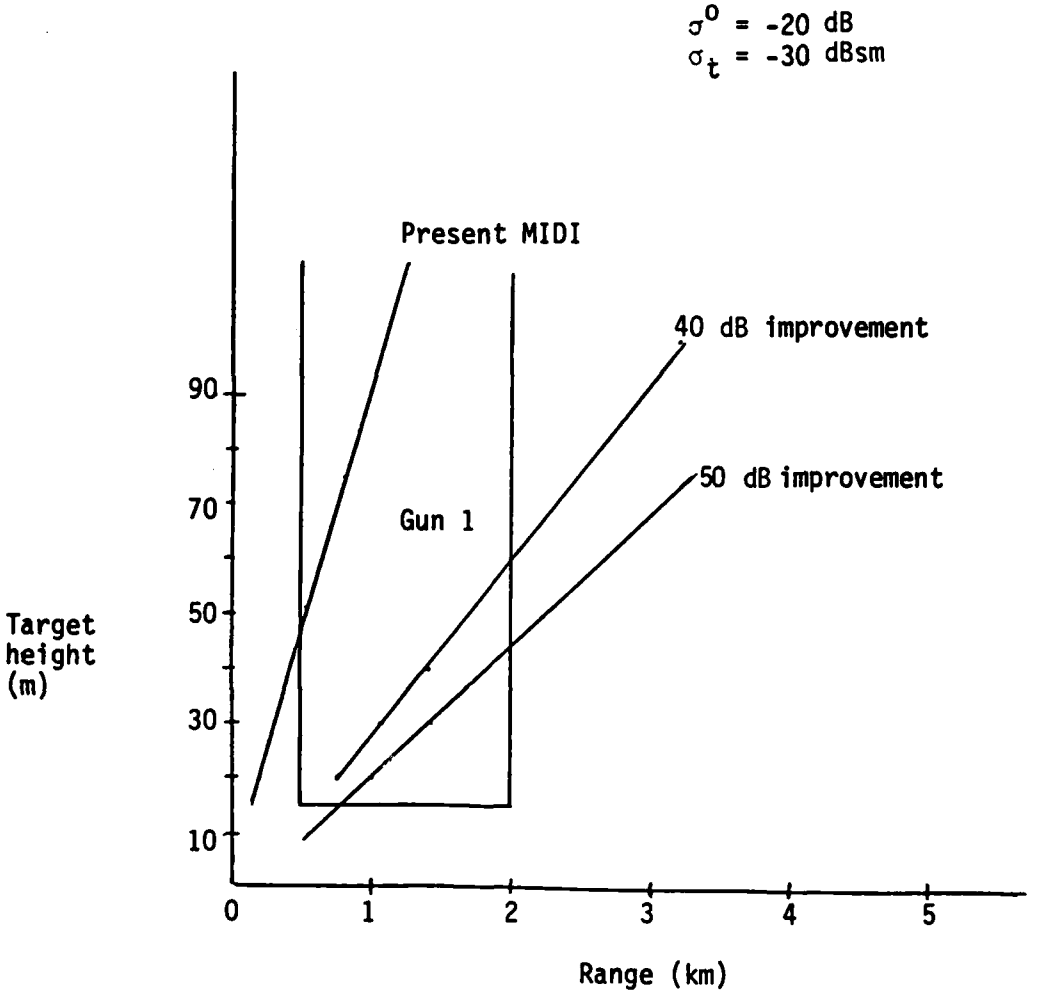

Figure 3-13. X-band MIDI 20 mm bullet scoring: X-band; 40 dB MTI improvement; 50 m target height.

TABLE 3-6. CLUTTER INTERFERENCE MODEL
TEST MATRIX

VARIABLE	VALUES
Projectile type/RCS (dBsm)	-30, -22, -5
Projectile scoring angle (BW)	.25, .5
Target Height (m)	15, 50, 150
Target Range (km)	.5 to 30
MTI Improvement Factor (dB)	40, 50
Clutter Reflectivity (dB)	-20

The computer model reproduced the angle error calculations discussed in Section 3.5.3. The program computations proceeded as follows:

1. Read in antenna pattern and compute MIDI calibration curves.
2. Read in user selected test variables (target RCS, height, etc.).
3. Select maximum range.
4. Compute projectile and clutter antenna gains.
5. Compute signal-to-clutter ratios after processing.
6. Compute tracking phase angle for projectile alone.
7. Compute tracking phase angle for projectile plus clutter for 200 samples of clutter-to-projectile phase angle.
8. Compute rms tracking error for uniform clutter-to-projectile phase distribution.
9. Output rms error.
10. Select new range and repeat steps 4 through 9.
11. Plot results.

The above procedure resulted in plots of rms tracking error as a function of range for a variety of targets and conditions. These results are discussed

A similar comparison was performed for the 40 mm projectile. Because of the increased bullet cross section, the scoring accuracy achievable at 2 km is much better than for the 20 mm projectile. The design goal for 40 mm projectile scoring, however, was a 15 m altitude target at 4 km. This corresponds to an elevation angle of 0.2^{o}. As can be seen in Figure 3-14, such low coverage is simply not possible with a 1.25^{o} beamwidth radar located behind the firing line. Some alternative solution must be considered for achieving these low altitude coverage regions.

The scoring performance analysis was not limited to projectile weapons but included a representative missile weapon as well. The very low angle coverage (0.17^{o}) required to score missiles at their performance limits necessitated a reduction in the antenna beamwidth. An X-band antenna large enough to produce a narrow enough beamwidth would be physically impractical. Consequently, the missile scoring performance analysis assumed a K_a-band MIDI system. A two meter antenna, such as in use in the present MIDI system, would have a K_a-band beamwidth of 0.35^{o}. This three-fold reduction in the beamwidth would allow considerably lower angle tracking coverage. The total rms error of 1 mil assumed in the previous analysis, however, is not sufficiently restrictive for 20 to 30 km ranges. At 20 km, a 1 mil error would be equivalent to 20 meters. This is insufficient accuracy for useful scoring information. For this reason, the missile analysis assumed an rms scoring error limit of 0.1 mil for clutter interference.

The results of the K_a-band MIDI missile scoring analysis are presented in Figure 3-15 superimposed over the desired missile coverage diagram. As with the projectile weapons, a second generation MIDI located behind the firing line cannot achieve the low angle missile coverage desired with the kind of accuracy needed for missile scoring. A 50 dB improvement, however, would allow accurate scoring for 100 meter altitude missile targets at 20 km. This is significantly better performance than could be achieved with the present MIDI system.

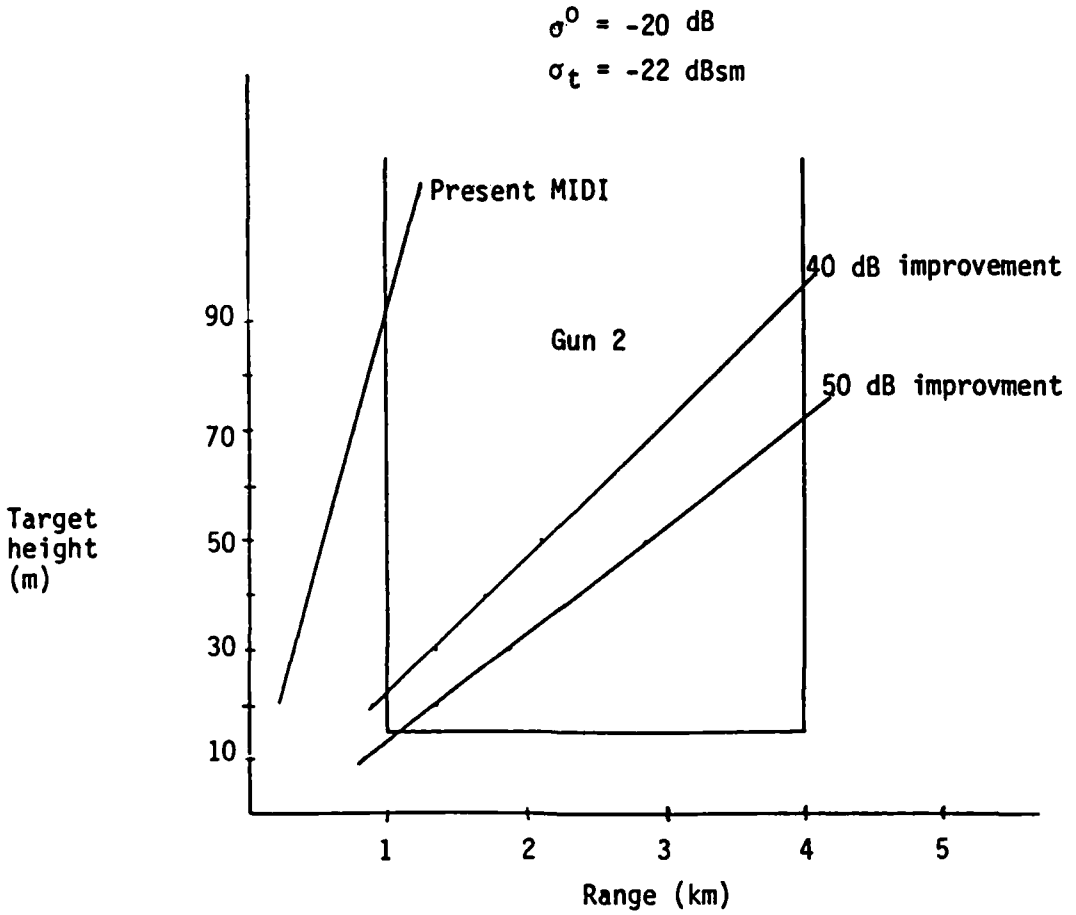

Figure 3-14. X-band MIDI 40 mm bullet scoring performance for a .5 mil rms error with and without MTI processing.

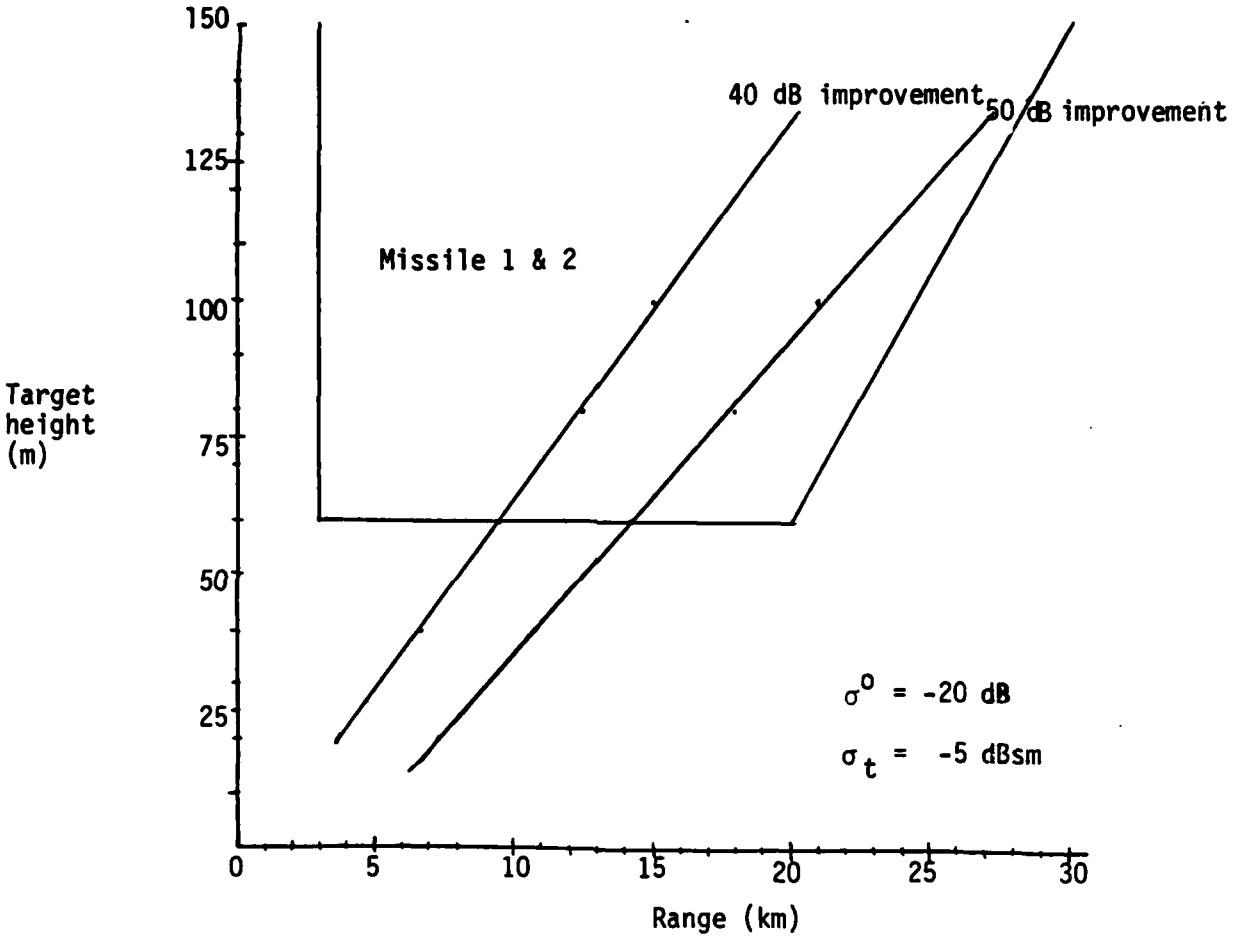

Figure 3-15. Ka-band MIDI missile scoring performance for a .1 mil rms error with and without MTI processing.

SECTION 4

MULTIPATH INTERFERENCE ANALYSIS

The primary tasks of the multipath interference analysis were:

1. Predict the MIDI scoring accuracy as a function of target altitude and range, antenna beamwidth, frequency, and terrain surface roughness (or more specifically, the ground reflection coefficient) and compare candidate radar mechanizations.

2. Determine the values of ground reflection coefficient which represent the terrain at Ft. Bliss and White Sands Missile Range. Analysis was started using values from 0.25 to 0.7. Subsequently, a computer program that models an area of the White Sands Missile Range predicted values from 0.25 to 0.67. Finally, a measured value of 0.35 was obtained during a limited test program at North McGregor Range.

3. Determine the correlation between errors in target tracking and errors in bullet miss distance measurement.

This section of the report describes the equations used, the computer programs that implement these equations, and the results.

4.1 CALCULATION OF ANGLE MEASUREMENT ACCURACY

The MIDI radar determines miss distance by tracking the gunnery target and performing off-boresight angle measurements of the projectiles at two ranges in the vicinity of the target.

The angle measurement errors due to multipath interference were calculated for two monopulse angle measurement methods, referred to as conventional monopulse and MIDI monopulse. The errors were calculated for two representations for interference -- a three dimensional model providing specular and diffuse reflections and a simple two dimensional specular reflection model. The angle measurement models and the two computer programs which implement the models are described herein.

4.1.1 ANGLE MEASUREMENT EQUATIONS

4.1.1.1 Conventional Monopulse The elevation sum (Σ) and elevation difference (Δ) patterns are inputs to this model. The off-boresight angle measurement calibration procedure consists of constructing a look-up table of Δ/Σ voltage ratios versus angle. The Δ/Σ ratios for angles below antenna boresight (negative angles) have a negative value. This represents an antenna which has been designed such that the response to a single signal in the Δ channel is either in phase or 180 degrees out of phase with the Σ response. If a second signal such as multipath interference is present, its Σ and Δ responses are in phase (or 180 degrees out of phase) with each other but may have any phase with respect to the first signal. Therefore, the vector sum of the Σ and Δ channels may have a quadrature component, as shown in Figure 4-1.

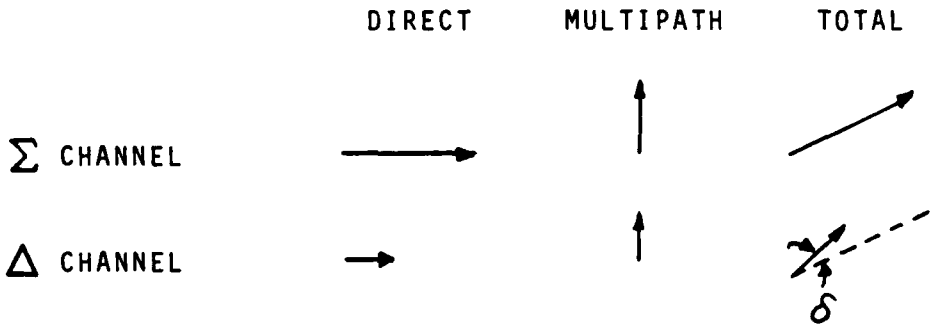

Figure 4-1. Vector relationships.

The phase sensitive detector used in some radars to perform the Δ/Σ ratio function and preserve the phase sense has the characteristic:

$$|\Delta/\Sigma| = \left|\frac{\Delta}{\Sigma}\right| \cos\delta \qquad 4.1$$

where δ = phase angle between Σ and Δ (ideally zero).

For a given target position, each signal, direct and reflected, is weighted by the antenna gain corresponding to its angle of arrival for both the Σ and Δ channels. Gain patterns from actual antennas and hypothetical shaped beams were used. These weighted signals within each channel are vectorially added to yield the total signal in that channel. Then $|\Delta/\Sigma|$ is computed using Equation 4.1 and the calibration look-up table is entered to determine the measured angle. The measurement error is the difference between the measured angle and the true angle. These error calculations are performed for a sequence of target positions along the flight path of the simulated firing mission.

The geometric definitions are shown in Figure 4-2. Note that the boresight of the antenna is maintained on the gunnery target. The angle measurement error is calculated for the object which is located at target altitude plus miss distance altitude. Setting miss distance equal to zero results in calculating the error corresponding to the target.

Three models were used to generate the input signals to the angle measurement process:

1. A three-dimensional facet model of the terrain at the White Sands Missile Range. The facet model is described in Appendix A.

2. A simplified two-dimensional specular reflection model of the radar two-way interference paths.

3. A two-dimensional specular reflection model of the beacon one-way interference path.

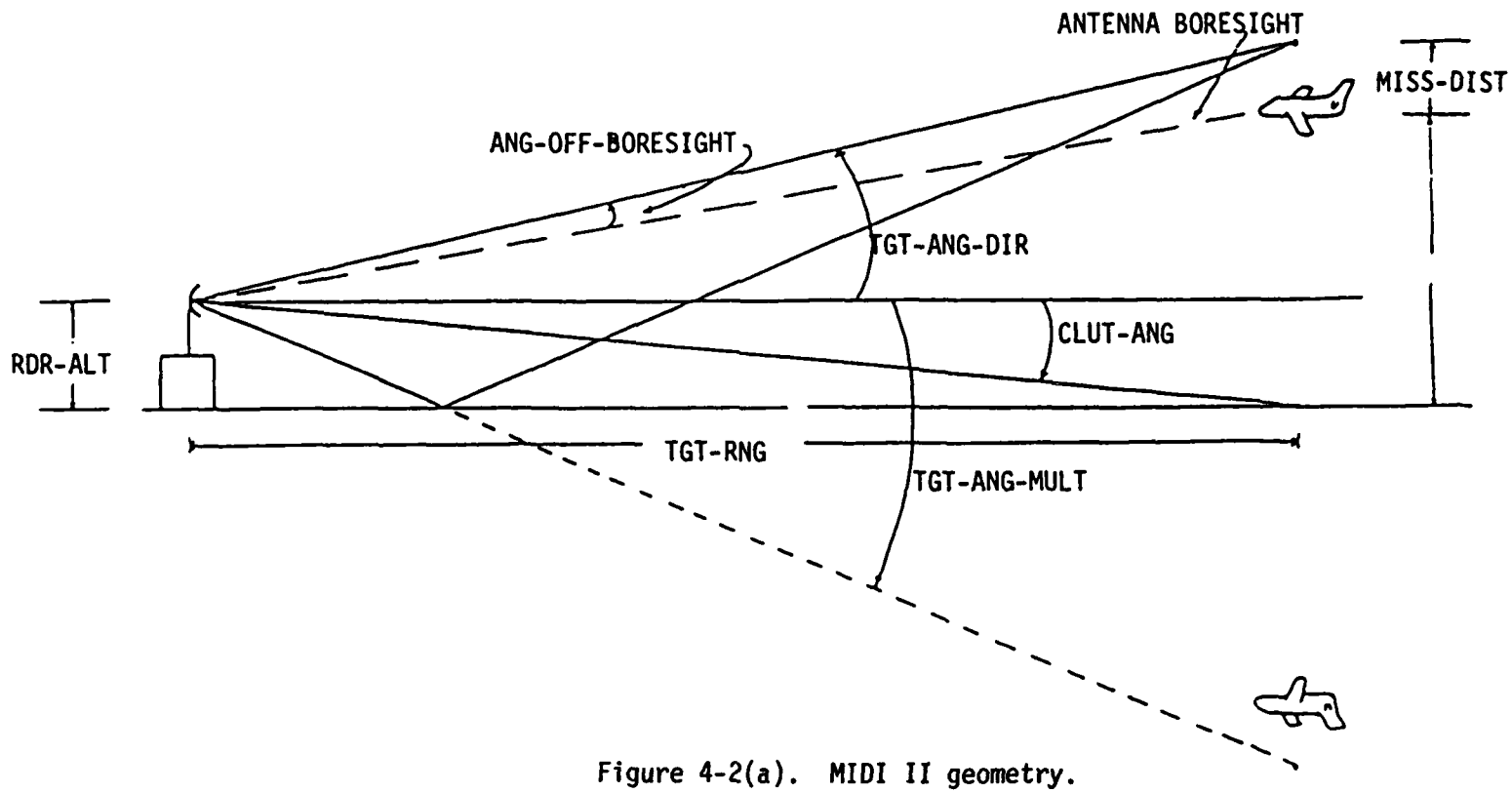

Figure 4-2(a). MIDI II geometry.

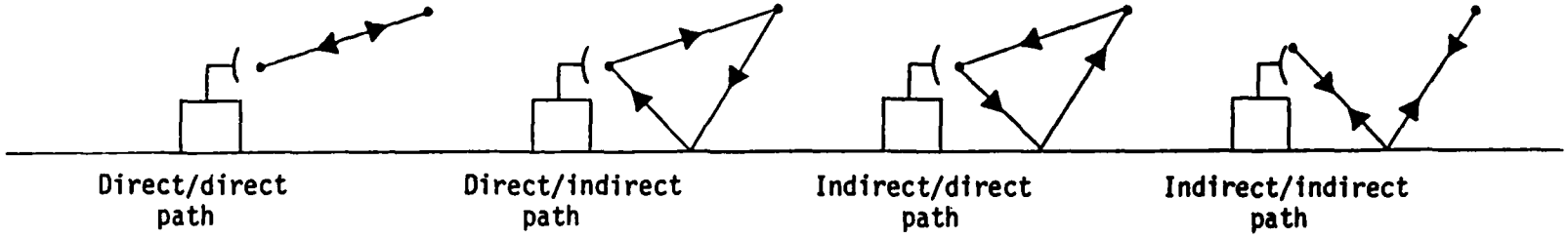

Figure 4-2(b). Multipath interference paths.

The signals for each of the radar (two-way) paths shown in Figure 4-2 are:

Path	Σ Channel	Δ Channel
Direct/Direct	$K\ G_{\Sigma}^{2}(T)$	$K\ G_{\Sigma}(T) \cdot G_{\Delta}(T)$
Direct/Indirect	$K\ G_{\Sigma}(T) \cdot G_{\Sigma}(M)\rho$	$K\ G_{\Sigma}(T) \cdot G_{\Delta}(M)\rho$
Indirect/Direct	$K\ G_{\Sigma}(M) \cdot G_{\Sigma}(T)\rho$	$K\ G_{\Sigma}(M) \cdot G_{\Delta}(T)\rho$
Indirect/Indirect	$K\ G_{\Sigma}(M)^{2}\ \rho^{2}$	$K\ G_{\Sigma}(M) \cdot G_{\Delta}(M)\ \rho^{2}$

For beacon tracking (one-way), the signals are:

Path	Σ Channel	Δ Channel
Direct	$K\ G_{\Sigma}(T)$	$K\ G_{\Delta}(T)$
Indirect	$K\ G_{\Sigma}(M)\ \rho$	$K\ G_{\Delta}(M)\ \rho$

where

- $G(\ )$ = Antenna gain as a function of angle off boresight
- T = Target angle off boresight
- M = Multipath interference angle off boresight
- ρ = Reflection coefficient
- K = Constant from the radar range equation
- Σ = Subscript denoting sum pattern
- Δ = Subscript denoting difference pattern

The magnitude of the voltage reflection coefficient is an input parameter to the computer programs which calculate the angular error. Another input is

the phase angle of the reflection, relative to the direct path, and represents the sum of the phase effects from path length difference and a complex reflection coefficient.

The quadrature component is also computed to determine its usefulness as a measurement quality indicator using:

$$QUAD = 10 \log_{10}\left(\left|\frac{\Delta}{\Sigma}\right| \sin \delta\right)^2 \qquad 4.2$$

The presence of a quadrature component indicates multipath interference; however, relative phase angles of 0 or 180 degrees between the direct and interfering signal produce no quadrature component but can result in significant angle errors. The simple specular reflection model exhibits deep nulls in the quadrature component; therefore, the quadrature component would not be a reliable track quality indicator if the surface is a smooth plane, e.g., a lake. The terrain of the test range, however, generally appears rough at microwave frequencies, thus giving rise to diffuse reflections. The returns from the individual facets have different amplitudes and phases. The vector sum of these returns does not exhibit deep nulls. Therefore, in the overland application of MIDI, the presence of a quadrature component may be a valuable track quality indicator.

4.1.1.2 MIDI Angle Measurement

In the current MIDI radar, a microwave network converts the basic Σ and Δ channels into $\left(\frac{\Sigma}{2} + j\frac{\Delta}{\sqrt{2}}\right)$ and $\left(\frac{\Sigma}{2} - j\frac{\Delta}{\sqrt{2}}\right)$channels (see Figure 4-3). The radar measures the phase angle, ϕ between the two channels. The off-boresight calibration procedure consists of constructing a look-up table of ϕ versus angle. For a single input signal as used in calibration, ϕ is computed from:

$$\phi(\Sigma)\ 2 \arctan\left(\sqrt{2}\ \Delta(\varepsilon)/\Sigma(\varepsilon)\right), \qquad 4.3$$

where

$\Delta(\varepsilon)$ = voltage gain of elevation difference pattern at angle ε,

$\Sigma(\varepsilon)$ = voltage gain of sum pattern at angle ε ,

and ε = elevation angle.

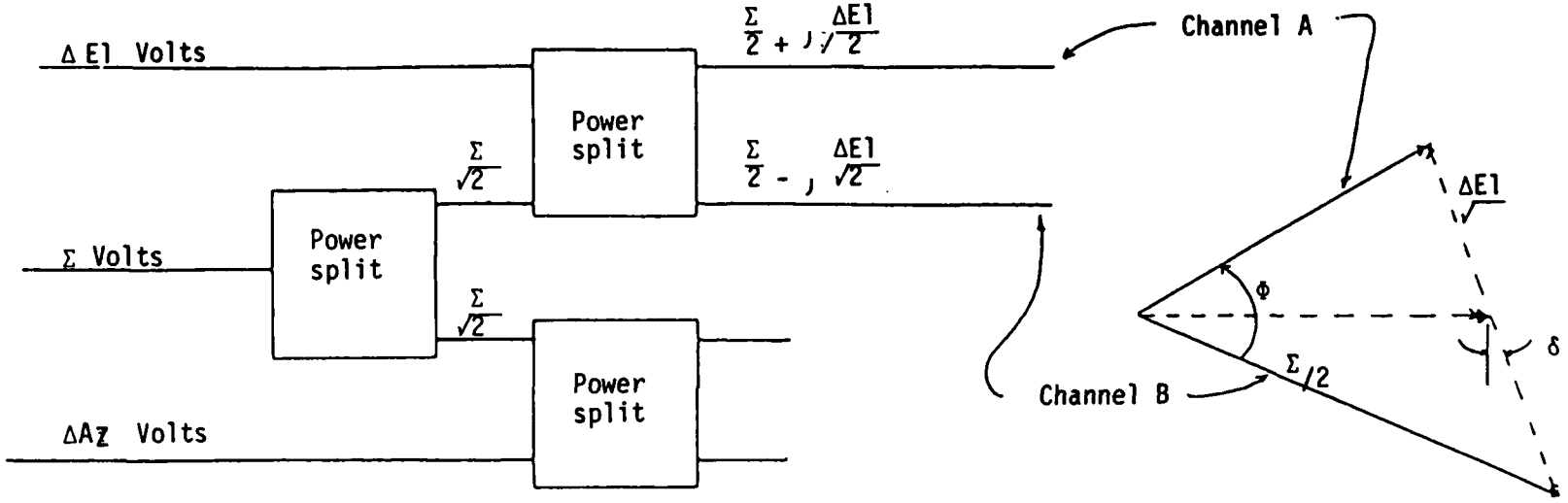

Figure 4-3. MIDI processing.

The vector sum of all received signals in the Σ and Δ channels is used in the MIDI angle measurement. Two channels are formed:

$$A = \frac{\Sigma}{2} + j\frac{\Delta}{\sqrt{2}} \qquad 4.4$$

and

$$B = \frac{\Sigma}{2} - j\frac{\Delta}{\sqrt{2}} . \qquad 4.5$$

Both Σ and Δ are complex voltages and are not generally in phase. The phase angle ϕ between A and B is calculated from:

$$\phi = -\arccos\left(\frac{AB^*}{|A|\,|B|}\right) , \qquad 4.6$$

where B^* = complex conjugate of B.

The calibration look-up table is used to transform ϕ into the measured angle. The measurement error is the difference between the measured angle and the true angle.

4.1.2 COMPUTER PROGRAM "COMPARE"

4.1.2.1 Program Summary

The program environment is shown in Figure 4-4. The input file structure is shown in Figure 4-5. This structure which has been used on several other MIDI computer programs.

The program performs the following operations:

1. Reads in the antenna patterns and calculates the conventional monopulse and MIDI calibration curves.
2. Generates the direct target-to-radar signal and specular reflection signals.
3. Weights each signal by the antenna gain corresponding to its arrival angle.
4. Computes the angle measured by both conventional monopulse and MIDI processing and the measurement errors.
5. Calculates the quadrature component.

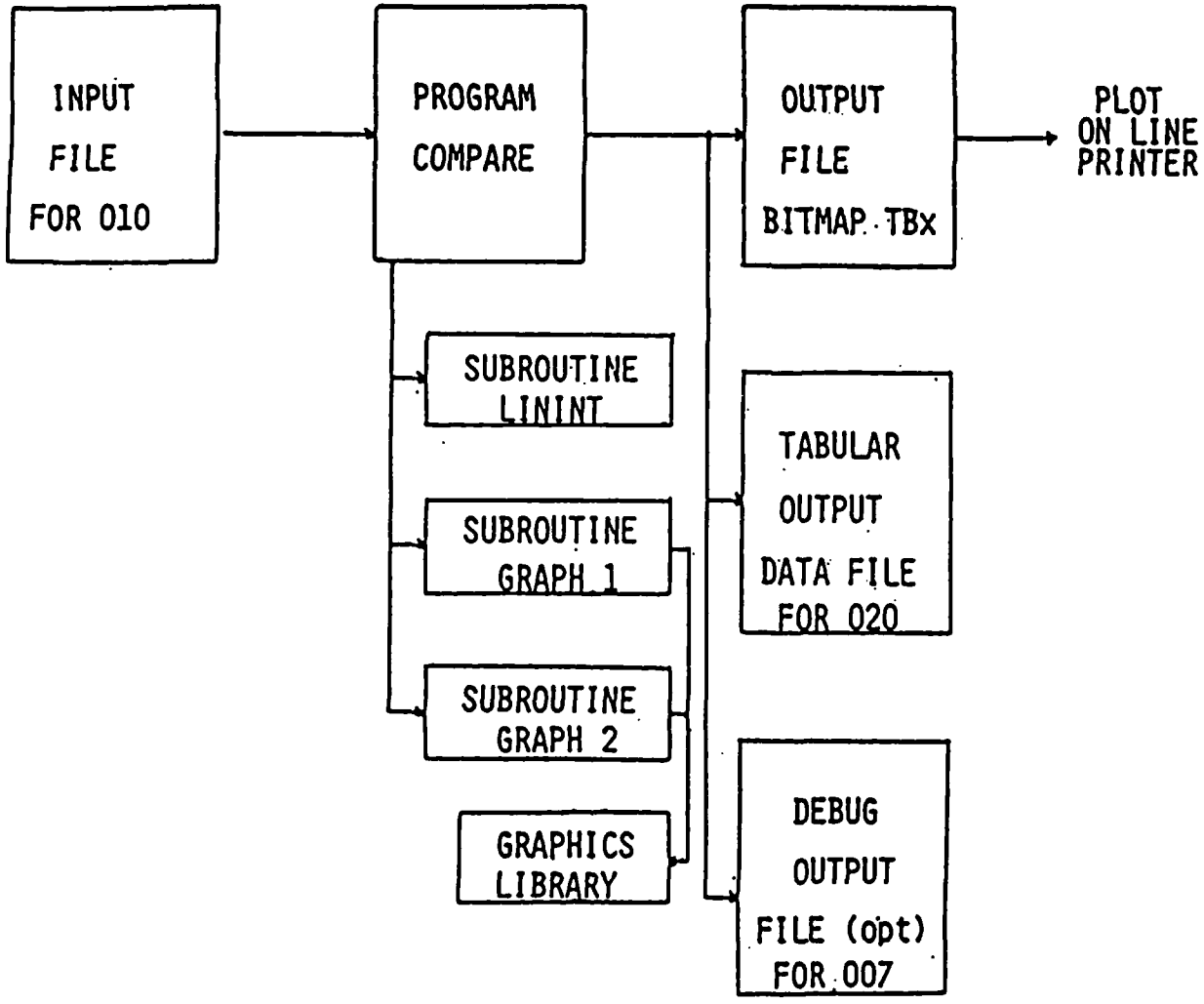

Figure 4-4. Program "COMPARE" environment.

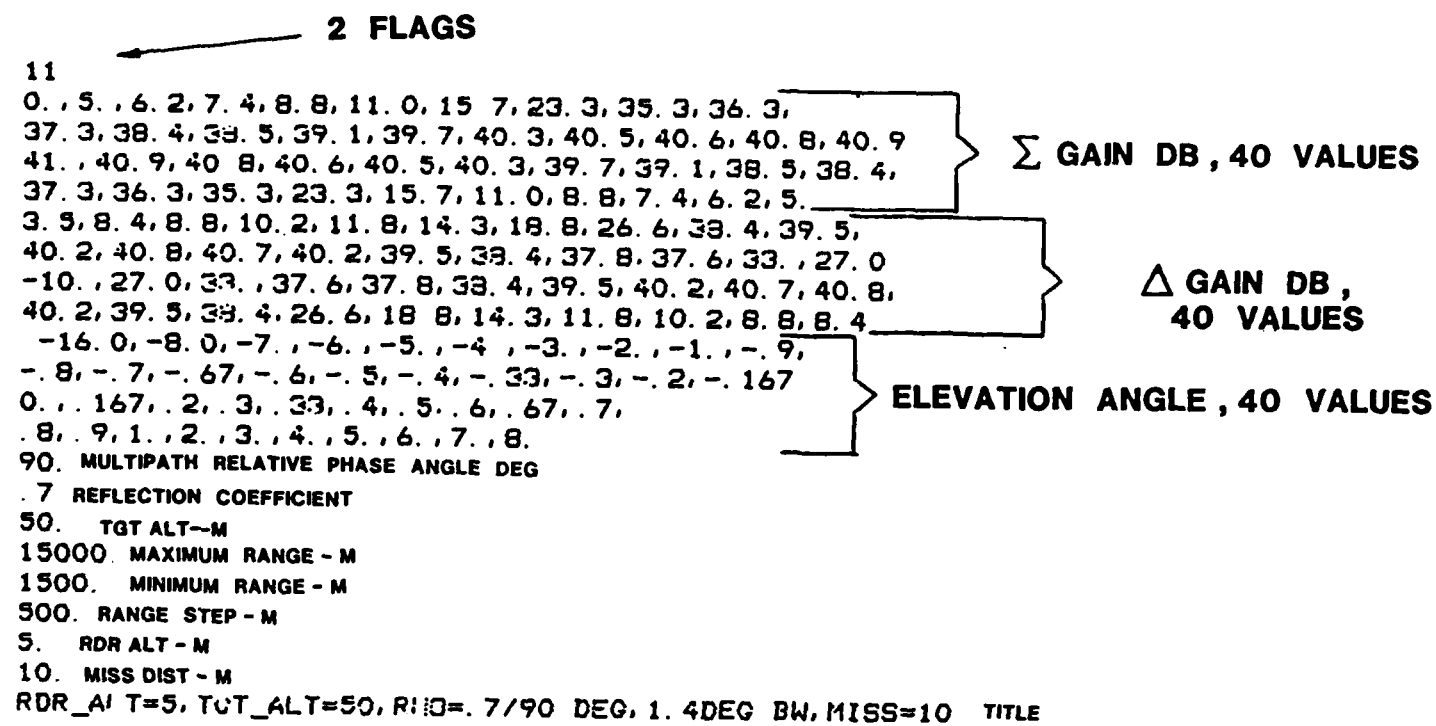

Figure 4-5. Input file FOR010 structure.

6. Repeats steps 2 through 5 for each target range.
7. Creates an output file containing plots of measurement error and quadrature component versus range.

The program was written in FORTRAN and was installed on the VAX-11/780 computer at the Georgia Tech Research Facility, Cobb County. The output file containing the graphs was labeled BITMAP.TBX. Figures 4-6 and 4-7 are representative plots. Tabular data were also output to files FOR007 and FOR020.

4.1.2.2 Program Description

Program listings are included in Appendix C. "COMPARE" models the one-way interference. "COMPARE 2" is identical except the two-way equations are used. Each program is separated by comments into the following sections:

Declarations
Internal Data
Input
Conversions, etc.
Monopulse Calibration Curve
MIDI Calibration Curve
Calculation Do Loop
    Generation of Direct and Reflected Signals
    Monopulse Measurement
    MIDI Measurement
Plot Results

The listing is largely self-explanatory, but some further comments are appropriate.

Internal Data - Contains four complex unit vectors which are used to convert real numbers into complex numbers.

Input - The first line contains two integers. Setting the first equal to "1" causes graphs to be generated. A zero supresses the plot. Setting the second to "1" causes debug data to be read to an output file.

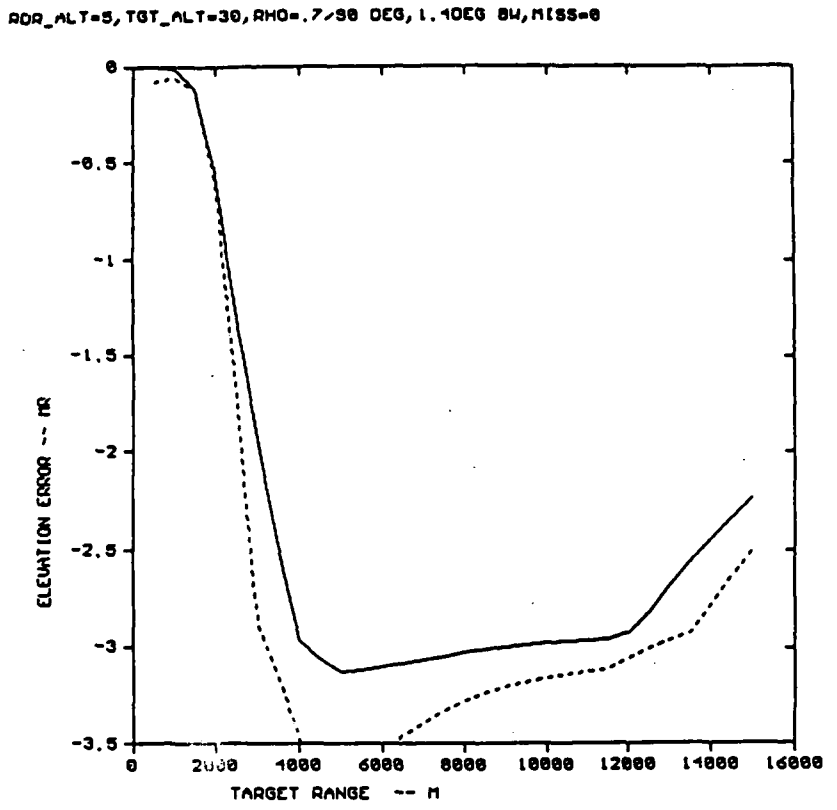

Figure 4-6. Error versus range.

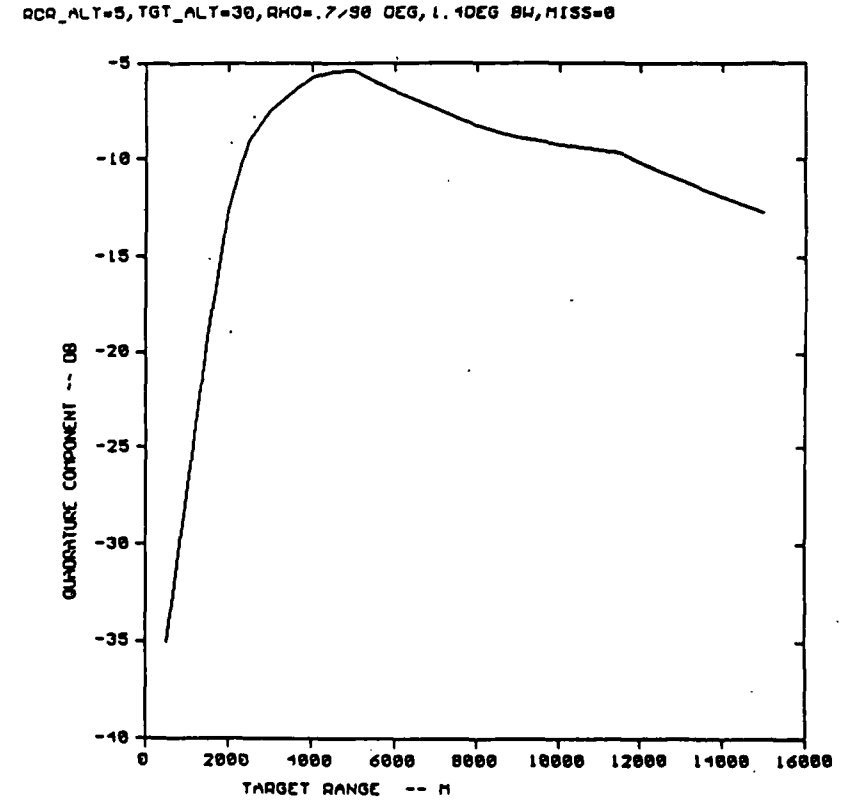

Figure 4-7. Quadrature component versus range.

Conversions - Within the program, most angles are expressed in milliradians and signals are expressed in volts.

Monopulse Calibration Curve - At large angles off boresight, the calculated $|\Delta/\Sigma|$ ratio decreases. Two values of angle produce the same $|\Delta/\Sigma|$ ratio. The program artifically resolves this ambiguity by altering the Δ/Σ versus angle characteristic to be monotonic. The program outputs a warning message and proceeds. Obviously in running specific cases, the miss distances and ranges must be chosen so that off boresight scoring is not attempted in this falsely calibrated region.

Calculation Do Loop - The antenna gain at each angle is computed by a call to subroutine LININT which performs a linear interpolation using the gain versus angle look-up table.

Internal subroutine ROTATE performs a phase rotation of a complex number.

Plot Results - The subroutine call to GRAPH1 creates output file BITMAP.TBX containing the plots, automatically scales the X and Y axes, and adds the X axis label, Y axis label, and title. The call to GRAPH2 adds the second plot on the same axes. GRAPH1 and GRAPH2 call several subroutines from the Graphics Library of the VAX.

4.1.3 COMPUTER PROGRAM "MULTIDATA"

4.1.3.1 Program Summary

This program is identical to COMPARE with one exception. Instead of a simple internal specular model, it uses an additional input file (FOR030) containing signal voltages from each of the ground facets computed by the three-dimensional multipath model. The program environment is shown in Figure 4-8, and the structure of input file FOR030 is shown in Figure 4-9.

The input file contains the "direct/direct" signal corresponding to the path from the radar to the target and back to the radar. The next input data point is the signal from the specular reflection facet. The mean and standard deviation of the return from each facet computed for a number of pulses, typically 200, are available within the file. The square of the standard deviation represents the average power received from that ground facet for the number of pulses.

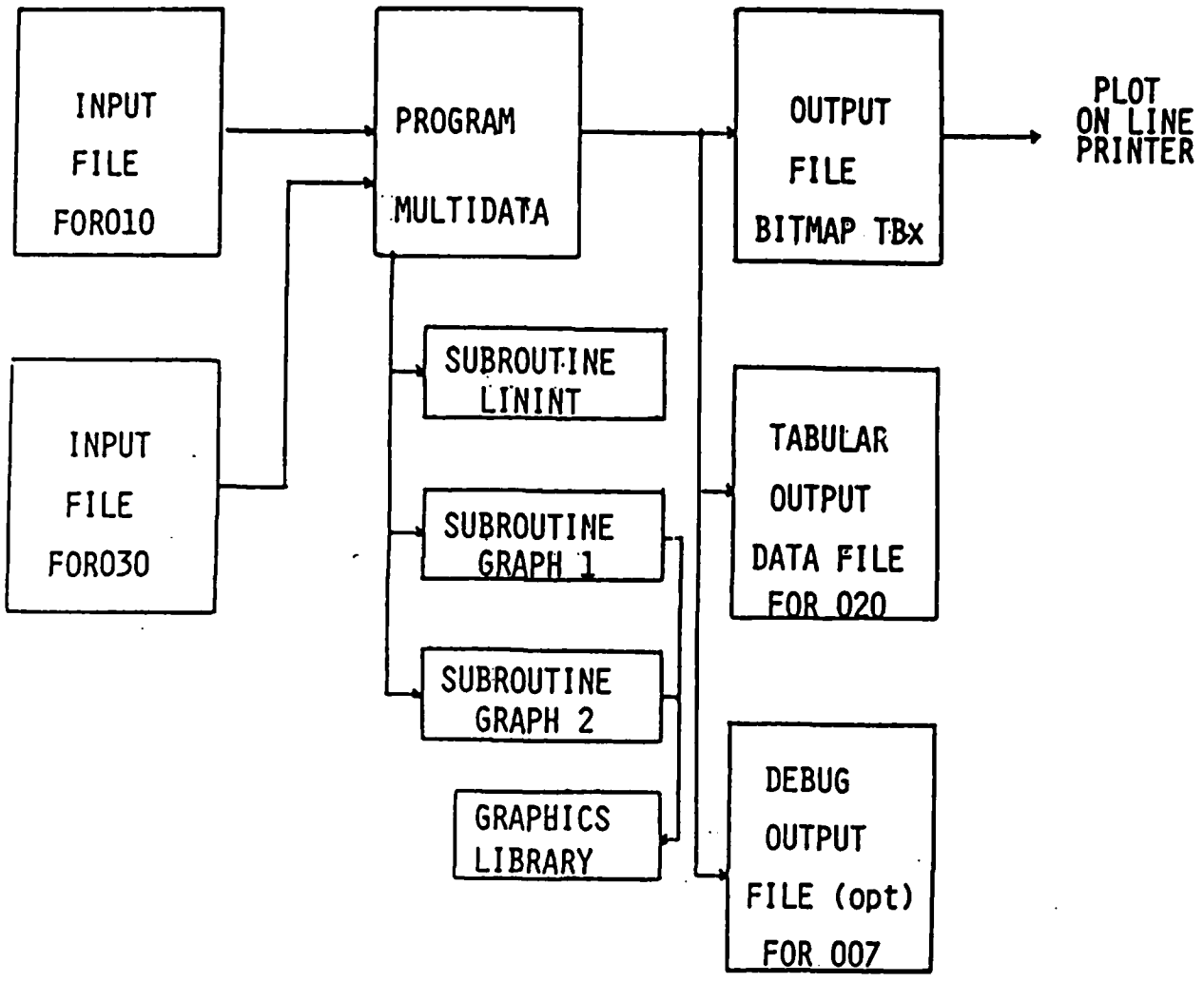

Figure 4-8. Program "MULTIDATA" environment.

```
  1000.000          3900.000          225.3000          0.0000000E+00     100.0000   } TARGET X,Y,Z,V_X,V_Y,
 0.0000000E+00                                                                        V_Z
  6.0E-6  <-------- DIRECT RETURN
  332.6002          3.0371454E-02                                                   } SPECULAR RETURN RNG,EL_ANGLE
(-1.2998741E-07, 2.9532708E-07) (-3.4758407E-09,-3.7949590E-09)                     }                 DI,II
       741  <-------- NFACETS
  1044.054         -3.4667987E-02 -3.0493166E-03                                    } DIFFUSE RETURN
(3.9250728E-10, 1.9516180E-10) (1.8280946E-11, 5.8238654E-09)                       }    RNG,EL_ANGLE,AZ_ANGLE
(1.7126392E-13, 9.2083144E-13) (3.7475955E-12, 6.2411127E-12)                       }    DIFFUSE_MEAN_DI,SD_DI
  1061.653         -3.4507692E-02 -3.0099689E-03                                    }    DIFFUSE_MEAN_II,SD_II
(-7.0280381E-10,-4.3323606E-10) (1.2223816E-09,-5.4824660E-09)
(-2.1783134E-12, 2.8590598E-12) (6.2073857E-12, 4.8122691E-12)
  1079.252         -3.4353598E-02 -2.9700999E-03                                    FOR EACH OF NFACETS
(6.3398053E-10,-1.4765533E-09) (6.0655747E-09,-6.5654338E-10)
(-4.5126500E-13,-5.2324670E-13) (6.3013718E-12, 5.9633331E-13)
  1096.851         -3.4204017E-02 -2.9092724E-03
(6.6565322E-09, 1.6595751E-08) (4.9751616E-08,-5.3496869E-08)
(1.9090717E-10, 1.3304087E-11) (1.1078493E-10, 3.7351108E-10)
  1114.450         -3.4057297E-02 -2.8471455E-03
(-1.6839763E-08, 9.6656638E-10) (4.3612104E-08, 2.9422402E-08)
(1.0980342E-10, 3.8875354E-11) (2.0828834E-10, 4.8776233E-10)
  1132.050         -3.3916965E-02 -2.8261330E-03
(-9.4433181E-09,-9.7750510E-09) (1.3362862E-08,-3.2876212E-08)
(-2.2979452E-10,-3.7313156E-11) (6.3620925E-10,-2.4570029E-10)
  1149.649         -3.3781353E-02 -2.8049629E-03
(4.0865120E-09,-1.5849535E-08) (7.5033697E-08, 3.7175440E-08)
(1.5384258E-10,-1.8461771E-10) (2.8993127E-10,-6.8048989E-10)
  1167.248         -3.3646964E-02 -2.7404726E-03
(4.1026810E-09, 2.6947133E-09) (5.6478225E-08, 1.1101386E-08)
(-1.8868242E-11,-1.2876504E-10) (1.5063356E-10,-7.1571427E-10)
```

•
•
•

Figure 4-9
Input File FOR030 Structure

1 ← FLAG INDICATING DATA FOR ANOTHER TARGET POSITION FOLLOWS

The diffuse returns from each facet are computed by the multipath model for the following signal paths:

1. Direct/indirect - The path from the radar to the target to the ground and back to the radar.
2. Indirect/direct - The path from the radar to the ground to the target and back to the radar.
3. Indirect/indirect - The path from the radar to the ground to the target and back to the ground and finally to the radar.

The signals of (1) and (2) above are equal and are added together within the multipath model program. Program MULTIDATA separates the two components so that they may weighted by the antenna gains.

Program MULTIDATA uses the direct signal and the standard deviations from each facet to calculate the total signal in both the Σ and Δ channels. Each signal generated by the three-dimensional multipath model is weighted by the antenna gain corresponding to its angle of arrival. The weightings used are:

Path	Σ Channel	Δ Channel
Direct/Direct	$G_\Sigma^2(T)$	$G_\Sigma(T) \cdot G_\Delta(T)$
Direct/Indirect	$G_\Sigma(T) \cdot G_\Sigma(M)$	$G_\Sigma(T) \cdot G_\Delta(M)$
Indirect/Indirect	$G_\Sigma(M) \cdot G_\Sigma(T)$	$G_\Sigma(M) \cdot G_\Delta(T)$
Indirect/Indirect	$G_\Sigma^2(M)$	$G_\Sigma(M) \cdot G_\Delta(M)$

$G(\theta)$ is the antenna gain as a function of angle off boresight and

Σ = subscript denoting sum pattern
Δ = subscript denoting difference pattern
T = target angle off boresight, and
M = multipath interference angle off boresight.

The total signals in each channel are used in exactly the same way as described for computer program COMPARE.

4.1.3.2 Program Description

A program listing is included in Appendix C. The program is separated by comments into the following sections;

Declarations
Internal Data
Input from Antenna Pattern File
Conversions, etc.
Monopulse Calibration Curve
MIDI Calibration Curve
Interative Calculation Loop
  Vector Summation of Returns from Facets
  Monopulse Measurement
  MIDI Measurement
Plots Results

The listing for MULTIDATA is very similar to that for COMPARE, and the same program description information presented in Section 4.1.2.2 is also applicable to MULTIDATA. The iterative calculation loop of MULTIDATA is controlled by a flag following the set of data for a given target position as shown in Figure 4-9. Therefore, the program can accept a variable number of target positions during a scenario and non-uniform steps in position between data points.

4.1.4 SUMMARY OF RESULTS

X-Band

Elevation error versus target range plots were produced for each of the cases shown in Tables 4-1, 4-2, and 4-3. The plots are included as Appendix B. As the target range decreases, the antenna elevation angle increases, and the gain in the direction of the multipath interference decreases. The target ranges at which the angle measurement errors decrease below a threshold value, e.g., 0.5 milliradians, were read from the plots and are shown in the tables.

The antenna pattern used in the calculation of the data in Table 4-1 is shown in Figures 4-10 and 4-11. The envelope of the antenna sidelobe structure was used rather than the detailed sidelobe structure. The sum pattern sidelobes are down 30 dB at angles greater than 3 times the beamwidth from boresight. This antenna pattern approximates the pattern of the current MIDI 6 foot diameter X-band antenna.

The error data from Table 4-1 are plotted in Figure 4-12. The errors due to multipath interference are less than 0.5 milliradian (approximately 0.03 beamwidths) at elevation angles greater than 15 milliradians (0.7 beamwidths). At an elevation angle of 12 milliradians, the errors are approximately 1 milliradian.

The results in Table 4-2 were computed using the antenna pattern shown in Figure 4-13. The difference pattern is shifted upward in elevation 0.33 degree, and the peak gain is reduced by 2.5 dB. The sum pattern remains the same as the one shown in Figure 4-11. Offset tracking is used. The target is tracked using a bias added into the monopulse error signal so that the boresight (point of maximum sum pattern gain) is pointed at the target. The errors of Table 4-2 are plotted with the corresponding non-squinted cases in Figure 4-14. The 0.33 degree (6 milliradian) upward squint permits the antenna boresight to be lowered by 5 milliradians.

The technique of offset tracking using a normal, non-squinted pattern was also investigated. The results are summarized in Figure 14-15. The minimum elevation angle is comparable to that achieved with the squinted pattern.

TABLE 4-1. 1.3 DEGREE (22 MILLIRADIAN) BEAMWIDTH CASES

CASE	RADAR ALTITUDE m	RHO MAG/PHASE (DEG)	TARGET ALTITUDE m	MISS m	MAXIMUM (m) RANGE FOR ERROR <1 mrad	<0.5 mrad
1	5	0.7/90	15	0	1250	1000
2	5	0.7/90	15	-5	2000	1300
3	5	0.7/90	15	+5	1500	1500
4	5	0.7/90	20	-5	1420	1170
5	5	0.7/90	20	0	1470	-
6	5	0.7/90	50	-10	4240	3710
7	5	0.7/90	50	10	4000	3500
8	5	0.7/90	50	15	5000	4800
9	5	0.7/90	50	-15	5200	3050
10	5	0.7/90	50	0	3910	3410
11	5	0.7/135	15	0	<1000	<1000
12	5	0.7/0	15	0	<1000	<1000
13	5	0.7/180	15	0	<1000	<1000
14	5	0.7/90	60	-10	≈ 5000	4000
15	5	0.25/90	15	0	All ranges	2000
16	5	0.7/90	70	-20	7240	4290
17	5	0.7/90	30	0	2300	1900
18	5	0.7/90	35	0	2750	2200
19	5	0.7/90	35	-5	2600	2300
20	15	0.7/90	50	0	4350	3760
21	15	0.7/90	50	10	4000	3500
22	15	0.7/90	50	-10	4240	3700
23	5	0.7/90	50	-20	3390	3200
31	5	0.7/90	15	0	1200	960
32	5	0.7/90	50	0	3780	3260
33	5	0.7/90	50	-10	4700	3850
34	5	0.7/90	50	10	4000	3480

TABLE 4-2. 1.3 DEGREE (22 MILLIRADIAN) BEAMWIDTH CASES, 0.33 DEGREE SQUINT

CASE	RDR ALT m	RHO MAG/PHASE (DEG)	TGT. ALT m	MISS m	MAX RANGE (m) FOR ERROR <1 mrad	<0.5 mrad
50	5	0.7/90	15	0	2000	<1000
51	5	0.7/90	15	-5	2000	1600
52	5	0.7/90	20	-5	3000	1900
53	5	0.7/90	30	0	4000	3000
54	5	0.7/90	30	-5	4400	2900
55	5	0.7/90	35	-5	5100	3300
56	5	0.7/90	60	-10	8900	5700
57	5	0.7/90	50	0	6900	4400
58	5	0.7/90	50	-15	8000	4600

TABLE 4-3. 0.4 DEGREE (6 MILLIRADIAN) BEAMWIDTH CASES

CASE	RDR ALT m	RHO MAG/PHASE (DEG)	TGT. ALT m	MISS m	MAX RANGE (m) FOR ERROR <0.5 mrad	<0.2mrad	<0.1 mrad
1	5	0.7/90	15	0	6000	4400	3900
2	5	0.7/90	20	0	8300	5600	5000
3	5	0.7/90	30	0	12500	8700	7600
4	5	0.7/90	50	0	20400	14300	12600
5	5	0.7/90	60	0	24000	17200	15000

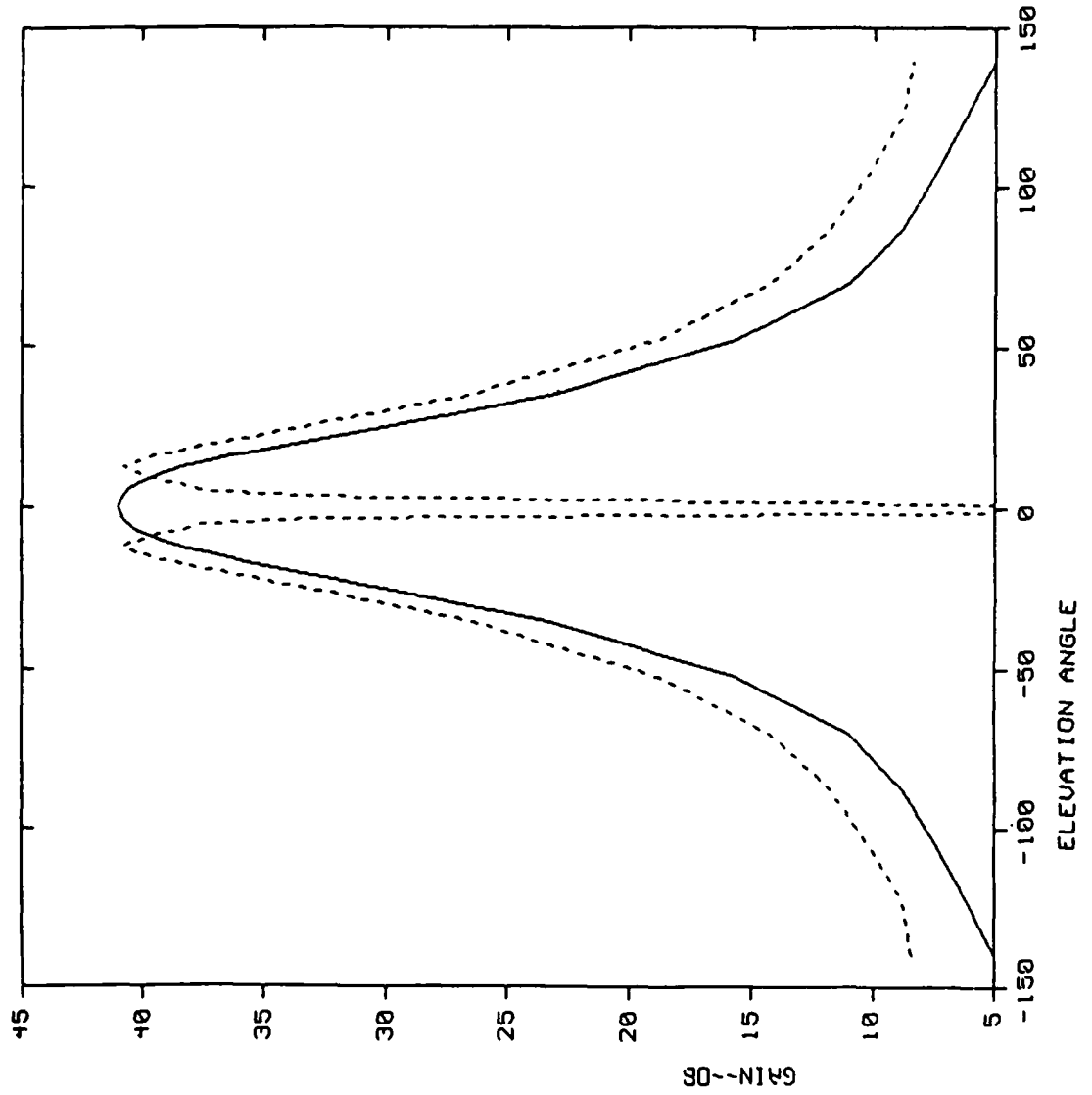

Figure 4-10. 1.3 Degree Beamwidth Antenna Pattern.

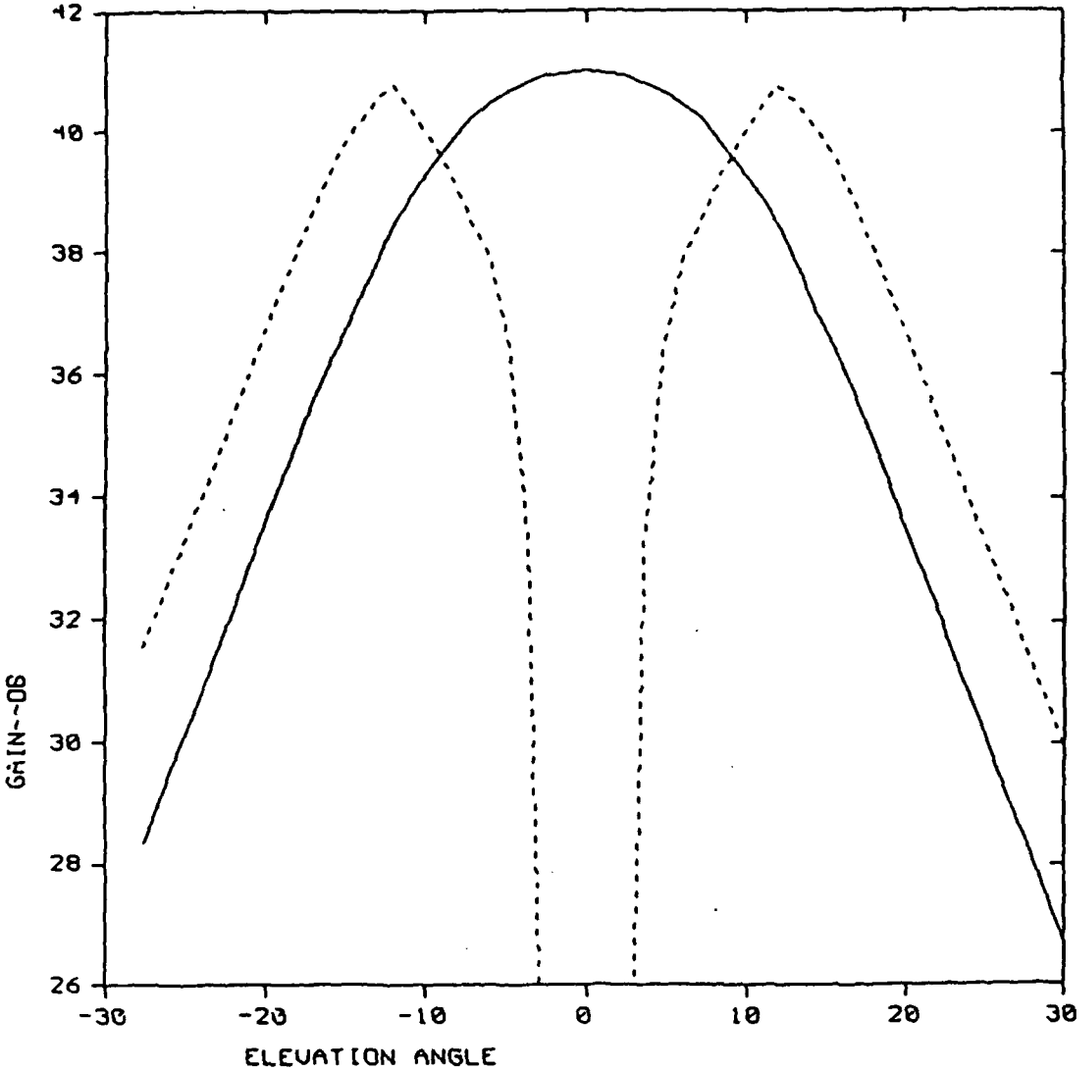

Figure 4-11. 1.3 Degree Beamwidth Antenna Pattern, Expanded.

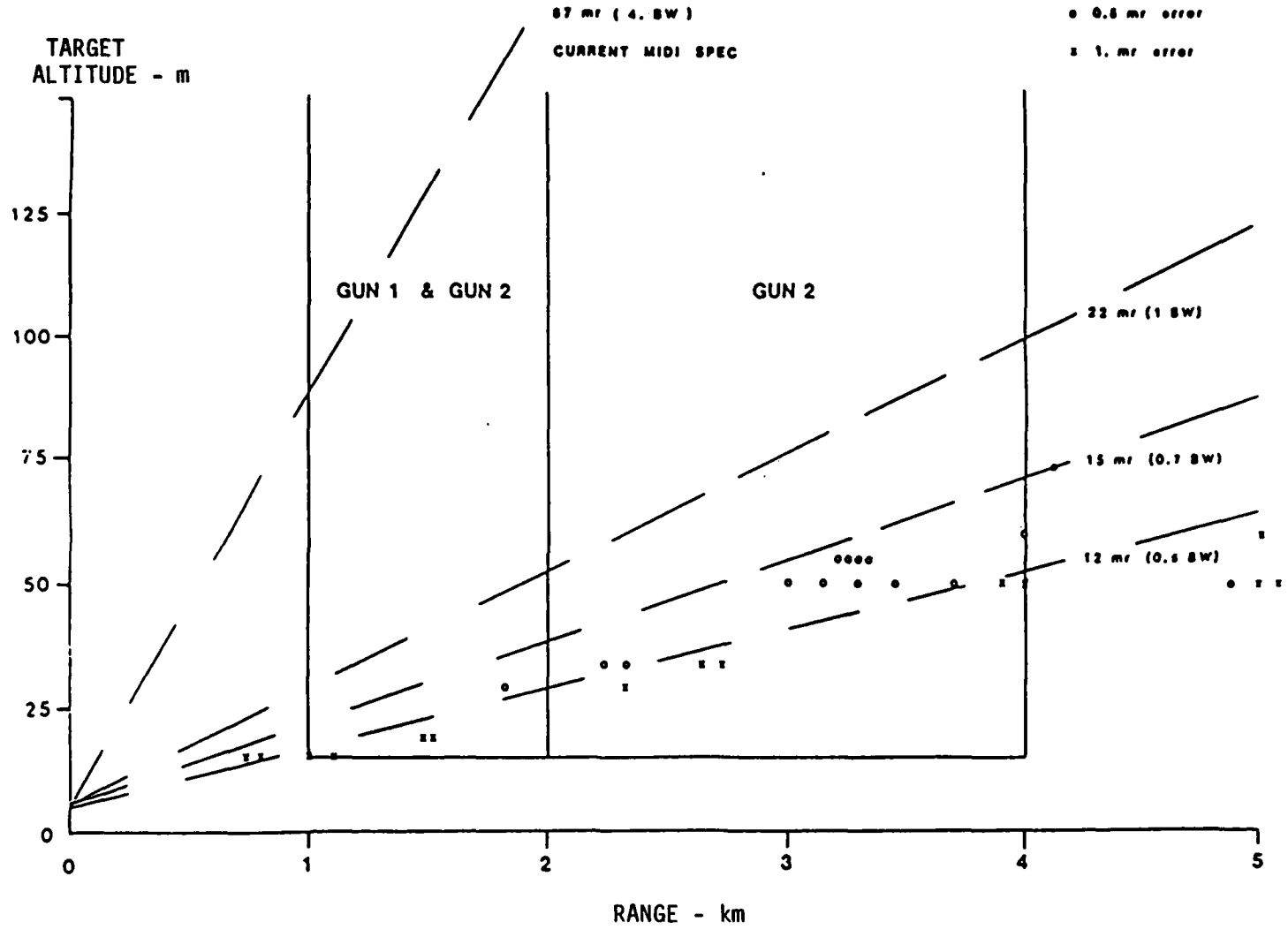

Figure 4-12 Performance Summary -- Xband

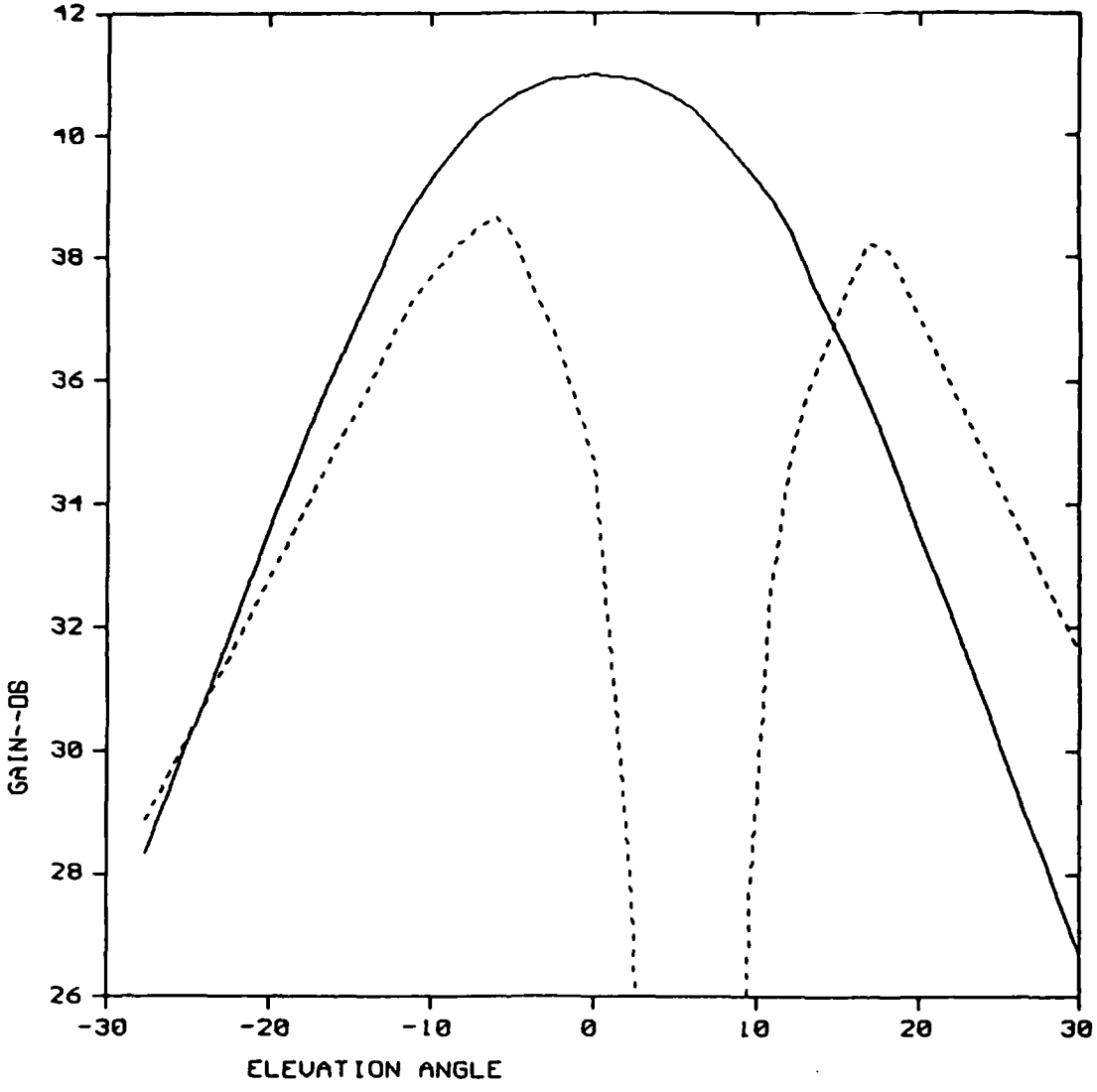

Figure 4-13 1.3 Degree Beamwidth Antenna Pattern, Squinted

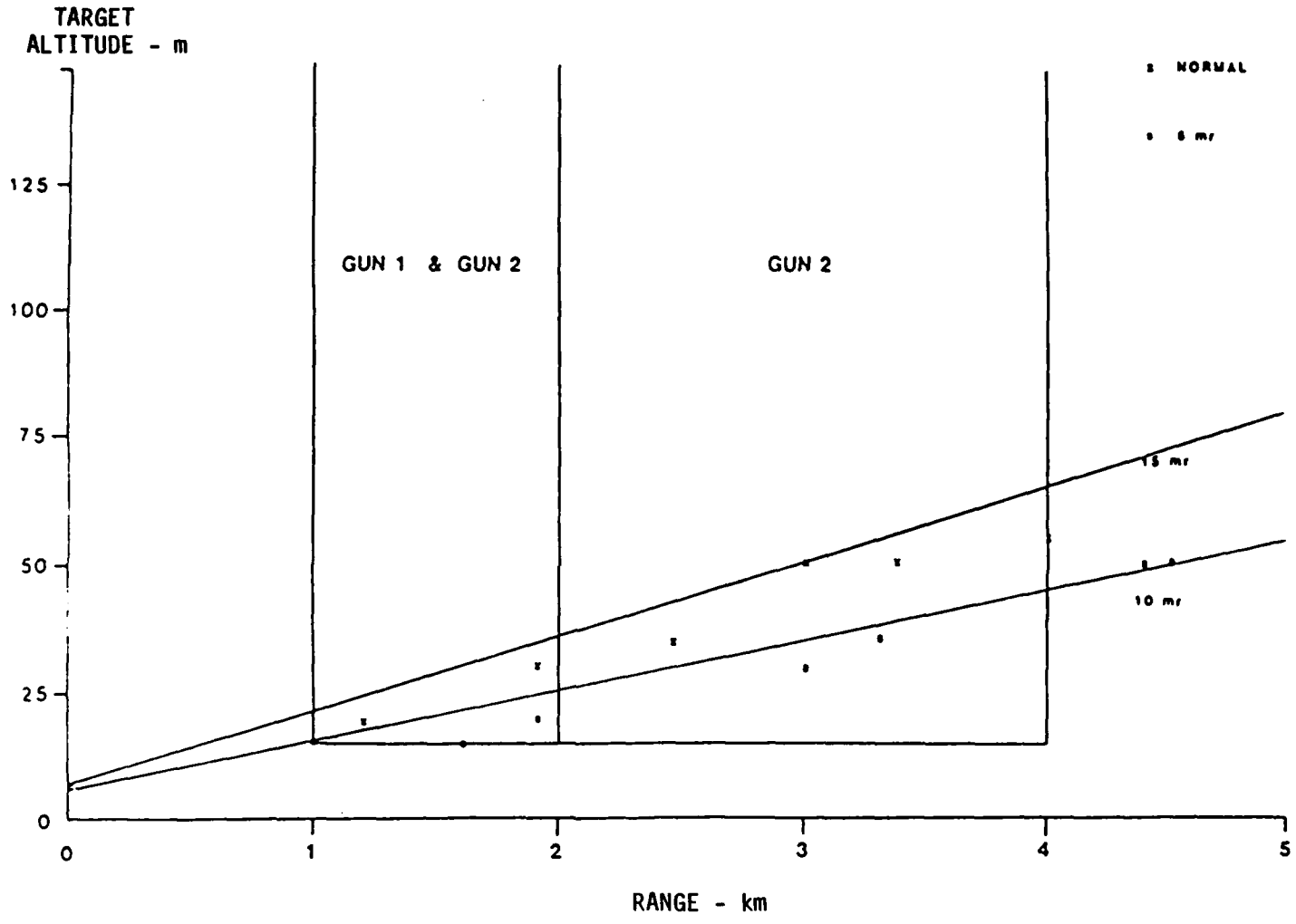

Figure 4-14 Performance Summary -- Xband, Squinted Difference Pattern

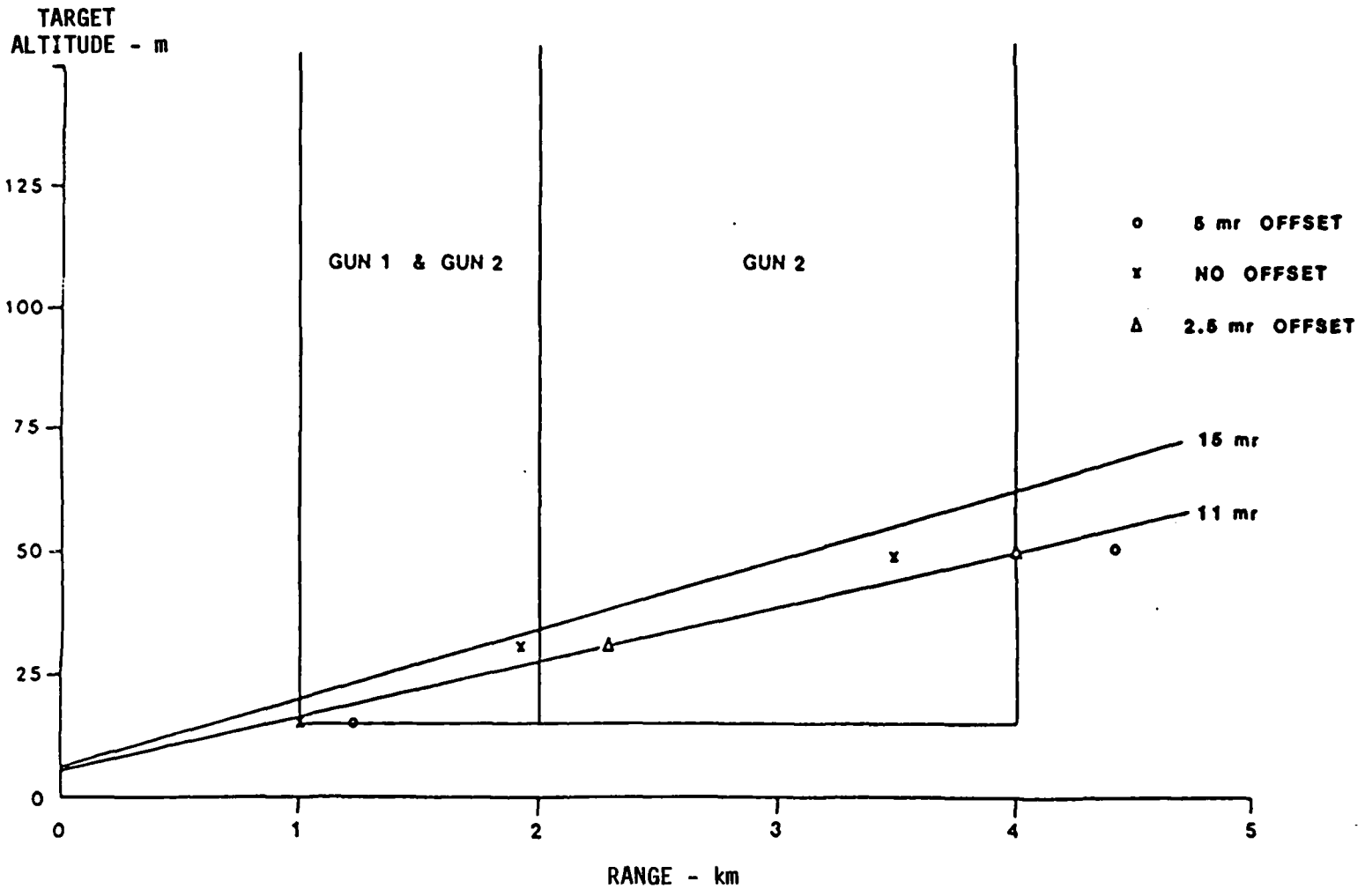

Figure 4-15 Performance Summary -- Xband Offset Tracking

K_A Band

Table 4-3 and Figure 4-16 summarize that K_A performance. The 0.4 degree (6 milliradian) antenna beamwidth corresponds to a 6 foot diameter antenna. At elevation angles above 4 milliradians (0.7 beamwidths), the errors are less than 0.1 milliradian (0.02 beamwidths). When normalized to the antenna beamwidth, these results closely follow the X-band results.

Other Results

The reflection coefficients predicted by the three dimensional facet model using the terrain characteristics of an area of the White Sands Missile Range are shown in Table 4-4. The conclusions presented herein were based on a constant reflection coefficient value of 0.7 for all ranges. The reflection coefficient determined from the tests at the North McGregor Range described in Section 4.2 is also shown.

The relative phase angles between the direct signal and the diffuse multipath interference signals from the ground facets are distributed throughout the region $\pm\pi/2$. Therefore, the presence of a quadrature component in the elevation difference channel is useful in indicating the presence of multipath interference.

4.2 MULTIPATH INTERFERENCE MEASUREMENTS

As was done for the clutter analysis, the present MIDI system was used to document the magnitude of multipath interference in a desert environment. A metallic balloon was used to measure the vertical lobing structure characteristic of multipath interference, from which estimate an of the average forward scattering reflection coefficient was derived. This reflection coefficient was compared to the values used in the theoretical models to determine the validity of the tracking error predictions. The following paragraphs describes the measurement procedure and the analysis of the results.

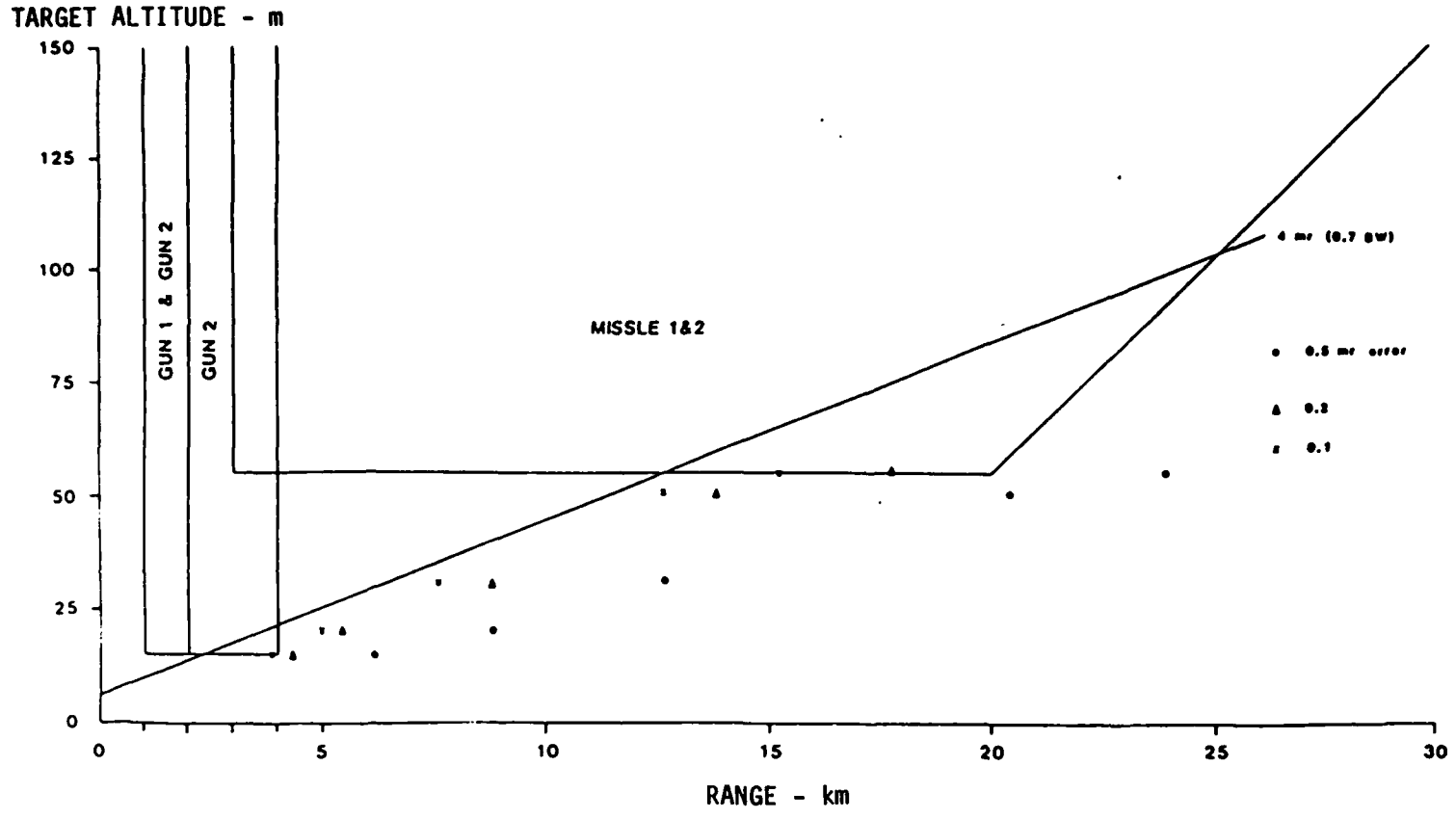

Figure 4-16 Performance Summary Ka Band

TABLE 4-4 REFLECTION COEFFICIENT COMPARISON

RANGE (m)	SIMPLE MODEL $\lvert\rho\rvert$	FACET MODEL $\sqrt{\rho_s^2 + \rho_d^2}$	TEST NORTH MCGREGOR
5800	0.7	-	0.35
3700	0.7	0.67	-
2700	0.7	0.39	-
1700	0.7	0.28	-
1200	0.7	0.25	-

4.2.1 MULTIPATH INTERFERENCE MEASUREMENT PROCEDURE

The multipath measurements were preceded by a step calibration of the receiver response using 10 dB attenuators. The procedure was identical to that used in the clutter measurements. Once calibration was completed, the multipath measurements proceeded as follows. A 1 m^2 RCS aluminum balloon was inflated with helium and attached to a string marked off in 2 foot increments. The balloon was positioned in an area that afforded allow clutter background while providing a clear line of sight to the desert surface. Such an area was located South south east of the MIDI site at a range of 5800 m. Once the balloon was positioned at the site, the antenna was pointed slightly above the horizon. Once measurements began, the antenna position remained fixed. Thus, during data collection, the only variable was the height of the balloon. This height was varied from 10 feet to 100 feet above the local terrain in 5 foot increments. At each position, several seconds of range gated, sum channel, video data were recorded. Once the vertical probe had veen completed, the balloon was raised to 200 feet, the antenna was boresighted on it, and several seconds of video data were collected. This calibration measurement provided a sample of balloon backscatter power in the absense of multipath interference. Once the measurement was completed, the balloon was moved slightly in range and azimuth and the entire process was repeated.

4.2.2 MULTIPATH MEASUREMENT RESULTS

The results of the two multipath measurements are presented in graphical form in Figures 4-17(a) and (b). The step calibration was used to convert the collected video data into dB relative to the maximum step calibration level. An attenuation level of 0 dB corresponded to 70 dB above noise level. The calibrated data at each balloon position were averaged, and the averaged values were plotted as a function of balloon position above ground level. The two figures exhibit a definite multipath lobing structure. While the structure is not perfectly uniform, it is strongly repeatable, as can be seen by overlaying the two plots. At the top of each figure is the video sample of the balloon in free space. The multipath lobing structure clearly oscillates around this value.

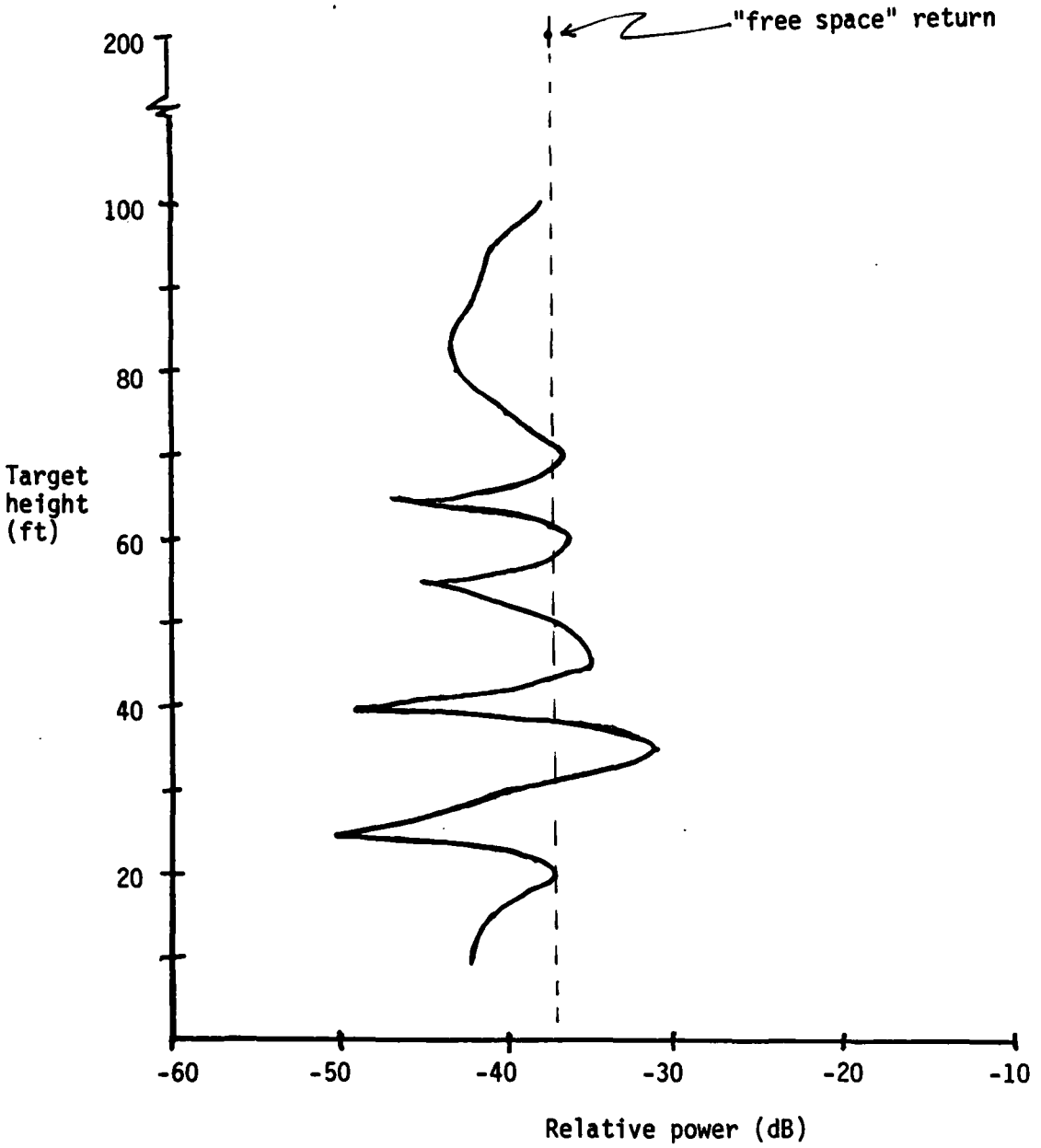

Figure 4-17a. Measured MIDI multipath interference pattern (set 1).

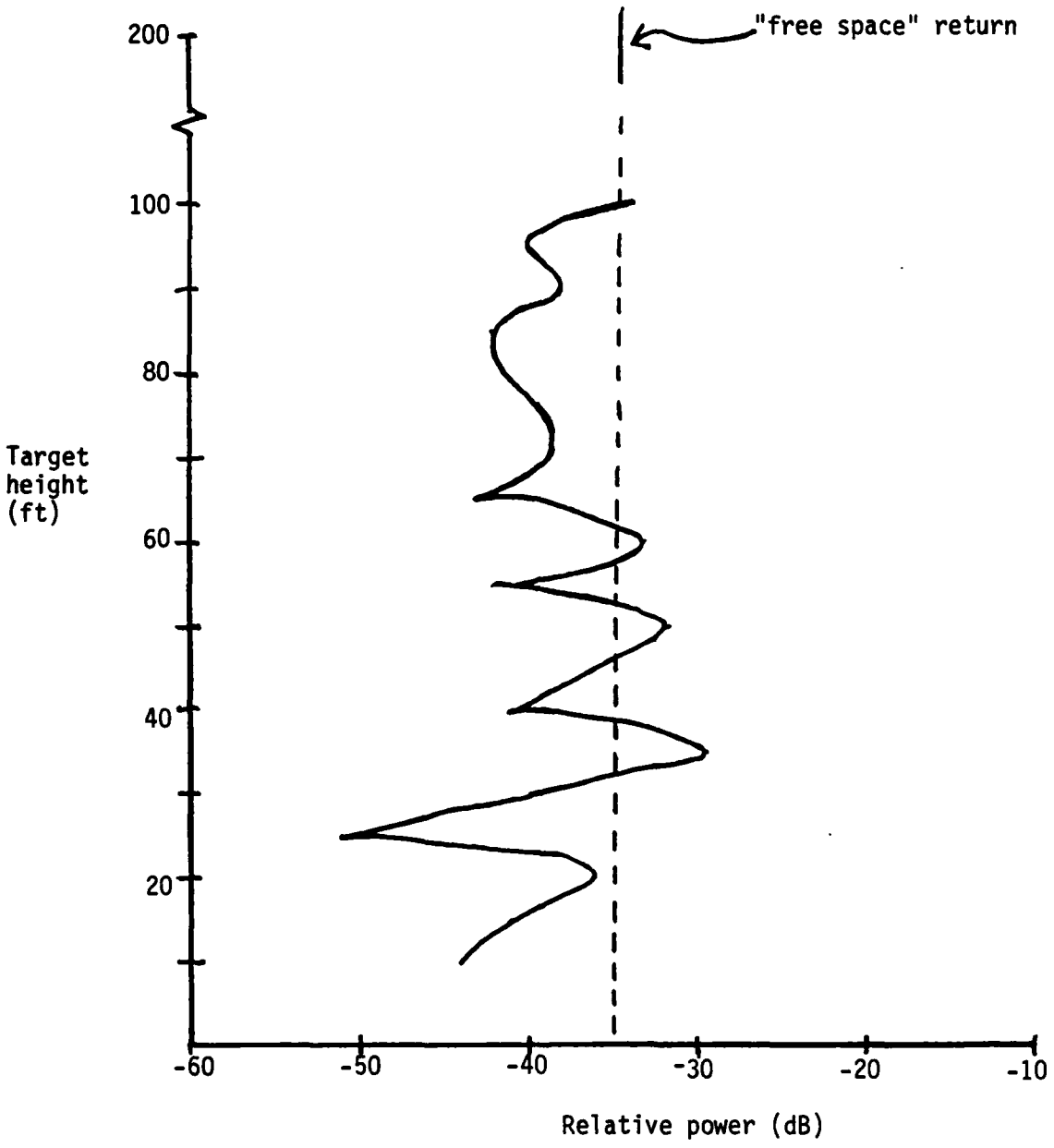

Figure 4-17b. Measured MIDI multipath interference pattern (set 2).

The results of the multipath interference measurement are presented in tabular form in Table 4-1. For each lobe, the peak-to-null signal variation and the lobe width are recorded. For data set #1, the average peak-to-null variation was 13.5 dB and the lobe width was 14 feet. For data set #2, the lobe width was the same and the amplitude variation was 12.1 dB. The average peak-to-null variation for both sets was 12.8 dB.

For monostatic (two-way) multipath interference, the peak-to-null variation is a function of the magnitude and phase of the reflection coefficient. At the low grazing angles considered in the present analysis the phase of the reflection coefficient is very close to 180^{o} for vertical polarization. The peak-to-null (PN) amplitude variation is given by

$$PN = \frac{1 + 2\rho + \rho^2}{1 - 2\rho + \rho^2}, \qquad 4.7$$

where ρ = the magnitude of the reflection coefficient.

This equation can be solved for ρ by converting it to the quadratic equation

$$(PN - 1)\rho^2 - (PN + 1)2\rho + PN - 1 = 0. \qquad 4.8$$

Equation 4.8 and an average peak-to-null value of 12.8 dB which corresponds to an amplitude ratio of 4.37 were used to calculate the reflection coefficient for the present MIDI environment; the result was 0.35. This value is less than that predicted by the diffuse multipath model and less than the value used in the multipath interference tracking error predictions. At longer ranges and lower elevation angles, however, the reflectivity will be greater than 0.35.

4.3 CORRELATION DISTANCE ANALYSIS

Multipath interference causes angle tracking errors when the MIDI is used to track a gunnery target during certain desired low altitude test scenarios. Similarly, multipath interference causes unacceptable errors in the measurement of angle off boresight of bullets and missiles fired at the

TABLE 4-5. MIDI MULTIPATH MEASUREMENT RESULTS.

Data set #1

Lobe	Peak-to-Null (dB)	Lobe Width (feet)
1	13	—
2	19 18	15
3	14 10	15
4	9 11	10
5	10 (6)	15
Results	average = 13.5	average = 14

Data set #2

Lobe	Peak-to-Null (dB)	Lobe Width (feet)
1	8 15	15
2	22 12	15
3	10 11	15
4	9 10	10
Results	average = 12.1	average ≈ 14
Total Results	average = 12.8	average ≈ 14 = 4.25 m

target. If the errors in target angle and projectile angle are highly correlated, they will tend to cancel in the miss distance calculation. The analysis described herein provides some insights into the size of the region about the gunnery target within which the projectile and target errors might be considered as being correlated.

The relative phase between the direct signal and the reflected signal is directly related to the geometric path length difference. If these relative phase angles for the gunnery target and the projectile are the same, then the resulting angular errors will be correlated and will tend to cancel in the miss distance calculation. The specific degree of error cancellation is dependent upon the characteristics of the radar, principally transmitter frequency and antenna patterns. This investigation consists of two analyses:

1. Calculating the geometric path length differences. The results are expressed in meters and are independent of radar characteristics.
2. Determining the error correlation produced by the path length differences using the characteristics of the current MIDI.

4.3.1 GEOMETRIC PATH LENGTH DIFFERENCE CALCULATION

The geometric definitions used throughout this analysis are shown in Figure 4-18. The difference between the reflected path length and the direct path length δ_1 for the gunnery target is given by:

$$\delta_1 = R1 + R2 - R \qquad 4.9$$

where $$R1 + R2 = ((h_T + h_R)^2 + G^2)^{1/2} \qquad 4.10$$

and $$R = ((h_T - h_R)^2 + G^2)^{1/2} \ . \qquad 4.11$$

Similarly, the path length difference for the projectile δ_2 is given by:

$$\delta_2 = R1' + R2' - R' \ , \qquad 4.12$$

where

$$R1' + R2' = ((h_T + h_R + M_Y)^2 + (G + M_X)^2)^{1/2} \qquad 4.13$$

and

$$R' = ((h_T - h_R - M_Y)^2 + (G + M_X)^2)^{1/2}. \qquad 4.14$$

The change Δ in path length difference between the projectile and the gunnery target is then:

$$\Delta = \delta_2 - \delta_1. \qquad 4.15$$

The quantity Δ is computed as a function of vertical miss distance M_Y while other parameters are held constant. A listing of the computer program CORRELATION-DISTANCE which calculates and plots Δ versus miss distance is included in Appendix C. The program inputs are radar altitude, gunnery target altitude and range, and relative range gate position, M_X.

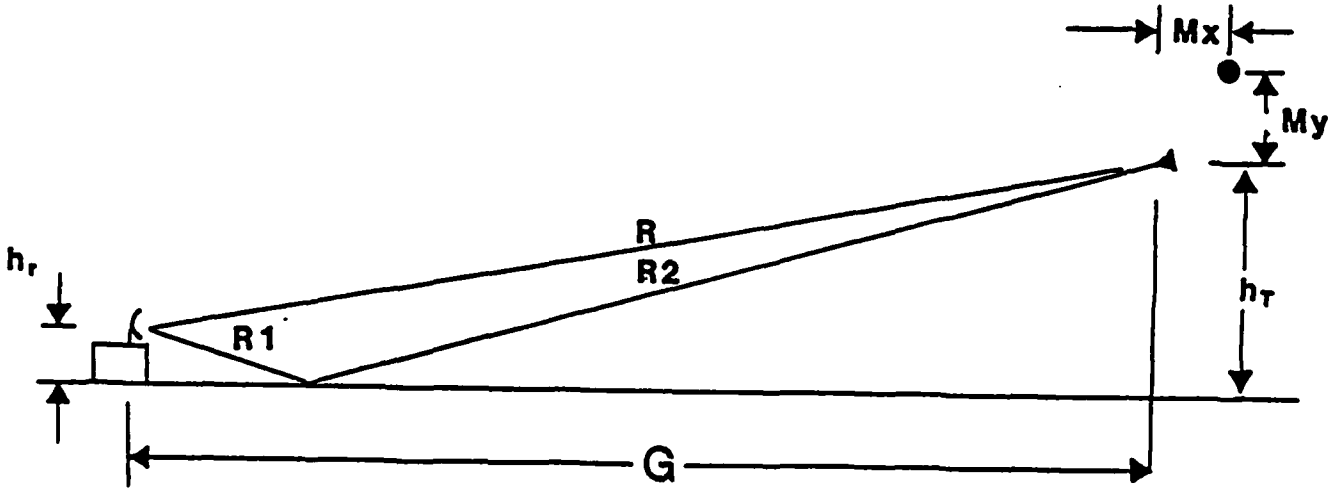

Figure 4-18. Geometric definitions.

4.3.2 ANGLE ERROR CALCULATION

Angle errors are calculated for both the target and projectile in the same way as previously described in Section 4.1, except as follows. Instead of using a constant value, such as 90 degrees, for the relative phase ϕ_M between the direct signal and the multipath interference signal, a value is computed for each gunnery target position and projectile position using:

$$\phi_M = \phi_\rho + \frac{2\pi}{\lambda} \delta \ , \qquad 4.16$$

where

ϕ_ρ = phase angle of ground reflection coefficient, taken as π , and
λ = transmitter wavelength, meters.

Figures 4-19, 4-21, and 4-23 show the relative error that result from the Δ values of Figures 4-20, 4-22, and 4-24, respectively. A reflection coefficient of 0.7 was used in each case. Figure 4-25 shows the results for the same geometry as Figure 4-24 but with a reflection coefficient of 0.25. The large error peaks occur when the relative phase between the direct path and the reflected signal is a multiple of π. The error budgets of 0.5 milliradian for ranges of 4000 meters or less and 0.2 milliradian for a range of 10,000 meters are exceeded for vertical miss distances greater than one to two meters. The results presented here tend to be somewhat pessimistic in that a diffuse reflecting surface would not exhibit the sharp error peaks.

In conclusion, the region about the target within which the path length differences were small compared to a wavelength was not large enough to be useful for MIDI gun scoring missions, which are typically performed at ranges of 4 km or less. At ranges of 10 km or greater, the technique may be applicable for an X-band or lower frequency radar. The technique must be verified experimentally before it can be relied upon to reduce the miss distance measurement errors in an operational system.

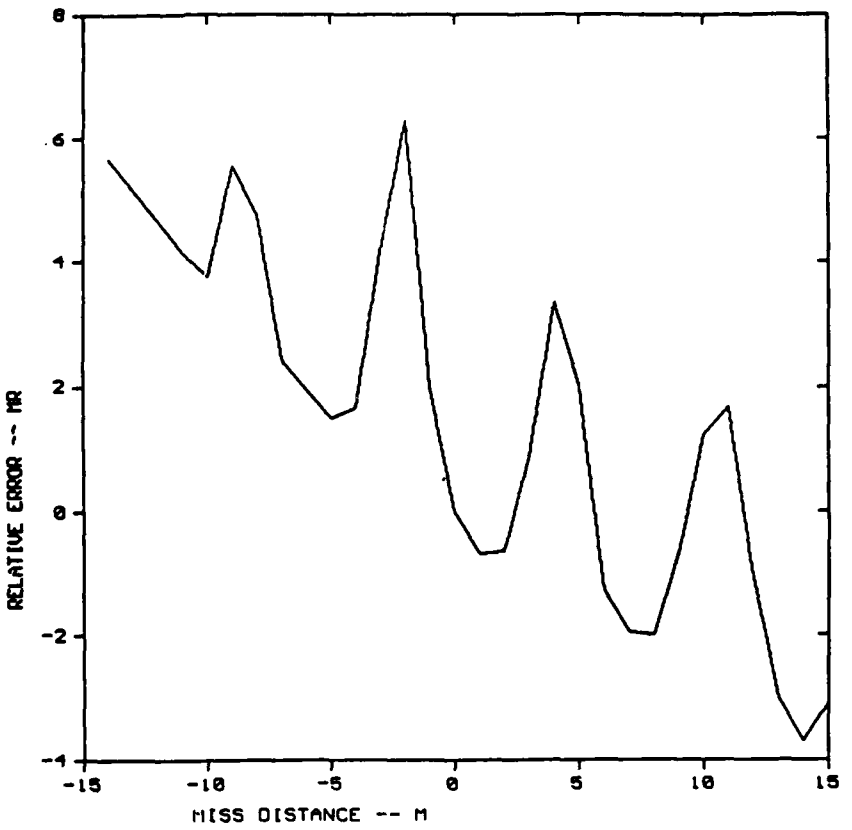

Figure 4-19. Relative error at 2,000 m.

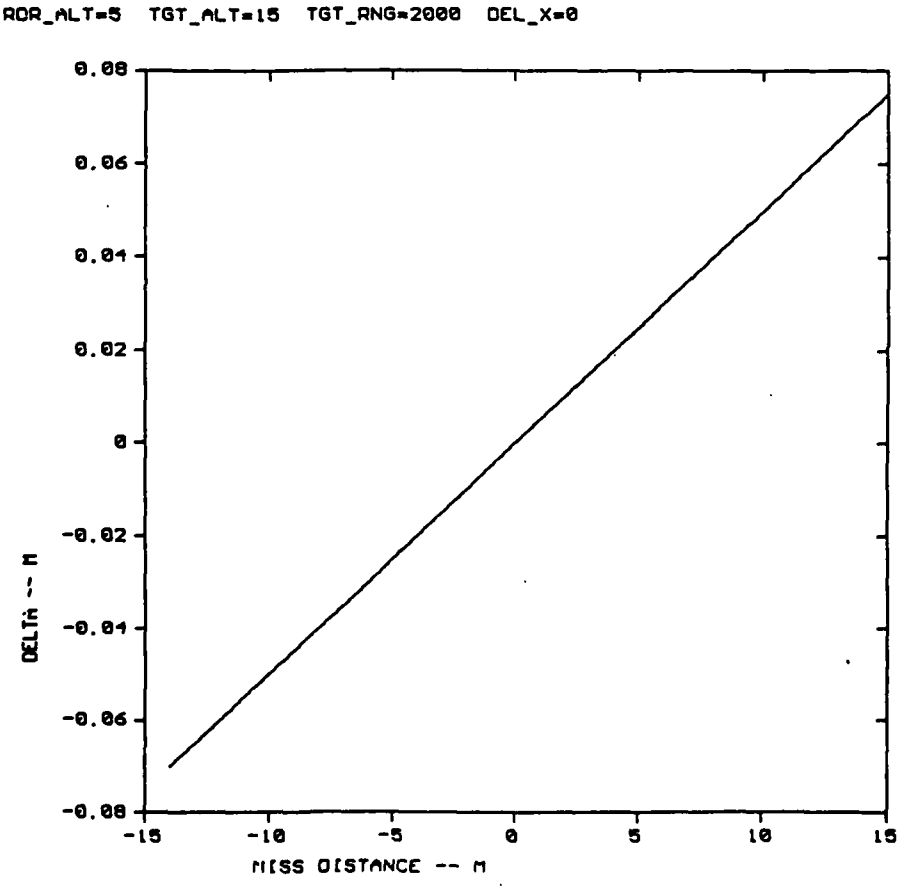

Figure 4-20. Path length difference at 2,000 m.

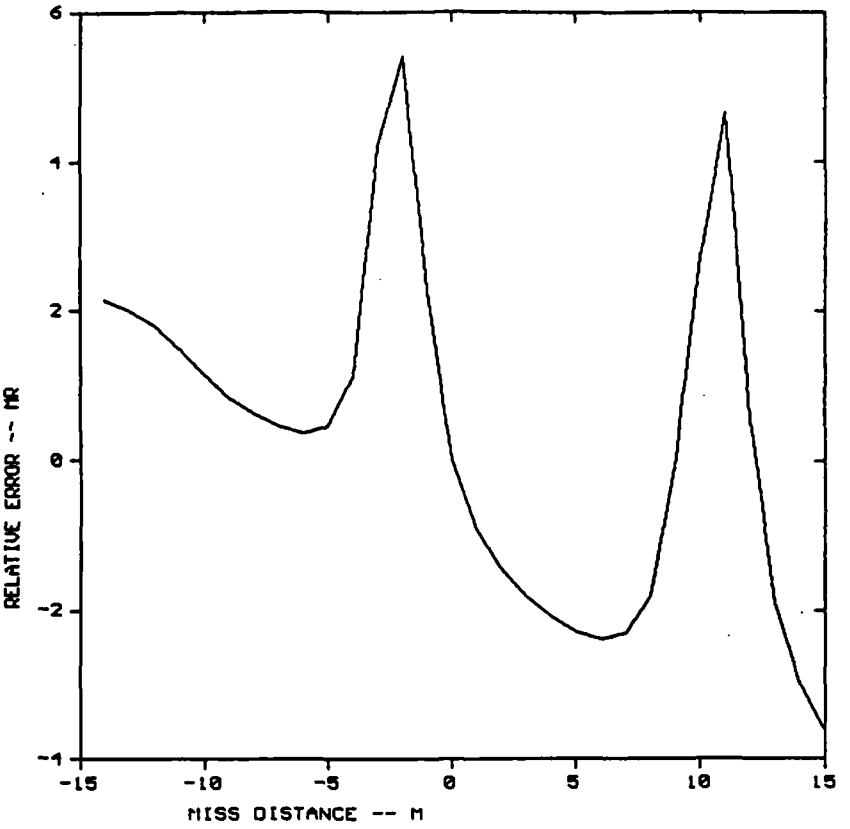

Figure 4-21. Relative error at 4,000 m.

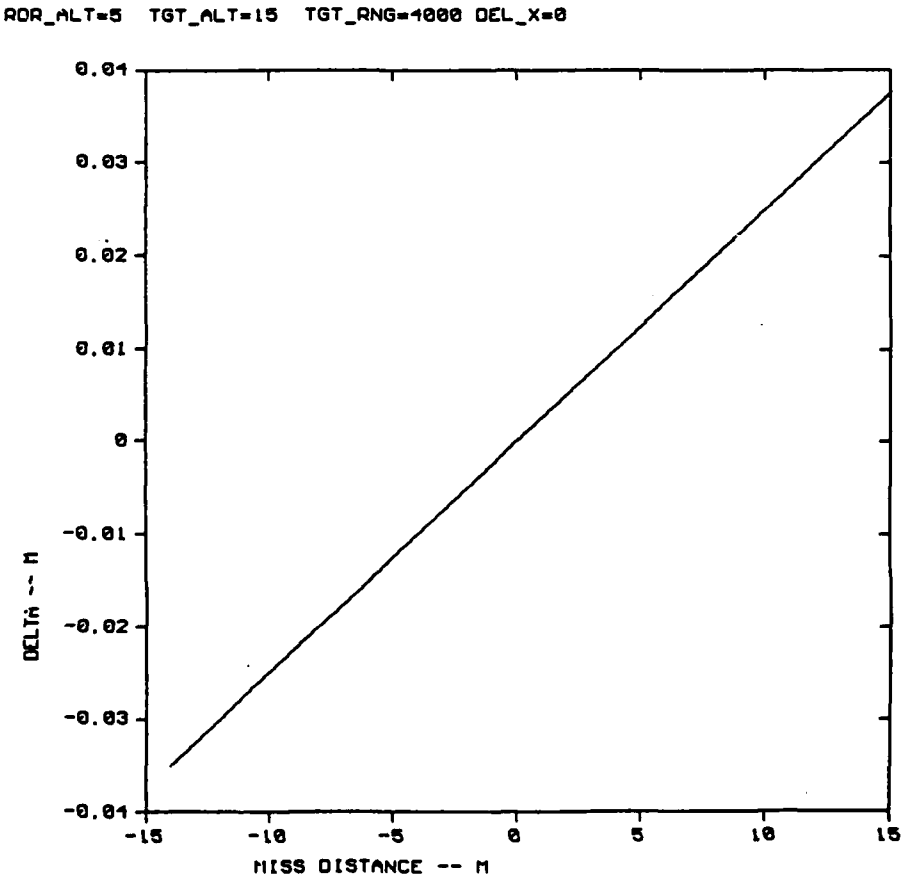

Figure 4-22. Path length difference at 4,000 m.

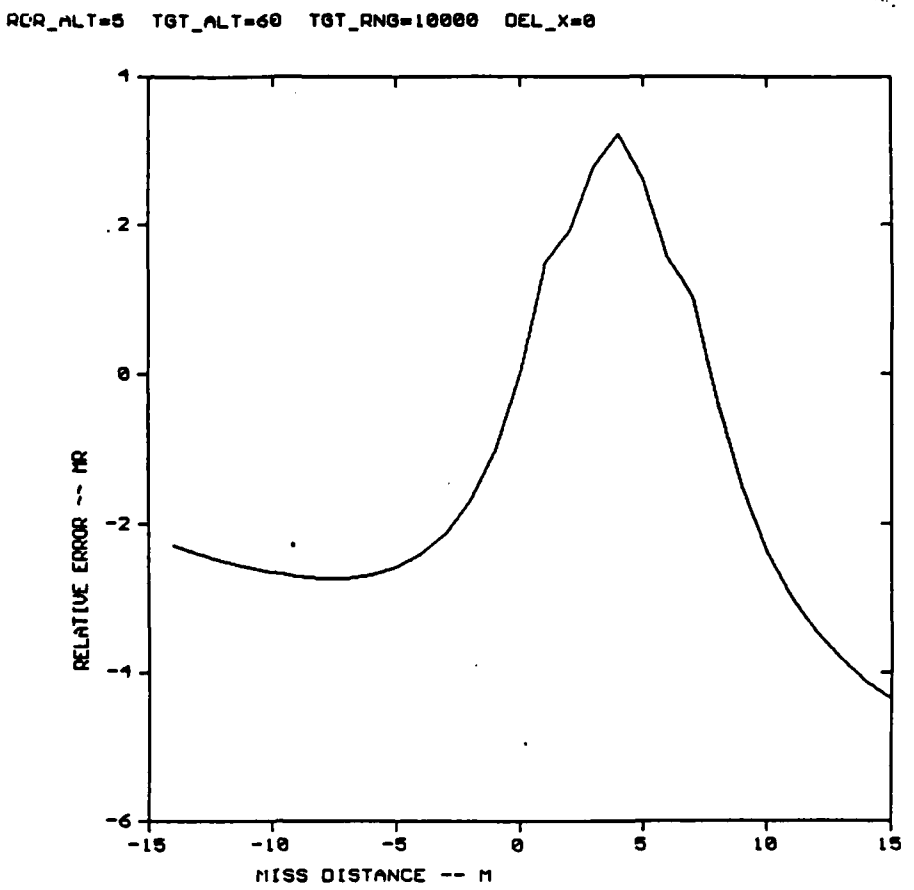

Figure 4-23. Relative error at 10,000 m.

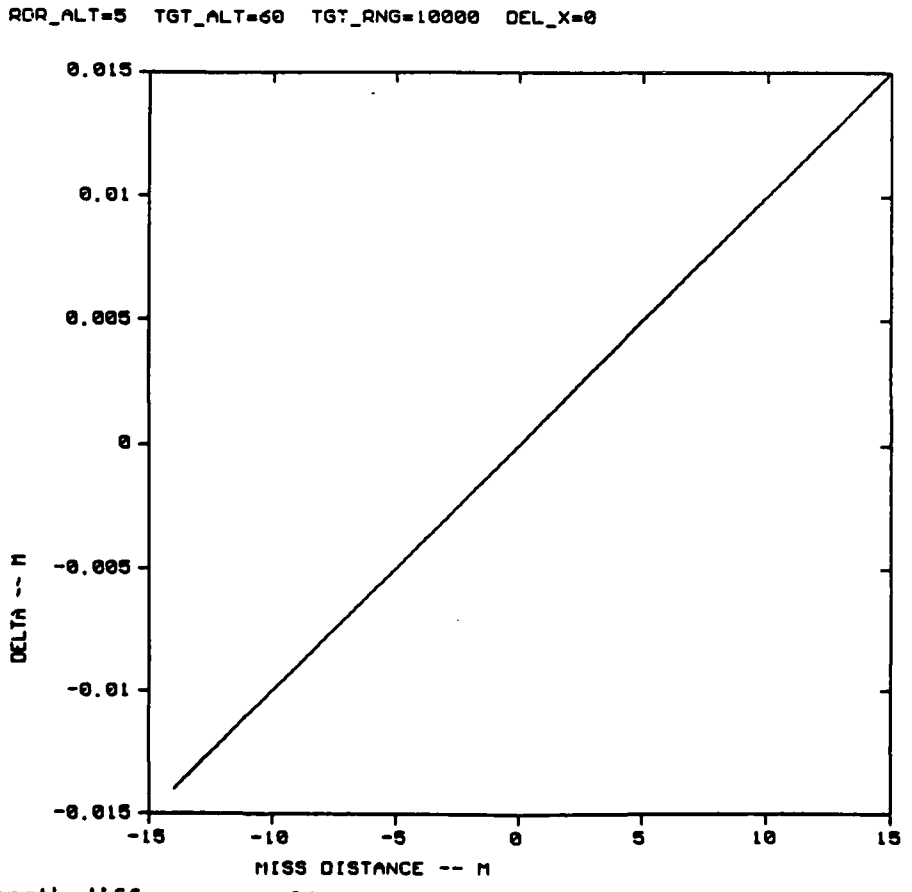

Figure 4-24. Path length difference at 10,000 m.

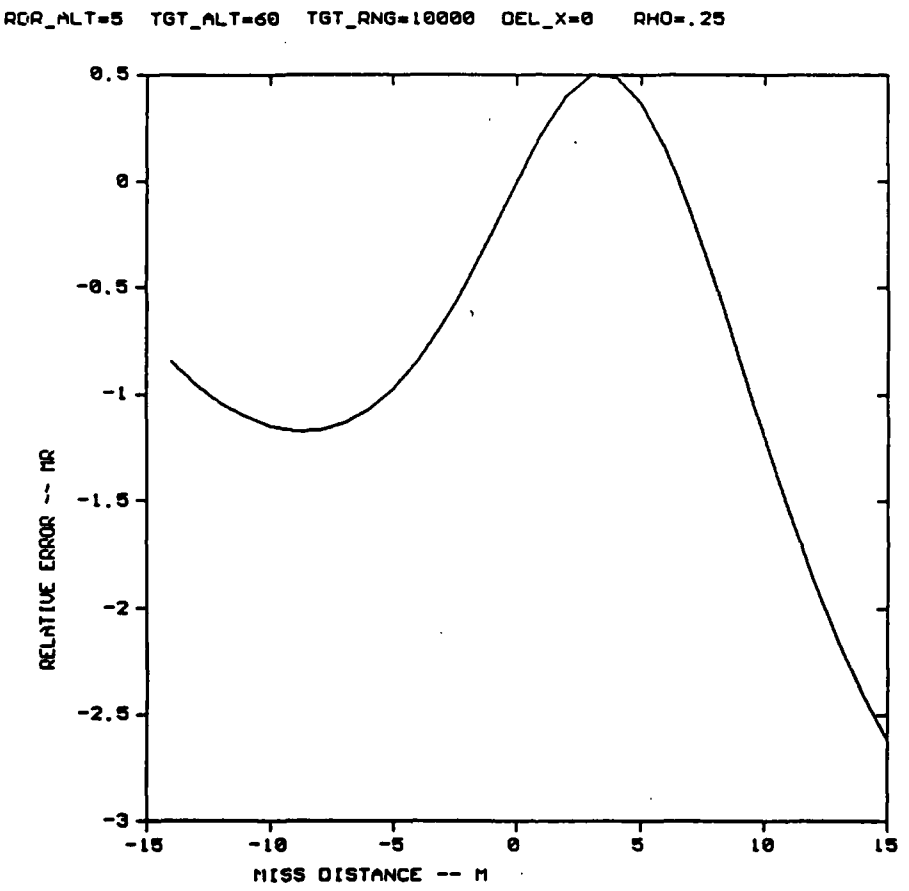

Figure 4-25. Relative error at 10,000 m, p = 0.25.

4.4 CALCULATION OF CLUTTER-TO-TARGET AND MULTIPATH INTERFERENCE-TO-TARGET RATIOS

The clutter-to-target ratios and multipath interference ratios for various MIDI II scenarios were calculated. This analysis provided an insight, expressed in the user coordinate system of target range and target altitude, into which interference, clutter, or multipath, would limit the radar tracking and scoring performance. Also, the effects of changing target altitude and antenna beamwidth could readily be evaluated. The model and the computer program that implements the model are described herein.

4.4.1 INTERFERENCE RATIO EQUATIONS

The MIDI II geometry is as defined previously in Figure 4-2. The radar target is, depending upon the mission, an actual gunnery target or a projectile fired at the gunnery target. By proper choice of radar cross section, calculations were made for various projectiles and gunnery targets.

The basic equations used for the sum channel are:

$$P_{RT} = K\, G_T^2\, \sigma_T\,, \tag{4.17}$$

$$P_{RC} = K\, G_C^2\, \sigma_C, \tag{4.18}$$

and

$$P_{RM} = K\, G_T G_M\, \rho^2\, \sigma_T, \tag{4.19}$$

where

P_{RT} = Power received from target,
P_{RC} = Power received from clutter,
P_{RM} = Power received from multipath,
ρ = Magnitude of ground reflection coefficient,
G = Antenna gain, sum channel,
σ = Radar cross section.

Subscripts T, C, M denote target, clutter, and multipath respectively.

K = Other parameters of the radar range equation which are constants for this purpose.

The clutter cross section is itself a function of range and was computed from:

$$\sigma_C = R\ BW\ \Delta R\ \sigma_o\ , \qquad 4.20$$

where

R = range to clutter patch,

BW = antenna azimuth beamwidth,

ΔR = range resolution,

σ_o = ground backscatter coefficient.

The quantities shown below are derived from equations 4.17 through 4.20.

$$\frac{P_{RC}}{P_{RT}} = \left(\frac{G_C}{G_T}\right)^2 \frac{R\ BW\ \Delta R\ \sigma_o}{\sigma_T}\ , \qquad 4.21$$

and

$$\frac{P_{RM}}{P_{RT}} = \frac{G_M\ \rho^2}{G_T}\ , \qquad 4.22$$

where all quantities are as previously described.

The basic equations for the difference (Δ) channel are similar to Equations 4.17, 4.18, and 4.19:

$$P_{RT\Delta} = K\ G_T\ G_{\Delta T}\ \sigma_T\ , \qquad 4.23$$

$$P_{RC\Delta} = K\ G_C\ G_{\Delta C}\ \sigma_C\ , \qquad 4.24$$

and

$$P_{RM\Delta} = K\ G_T\ G_{\Delta M}\ \sigma_T, \qquad 4.25$$

where G_Δ = difference channel antenna gain and the other quantities are as previously defined. The expressions shown below are derived from Equations 4.20, 4.23, 4.24 and 4.25.

$$\frac{P_{RC\Delta}}{P_{RT\Delta}} = \frac{G_c\, G_{\Delta C}\, \sigma_C}{G_T\, G_{\Delta T}\, \sigma_T} \quad . \qquad 4.26$$

$$\frac{P_{RM\Delta}}{P_{RT\Delta}} = \frac{G_{\Delta M}\, \rho^2}{G_{\Delta T}} \quad . \qquad 4.27$$

Equations 4.21 and 4.26 are computed as a function of range while all other parameters are held constant and plotted on the same axes. A representative output is shown as Figure 4-26. Equations 4.22 and 4.27 are similarly computed and plotted; Figure 4-27 is a representative plot.

4.4.2 COMPUTER PROGRAM "INTERFER_TO_SIG"

4.4.2.1 Program Summary

The program environment is shown in Figure 4-28. The input file is of the structure previously shown in Figure 4-5, a structure which has been used on several other MIDI computer programs. The other inputs requested by the program via the terminal are backscatter coefficient in dB, target cross section in dBsm, azimuth beamwidth in degrees, range resolution in meters, and a title for the plot output.

The program was written in FORTRAN and was installed on the VAX 11/780 computer at the Georgia Tech Research Facility, Cobb County. The program creates an output file labled BITMAP.TBX, which is subsequently printed on the line printer.

4.4.2.2 Program Description

A listing is included in Appendix C. The program is separated by comments into the following sections:

Declarations
Internal data
Input from file
Input from terminal

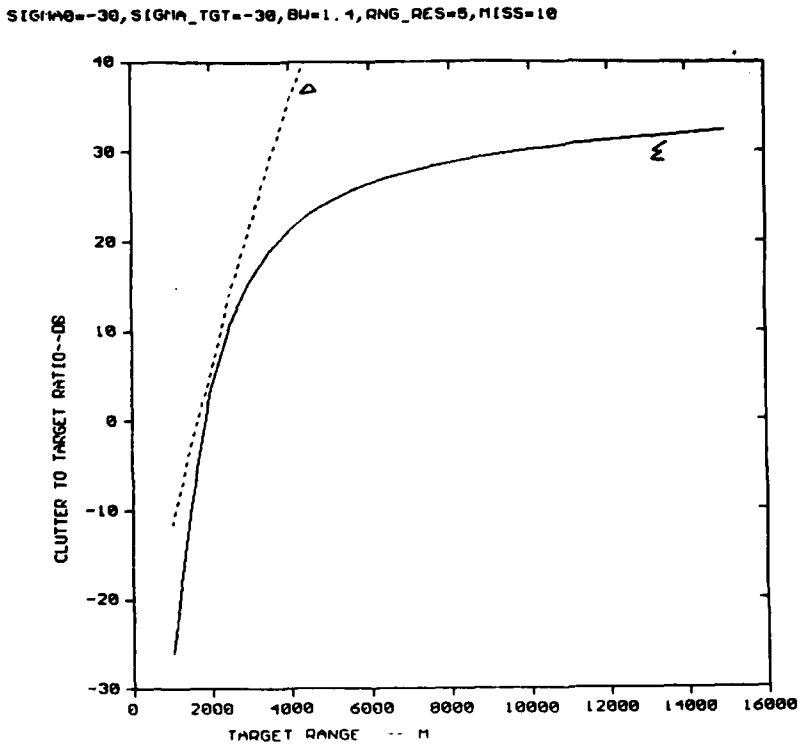

Figure 4-26. Clutter to target ratio versus range.

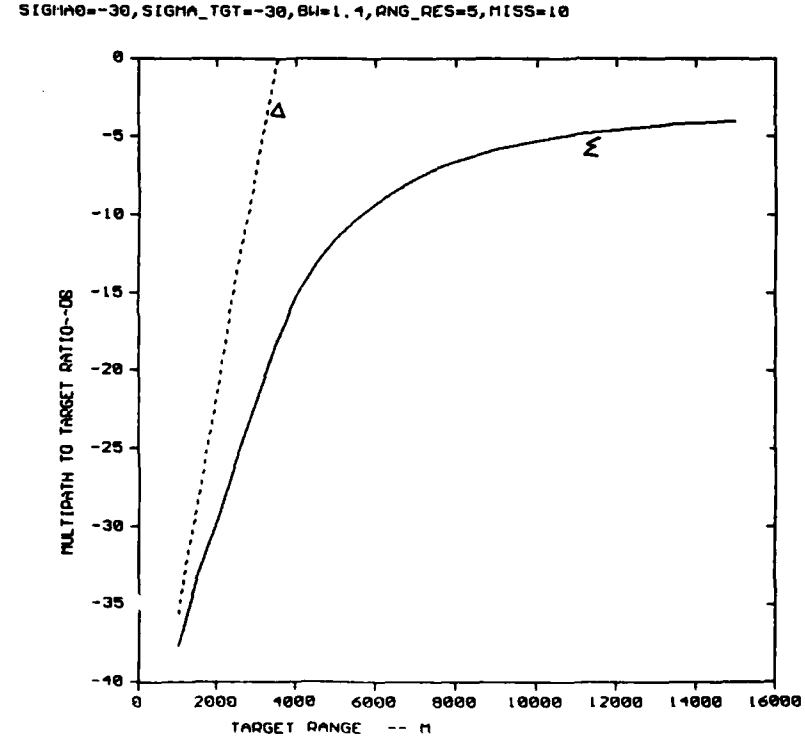

Figure 4-27. Multiptath interference ratio versus range.

AD-A148 467 METHODOLOGY IMPROVEMENT PROGRAM FOR THE SECOND GENERATION MISS DISTANCE R..(U) GEORGIA INST OF TECH ATLANTA ENGINEERING EXPERIMENT STATION 2/3

UNCLASSIFIED G V MORRIS ET AL. 30 OCT 84 F/G 17/9 NL

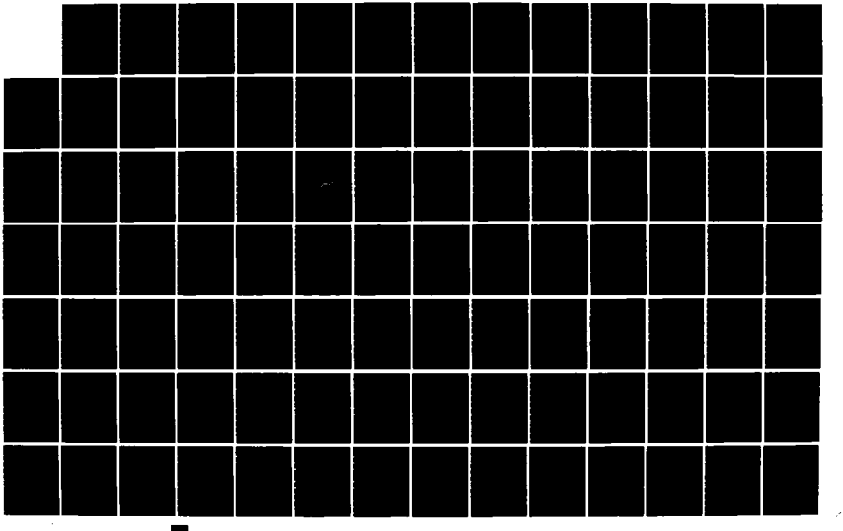

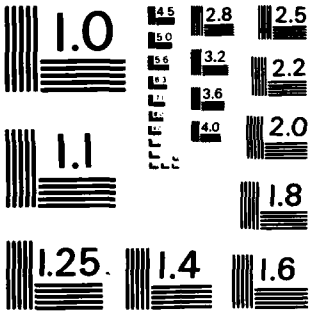

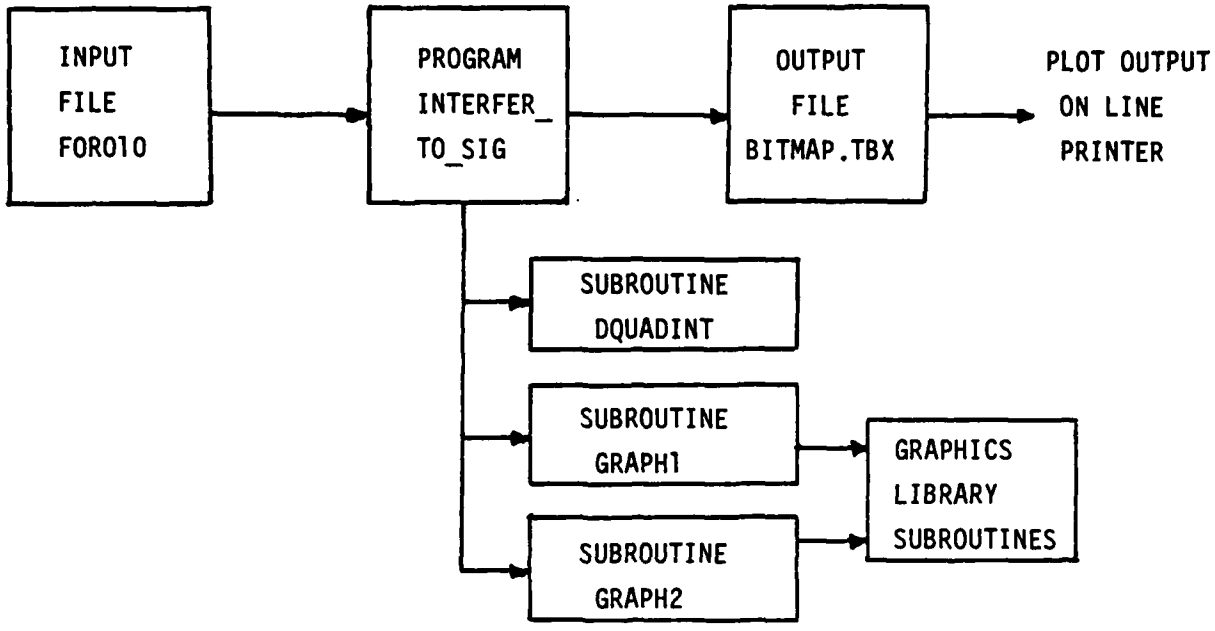

Figure 4-28 Program "INTERFER-TO-SIG" environment

Conversions

Calculation do loop

Plot results

The listing is largely self-explanatory, but some further comments are appropriate.

The following sequence is repeated as the target position is stepped from the minimum to maximum range. The program maintains the antenna boresight pointed at the target. The angles, referenced to antenna boresight, to the clutter patch and to the specular reflection point are calculated. The antenna gain at each angle is computed by a call to subroutine DQUADINT which performs a quadratic interpolation using the gain versus angle look-up table. The multipath interference ratio, clutter to target signal ratio, and target range are stored in arrays MULT_TO_TGT, CLUT_TO_TGT, and TGT_RNG, respectively.

The subroutine call to GRAPH1 creates an output file containing a plot, automatically scales the X and Y axes, and adds the X axis label, Y axis label, and title. The subroutine call to GRAPH2 plots the second curve on the same set of axes. GRAPH1 and GRAPH2 call several other subroutines from the Graphics Library of the VAX.

SECTION 5
HARDWARE FEASIBILITY

This section reviews those hardware subsystems which are key to the performance of the radar described in this report. The key subsystems reviewed include the transmitter, the signal processor, and the computer. The objective of this review is to demonstrate that a radar can be assembled using major subsystems which are known to be off-the-shelf items.

For the transmitter, the goal is a single-pulse signal-to-noise ratio of 20 dB at the maximum scoring ranges for each projectile with a standard frequency and standard power transmitter tube.

The signal processing data rate was calculated in order to estimate the size and complexity of the signal processor.

For the computer requirements, the goal is to identify at least one commercial product which meets the requirements of MIDI II and which is well supported logistically both in hardware and software.

The data processing should retain the essential features of the current MIDI. The signal processing and data processing discussions of this section treat primarily (1) the new or modified requirements which result from using a Doppler radar with a large number of range gates and (2) upgrading the computing equipment to provide the final vector miss distance calculation within two minutes.

5.1 TRANSMITTER POWER REQUIREMENTS

Table 5-1 lists the terms of the range equation for three frequencies (10, 17, and 35 GHz) for a 3 foot diameter antenna and a transmitter with a peak power of 50 kilowatts. At a range of 1000 meters, the calculated signal-to-noise ratios are 36.6, 41.1, and 48.4 dB, respectively, for these three frequencies. These calculated values include 13 dB from the pulse compression but do not include the 15 dB signal-to-noise ratio maximum improvement due to the Doppler processing.

TABLE 5-1. MIDI II SIGNAL-TO-NOISE RATIO (SNR)
(σ = 0.001 m^2 = -30 dBsm)

FACTOR	VALUE	EQUATION VALUE (dB) PLUS 10 GHz	PLUS 17 GHz	PLUS 35 GHz	MINUS 10 GHz	MINUS 17 GHz	MINUS 35 GHz
P_T	50 kW	46.9	46.9	46.9	--	--	--
$G_T G_R$	3 ft. dia ant.	73.6	82.8	95.4	--	--	--
λ^2	0.03/0.02/0.009 m	--	--	--	30.4	35.1	41.0
σ	0.001 m^2	--	--	--	30.0	30.0	30.0
L	0.5	--	--	--	3.0	3.0	3.0
$(4\pi)^3$	1984.4	--	--	--	33.0	33.0	33.0
R^4	1000 m	--	--	--	120.0	120.0	120.0
K T_o	4.14 x 10^{-21}	204	204	204	--	--	--
B	16 ft. Res./30.75 MHz	--	--	--	74.9	74.9	74.9
N_f	9.12	--	--	--	9.6	9.6	9.6
Pulse Comp.	13:1	13	13	13	--	--	--
		337.5	346.7	359.3	300.9	305.6	311.5
SNR Single Pulse		36.6	41.1	47.8			
SNR After Doppler Processing		51.6	56.1	62.8			

TABLE 5-2. MIDI II MATRIX OF POSSIBILITIES

TRANSMITTER POWER (kW)	PULSE COMPRESSION	TARGET SIZE (dBsm)	ANTENNA DIAMETER (feet)	FREQUENCY (GHz)	RANGE AT 20 dBS/N (km)	BEAMWIDTH (deg/mrad)
50	13:1	-30	3	10	2.7	2.5/43.6
50	13:1	-30	3	17	3.5	1.5/26.2
50	13:1	-30	3	35	.5	0.7/12.2
50	13:1	-5	3	10	>10	2.5/43.6
50	13:1	-5	3	17	>10	1.5/26.2
50	13:1	-5	3	35	>10	0.7/12.2
50	13:1	-30 dBsm	10.5	10 GHz	>5	0.7/12.2

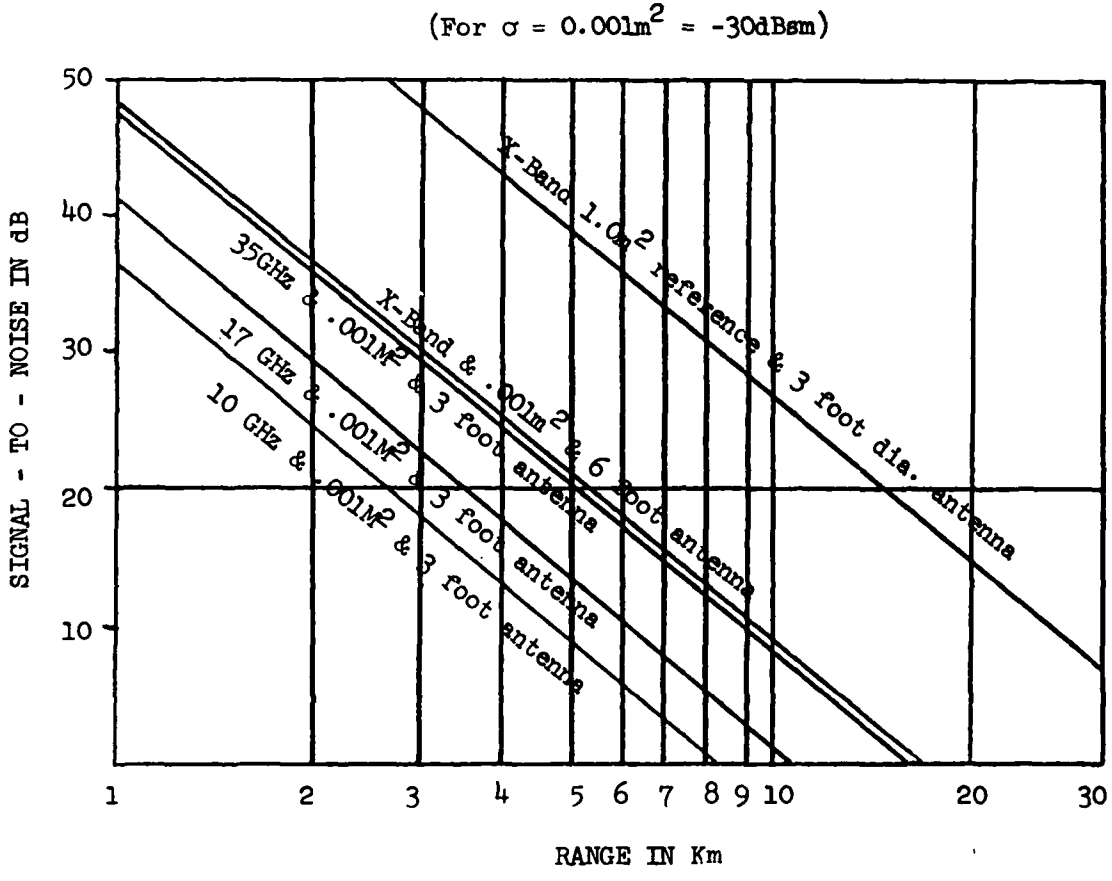

Notes:
(1) Doppler processing gain of 15dB is not included in this graph.
(2) Pulse compression gain of 13dB is included in this graph.
(3) Curve for 10 GHz and 6 foot antenna overlays curve for 35 GHz and 3 foot antenna.

Figure 5-1. Bullet scoring signal to noise ratio.

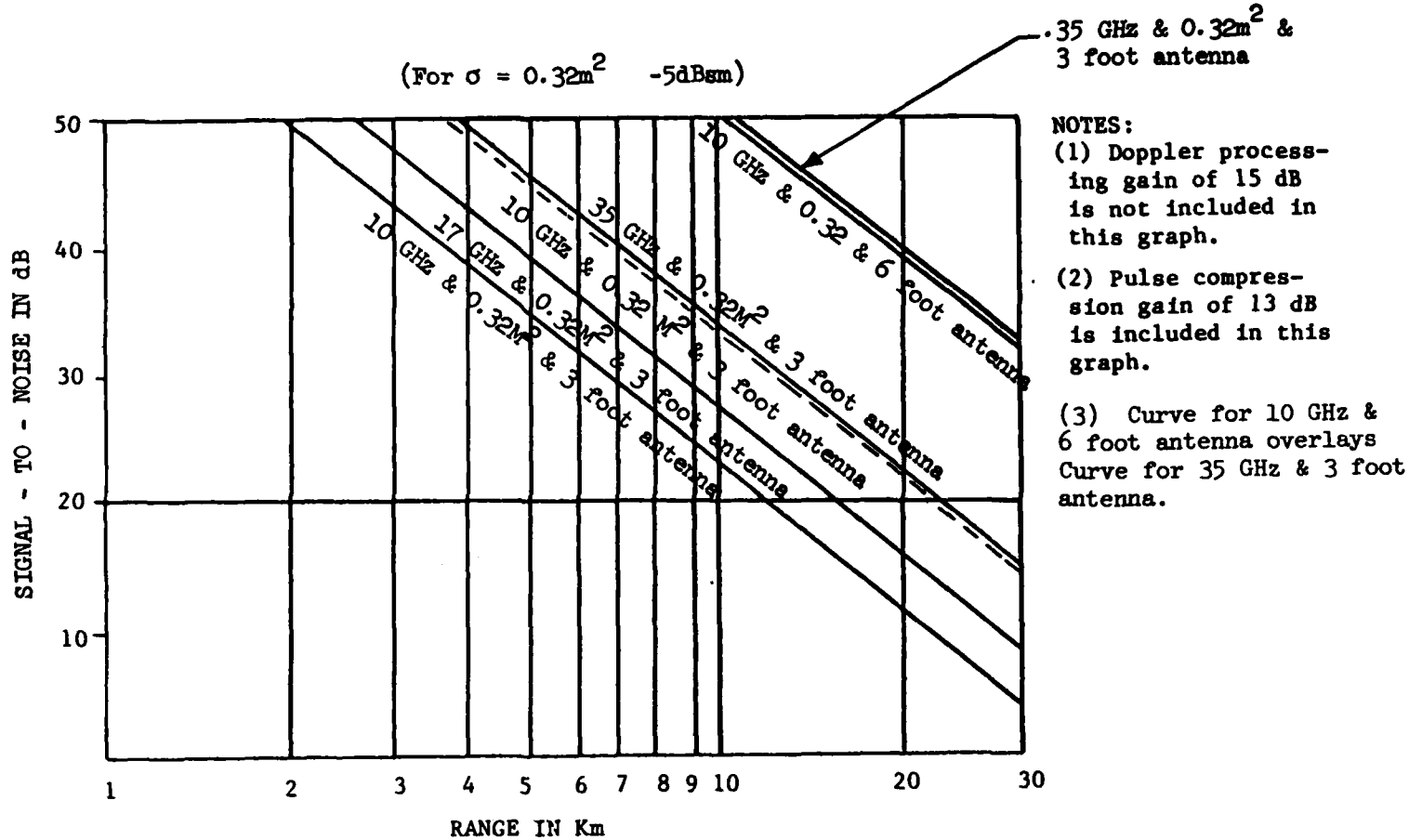

Figure 5-2. Missile scoring signal to noise ratio.

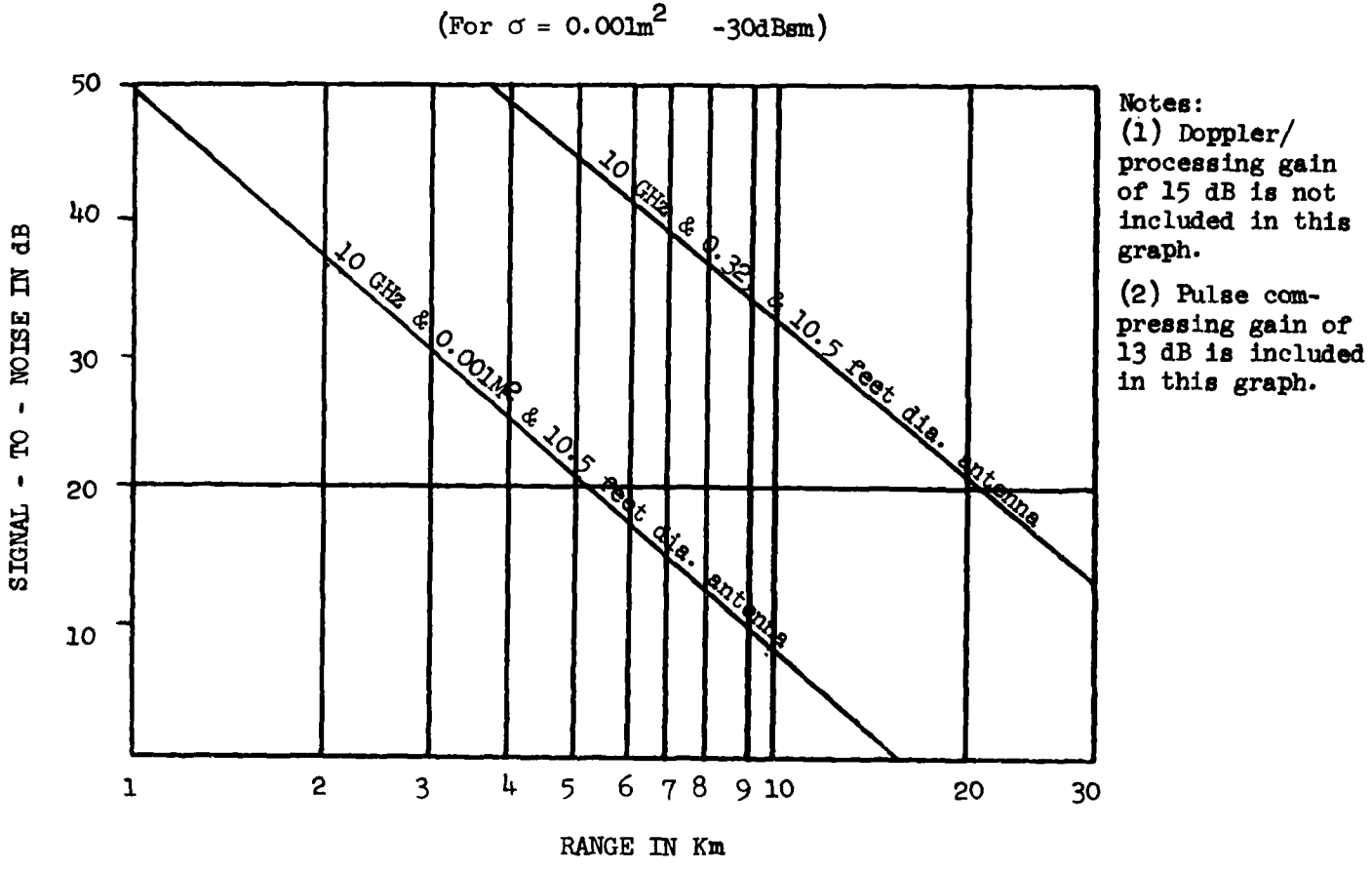

Figure 5-3. Signal to noise -- 10.5 foot X band antenna.

Figures 5-1, 5-2, and 5-3 are extensions of the data from Table 5-1 for different frequencies, target sizes, antenna diameters, and target ranges. The key point is the ability of a 50 kilowatt peak power transmitter to develop adequate (i.e., 20 dB) single-pulse, signal-to-noise ratios for selected combinations of frequency and antenna diameter.

Table 5-3 shows frequency, coherency, tube type, duty percent (%), price, pulsewidth, peak power, and tube delivery time. There are no significant differences in the tubes required for the different frequencies. In general, 10 GHz tubes are better understood and, therefore, easier to engineer into a transmitter than either the 17 GHz or the 35 GHz alternative. A 50 kW, 10 GHz transmitter with a pulse compression ratio of 13 to 1 achieves the same range performance as a short pulse radar with a transmitter peak power of approximately 650 kW. At X-band, 1 MW tubes exist, and a short pulse transmitter could be used. At 17 GHz or 35 GHz, the required peak power of a tube to implement a short pulse radar exceeds 500 kW, and tubes are not readily available.

5.2 SIGNAL PROCESSING DATA RATE

Figure 5-4 is a representation of the MIDI II sampling space. The sampling space is composed of 141 contiguous range bins, and each bin's range extent is 16 feet. The total extent of the range window is 2256 feet. The 141 samples are reduced by the pulse compression process to 141 - 13 = 128 range bins. The total energy is illustrated as contained in an angular space bounded by ΔEL and ΔAZ, the 3 dB beamwidths of the antenna.

The sampling space of Figure 5-4, a projectile velocity range of 500 to 1000 meters per second, and a PRF rate of 4000 Hertz were used to develop the following reference values:

Range Bin	-	16 feet/4.88 meters
Projectile Velocity	-	500 to 1000 m/s
PRF	-	4000 Hz
Projectile Time Per Range Bin	-	0.005 to 0.01 seconds

TABLE 5-3. TRANSMITTER TUBE REVIEW

FREQUENCY (GHz)	COHERENT	TUBE TYPE	DUTY (%)	PRICE (K $)	PULSEWIDTHS POSSIBLE (ns)	PREFERRED (ns)	PEAK POWER (mw)	AVAILABILITY (Months)
10	Yes	TWTA(1)	10	200	30	50-500	.05 - 1.0	6 - 9
17	Yes	TWTA(1)	10	200	30	50-500	.05	6 - 9
35	Yes	TWTA(1)	10	200	30	50-500	.05	6 - 9

NOTES:
1. TWTA - Traveling wave tube amplifier.

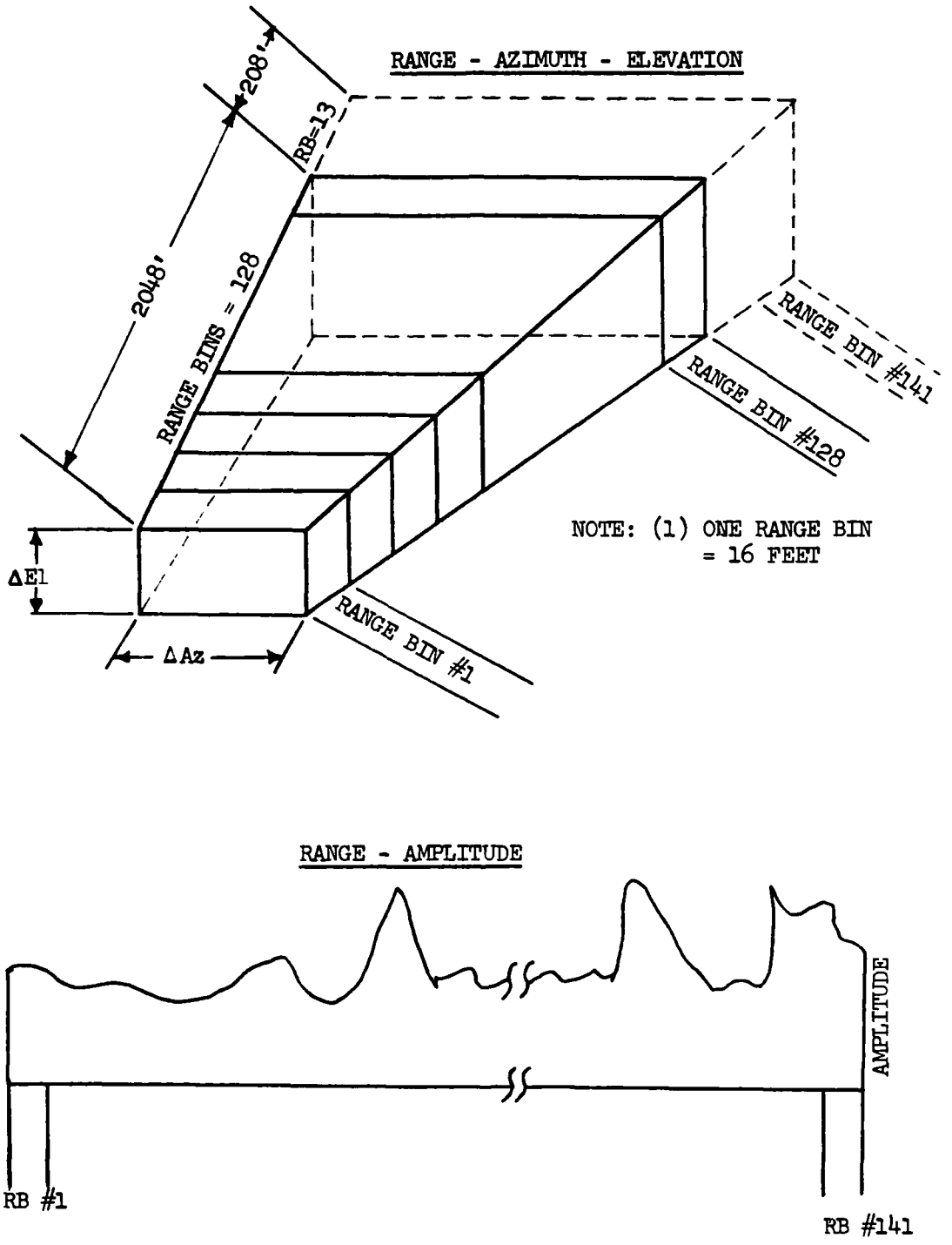

Figure 5-4. MIDI II sampling space.

Number of Samples
Per Range Bin
Per Projectile - 20 to 40 samples

Figure 5-5 contains a high level analysis of the signal functional flow. The signal flow of this figure is composed of these parts:

1. A transmitter and receiver develop four bipolar voltages of the form $\pm\Sigma/2 \pm j\ \Delta(\ )/\sqrt{2}$.

2. The four bipolar signals are in-phase and quadrature-phase sampled once for each 16 foot range bin. This requires a sample rate of approximately 32 MHz. A nine-bit, analog-to-digital (A-to-D) device was chosen because of their availability and the attendant 54 dB of dynamic range.

3. The eight nine-bit samples are stored in a memory for 32 PRI's. The structure of this memory is shown in Figure 5-6.

4. The fast Fourier transform is applied to each of the four complex sampled signals for the 32 PRI's. The energy of each signal is resolved into Doppler bins of width 125 Hertz. Because the maximum Doppler shift corresponds to 60,000 Hertz, the PRF of 4000 Hertz undersamples the Doppler by a factor of 15. This creates a 15 to 1 Doppler foldover in the FFT output, but the foldover is not a problem as the velocity of the projectile will be accurately known before the radar detects the projectile. This prior knowledge can be used to resolve this Doppler foldover (Doppler ambiguity).

The FFT's required per second if the FFT is calculated for each batch of 32 PRI's are:

$$\frac{\text{FFT's}}{\text{SEC}} = (141\ \frac{\text{RANGE}}{\text{BINS}})\ (\frac{4\ \text{COMPLEX SIGNALS}}{\text{BIN}})\ (\frac{4000}{32}\ \frac{\text{PRI}}{\text{SEC}}) \qquad 5.1$$

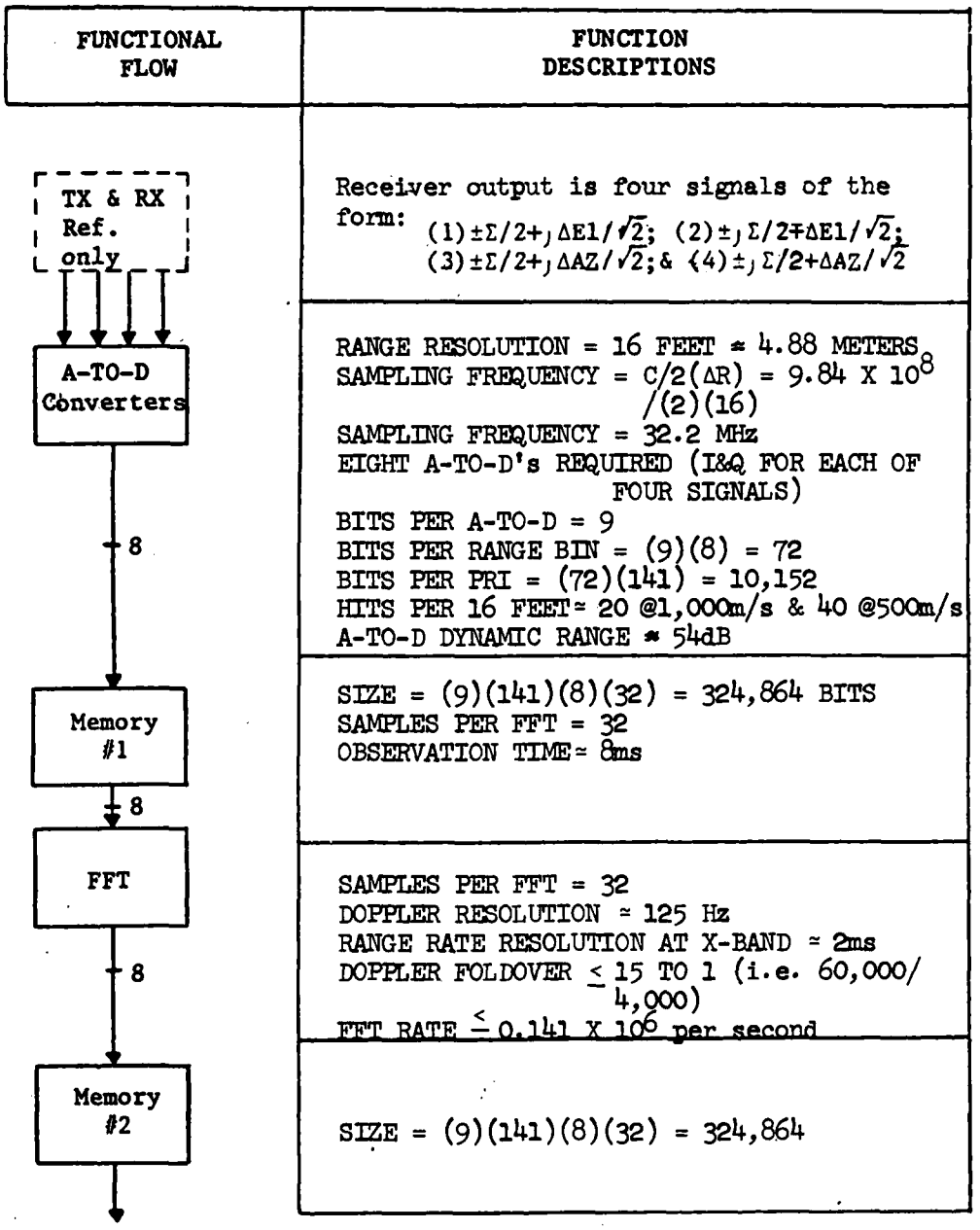

Figure 5-5. Signal functional flow.

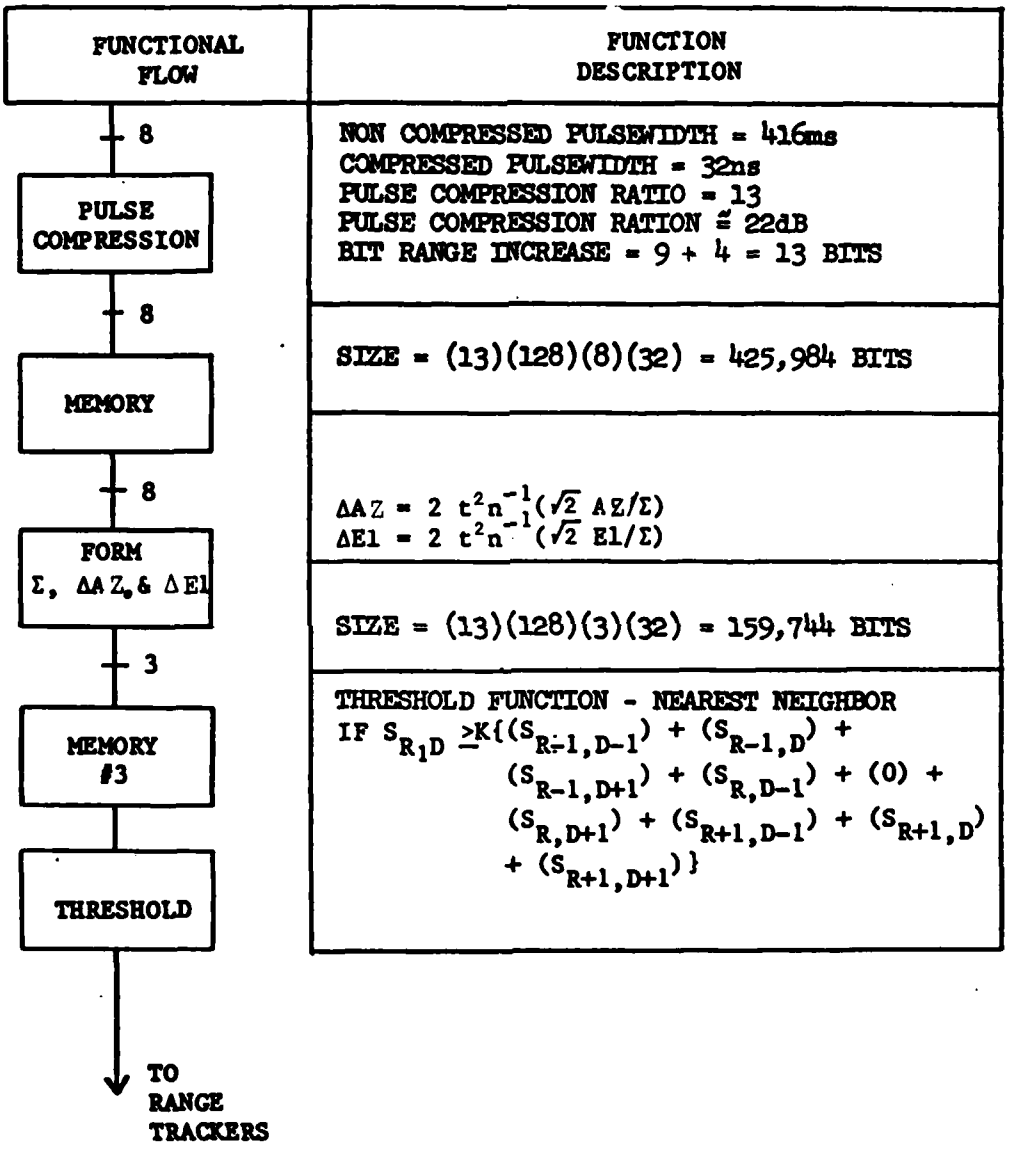

Figure 5-5 (continued)

MEMORY SIZE = (9 BITS/RANGE CELL) (141 RANGE CELLS/MEASUREMENT)
(8 MEASUREMENTS/PRI) (32 PRI)
= 324,864 BITS

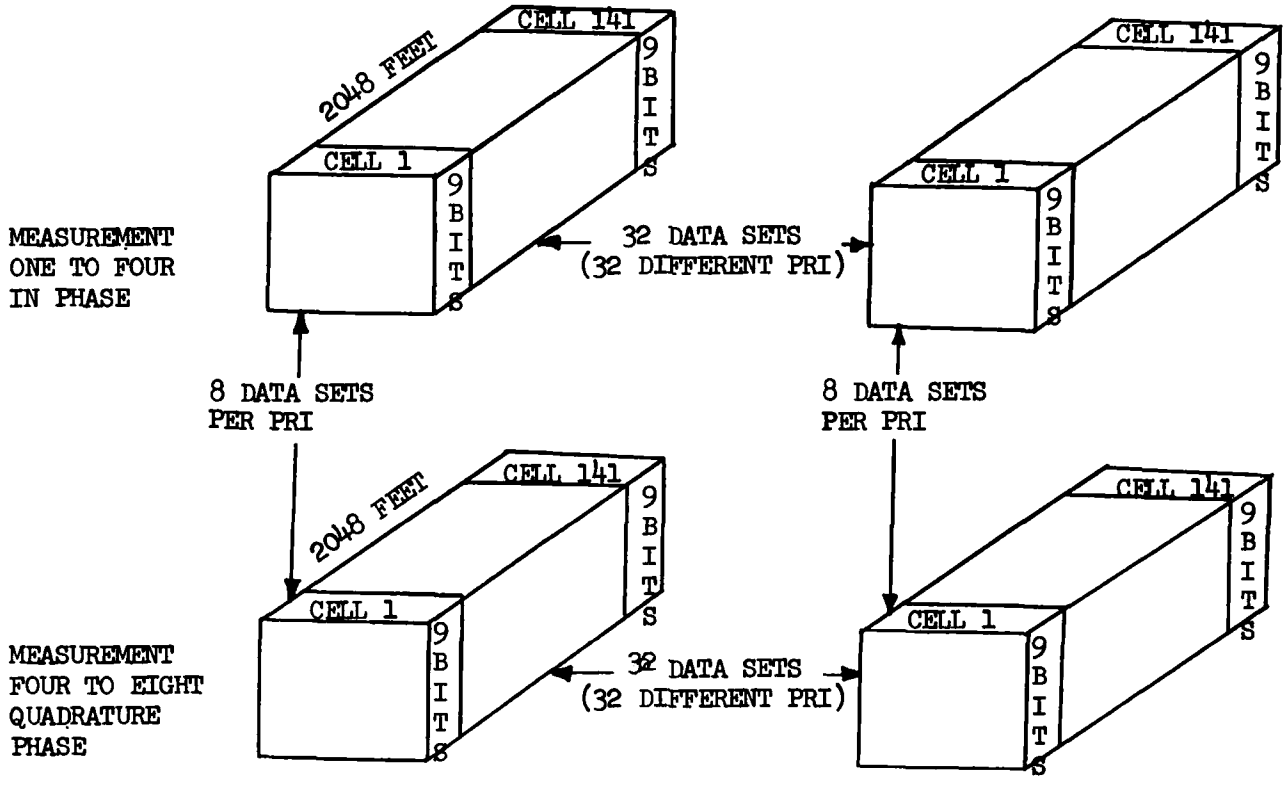

Figure 5-6. Memory number 1 structure.

$\frac{FFT'S}{SEC} = 70,500$.

The Westinghouse, Inc., Very High Speed Integrated Circuit (VHSIC) contract calls for a Complex Arithmetic Vector Processor (CAVP) which computes a 1024-point FFT in 131 microseconds. A recent proposal by another manufacturer contained a hardware description for a 1024-point FFT in 50 microseconds.

The computational complexity controls the time execution of an FFT. The computational complexity for an N-point FFT is N $\log_2$ N. A 1024-Point FFT has a computational complexity of 10,240 while a 32-point FFT has computational compelxity of 160. The complexity ratio these two different length FFT's is 64 to 1. This ratio gives a 32-point FFT performance time of approximately 2 microseconds. The CAVP is expected to produce 500,000 FFT's per second. Also, this computation rate is within the capability of some commercial array processors such as the one described later inthis section. The components required to meet the MIDI II FFT requirements will be available.

6. The FFT data are stored in an amplitude - range - Doppler map (i.e., memory #2).

7. A pulse compression ratio of 13 to 1 is applied to the data of the amplitude - range - Doppler map. A thirteen-bit correlation process is one method of performing the pulse compression. This process has been performed at rates of 100 MHz for codes of 64 bits by Georgia Tech. The number of correlations which can be performed during a time period corresponding to 32 PRI is 80,000. The required number of correlations is 4512 per 32 PRI.

8. The compressed pulse data are stored in an amplitude - range - Doppler map. This map is contained in memory #3 whose structure is illustrated in Figure 5-7.

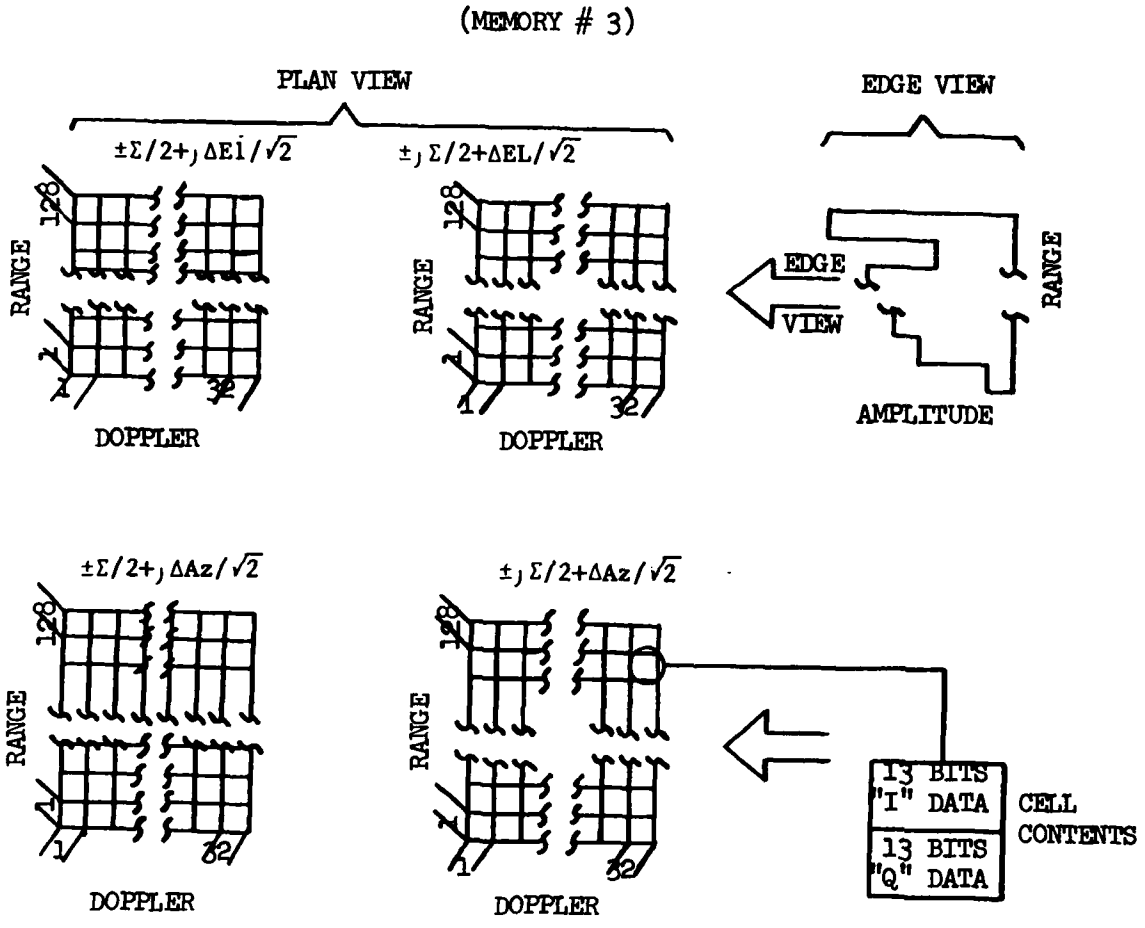

Figure 5-7. Memory number 3 structure.

9. The sum and angle error terms are formed. The required computation rate is estimated as:

$$\text{Req. Op. Rate} = \frac{(20 \text{ Ops})\ (128 \text{ Range Bins})\ \left(32 \frac{\text{Doppler Bins}}{\text{Range Bin}}\right)}{8 \text{ ms}} \qquad 5.2$$

$$\text{Req. Op. Rate} = 10.24 \times 10^{6} \text{ Ops/sec.}$$

10. The sum and angle error voltage are stored in memory #4.

11. A nearest neighbor or "thumb tack" threshold function is applied to detect targets. This requires less than ten operations per range - Doppler bin. There are 4096 range - Doppler bins so the required operations are 40960 or less. The required operations rate is:

$$\text{Req. Op. Rate} = \frac{4096}{8 \times 10^{-3}} = 512{,}000 \text{ Ops per sec.} \qquad 5.3$$

12. Not shown in Figure 5-2 are the range trackers. This function divides into the three functions of:
    (a) Real time track of the projectile target.
    (b) Near real time sorting of the data into subsets which are associated with a particular projectile.
    (c) Near real time fitting of a projectile trajectory to each subset of projectile data.

The real time track of the target can be implemented in a early-late gate tracker followed by double integration of the error from the early-late gate tracker. The tracker will use the data from the threshold function as input to a digital tracker implemented in software. The target tracker will remain on the target because of prior track data, because of Doppler difference between the projectile and the target, and because of the amplitude difference between the projectile and the target returns.

The near real time sorting of the projectile data will be based primarily on the projectile Doppler shifts. The initial range separation between projectiles is equal to or greater than approximately 55 feet if the muzzle velocity is equal to or less than 1000 meters per second and the firing rate

is equal to or less than 3600 rounds per minute. For a five second or less projectile time-of-flight, the differential velocity required for two projectiles to pass each other is 11 feet per second or greater. The Doppler resolution of the FFT is 125 Hz, or 6.8 feet per second, at a radar center frequency of 10 GHz. Therefore, the FFT output combined with the firing time of the projectiles will allow the data set to be subdivided by projectile. The near real time trajectory fit could be executed as a Kalman Filter. The maximum data points per projectile will be approximately 150 for a 2048 foot range data structure and a projectile with a velocity of 500 meters per second. The trajectory fit will use 150 or less data points composed of T, R, $\dot{R}$, A_Z, and E_l (Time, Range, Range rate, Azimuth, and Elevation).

5.3 COMPUTER SELECTION

Several hardware sets exist that can perform the high speed signal processing required to reduce the front end data to a data-stream which is within the performance envelope of a general purpose embedded computer. One choice is the SPS-1000 array processor shown in Figure 5-8. This machine is available off-the-shelf from Signal Processing, Inc. of Waltham, Massachusetts, and it possesses the capabilities needed to do the MIDI II front end processing. With the addition of the eight, 9-bit, 32 MHz, analog-to-digital converters, the SPS-1000 array processor could perform the signal processing functions at the required data rates (i.e., 32-point FFT in 10 microseconds) for the signal processing flow developed in Figure 5-2.

The General Purpose Processor attached to one of the SPS-1000 ports could be a PDP-11 class machine with a software development environment for both the PDP-11 and the SPS-1000. This approach will ensure that the computer software can be supported in the field for both machines.

A General Purpose Mini-Computer of the PDP-11 class is needed to perform the functions required. The three most critical functions are:

1. To supply a well supported software development environment for the signal processing hardware.

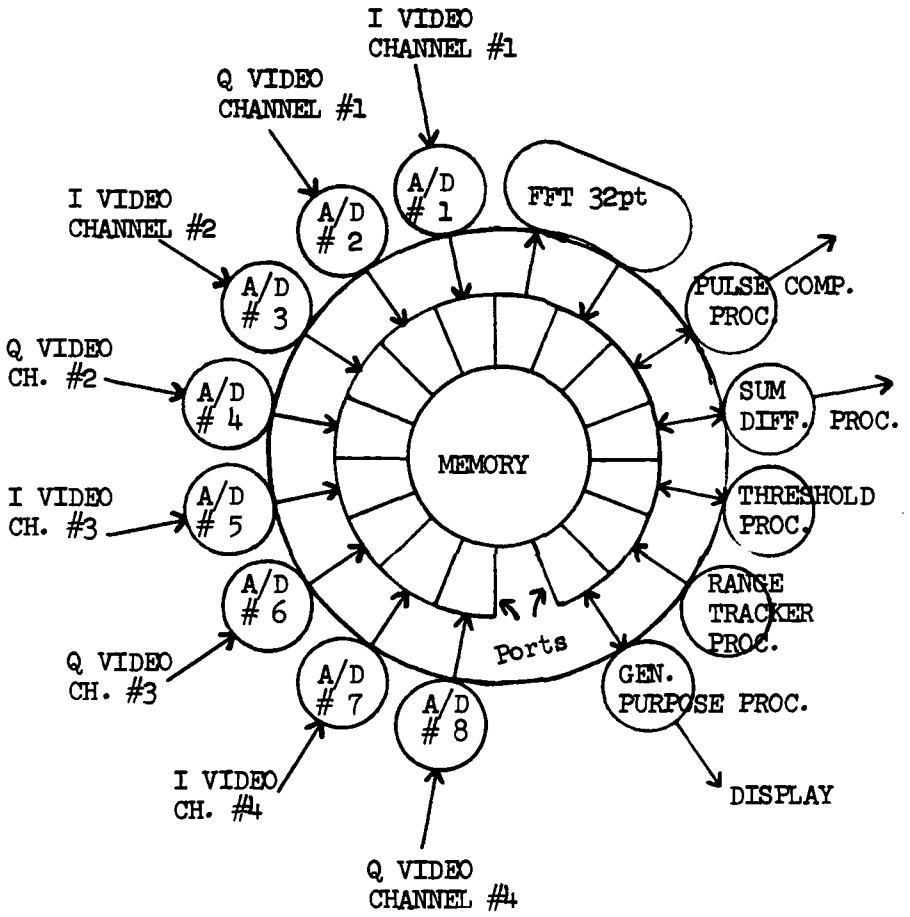

Figure 5-8. SPS-1000 processing architecture.

2. To route the reduced raw data from the SPS-1000 class machine to a disk or tape storage machine.

3. To perform the miss distance calculation.

The first function is ensured by the wide range of applications for which PDP-11 machine have been used.

Some characteristics of the PDP-11/44M are shown in Table 5-4.

TABLE 5-4. PDP-11/44M CHARACTERISTICS

Instruction	Timing
Move	1.19 microsecond
Add 1.01 microsecond	
Multiply	6.38 microsecond
Divide	10.76 microsecond
Floating Point Processor	
Add-32 Bit-Single Precision	8.9 microsecond
Multiply-32 Bit-Single Precision	16.2 microsecond
Memory	
Cycle Time-Core	900 microsecond
Read Access	452 microsecond
Input/Output	
I/O Rate	< 1.1 Mega-Words per second

The calculated I/O Rate for the MIDI II is 15,000 16-bit words per second. This is well within the 1.1 MW/s of the PDP-11/44M.

The processing rates of the PDP-11/44M are adequate to complete the miss distance calculation for 40 targets within a few minutes after the test is completed.

In Figure 5-9, a conceptual organization of the remote radar is shown. This figure is based on the assumption that all the digitized data would be transmitted via a fiber optics communications system to the signal processor van. Further analysis of the remote radar concept is contained in Section 6.

In Figure 5-10, a conceptual organization of the radar and the signal processing are shown. The signal processing concept selection was chosen to meet these objectives:

1. Transmit the full raw digitized data set to the SPS-1000.
2. Process the raw data set to produce raw detected-target data set.
3. Record the full detected-target raw data set on the disk.
4. Post operation, record the detected-target raw data and the processed data on the tape.
5. Select a computer and software development environment which allows both development and maintenance of the software for both the PDP-11 and the SPS-1000.
6. Make all operational programs available in either the memory of the SPS-1000 or the PDP-11.
7. Make quick load programs available on the disk.

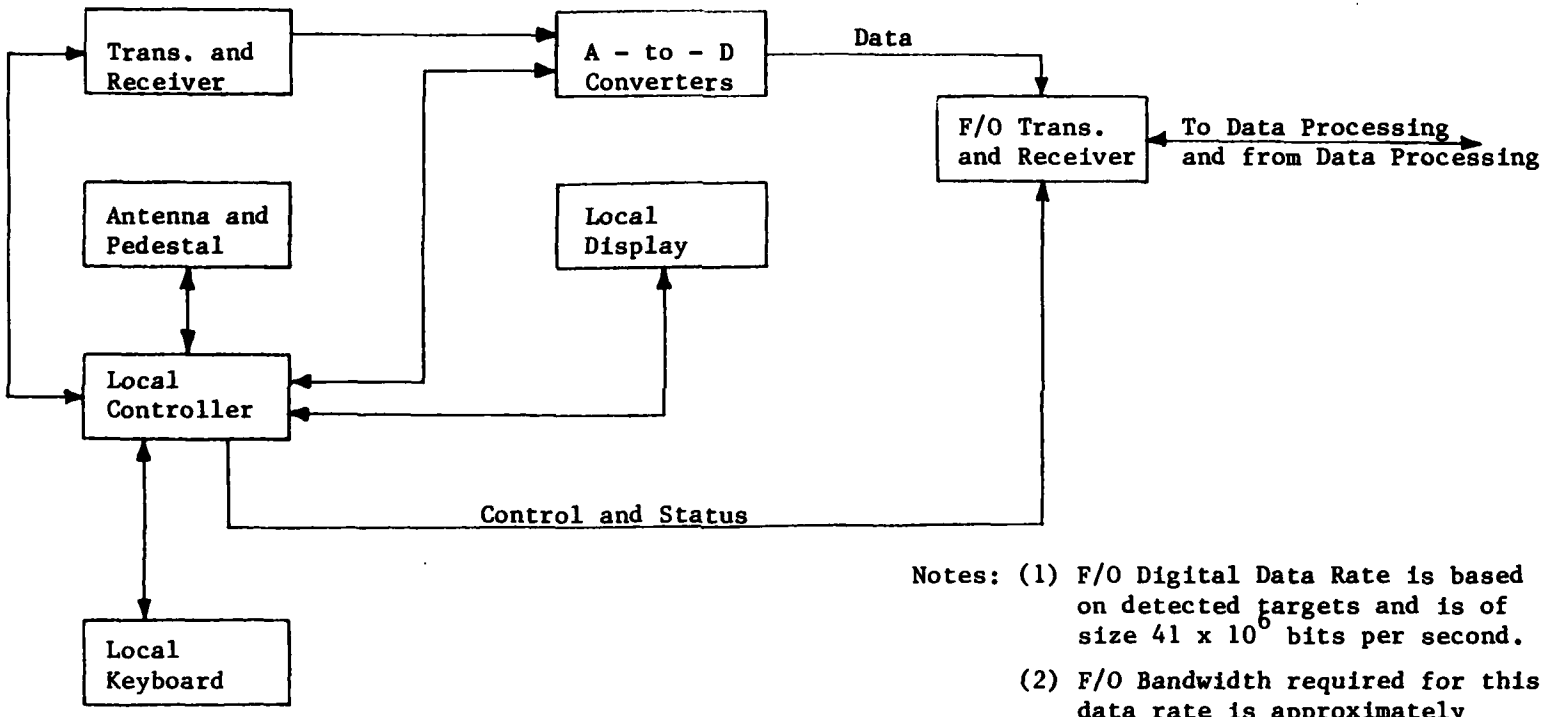

Notes: (1) F/O Digital Data Rate is based on detected targets and is of size 41 x 10^6 bits per second.

(2) F/O Bandwidth required for this data rate is approximately 410 x 10^6 Hertz.

(3) The F/O System will use an injection laser diode (ILD) and avalanche photodiodes.

Figure 5-9. Remote radar concept.

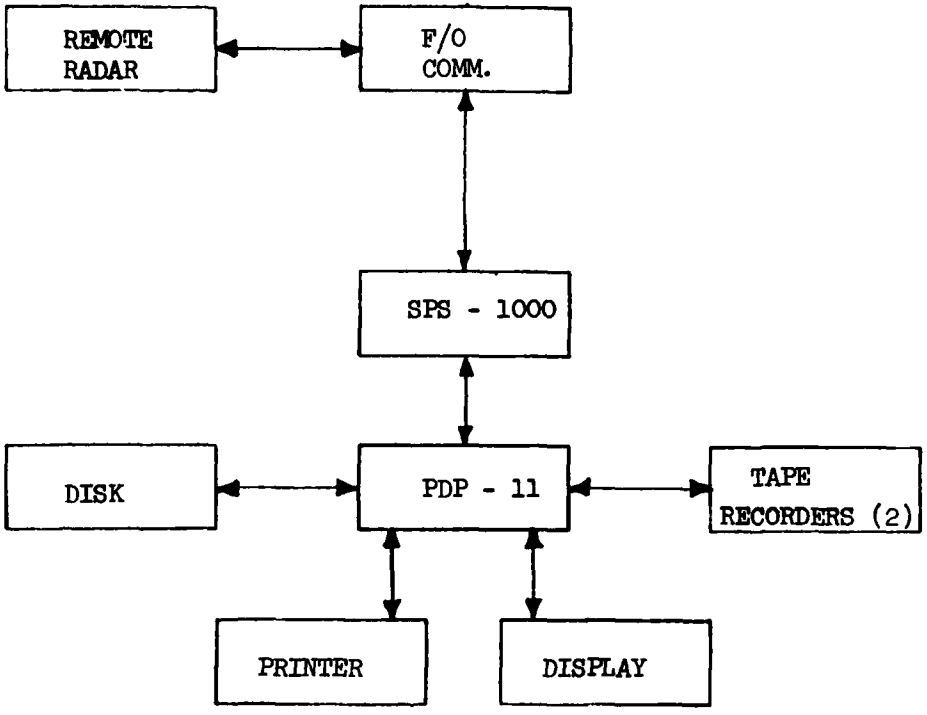

Figure 5-10. Radar and data processing.

SECTION 6

REMOTE ANTENNA CONCEPT

Without Doppler processing, the MIDI II would be limited to tracking targets at 3.5 or more beamwidths above the ground. With Doppler processing, the MIDI II would be limited to tracking targets at 0.8 or more beamwidths above the ground. Even with Doppler processing, the desired coverage is not completely provided when the MIDI II is located behind the gun or missile launcher.

A low risk technical alternative to a multifrequency radar for increasing the coverage is the remote location of the radar as initially shown in Figure 5-9.

The prefered solution is composed of these elements:

1. A coherent X-band transmitter.
2. A general purpose computer for local and remote control of the remote radar.
3. A fiber optics communication system to route the data between the signal processing van and the remote radar.

These elements are shown in the concept drawing Figure 5-10.

In Figures 6-1 and 6-2 a remote X-band system with beamwidths of 2.5 and 1.25 degrees is shown overlaid on the missile and gun scoring envelopes of the MIDI II requirements. The remote antenna is located at 11.5 km for the missile case and 2.5 km for the gun case. The coverage percentage for the missile case is approximately 50 percent per site location for the large antenna at one beamwidth ground clearance. The coverage percentage for the gun case is approximately 90 percent per site location for the large antenna at one beamwidth ground clearance. Army test personnel can easily construct other examples for specific test scenarios.

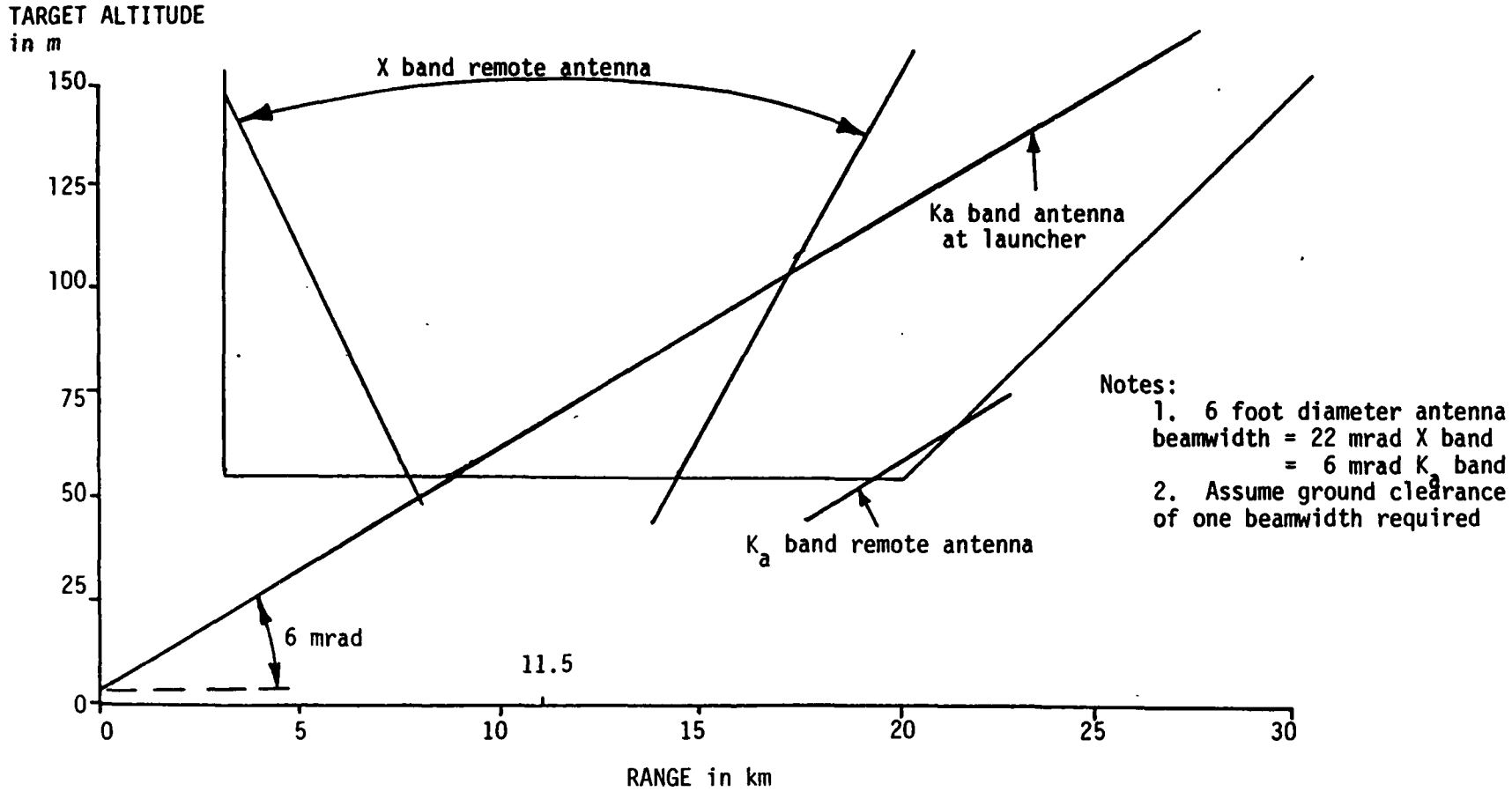

Figure 6-1. Remote antenna coverage -- missile scoring.

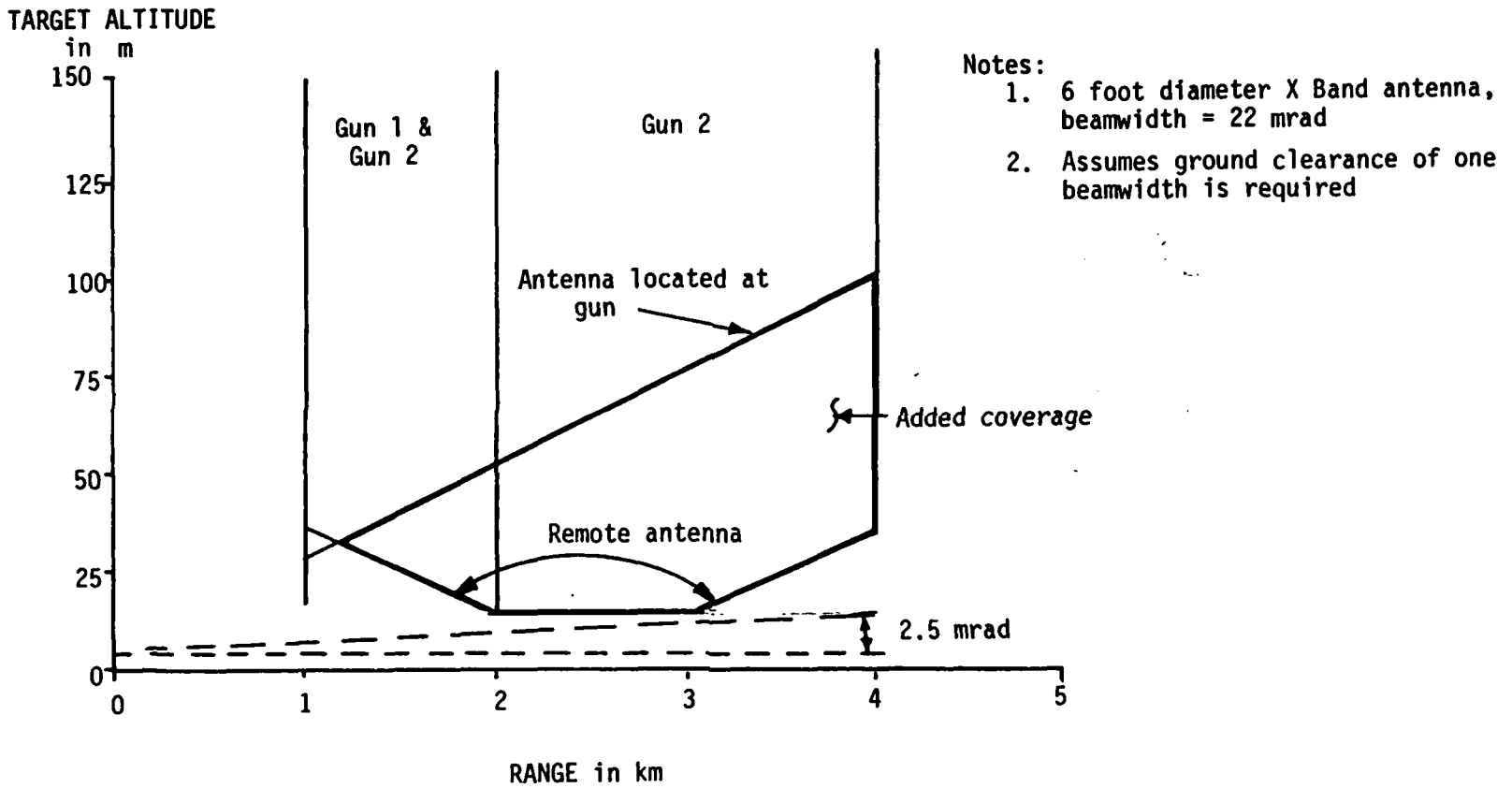

Figure 6-2. Remote antenna coverage - - gun scoring.

SECTION 7
CONCLUSIONS

The major conclusion of this study is that the MIDI I limitation when operating against targets 500 feet (150 meters) or more above ground level can be improved down to 15 meters for gun scoring and 60 meters for long range missile scoring by applying the combination of radar techniques listed below.

1. Pulsed Doppler (Moving Target Indicator) is required to operate at elevation angles less than 3.5 radar antenna beamwidths above the ground to attenuate the ground clutter. MTI permits operation down to 0.8 beamwidths above the ground.
2. Errors due to multipath interference will be less than 0.03 beamwidth when operating at elevation angles of 0.7 beamwidth or greater using conventional tracking and off-boresight scoring. If an elevation tracking bias is inserted to lift the antenna beam further off the ground, operation down to 0.5 beamwidths should be possible.
3. The radar must have multiple, selectable beamwidths to meet both the low altitude operation and the scoring volume requirements. Multiple transmitter frequencies, multiple antenna sizes, or a combination of both can be used.
4. A remote antenna/receiver/transmitter should be considered as a method for providing a favorable elevation ge metry. A second benefit is an increase in signal-to-noise ratio.
5. All of the candidate systems can be implemented with current technology.

SECTION 8
REFERENCES

1. "Mobile Miss Distance Indicator (MIDI) Final Technical Report," Westinghouse Electric Corporation, Data Item A003, Contract DAAD07-72-C-0155, May 1973.
2. Ruck, G. T., Editor, Radar Cross Section Handbook, Plenum Press, 1970.
3. Barton, D. K. and Ward, H. R., Handbook of Radar Measurements, Prentiss-Hall, 1969.
4. Skolnik, M. I., Radar Handbook, McGraw-Hill, Inc., 1970.

APPENDIX A
THREE DIMENSIONAL MULTIPATH INTERFERENCE MODEL

THREE DIMENSIONAL MULTIPATH INTERFERENCE MODEL

The Multipath Interference Model is used to calculate the signals arriving at the radar via each of the principal ground reflection paths. The model software was developed by John Peifer and Mike West in March through June, 1982, and was revised by Mike West in May, 1984 and Mark Clinard in June and July of 1984. The multipath returns parameter are calculated and output for an isotropic, unity gain antenna and a target with a unity cross section. Other computer programs which use these outputs must account for radar system parameters such as varying antenna directional patterns, beamwidths, etc. This appendix provides the following information:

1. A description of the output of the multipath model.
2. A description of the information needed to use the multipath model.
3. A synopsis of the mathematical and computational techniques used to produce the output parameters.

The multipath model considers a terrain composed of 24 x 175 square facets of equal area with sides of 88 meters. Indexing the facets with integers specifying the latitudinal and longitudinal coordinates, the model references an input file to provide parameters characteristic of each individual facet (terrain height, terrain type, etc.). Figure A-1 shows the faceting technique for a similar 40 x 40 facet terrain. Figure A-1c shows how the radar site, a target, and the surface in between the underlying facets would typically be located with respect to the faceted terrain.[A1]

The most fundamental physical parameter describing the reflection properties for the terrain facet is its dielectric constant. Given the user's information specifying a wet or dry scenario, the model considers six different types of terrain that may characterize each facet:

A1. M. S. West, "A Multipath-Clutter Model for SAMS," Final Report on Contract F33615-81-C-1487, Georgia Institute of Technology, Engineering Experiment Station, December 1983.

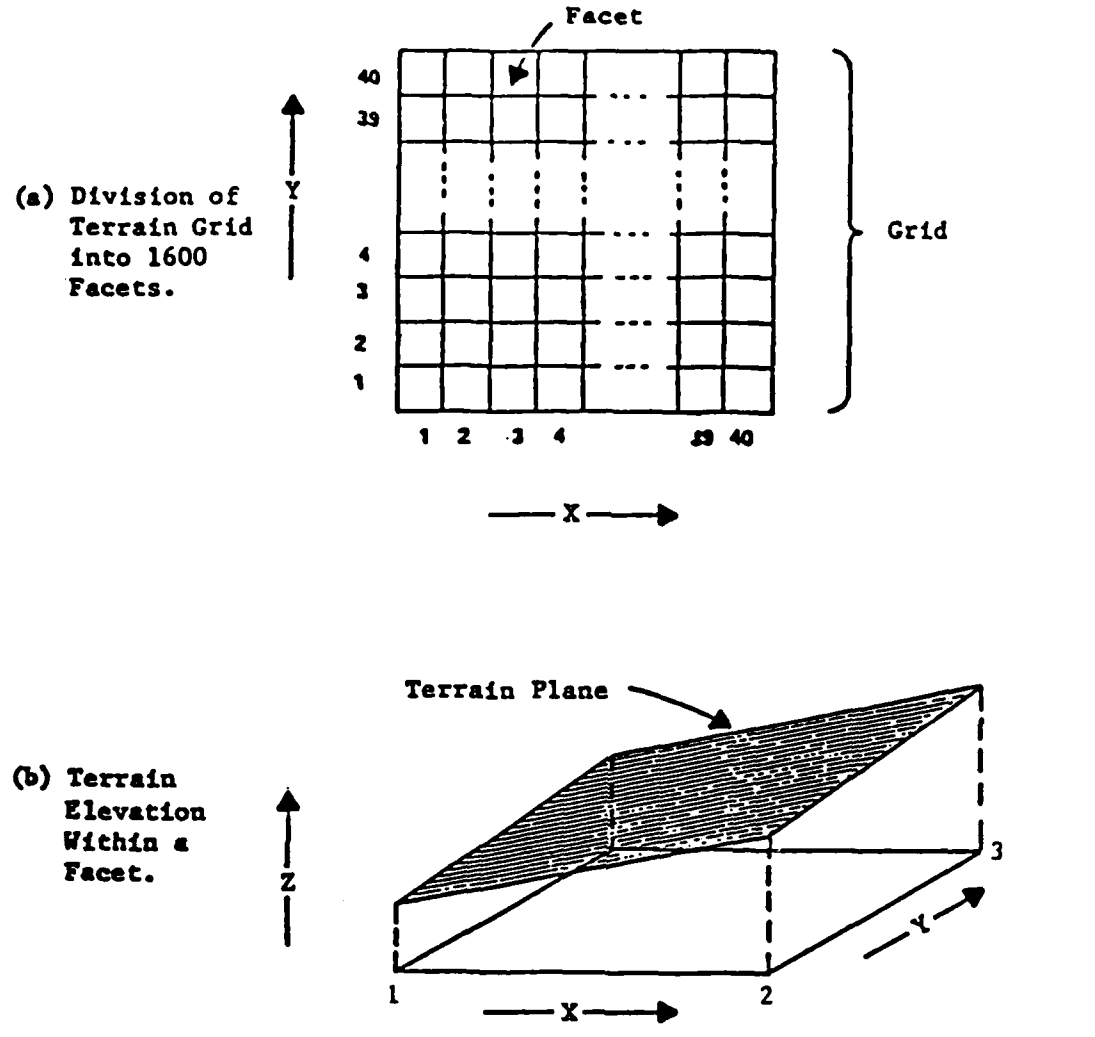

Figure A-1. Overview of the faceting technique.

1. Sea	4. Crops
2. Soil	5. Trees
3. Grass	6. Sand

The dielectric constants were experimentally determined for the X-band frequency range. They are shown in Table A-1. The Fresnel reflection coefficient ρ_o is evaluated for either horizontal or vertical polarizations:

$$\rho_o = \frac{\varepsilon_r \sin\psi - (\varepsilon_r - \cos^2\psi)^{1/2}}{\varepsilon_r \sin\psi + (\varepsilon_r - \cos^2\psi)^{1/2}} \quad \text{for vertical polarization} \qquad (A1)$$

$$\rho_o = \frac{\sin\psi - (\varepsilon_r - \cos^2\psi)^{1/2}}{\sin\psi + (\varepsilon_r - \cos^2\psi)^{1/2}} \quad \text{for horizontal polarization} \qquad (A2)$$

where:

ψ = the incident angle on the facet

and ε_r = the dielectric constant

With the scenario geometry, the terrain characteristics, the operating frequency, the transmitted power, the gain of the transmitter, and target established, the multipath program computes the following output:

1. The direct return from the target:* (real number).
2. The range and elevation angle from the receiver to the specular facet at which the reflected RF energy from the target to the surface to the receiver obeys Snell's Law.
3. The returns from the target to the receiver via two different paths, both of which involve the specular facet: (complex number).

---

* Note that all returns are in terms of voltages; therefore, the returns are proportional to $1/R^2$ instead of $1/R^4$.

TABLE A-1 DIELECTRIC CONSTANTS

	TERRAIN TYPE	CONDITION	REAL	IMAGINARY
1.	Sea	WET	65..0	30.7
		DRY	65.0	30.7
2.	Soil	WET	20.0	2.4
		DRY	2.44	.00267
3.	Grass	WET	20.0	0.0
		DRY	2.0	0.0
4.	Crops	WET	0.0	0.0
		DRY	0.0	0.0
5.	Trees	WET	0.0	0.0
		DRY	0.0	0.0
6.	Sand	WET	13.1	5.8
		DRY	2.4	0.1

a. The direct-indirect path composed of the ray from the radar to the target, the ray from the target to the specular facet, and the returning ray to the receiver.†

b. The indirect-indirect path composed of the transmitted ray from the radar to the specular facet, the reflected ray to the target, and the identical return path taken by the direct-indirect path back through the specular facet.

4. The diffuse multipath return coefficients from the individual facets for the indirect-indirect and direct-indirect paths provided that the sub-facets satisfy the following criteria enumerated by West:
   a. The sub-facet is sufficiently illuminated.
   b. The radar echo of the sub-facet is not clearly separated from the radar echo of the target.
   c. The facet is not shadowed by surrounding facets as illustrated in Figure[A-2].
5. The range, elevation angle, and azimuth angle to each sub-facet from the radar site from which the diffuse multipath is calculated.

Item #4, the diffuse return, is given in the form of the mean of the Gaussian phase distribution of the return voltages and the standard deviation of the distribution; thus, the standard deviation for the two paths is a measure of the returned voltage. (Both the mean and standard deviation are complex quantities.)

Figure A-3 illustrates the three possible return paths.[A-1]

Several inputs which are qualitatively described here are needed to use the multipath model. First, a file describing the terrain and each of its facets must be accessed to provide:

1. The longitudinal and latitudinal dimensions of the terrain in units of facets along with scaling factors and offsets.

---

† Note that the indirect-indirect return and the indirect-direct return are considered equivalent by this particular model since the model uses an isotropic transmitter and receiver.

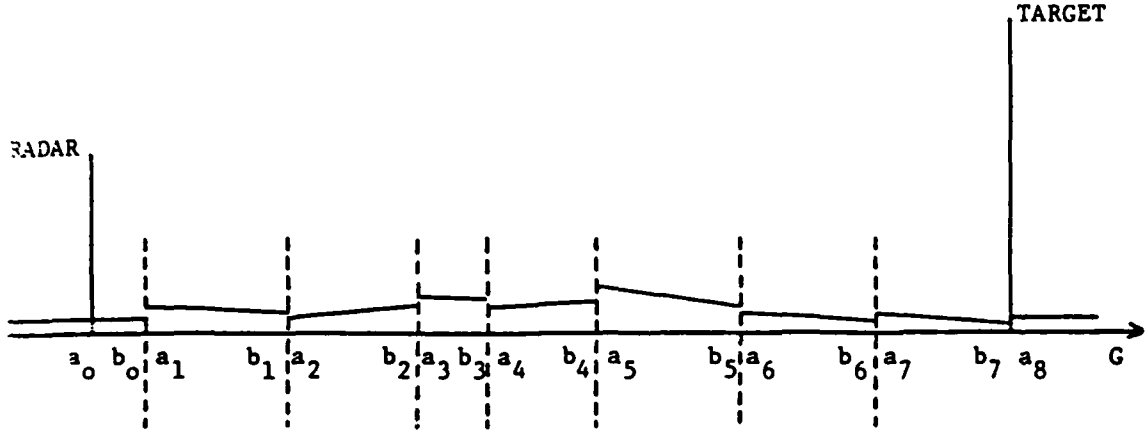

Profile of terrain cross section as approximated by facets.

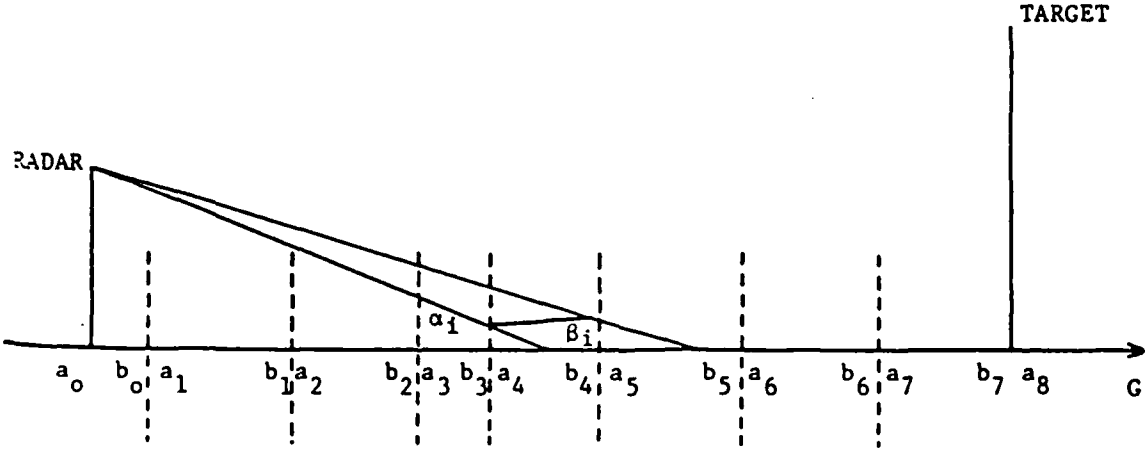

A facet is shadowed if $\beta_i > \min[\alpha_1, \cdots, \alpha_i, \beta_o, \cdots, \beta_{i-1}]$.

Figure A-2. Elevation view of facets.

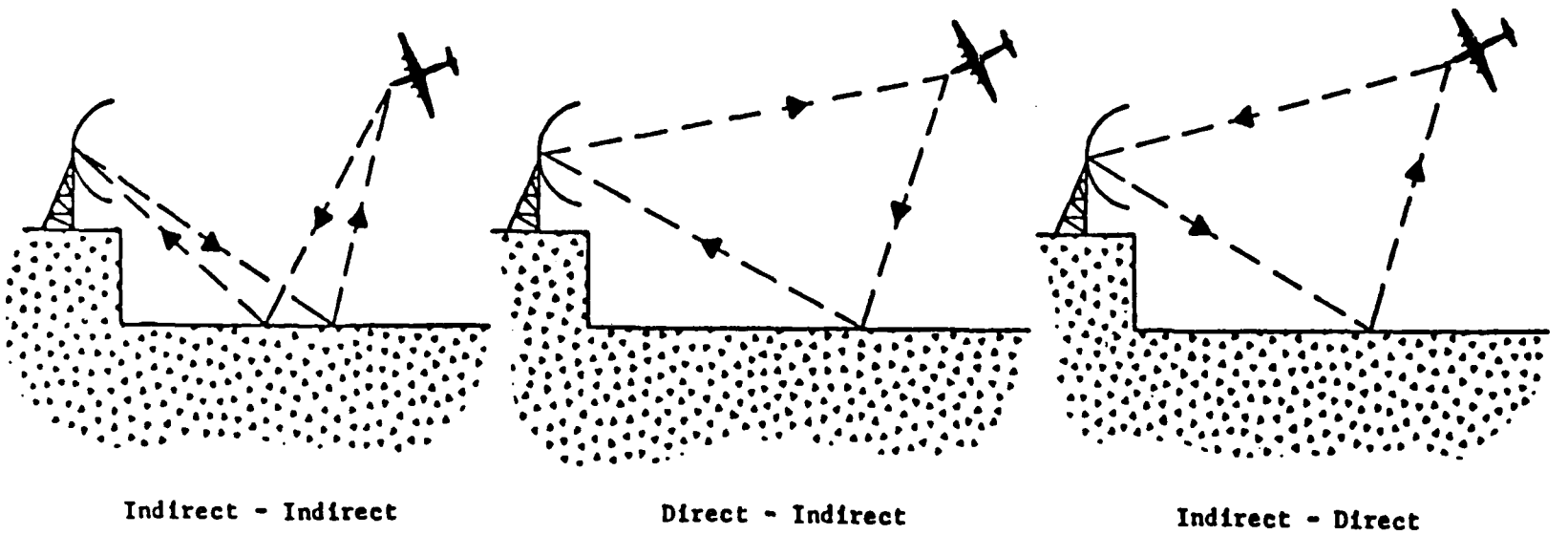

Figure A-3. Examples of multipath signal paths.

2. The three dimensional normal vector the surface of each facet.
3. The terrain height of each facet.
4. The terrain type of each facet.

A user input file provides three vectors: the position of the target, the velocity of the target, and the velocity of the receiver (normally set equal to [0,0,0]).

Each time the multipath program is run for a new scenario, the user is prompted for these mutable conditions:

1. Horizontal or vertical polarization?
2. Wet or dry terrain?
3. The receiver half-bandwidth?
4. Site height is meters above the terrain surface?
5. RMS surface deviation for the entire terrain?

The location of the radar site is currently set in the middle of the 24-facet-wide field at 1000 meters latitude and 276 meters down-range. The radar site height is set by the coinciding facet height plus the input site height, as described in item #4 above.

The qualitative outputs of the multipath model have been described along with the inputs needed to use the program. The exact equations used, the exact criteria for evaluating contributions to the multipath return, and the particular parameters and results of the MIDI analysis are then ready to be specified.

The direct return coefficient is calculated from the radar equation:

$$\text{DIRECT} = (2\pi/k_d)\sqrt{P_t/(4\pi)^3}\, G_t/R^2 , \qquad \text{(A-3)}$$

where:

k_d = the Doppler shifted wave number at the receiver,
R = the line-of-site range from the receiver to the target,
P_t = the transmitted power,
G_t = the gain of the transmitter antenna.

In the runs for the MIDI analysis, the operating frequency was 10.125 GHz. Typically, the target was approaching the receiver at a velocity of 100 m/s. The transmitter antenna gain, an internal variable of the program, was set equal to unity.

For the return from the specular facet, the model first locates the specular facet at which the RF energy is reflected according to Snell's Law by considering the coordinates of the receiver and the target. The line-of-sight range from the receiver to the specular facet and the elevation angle at the receiver down to the specular facet is output. (The elevation angle is equal to the complement of the off-normal incident angle and the reflected angle.) The direct-indirect and the indirect-indirect return coefficients are then computed.

The direct-indirect and indirect-direct returns are equivalent for the case of an isotropic antenna as assumed in the MIDI analysis and are summed together for the output. The summed direct-indirect (DI) coefficient is calculated from the radar equation and the reflection coefficients described below:

$$DI = (2\rho_v \rho_o \rho_{rms} \kappa G_t / R^2) \exp(jk\Delta R) \qquad (A-4)$$

where:

- κ = $\lambda\sqrt{P_t/(4\pi)^3}$
- k = the transmitted wave number (ω/c)
- ΔR = (receiver to the specular facet range) + (target to the specular facet range) - R
- ρ_v = the vegetation reflection coefficient ($0 \leq \rho_v \leq 1$ and $\rho_v = 1.0$ for sea, soil, and sand.)
- ρ_o = the Fresnel reflection coefficient
- ρ_{rms} = $\exp(-2(k\sigma_h \sin\psi)^2)$
- σ_h = the user-input rms surface deviation

All of the terrain used for the MIDI analysis was of the type "sand." The input rms surface height deviation was 0.2 meters. The terrain was dry and the radar transmitted vertically polarized energy. The indirect-indirect (II) specular return coefficient is calculated from:

$$II = (\rho_v \rho_o \rho_{rms})^2 \kappa (G_t/R^2) \exp(jk\Delta R) \ . \qquad (A\text{-}5)$$

The consideration of the diffuse multipath return involves a much more complex analysis of the geometry of the model. All of the facets inside a rectangle whose sides are defined by the edges of the terrain and the downrange coordinates of the radar site and the target are initially considered for possible contributions to the multipath return at the receiver. First, criteria are applied to decide which of the 88 x 88 square meter facets will be subdivided into smaller subfacets so as to obtain better approximations for Doppler shifted returns. Secondly, criteria are applied to each facet or subfacet to determine if its contribution to the diffuse return is negligible or is to be evaluated. Finally, the location of each evaluated subfacet or facet, its DI return, and its II return are output in the form of range, elevation angle, azimuth angle, and the standard deviation and mean of the Gaussian phase distribution.

Ideally, Figure A-4 shows the facets which will be considered for diffuse multipath evaluation, but the program model used here considers (and perhaps tosses out) a much wider area for the prospective facets as described above.[A-2] Still, the facets darkened in Figure A-4 for the general case of a radar site and target placed in a faceted terrain will be the primary contributors of diffuse multipath return.

The model proceeds to loop over all the facets in the rectangular area between the site and the target, evaluating them one at a time. Each facet is divided into 25 subfacets of equal area to be evaluated in series along with

---

A2. S. P. Stuk, "TAC-ZINGER Clutter and Multipath Models for Track-While-Scan Systems," Software Documentation on Contract F49620-79-C-0222, Georgia Institute of Technology, Engineering Experiment Station, October 1980.

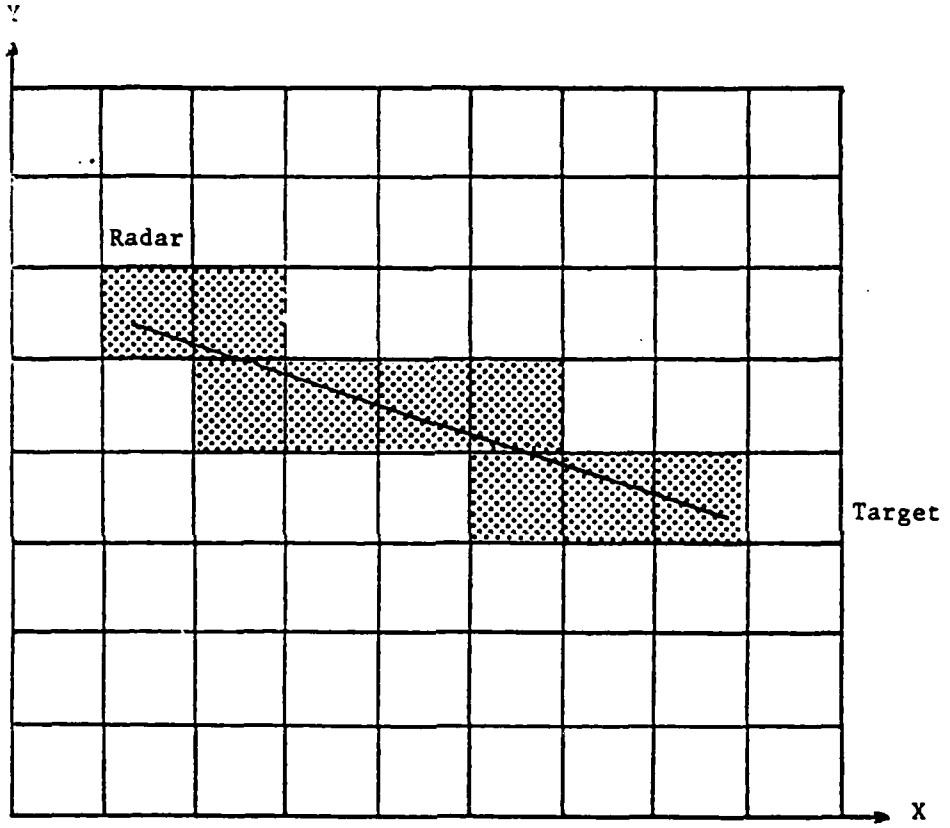

Figure A-4. Facets considered for use in diffuse multipath evaluation.

the remaining facets if its center is located at a line-of-site range greater than 3000 meters from either the target or the radar site. Thus, if large Doppler frequency variations occur over the area of the facet, it is to be subdivided.

As the facets and subfacets are evaluated serially, their contributions are neglected if:

1. The facet or subfacet lies outside of the cone defined by the receiver's half-beamwidth.
2. The line-of-sight (LOS) receiver-to-target range divided by the product of the LOS receiver-to-facet range and the LOS target-to-facet range is less than 1×10^{-9}.
3. $\tan^2\beta/\tan^2\beta_o < 50$

where:

β = the angle between the vector normal to the facet surface and the bisector of the angle between the LOS vectors from the facet to the receiver and from the facet to the target.

β_o = 0.2 (for our model)

If a subfacet or facet is not eliminated by any of these criteria, the model proceeds to calculate its contribution to the diffuse multipath return.

First, the diffuse reflection coefficients must be calculated for each of the two paths DI and II. A geometric mean factor involving the incident angles shown in Figure A-5 as ψ_1 and ψ_2 and the rMS surface height deviations is first calculated:[A1]

$$F_D^2 = (1 - \rho_{s1}{}^2)(1 - \rho_{s2}{}^2) , \qquad \text{(A-6)}$$

where:

$$\rho_{s1} = \exp(-2(k\sigma_h \sin\psi_1)^2)$$
$$\rho_{s2} = \exp(-2(k\sigma_h \sin\psi_2{}^2) .$$

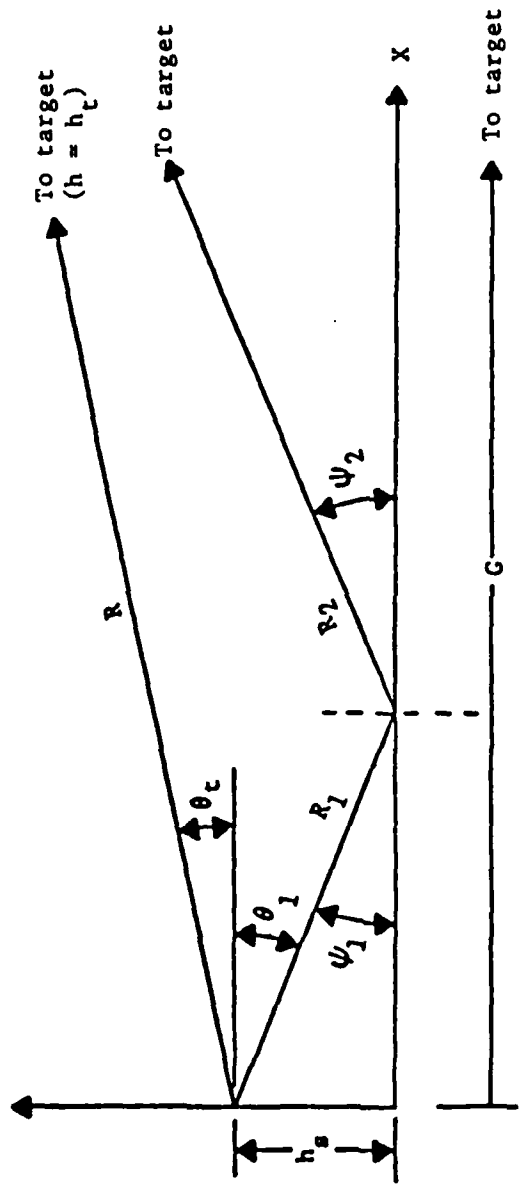

Figure A-5. Geometry of diffuse multipath reflection.

The diffuse part of the model assumes a vertical polarization. The diffuse reflection coefficient for the DI path then follows:

$$DI = \frac{\lambda\ \sigma_o F_D^2 |(\rho_o \rho_v)^2| F_t P_t \times SIDE}{R_1 R_2 (4\pi)^2}, \qquad \text{(A-7)}$$

where:

R_1 = LOS range from the facet to the receiver

R_2 = LOS range from the facet to the target

SIDE = the length of the side of the subfacet or facet

$\sigma_o = \exp(-\tan^2\beta/\tan^2\beta_o)/\tan^2\beta_o$

F_t = the antenna directional gain pattern (set = 1)

The reflection coefficient for the II path is:

$$II = \frac{\sigma_o F_D^2 |\rho_{o_1} \rho_v| (SIDE)^2\ P_t\ (F_t)^2 |\rho_{o_2} \rho_v|}{(R_1 R_2)^2 (4\pi)^{5/2}}, \qquad \text{(A-8)}$$

where:

ρ_{o_1} = the Fresnel reflection coefficient for ψ_1

ρ_{o_2} = the Fresnel reflection coefficient for ψ_2 .

Given the voltage reflection coefficients for the two paths weighted by the transmitter pattern and the area of the glistening subfacet, the model can calculate the reflected power from the facet (or reflected voltage).

The multipath model assumes that the reflected voltages are distributed in phase in the shape of a Gaussian curve. The model uses a Gaussian weighted random number generator to distribute the phases of 200 samples of the return from the subfacet being evaluated. Statistics are then extracted from the set of samples to provide the mean of the Gaussian phase distribution and the standard deviation. Thus, the standard deviation of the Gaussian is a relative measure of the energy inside the envelope and reflected from the subfacet. The LOS range to the center of the subfacet, the elevation angle, and the azimuthal angle with respect to the receiver are then output along

with the statistics for the DI and II paths. The total number of subfacets and facets evaluated for the diffuse multipath calculations are also output with the return data.

Options are available and were developed by Mark Clinard to map the diffuse return contributions in decibels on a printout of the 24 x 175 array representing the faceted terrain. Along with the total contribution of each facet being mapped, a map is provided detailing the number of subfacets that have evaluated inside each facet.

REFERENCES

A1. M. S. West, "A Multipath-Clutter Model for SAMS," Final Report on Contract F33615-81-C-1487, Georgia Institute of Technology, Engineering Experiment Station, December 1983.

A2. S. P. Stuk, "TAC-ZINGER Clutter and Multipath Models for Track-While-Scan Systems," Software Documentation on Contract F49620-79-C-0222, Georgia Institute of Technology, Engineering Experiment Station, October 1980.

APPENDIX B

ANGULAR ERROR VERSUS RANGE CURVES

This appendix contains the angular error versus range curves for the cases shown in Tables B-1, B-2, and B-3. Most cases contain curves for both conventional monopulse processing and MIDI processing. Each case is individually labeled.

TABLE B-1

1.3 DEGREE (22 MILLIRADIAN) BEAMWIDTH CASES

CASE	RDR ALT M	RHO MAG/PHASE DEG	TGT. ALT M	MISS M	MAX RANGE (M) FOR ERROR <1 MR	<0.5 MR
1	5	0.7/90	15	0	1250	1000
2	5	0.7/90	15	-5	2000	1300
3	5	0.7/90	15	+5	1500	1500
4	5	0.7/90	20	-5	1420	1170
5	5	0.7/90	20	0	1470	-
6	5	0.7/90	50	-10	4240	3710
7	5	0.7/90	50	10	4000	3500
8	5	0.7/90	50	15	5000	4800
9	5	0.7/90	50	-15	5200	3050
10	5	0.7/90	50	0	3910	3410
11	5	0.7/135	15	0	<1000	<1000
12	5	0.7/0	15	0	<1000	<1000
13	5	0.7/180	15	0	<1000	<1000
14	5	0.7/90	60	-10	≈ 5000	4000
15	5	0.25/90	15	0	All ranges	2000
16	5	0.7/90	70	-20	7240	4290
17	5	0.7/90	30	0	2300	1900
18	5	0.7/90	35	0	2750	2200
19	5	0.7/90	35	-5	2600	2300
20	15	0.7/90	50	0	4350	3760
21	15	0.7/90	50	10	4000	3500
22	15	0.7/90	50	-10	4240	3700
23	5	0.7/90	50	-20	3390	3200
31	5	0.7/90	15	0	1200	960
32	5	0.7/90	50	0	3780	3260
33	5	0.7/90	50	-10	4700	3850
34	5	0.7/90	50	10	4000	3480

TABLE B-2

1.3 DEGREE (22 MILLIRADIAN) BEAMWIDTH CASES, 0.33 DEGREE SQUINT

CASE	RDR ALT M	RHO MAG/PHASE DEG	TGT. ALT M	MISS M	MAX RANGE (M) FOR ERROR <1 MR	<0.5 MR
50	5	0.7/90	15	0	2000	<1000
51	5	0.7/90	15	-5	2000	1600
52	5	0.7/90	20	-5	3000	1900
53	5	0.7/90	30	0	4000	3000
54	5	0.7/90	30	-5	4400	2900
55	5	0.7/90	35	-5	5100	3300
56	5	0.7/90	60	-10	8900	5700
57	5	0.7/90	50	0	6900	4400
58	5	0.7/90	50	-15	8000	4600

TABLE B-3

0.4 DEGREE (6 MILLIRADIAN) BEAMWIDTH CASES

CASE	RDR ALT M	RHO MAG/PHASE DEG	TGT. ALT M	MISS M	MAX RANGE (M) FOR ERROR <0.5 MR	<0.2	<0.1
1	5	0.7/90	15	0	6000	4400	3900
2	5	0.7/90	20	0	8300	5600	5000
3	5	0.7/90	30	0	12500	8700	7600
4	5	0.7/90	50	0	20400	14300	12600
5	5	0.7/90	60	0	24000	17200	15000

RDR_ALT=5,TGT_ALT=15,RHO=.7/90 DEG,1.3DEG BW,MISS=0

MONO —, CASE 1

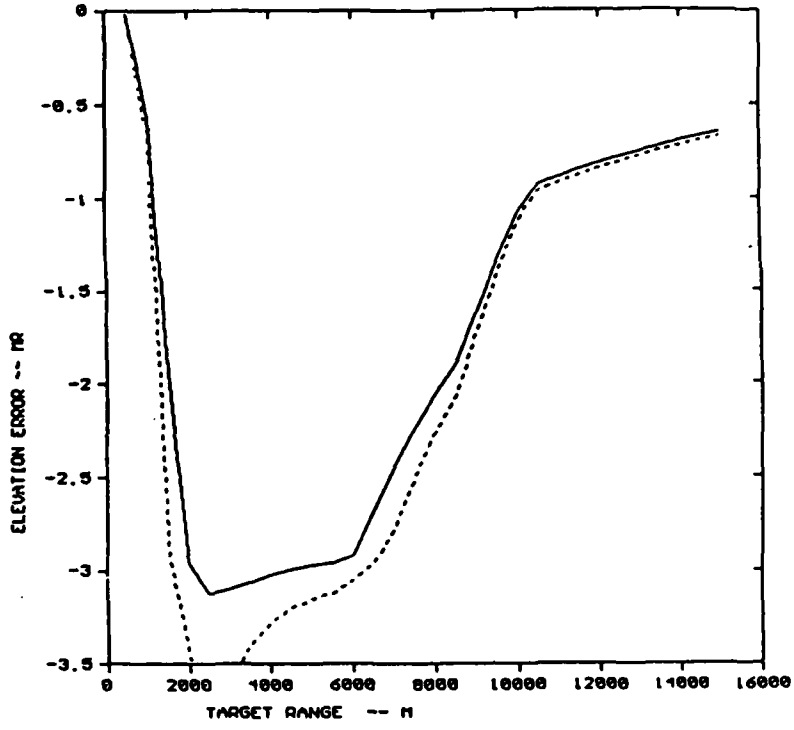

RDR_ALT=5,TGT_ALT=15,RHO=.7/90 DEG,1.3DEG BW,MISS=-5

MONO —, CASE 2

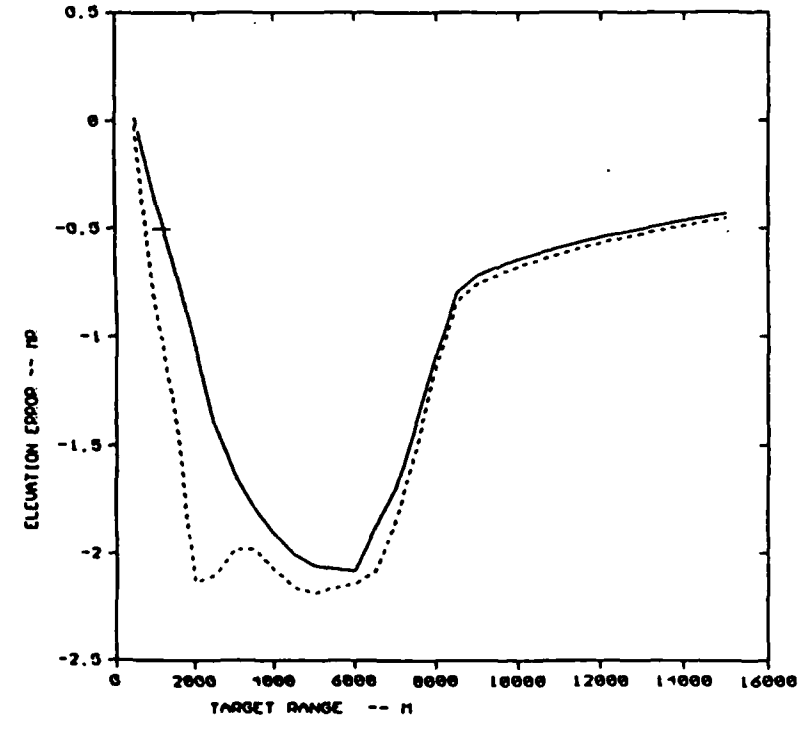

MONO —, CASE 3

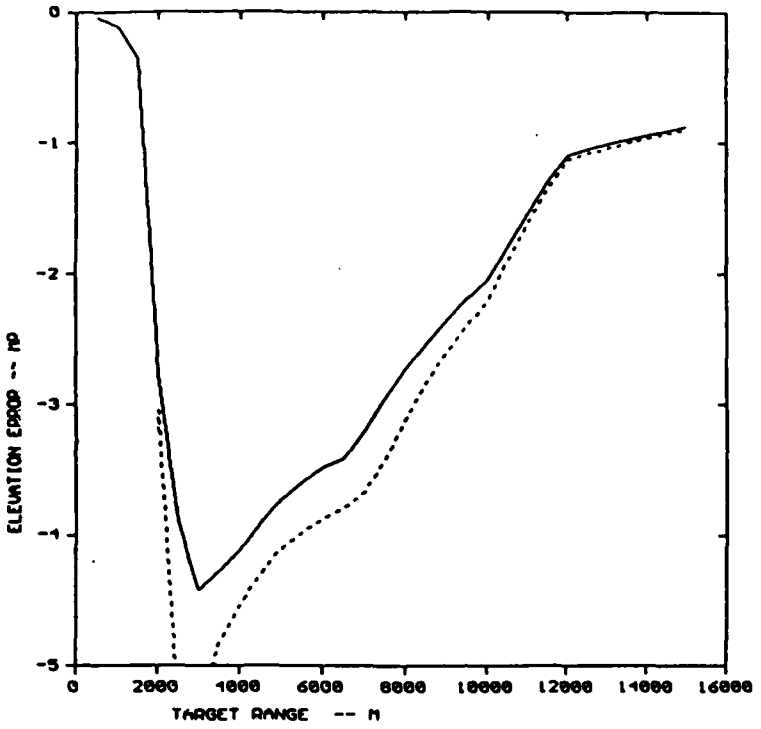

MONO —, CASE 4

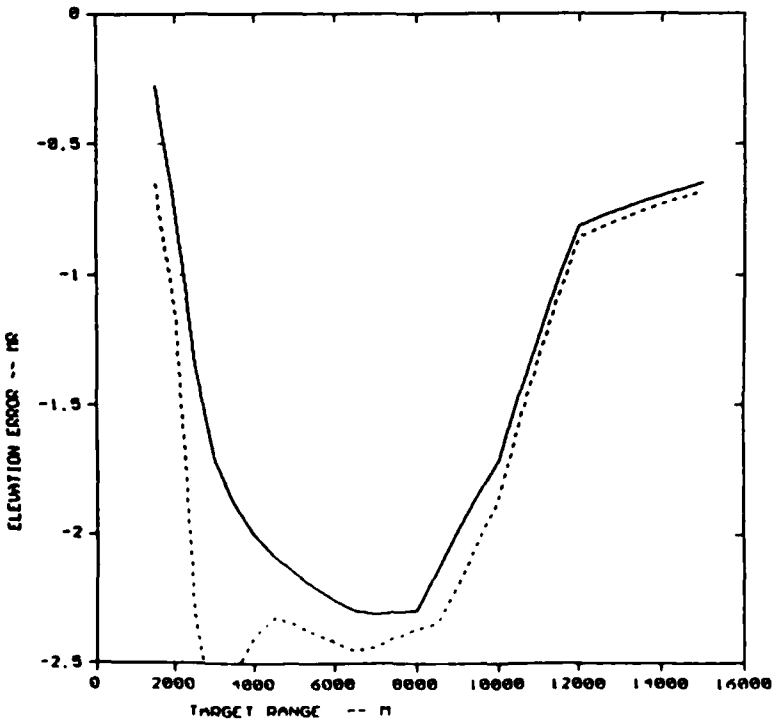

ROA_ALT=5, TGT_ALT=20, RHO=.7/30 DEG, 1.3DEG BW, MISS=0

MONO —, CASE 5

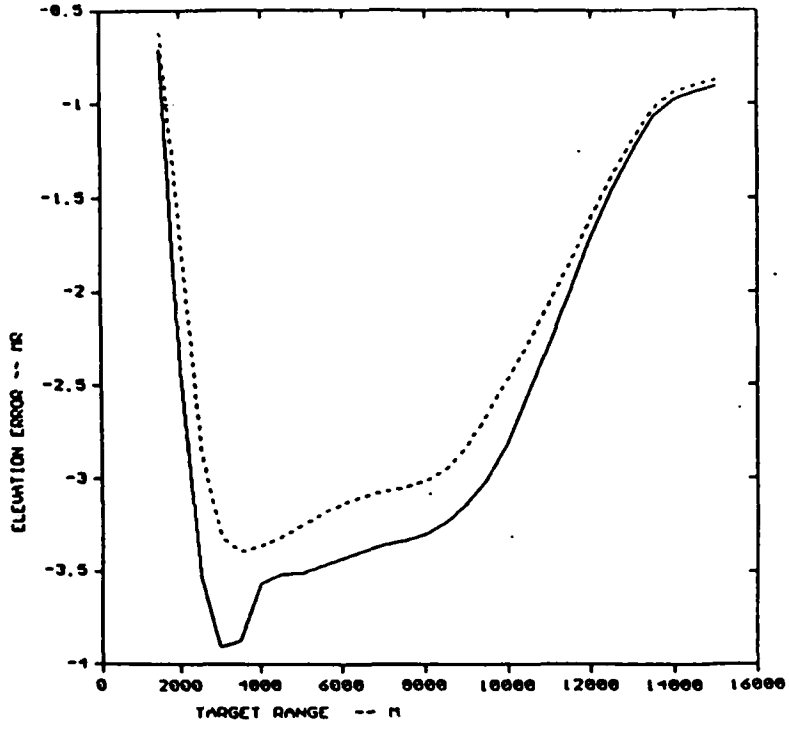

ROA_ALT=5, TGT_ALT=50, RHO=.7/30 DEG, 1.3DEG BW, MISS=-10

MONO —, CASE 6

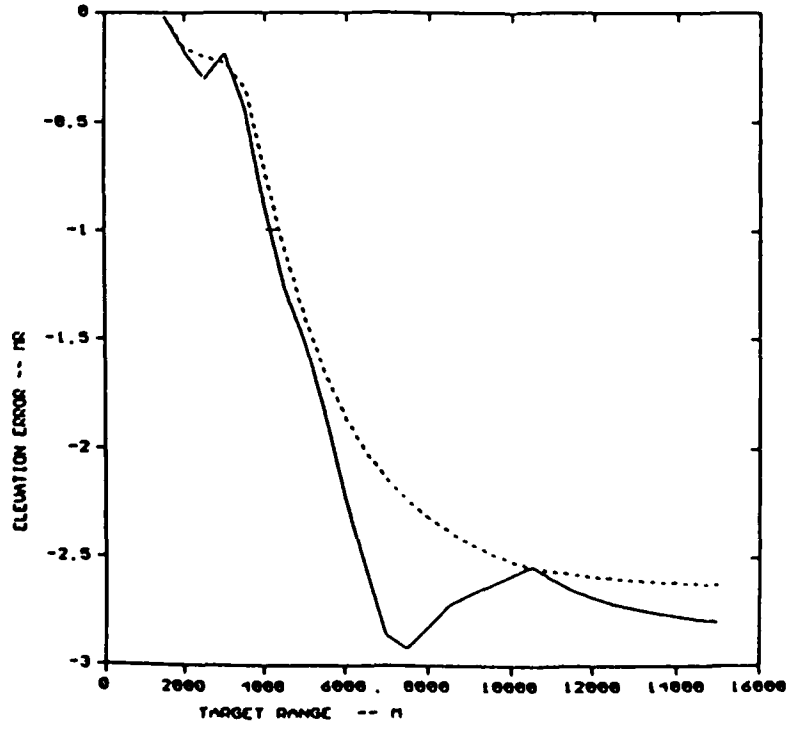

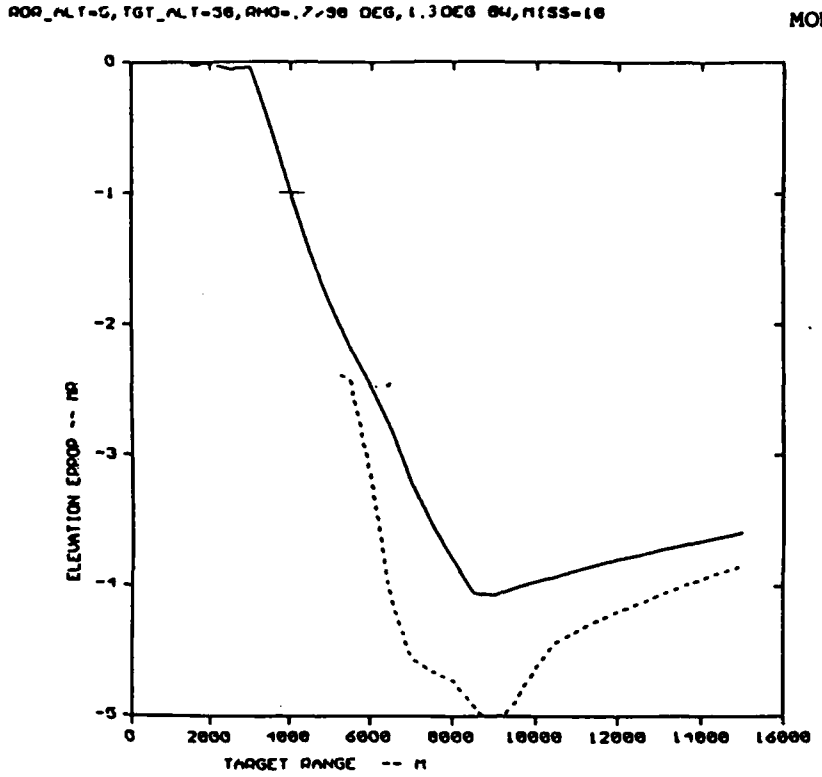
ROR_ALT=6, TGT_ALT=36, RHO=.7/90 DEG, 1.3DEG BW, MISS=16
MONO —-, CASE 7
0
-1
-2
-3
-4
-5
ELEVATION ERROR -- MR
0
2000
4000
6000
8000
10000
12000
14000
16000
TARGET RANGE -- M

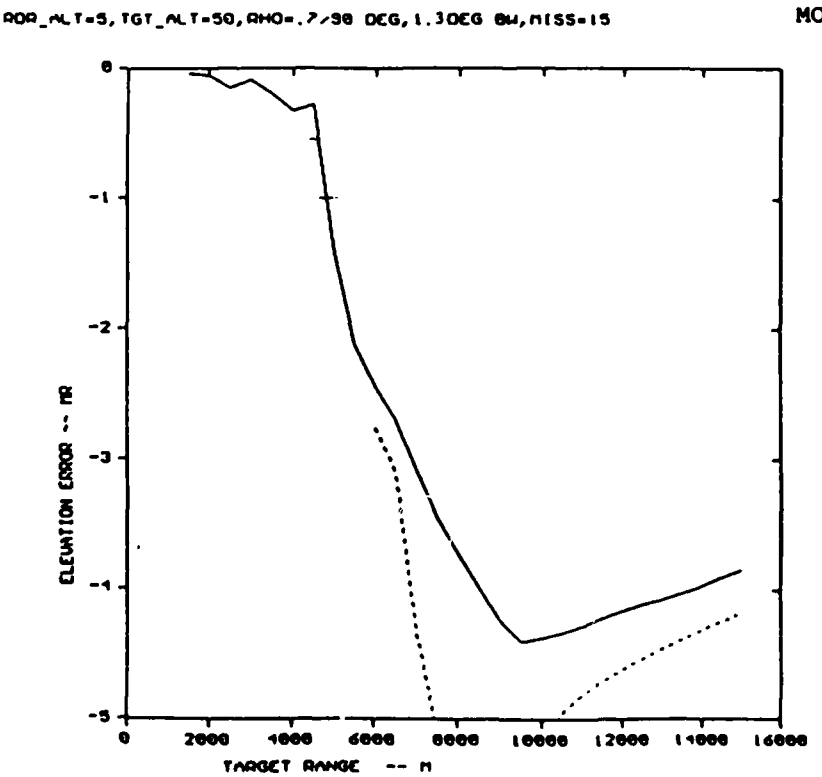
ROR_ALT=5, TGT_ALT=50, RHO=.7/90 DEG, 1.3DEG BW, MISS=15
MONO —, CASE 8
0
-1
-2
-3
-4
-5
ELEVATION ERROR -- MR
0
2000
4000
6000
8000
10000
12000
14000
16000
TARGET RANGE -- M

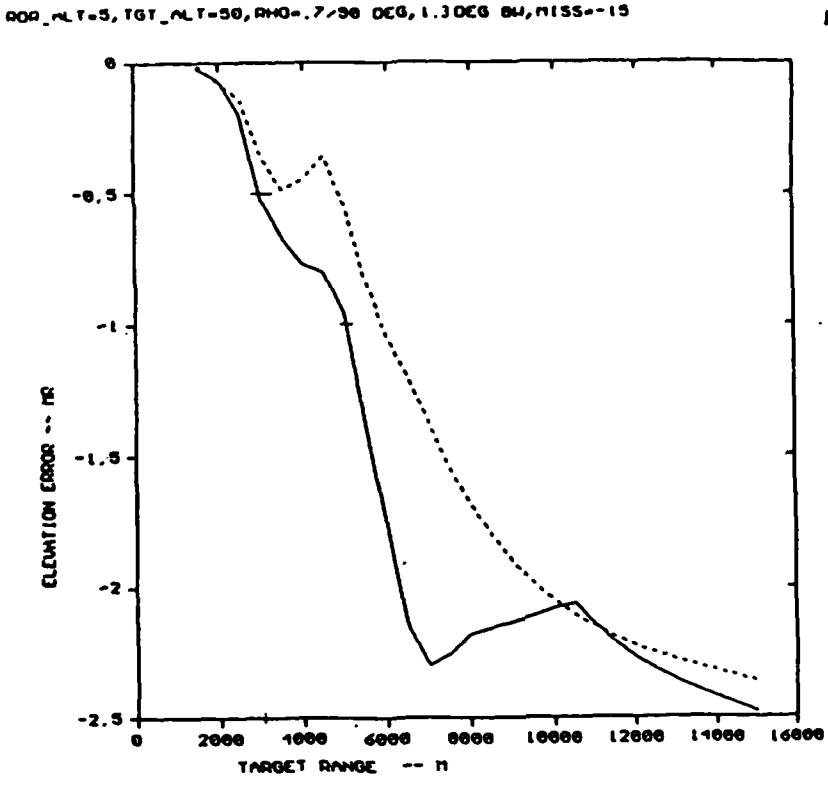

MONO —, CASE 9

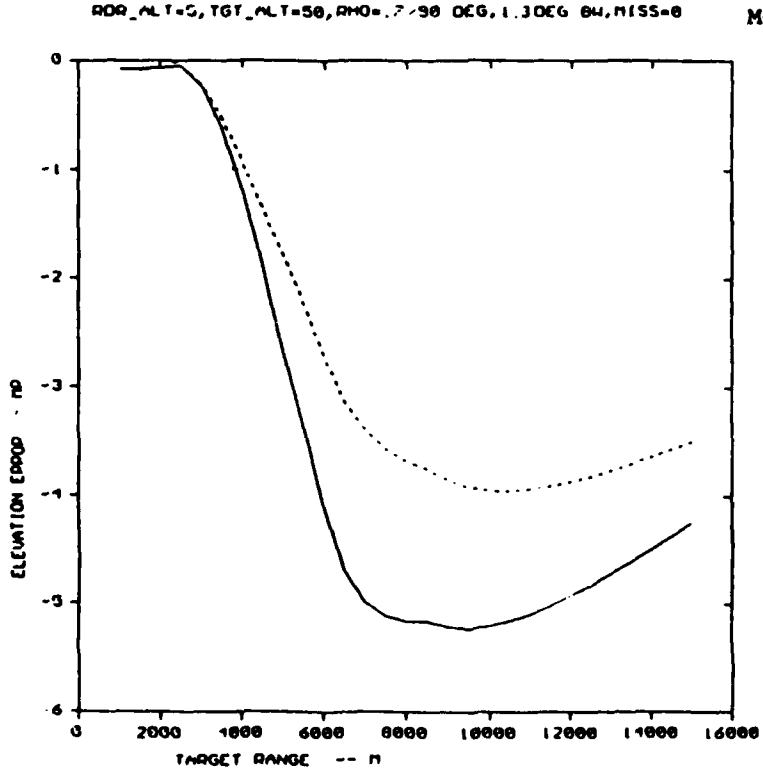

MONO --, CASE 10

RDR_ALT=0, TGT_ALT=15, RHO=.7/135 DEG, 1.3DEG BW, MISS=0

MONO —, CASE 11

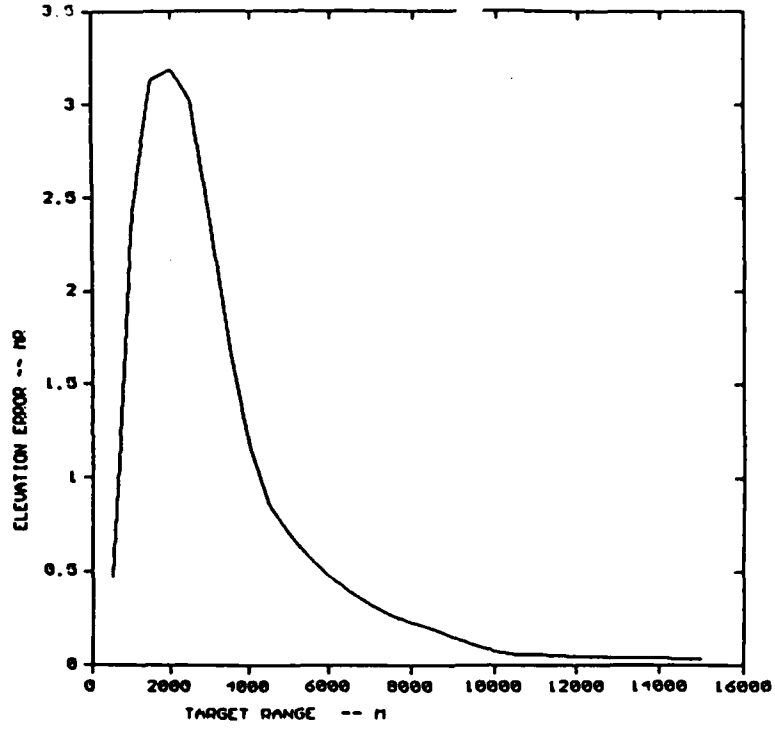

RDR_ALT=0, TGT_ALT=15, RHO=.7/0 DEG, 1.3DEG BW, MISS=0

MONO —, CASE 12

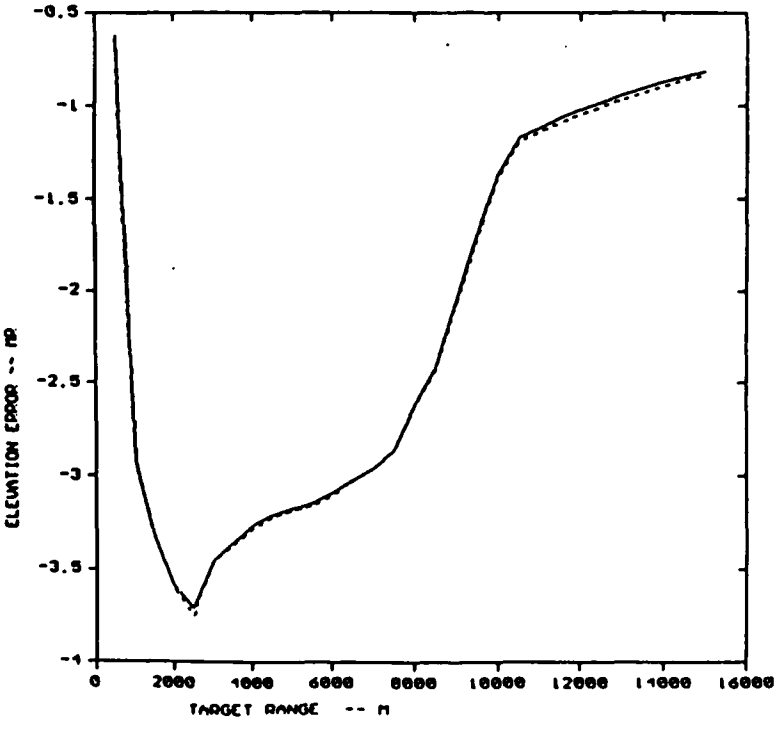

RDR_ALT=5,TGT_ALT=15,RHO=.7/180 DEG,1.3DEG BW,MISS=0

MONO —, CASE 13

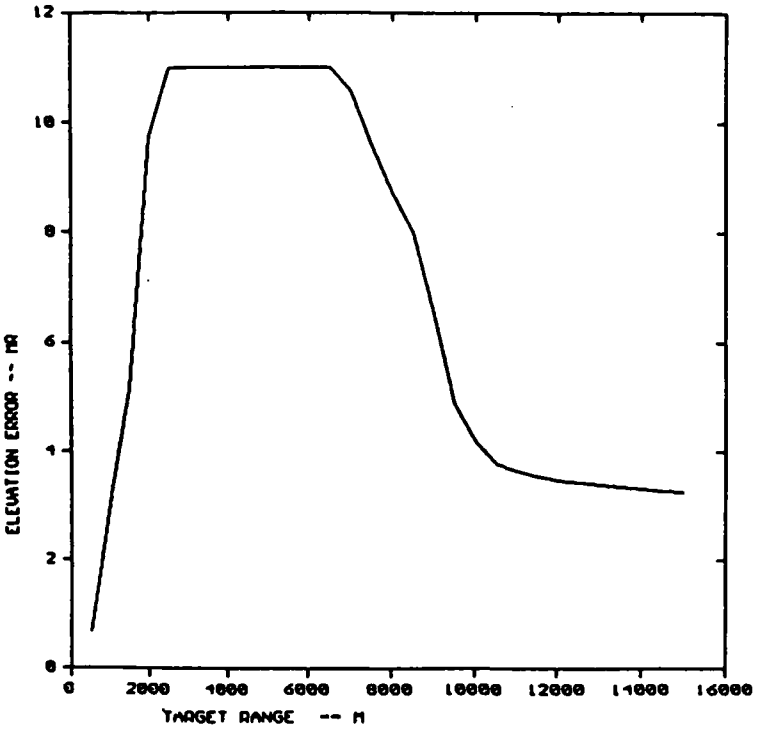

RDR_ALT=5,TGT_ALT=60,RHO=.7/90 DEG,1.3DEG BW,MISS=-10

MONO —, CASE 14

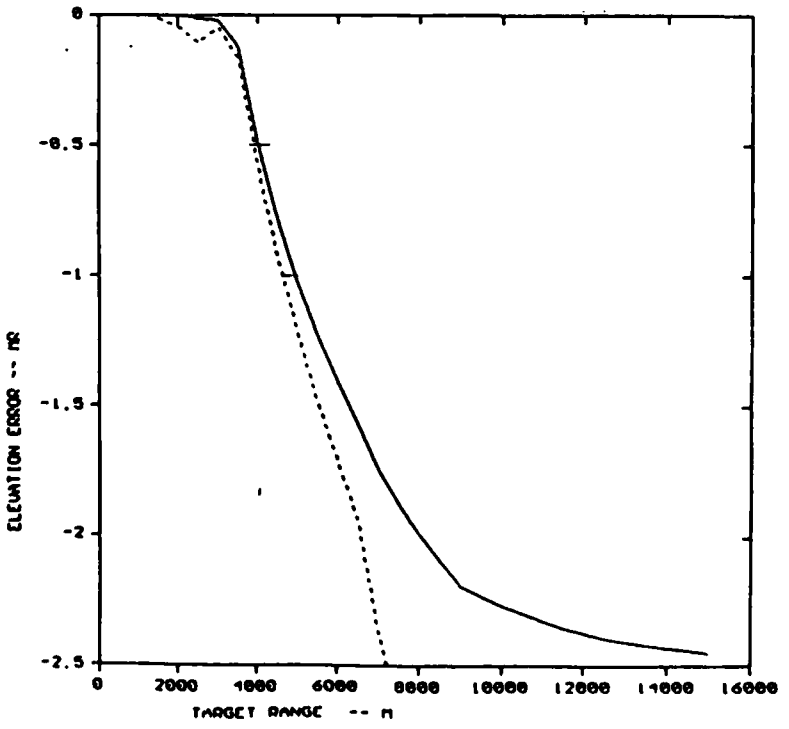

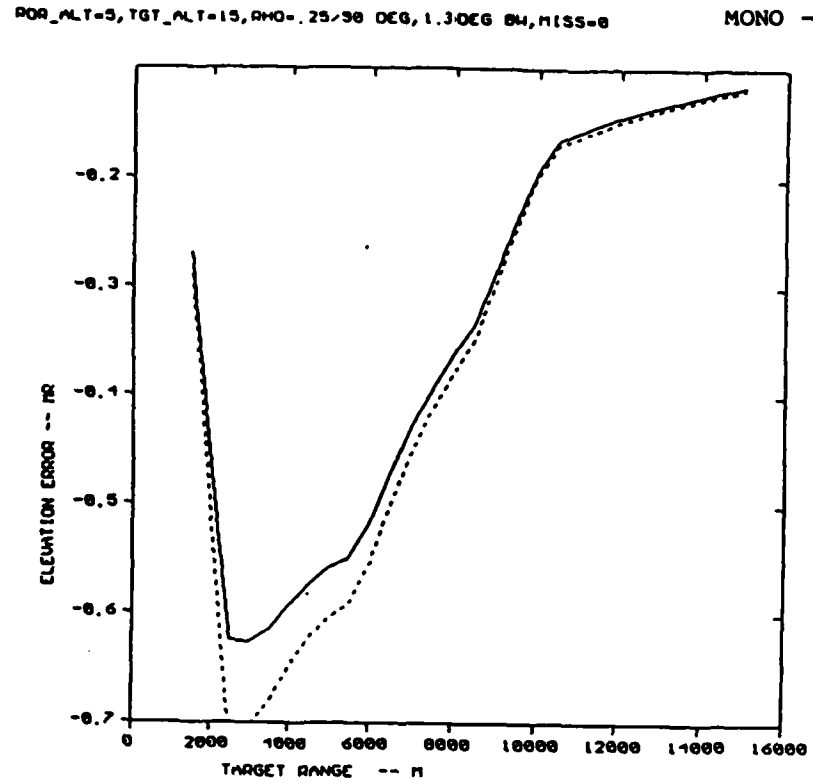
ROR_ALT=5,TGT_ALT=15,RHO=.25/90 DEG,1.3DEG BW,MISS=0
MONO —, CASE 15
-0.2
-0.3
-0.4
-0.5
-0.6
-0.7
ELEVATION ERROR -- MR
0
2000
4000
6000
8000
10000
12000
14000
16000
TARGET RANGE -- M

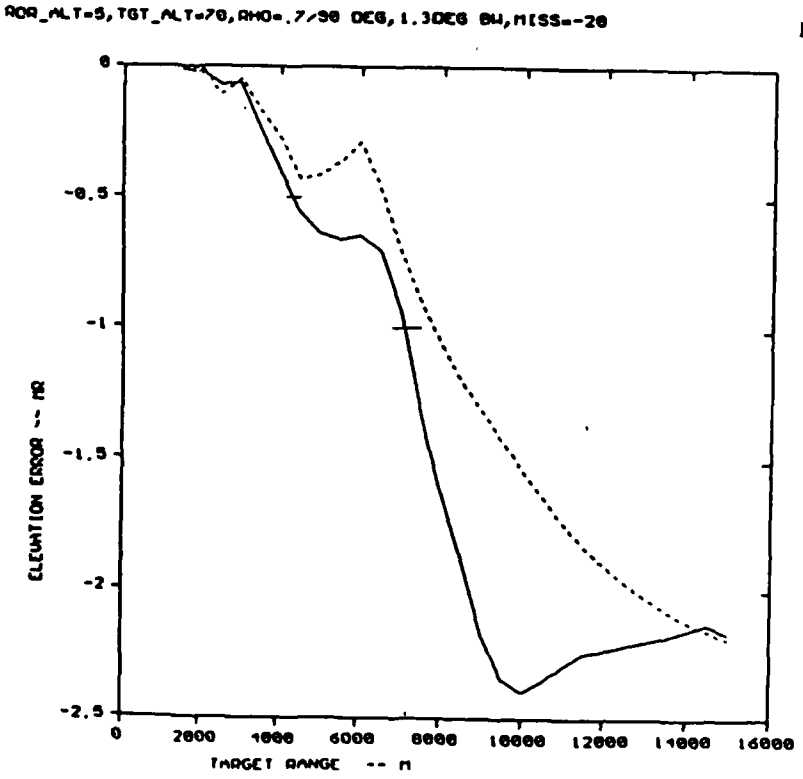
ROR_ALT=5,TGT_ALT=70,RHO=.7/90 DEG,1.3DEG BW,MISS=-20
MONO —, CASE 16
0
-0.5
-1
-1.5
-2
-2.5
ELEVATION ERROR -- MR
0
2000
4000
6000
8000
10000
12000
14000
16000
TARGET RANGE -- M

RDR_ALT=5,TGT_ALT=30,RHO=.7/90 DEG,1.3DEG BW,MISS=0

MONO —, CASE 17

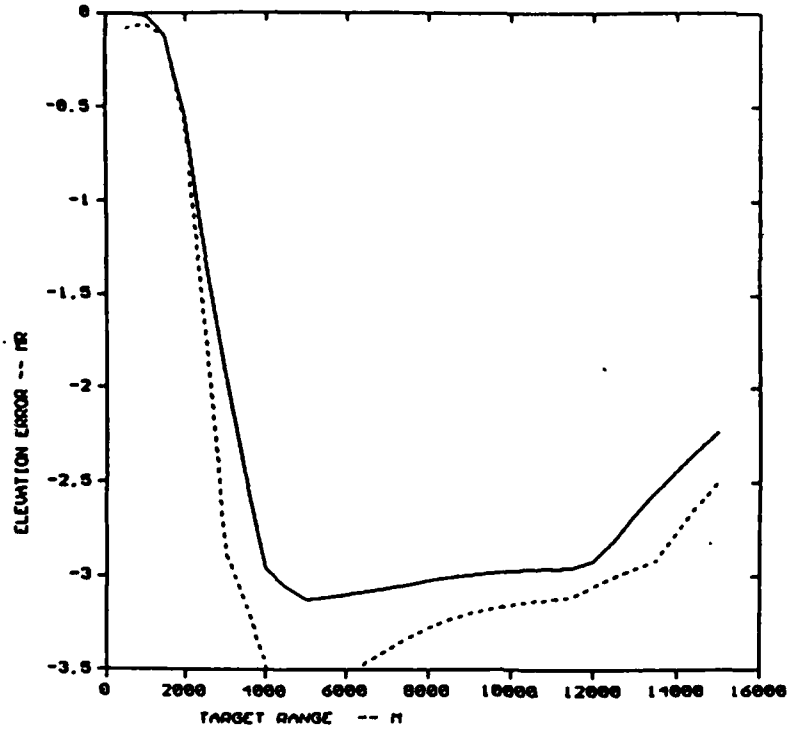

RDR_ALT=5,TGT_ALT=35,RHO=.7/90 DEG,1.3DEG BW,MISS=0

MONO —, CASE 18

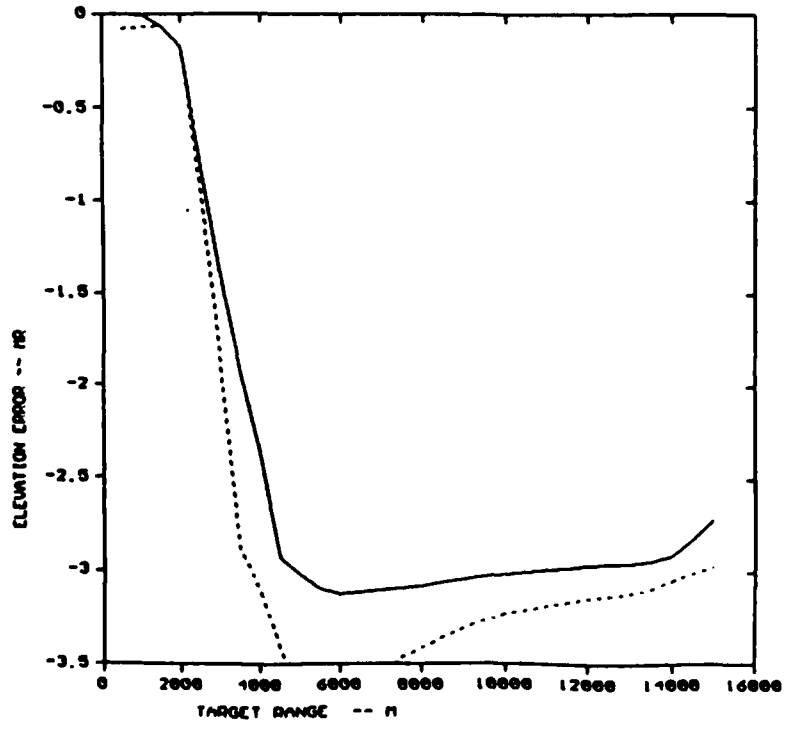

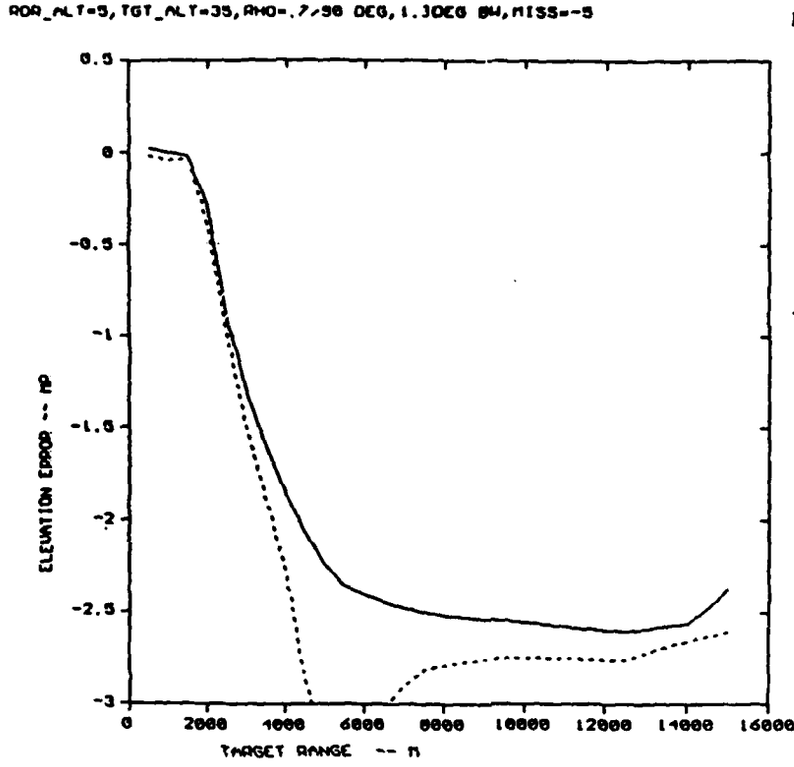
ROR_ALT=5, TGT_ALT=35, RHO=.7/90 DEG, 1.3DEG BW, MISS=-5
MONO —, CASE 19
ELEVATION ERROR -- MR
TARGET RANGE -- M
0.5
0
-0.5
-1
-1.5
-2
-2.5
-3
0
2000
4000
6000
8000
10000
12000
14000
16000

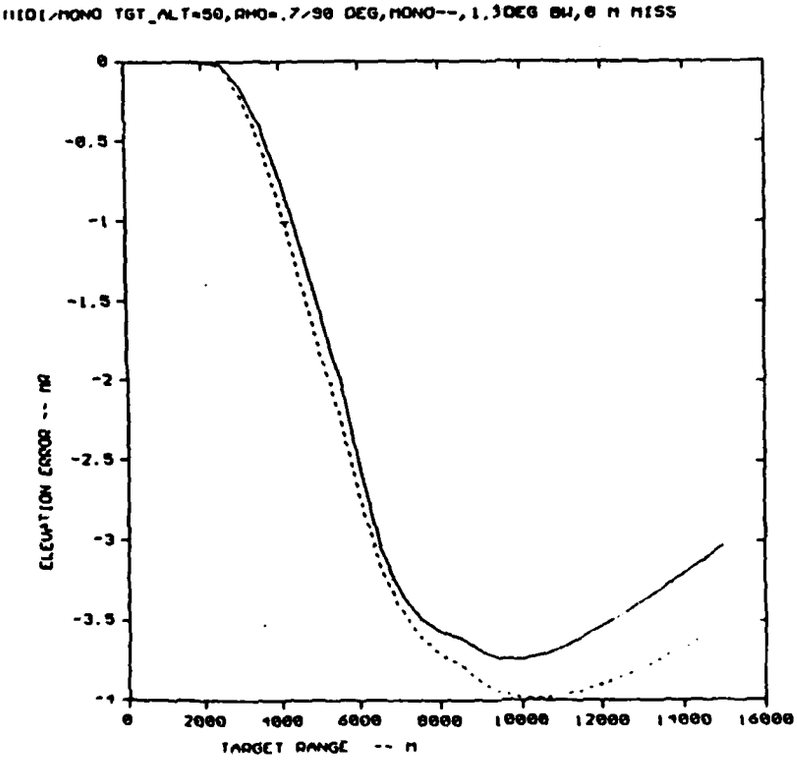
MONO TGT_ALT=50, RHO=.7/90 DEG, MONO--, 1.3DEG BW, 0 M MISS
MONO --, CASE 20
ELEVATION ERROR -- MR
TARGET RANGE -- M
0
-0.5
-1
-1.5
-2
-2.5
-3
-3.5
0
2000
4000
6000
8000
10000
12000
14000
16000

RDR_ALT=15,TGT_ALT=50,RHO=.7/90 DEG,1.3DEG BW,MISS=10

MONO —, CASE 21

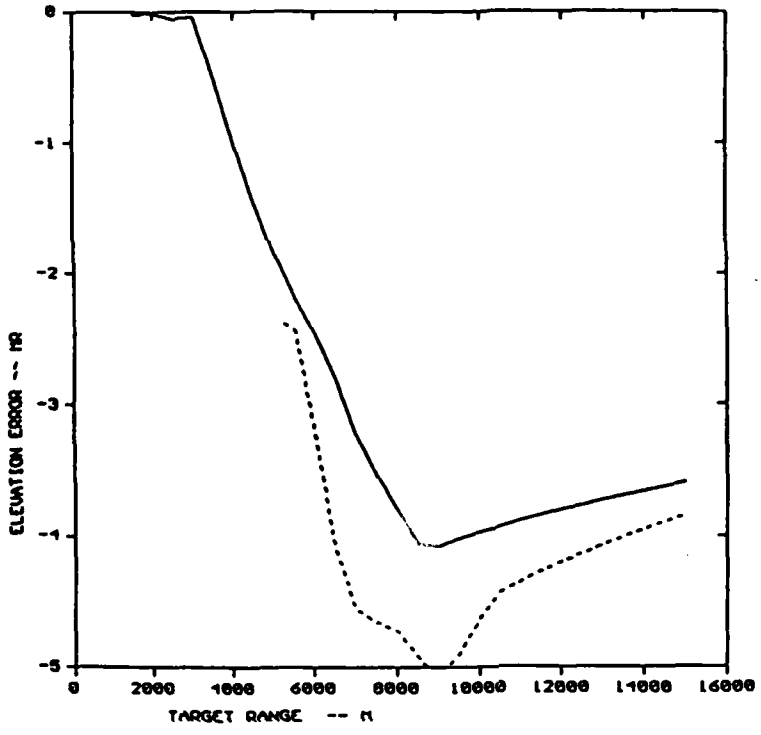

RDR_ALT=15,TGT_ALT=50,RHO=.7/90 DEG,1.3DEG BW,MISS=-10

MONO —, CASE 22

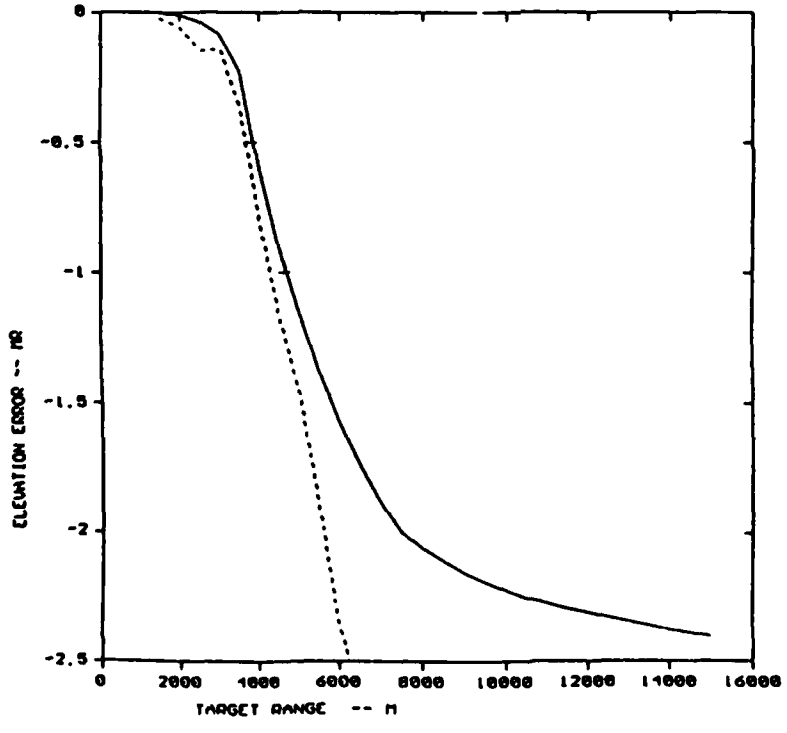

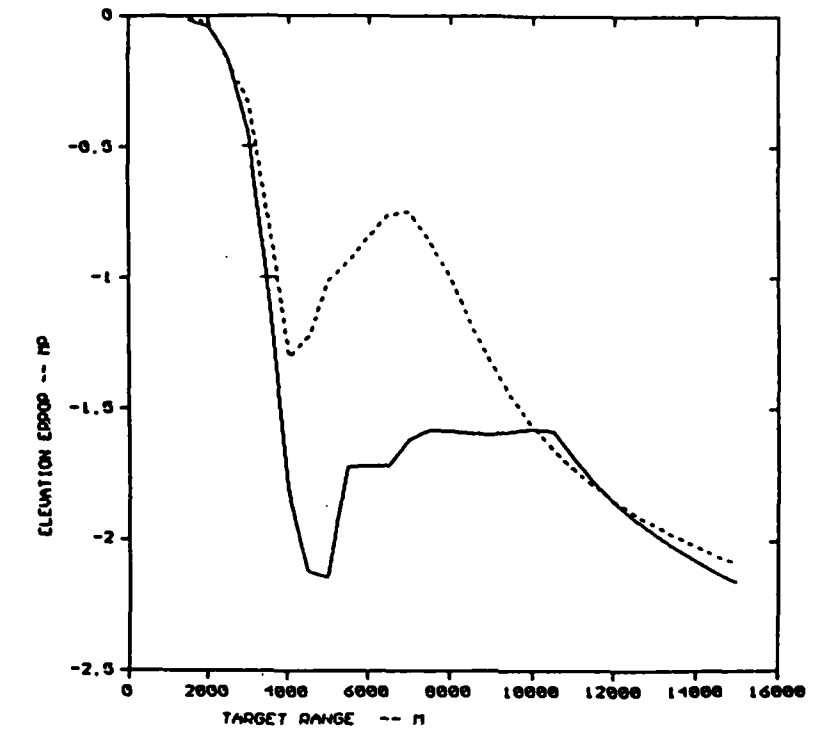
ROR_ALT=0,TGT_ALT=30,RHO=.7/90 DEG,1.3DEG BW,MISS=-20
MONO —, CASE 23
0
-0.5
-1
-1.5
-2
-2.5
ELEVATION ERROR -- MR
0
2000
4000
6000
8000
10000
12000
14000
16000
TARGET RANGE -- M

RGR_ALT=5, TGT_ALT=15, RHO=.7/90 DEG, 1.3DEG BW, MISS=0 MONO —, CASE 50

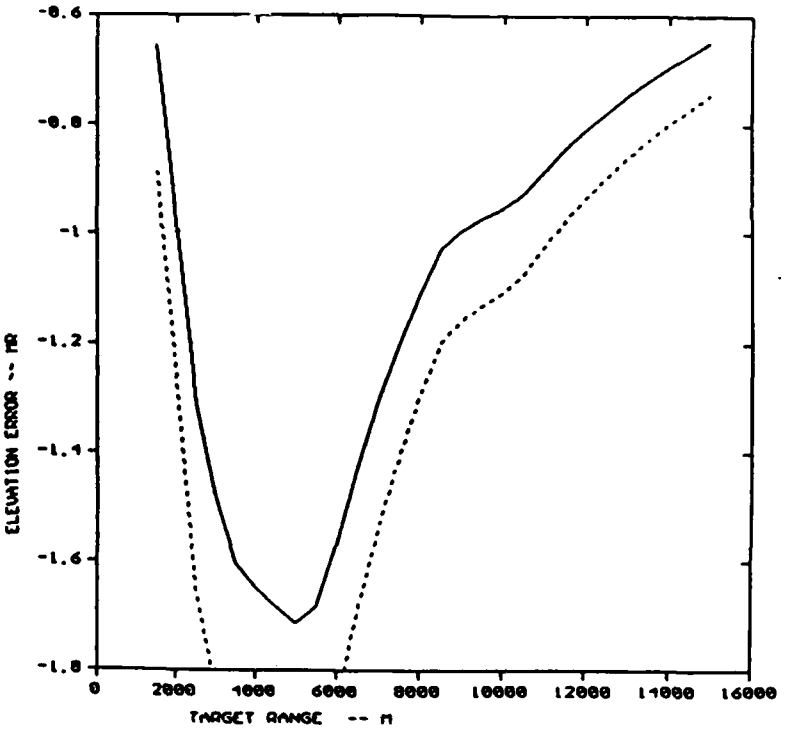

RGR_ALT=5, TGT_ALT=15, RHO=.7/90 DEG, 1.3DEG BW, MISS=-5 MONO —, CASE 51

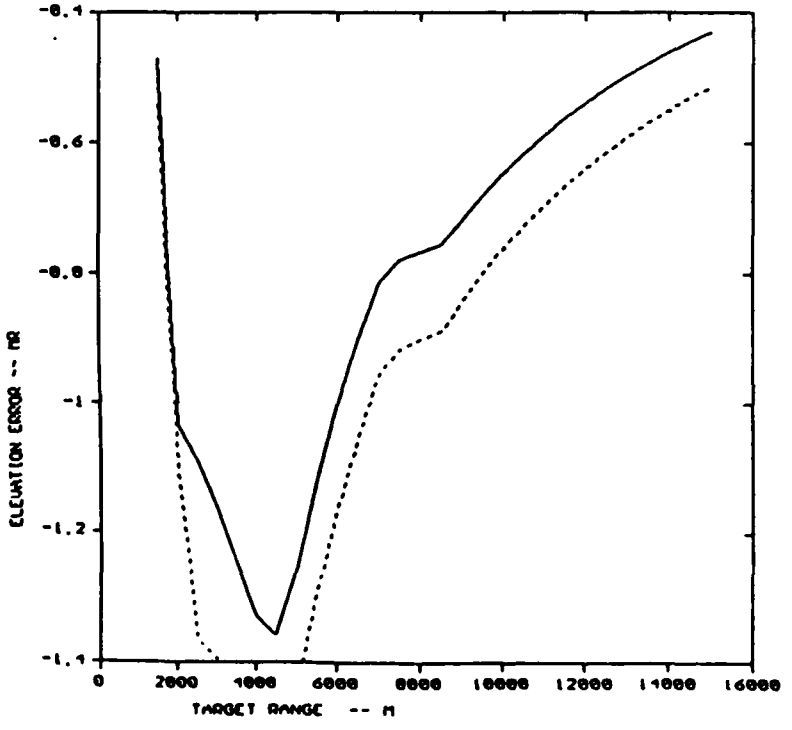

RDR_ALT=5,TGT_ALT=20,RHO=.7/90 DEG,1.3DEG BW,MISS=-5 MONO —, CASE 52

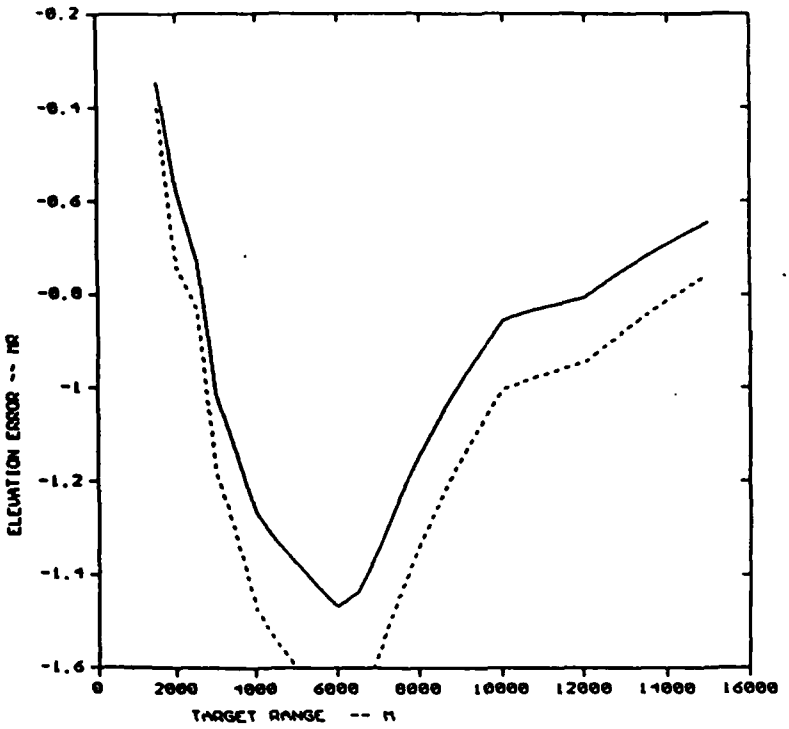

RDR_ALT=5,TGT_ALT=30,RHO=.7/90 DEG,1.3DEG BW,MISS=0 MONO —, CASE 53

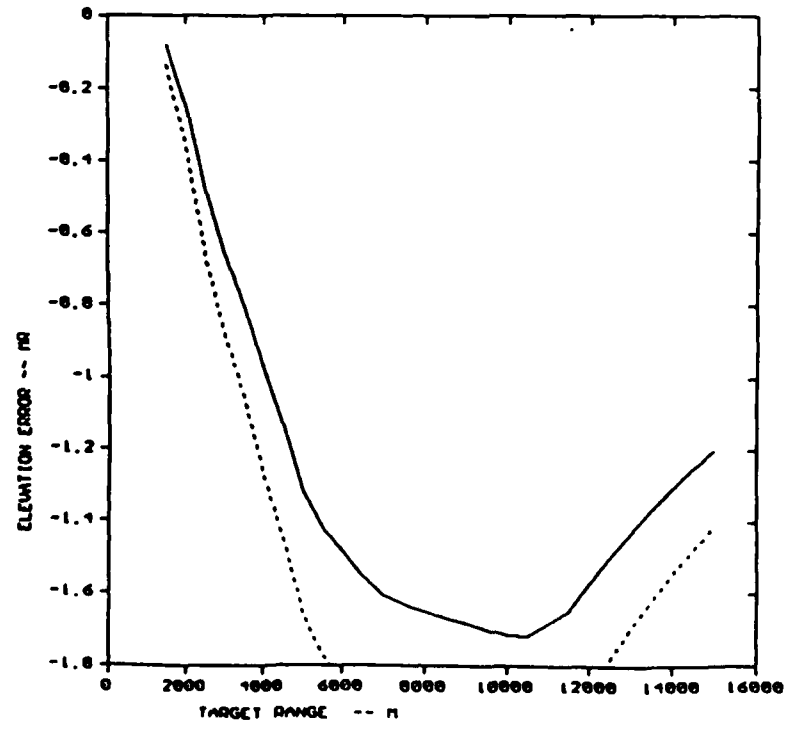

RDR_ALT=5,TGT_ALT=30,RHO=.7/90 DEG,1.3DEG BW,MISS=-6 MONO —, CASE 54

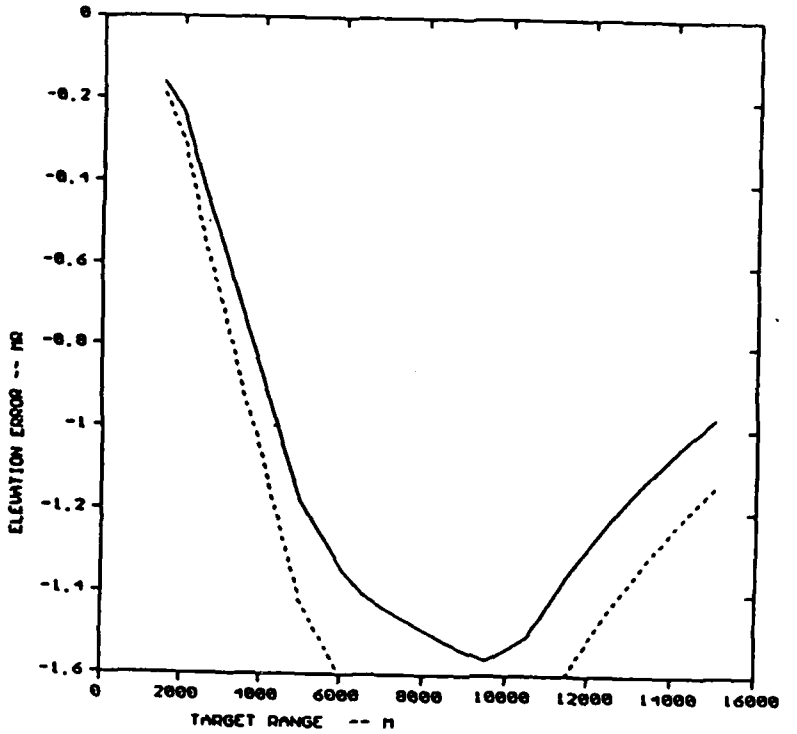

RDR_ALT=5,TGT_ALT=35,RHO=.7/90 DEG,1.3DEG BW,MISS=-6 MONO —, CASE 55

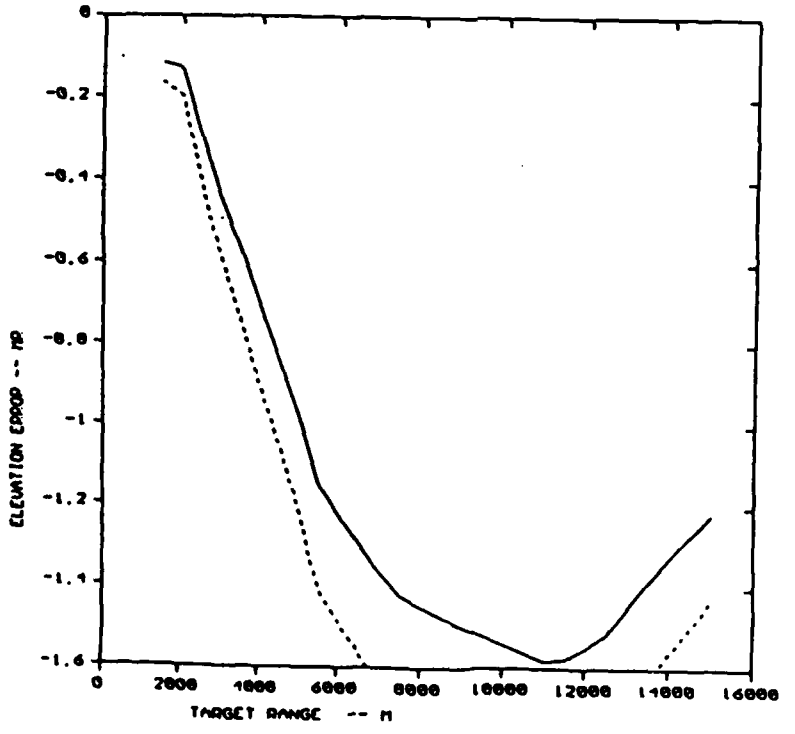

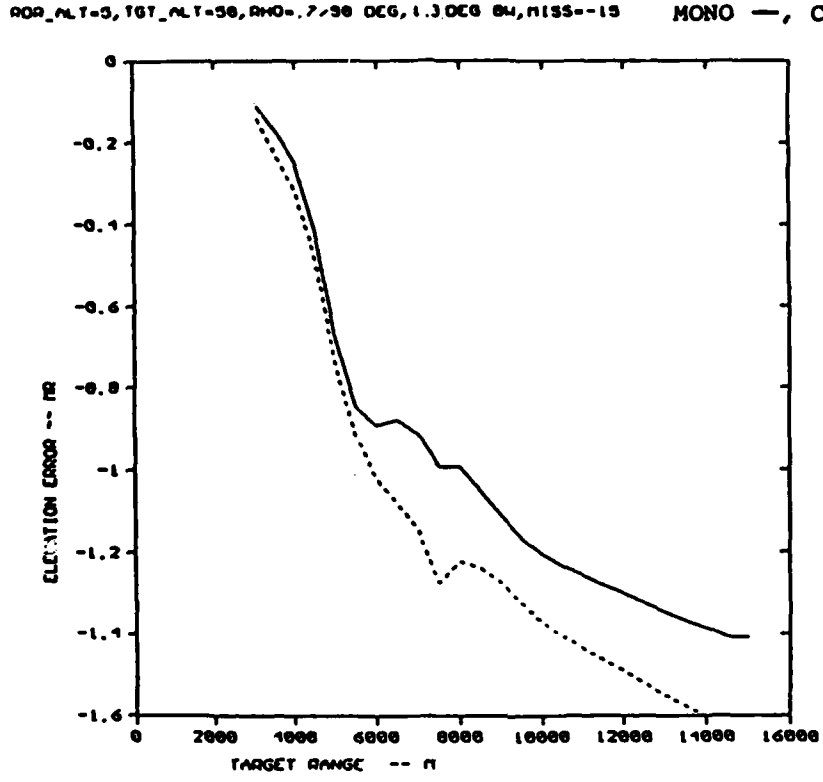
MONO —, CASE 58
0
-0.2
-0.4
-0.6
-0.8
-1
-1.2
-1.4
-1.6
0
2000
4000
6000
8000
10000
12000
14000
16000
TARGET RANGE -- M

RDR_ALT=5,TGT_ALT=15,RHO=.7/90 DEG,1.3DEG BW,MISS=0 MONO,CASE 31

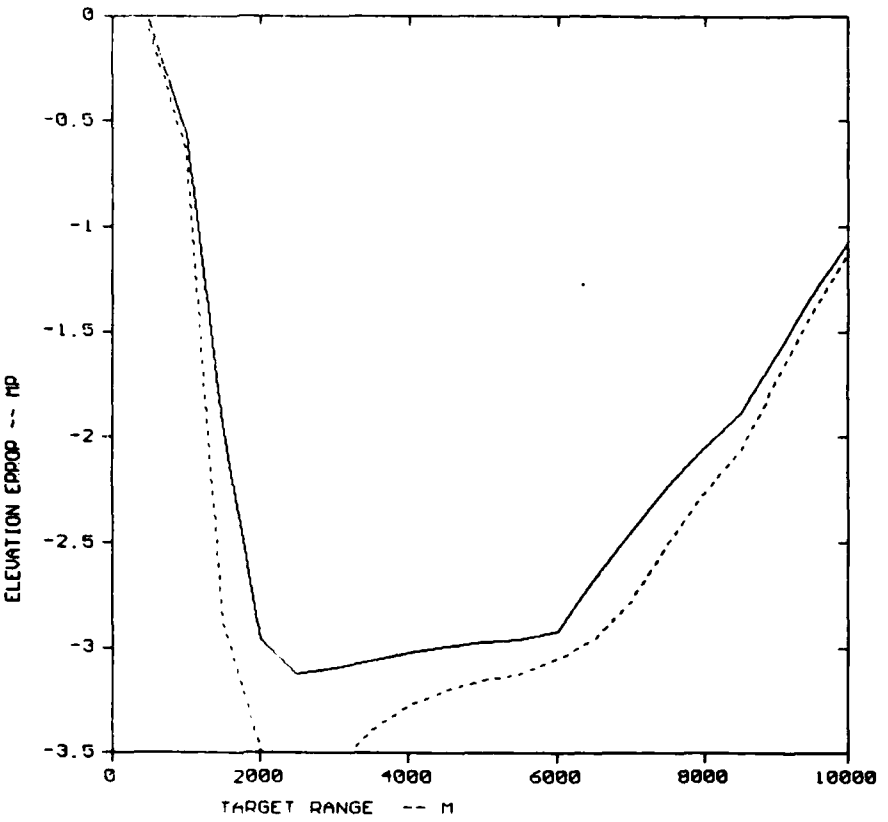

RDR_ALT=5,TGT_ALT=50,RHO=.7/90 DEG,1.3DEG BW,MISS=0 MONO___,CASE 32

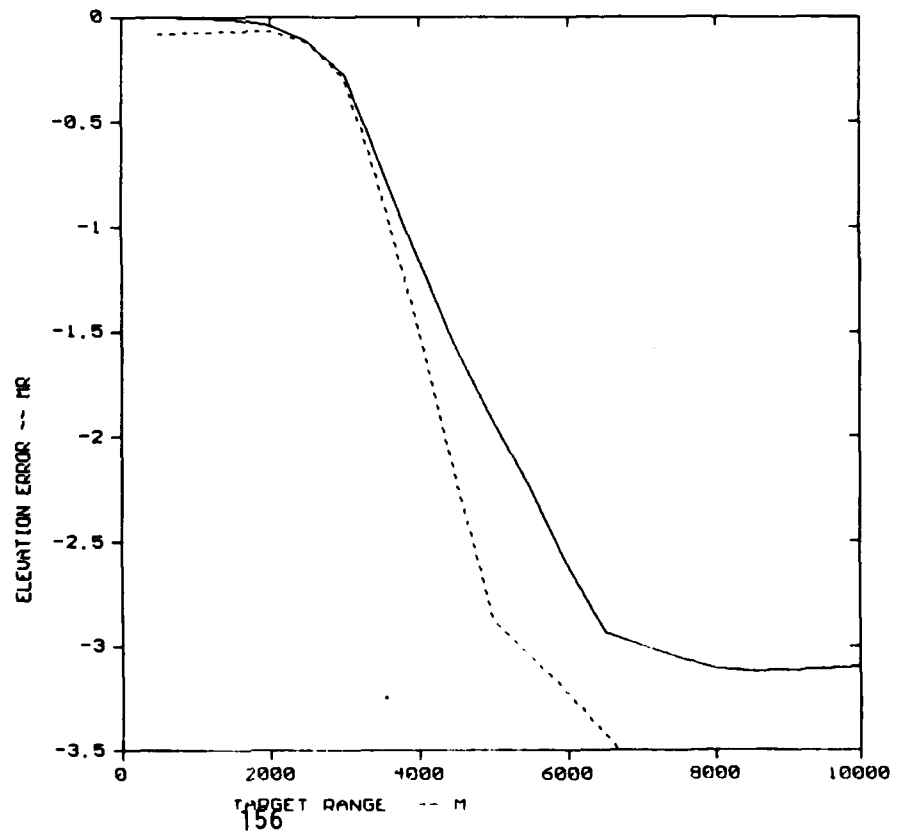

RDR_ALT=5,TGT_ALT=50,RHO=.7/90 DEG,1.3DEG BW,MISS=-10 MONO,CASE 33

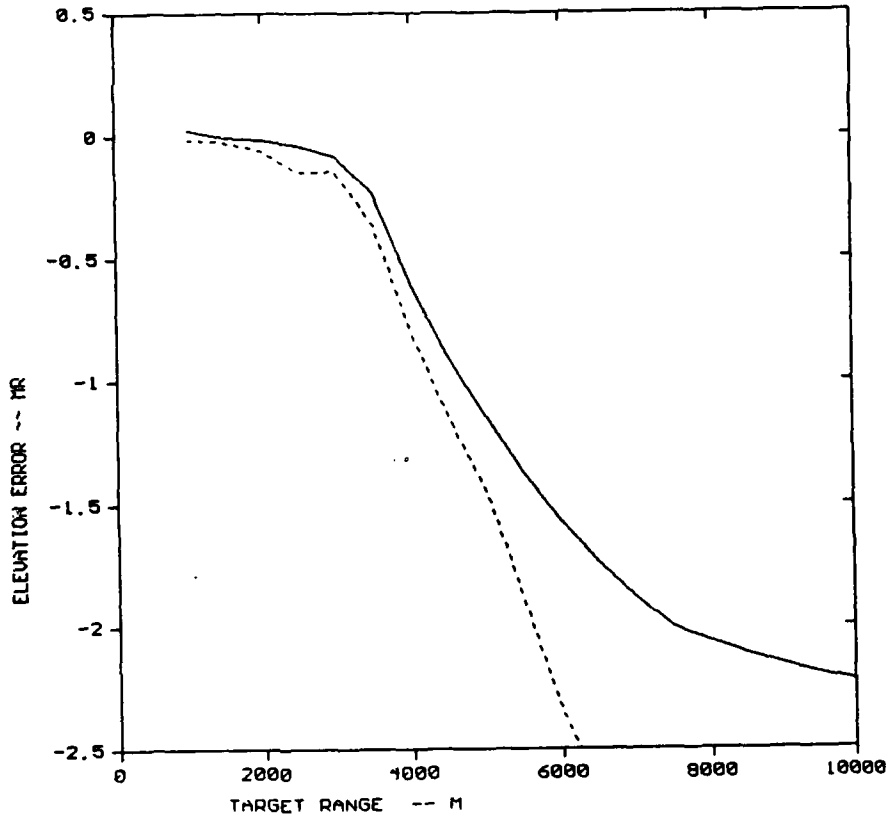

RDR_ALT=5,TGT_ALT=50,RHO=.7/90 DEG,1.3DEG BW,MISS=10 MONO__,CASE 34

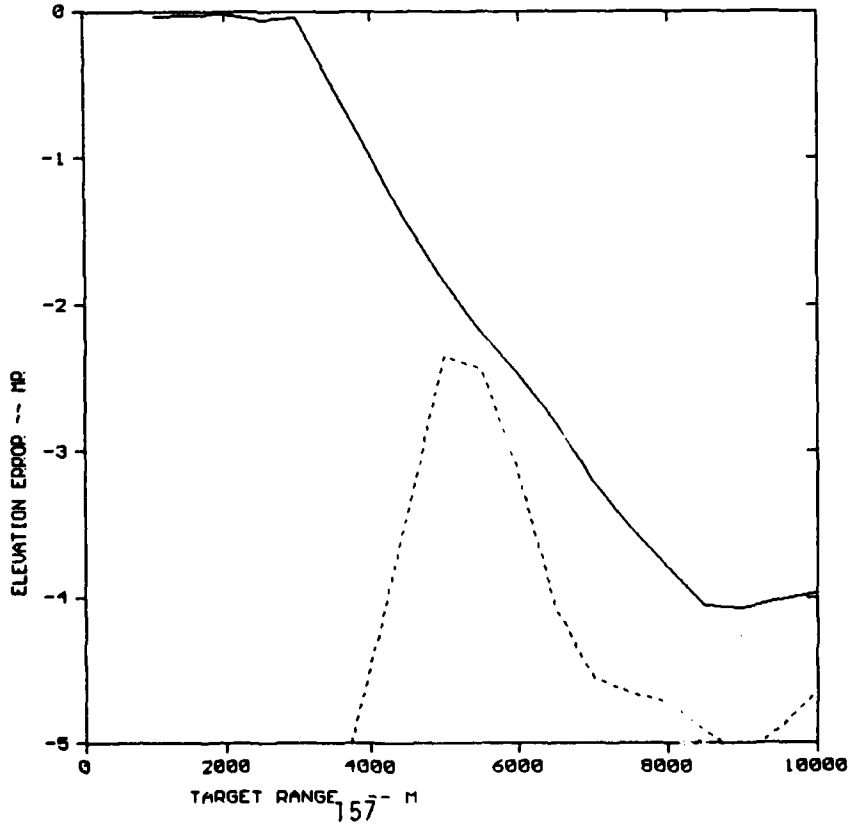

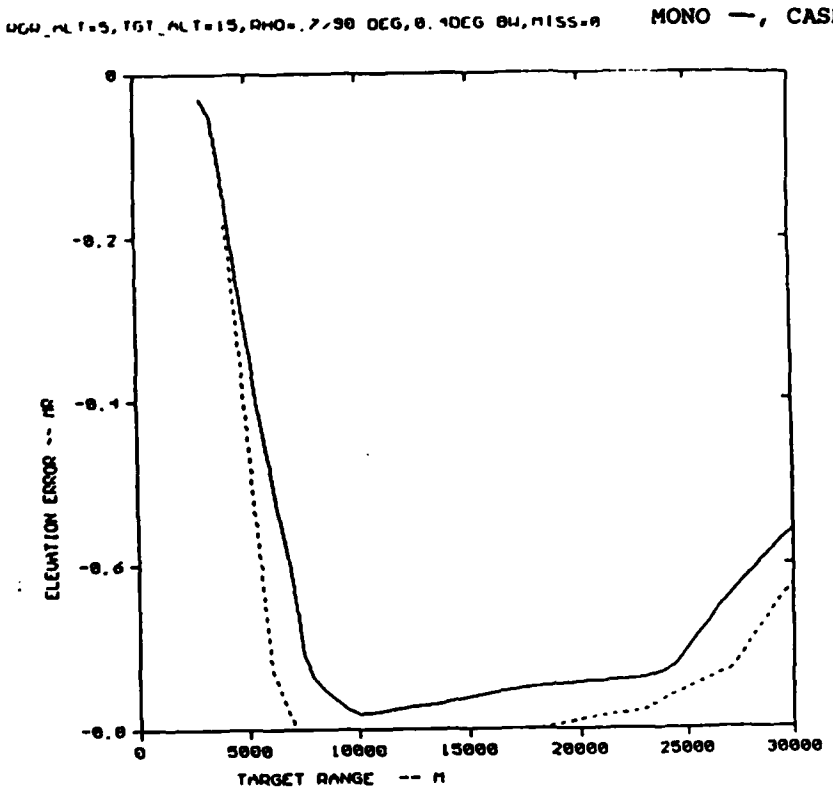
DGW_ALT=5,TGT_ALT=15,RHO=.7/90 DEG,0.4DEG BW,MISS=0
MONO —, CASE 1
0
-0.2
-0.4
-0.6
-0.8
ELEVATION ERROR -- MR
0
5000
10000
15000
20000
25000
30000
TARGET RANGE -- M

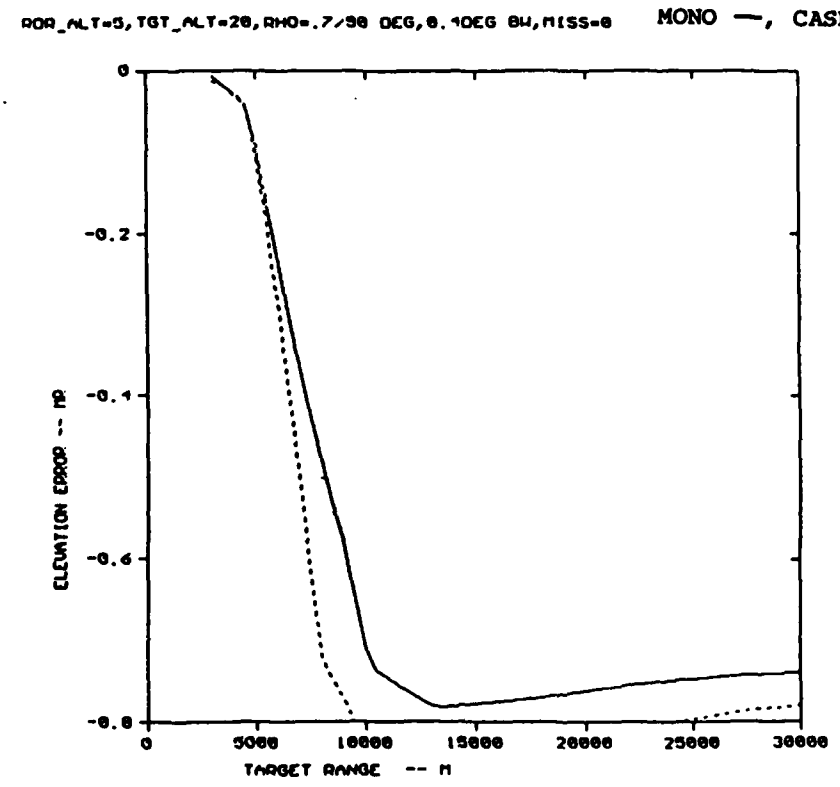
ROR_ALT=5,TGT_ALT=20,RHO=.7/90 DEG,0.4DEG BW,MISS=0
MONO —, CASE 2
0
-0.2
-0.4
-0.6
-0.8
ELEVATION ERROR -- MR
0
5000
10000
15000
20000
25000
30000
TARGET RANGE -- M

AGR_ALT=5,TGT_ALT=30,RHO=.7/90 DEG,0.1DEG BW,MISS=0 MONO —, CASE 3

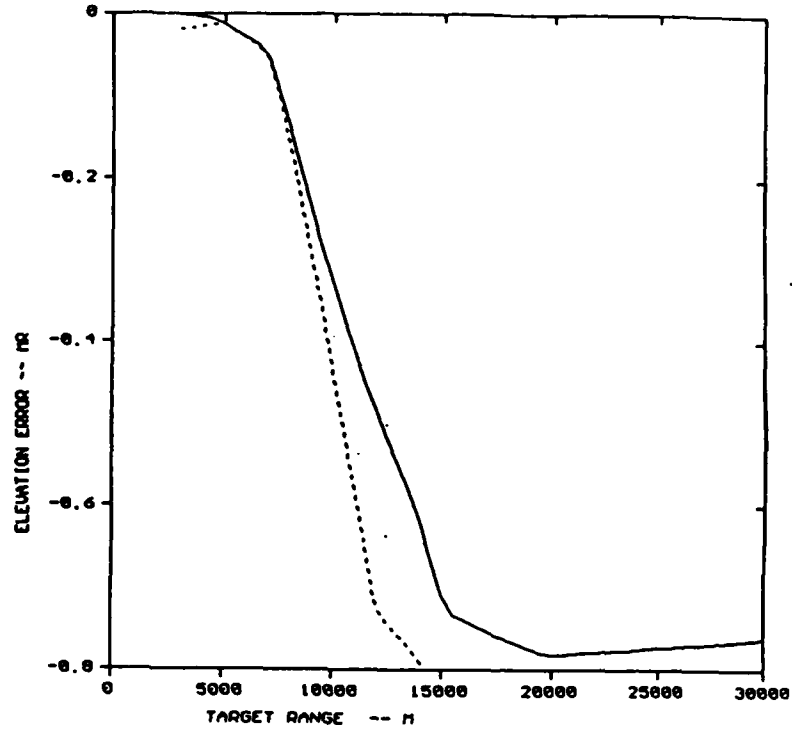

AGR_ALT=5,TGT_ALT=50,RHO=.7/90 DEG,0.1DEG BW,MISS=0 MONO —, CASE 4

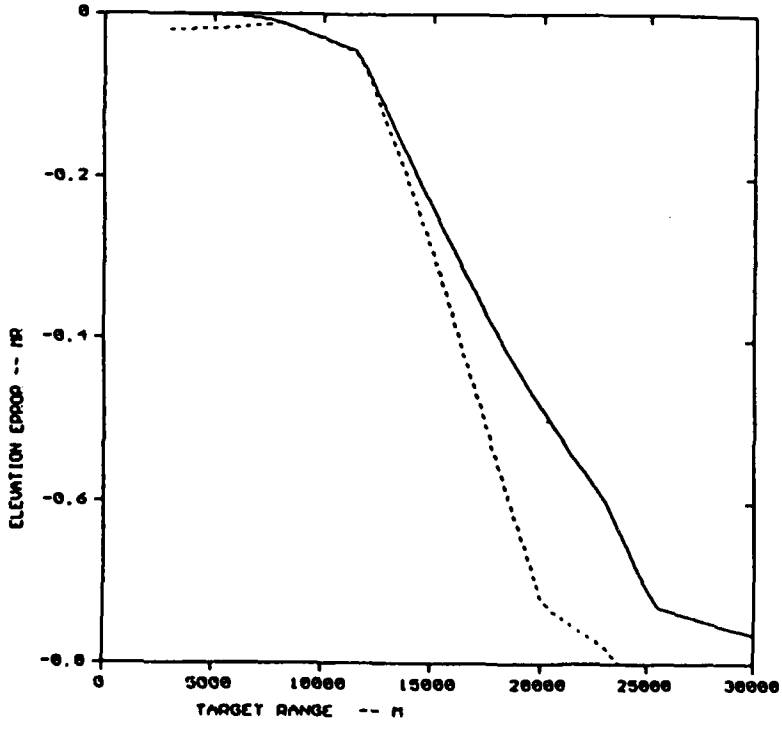

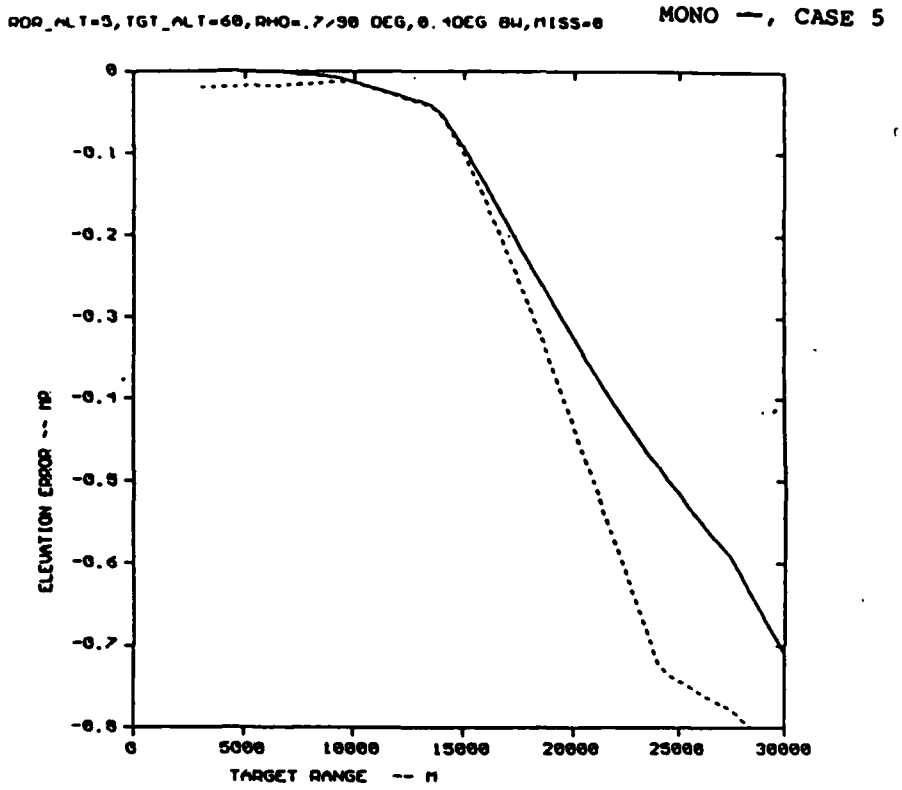
RDR_ALT=5,TGT_ALT=60,RHO=.7/90 DEG,0.4DEG BW,MISS=0
MONO —, CASE 5
0
-0.1
-0.2
-0.3
-0.4
-0.5
-0.6
-0.7
-0.8
ELEVATION ERROR -- MR
0
5000
10000
15000
20000
25000
30000
TARGET RANGE -- M

APPENDIX C

COMPUTER PROGRAM LISTINGS

```
      PROGRAM COMPARE
C
C     COMPARE CONVENTIONAL MONOPULSE AND MIDI
C
      DIMENSION SUM_DB(40),DEL_DB(40),ELANG_DEG(40),
     1                    CAL_MONO(40),
     2                    ELANG_MR(40),CAL_MIDI(40),
     3                    SUM_VOLT(40),DEL_VOLT(40)
      DIMENSION QUAD(200)
      DIMENSION TGT_RNG(200),ERROR_MONO(200),ERROR_MIDI(200)
C
      CHARACTER*80 TITLE
      CHARACTER*40 LABX
      CHARACTER*40 LABY
      CHARACTER*40 LABY1
      CHARACTER*6  TYPE_LINE
C
      COMPLEX SUM_SIG_DIR,SUM_SIG_MULT,DEL_SIG_DIR,DEL_SIG_MULT
      COMPLEX RHO_CPLX,A,B,SUM_TOTAL,DEL_TOTAL
      COMPLEX DEL_ROTATED,UNIT_IN,UNIT_QUAD
C
      REAL  IN_PHASE,MISS_DIST
C
C     INTERNAL DATA
C
      DATA SUM_SIG_DIR/(1.,0.)/
      DATA DEL_SIG_DIR/(1.,0.)/
      DATA UNIT_IN/(1.,0.)/
      DATA UNIT_QUAD/(0.,1.)/
      LABX='TARGET RANGE  -- M'
      LABY='ELEVATION ERROR -- MR'
      LABY1='QUADRATURE COMPONENT -- DB'
      TYPE_LINE='DASH'
C
C     INPUT
C
      READ (10,1005) IPLOT,IBUG
      READ (10,1006) (SUM_DB(I),I=1,40)
      READ (10,1006) (DEL_DB(I),I=1,40)
      READ (10,1006) (ELANG_DEG(I),I=1,40)
      READ (10,1007) PHASE_ANG_DEG
      READ (10,1007) RHO
      READ (10,1007) TGT_ALT
      READ (10,1007) TGT_MAX_RNG
      READ (10,1007) TGT_MIN_RNG
      READ (10,1007) RNG_STEP
      READ (10,1007) RDR_ALT
      READ (10,1007) MISS_DIST
      READ (10,1100) TITLE
C
C     CONVERSIONS,ETC
C
      SQRT2=SQRT(2.)
      PI=4*ATAN(1.)
      PI_OVER_2=PI/2.
      DEG_TO_MR=PI/.180
      SIGN=-1.
      DO 5 I=1,40
      IF(DEL_DB(I).LT.0.) SIGN=1.
      SUM_VOLT(I)=10.**(SUM_DB(I)/20.)
      DEL_VOLT(I)=SIGN*10.**(DEL_DB(I)/20.)
      ELANG_MR(I)=ELANG_DEG(I)*DEG_TO_MR
5     CONTINUE
```

```
C
C       MONOPULSE CALIBRATION CURVE
C
        DO 10 I=1,40
        CAL_MONO(I)=DEL_VOLT(I)/SUM_VOLT(I)
 10     CONTINUE
C
C       PREVENT CALIBRATION CURVE FROM BEING DOUBLE VALUED
C
        DO 15 I=1,39
        IF(CAL_MONO(I).LT.0.) GO TO 15
        IF(CAL_MONO(I+1).GT.CAL_MONO(I)) GO TO 15
        CAL_MONO(I+1)=CAL_MONO(I)+.0001
        WRITE(6,1001) I
 15     CONTINUE
        DO 16 I=40,2,-1
        IF(CAL_MONO(I).GT.0.) GO TO 16
        IF(CAL_MONO(I-1).LT.CAL_MONO(I)) GO TO 16
        CAL_MONO(I-1)=CAL_MONO(I)-.0001
        WRITE(6,1008) I
 16     CONTINUE
        IF(IBUG.LT.1) GO TO 25
        WRITE(7,1012)
        DO 22 I=1,40
        WRITE(7,1011) CAL_MONO(I),ELANG_MR(I)
 22     CONTINUE
 25     CONTINUE
C
C       MIDI CALIBRATION CURVE
C
        DO 20 I=1,40
        CAL_MIDI(I)=2.*ATAN(CAL_MONO(I)*SQRT2)
 20     CONTINUE
        IF(IBUG.LT.1) GO TO 24
        WRITE(7,1013)
        DO 23 I=1,40
        WRITE(7,1011) CAL_MIDI(I),ELANG_MR(I)
 23     CONTINUE
 24     CONTINUE

C       PRELIMINARIES
C
        PHASE_ANG_RAD=PHASE_ANG_DEG*DEG_TO_MR/1000.
        NTOINTS=0
        TGT_RNG(1)=TGT_MIN_RNG-RNG_STEP
        NSTEPS=INT((TGT_MAX_RNG-TGT_MIN_RNG)/RNG_STEP)+1
C
C       TABULAR DATA HEADERS
C
        WRITE (20,1002) TITLE
        WRITE (20,1003)
C
C       BEGIN ENORMOUS DO LOOP
C
        DO 30 I=1,NSTEPS
C
C       GENERATION OF DIRECT AND REFLECTED SIGNAL
C
        TGT_RNG(I+1)=TGT_RNG(I)+RNG_STEP
        ANG_OFF_BORESIGHT=1000.*MISS_DIST/TGT_RNG(I+1)
        ANT_ANG_DIRECT=ANG_OFF_BORESIGHT
        CALL LININT(ELANG_MR,SUM_VOLT,40,ANT_ANG_DIRECT,GAIN_SUM,
     1              IVIEWO)
```

```
      CALL LININT(ELANG_MR, DEL_VOLT, 40, ANT_ANG_DIRECT, GAIN_DEL,
     1                IVIEW0)
      IF(IVIEW0. NE. 0. ) WRITE(6, 1009) IVIEW0
      TGT_ANG_DIR=1000. *(TGT_ALT-RDR_ALT+MISS_DIST)/TGT_RNG(I+1)
      TGT_ANG_MULT=-1000. *(TGT_ALT+RDR_ALT+MISS_DIST)/TGT_RNG(I+1)
      ANT_ANG_MULT=TGT_ANG_MULT+ANG_OFF_BORESIGHT-TGT_ANG_DIR

      CALL LININT(ELANG_MR, SUM_VOLT, 40, ANT_ANG_MULT, VOLT_MULT,
     1                IVIEW1)
      SUM_SIG_MULT=VOLT_MULT*RHO*UNIT_IN
      CALL ROTATE(SUM_SIG_MULT, PHASE_ANG_RAD)
      CALL LININT(ELANG_MR, DEL_VOLT, 40, ANT_ANG_MULT, VOLT_MULT,
     1                IVIEW2)
      DEL_SIG_MULT=VOLT_MULT*RHO*UNIT_IN
      CALL ROTATE(DEL_SIG_MULT, PHASE_ANG_RAD)
C
C     TOTAL SUM AND DIFFERENCE SIGNALS
C
      IF((IVIEW1+IVIEW2). GT. 1) WRITE(6, 1080) IVIEW1, IVIEW2, I
      SUM_TOTAL=SUM_SIG_DIR*GAIN_SUM+SUM_SIG_MULT
      DEL_TOTAL=DEL_SIG_DIR*GAIN_DEL+DEL_SIG_MULT
C
C     MONOPULSE MEASUREMENT AND CALCULATION OF QUADRATURE COMPONENT
C
      S1=CABS(SUM_TOTAL)
      D1=CABS(DEL_TOTAL)
      R1=REAL(SUM_TOTAL*CONJG(DEL_TOTAL))
      IN_PHASE=R1/(S1**2)
      IF(IN_PHASE. GE. 1. 2) IN_PHASE=1. 2
      IF(IN_PHASE. LE. -1. 2) IN_PHASE=-1. 2
      ANG=ACOS(R1/(D1*S1))
      QUAD(I+1)= D1*SIN(ANG)/S1
      QUAD(I+1)=QUAD(I+1)**2
      IF(QUAD(I+1). LT. . 0001) QUAD(I+1)=. 0001
      QUAD(I+1)=10. *ALOG10(QUAD(I+1))

      CALL LININT(CAL_MONO, ELANG_MR, 40, IN_PHASE,
     1                ANT_TGT_ANG_MES, IVIEW3)
      TGT_ANG_MES=ANT_TGT_ANG_MES-ANG_OFF_BORESIGHT
      IF(IBUG. EQ. 1) WRITE(7, 1020) IN_PHASE, TGT_ANG_MES
      ERROR_MONO(I+1)=TGT_ANG_MES
C
C     MIDI MEASUREMENT
C
      DEL_ROTATED=DEL_TOTAL/SQRT2
      CALL ROTATE(DEL_ROTATED, PI_OVER_2)
      A=SUM_TOTAL/2. +DEL_ROTATED
      B=SUM_TOTAL/2. -DEL_ROTATED
      DUM1=REAL(A*CONJG(B))
      DUM2=CABS(A)*CABS(B)
      IF(DUM1. GE. DUM2) GO TO 27
      C=-ACOS(DUM1/DUM2)
      IF(C. GE. 2. ) C=2.
      IF(C. LE. -2. ) C=-2.
      GO TO 26
C     USE LAST VALUE OF C
 27   CONTINUE
      WRITE(6, 1016) I
      IF(IBUG. EQ. 1) WRITE(7, 1016) I
 26   CALL LININT(CAL_MIDI, ELANG_MR, 40, C, ANT_TGT_ANG_MES, IVIEW4)
      TGT_ANG_MES=ANT_TGT_ANG_MES-ANG_OFF_BORESIGHT
      IF((IVIEW3+IVIEW4). GT. 1) WRITE(6, 1081) IVIEW3, IVIEW4, I
      ERROR_MIDI(I+1)=TGT_ANG_MES
```

```
      IF(IBUG.EQ.1) WRITE(7,1021) C,TGT_ANG_MES
      NPOINTS=NPOINTS+1
      WRITE(20,1004) TGT_RNG(I+1),TGT_ANG_DIR,
     3                                ERROR_MONO(I+1),
     1                                ERROR_MIDI(I+1),QUAD(I+1),IVIEW1,
     4                                IVIEW2,
     2                                IVIEW3,IVIEW4
      IVIEW1=0
      IVIEW2=0
      IVIEW3=0
      IVIEW4=0
 30   CONTINUE
C
C     END DO LOOP
C
      ERROR_MONO(1)=NPOINTS
      ERROR_MIDI(1)=NPOINTS
      QUAD(1)=NPOINTS
      TGT_RNG(1)=NPOINTS
C
C     PLOT RESULTS
C
      IF(IPLOT.EQ.0) GO TO 99
      CALL GRAPH1(TGT_RNG,ERROR_MONO,LABX,LABY,TITLE,2,XMIN,XMAX,YMIN,YMAX)
      CALL GRAPH2(TGT_RNG,ERROR_MIDI,TYPE_LINE,1)
      WRITE(6,1015) XMIN,XMAX,YMIN,YMAX
C
      CALL GRAPH1(TGT_RNG,QUAD,LABX,LABY1,TITLE,1,XMIN,XMAX,YMIN,YMAX)
      WRITE(6,1015) XMIN,XMAX,YMIN,YMAX
 99   CONTINUE
C
C     FORMAT STATEMENTS
C
 1000 FORMAT(1X,'MONO ERROR',I4)
 1001 FORMAT(1X,'POSITIVE MONO_CAL ERROR AT I=',I4)
 1002 FORMAT('1',A80)
 1003 FORMAT(1X,'   TGT_RNG  TGT_ANG_MR   ERROR_MONO  ERROR_MIDI
     1    QUAD       IVIEW1     IVIEW2     IVIEW3     IVIEW4')
 1004 FORMAT(1X,4(2X,F10.2),2X,F10.5,4(3X,I4,3X))
 1005 FORMAT(2I1)
 1006 FORMAT(10F10.3)
 1007 FORMAT(F10.2)
 1008 FORMAT(1X,'NEGATIVE MONO_CAL ERROR AT I=',I4)
 1009 FORMAT(1X,'IVIEWO ERROR',I4)
 1010 FORMAT(1X,'MIDI ERROR',I4)
 1011 FORMAT(1X,2(2X,F10.5))
 1012 FORMAT(1X,'CAL_MONO          ELANG_MR')
 1013 FORMAT(1X,'CAL_MIDI          ELANG_MR')
 1015 FORMAT(1X,'XMIN,XMAX,YMIN,YMAX',4E12.4)
 1016 FORMAT(1X,'DUM ERROR AT I=',I4)
 1020 FORMAT(1X,'MONO IN_PHASE,TGT_ANG_MES',2(2X,E12.5))
 1021 FORMAT(1X,'                    C,TGT_ANG_MES',2(2X,E12.5))
 1023 FORMAT(1X,3(2X,E10.3))
 1070 FORMAT(1X,'VOLT ERRORS',2I4)
 1080 FORMAT(1X,'IVIEW ERRORS 1&2',3I4)
 1081 FORMAT(1X,'IVIEW ERRORS 3&4',3I4)
 1100 FORMAT(A80)
C
C
      STOP
      END
C
C
```

```
SUBROUTINE ROTATE(XCOMPLEX, ANGLE)
DIMENSION XCOMPLEX(2)
A=XCOMPLEX(1)
B=XCOMPLEX(2)
C COS(ANGLE)
S-SIN(ANGLE)
XCOMPLEX(1)= A*C+B*S
XCOMPLEX(2)=-A*S+B*C
RETURN
END
```

```
      PROGRAM MULTIDATA
C
C     COMPARE CONVENTIONAL MONOPULSE AND MIDI
C
      DIMENSION SUM_DB(40),DEL_DB(40),ELANG_DEG(40),
     1                  CAL_MONO(40),
     2                  ELANG_MR(40),CAL_MIDI(40),
     3                  SUM_VOLT(40),DEL_VOLT(40)
      DIMENSION QUAD(200)
      DIMENSION TGT_RNG(200), ERROR_MONO(200),ERROR_MIDI(200)
C
      CHARACTER*80 TITLE
      CHARACTER*40 LABX
      CHARACTER*40 LABY
      CHARACTER*40 LABY1
      CHARACTER*6  TYPE_LINE
C
      COMPLEX SUM_SIG_DIR,SUM_SIG_MULT,DEL_SIG_DIR,DEL_SIG_MULT
      COMPLEX RHO_CPLX,A,B,SUM_TOTAL,DEL_TOTAL
      COMPLEX DIFFUSE_MEAN_DI,DIFFUSE_SD_DI,DIFFUSE_SD_II,
     1        SPECULAR_DI,SPECULAR_II,
     2        DIFFUSE_MEAN_II
      COMPLEX DEL_ROTATED,UNIT_IN,UNIT_QUAD
C
      REAL  IN_PHASE,MISS_DIST,FACET_ANG_ANT
C
C     INTERNAL DATA
C
      DATA SUM_SIG_DIR/(1.,0.)/
      DATA DEL_SIG_DIR/(1.,0.)/
      DATA UNIT_IN/(1.,0.)/
      DATA UNIT_QUAD/(0.,1.)/
      LABX='TARGET RANGE  -- M'
      LABY='ELEVATION ERROR -- MR'
      LABY1='QUADRATURE COMPONENT -- DB'
      TYPE_LINE='DASH'
C
C     INPUT FROM ANTENNA PATTERN FILE
C
      READ (10,1005) IPLOT,IBUG
      READ (10,1006) (SUM_DB(I),I=1,40)
      READ (10,1006) (DEL_DB(I),I=1,40)
      READ (10,1006) (ELANG_DEG(I),I=1,40)
      READ (10,1007) PHASE_ANG_DEG
      READ (10,1007) RHO
      READ (10,1007) TGT_ALT
      READ (10,1007) TGT_MAX_RNG
      READ (10,1007) TGT_MIN_RNG
      READ (10,1007) RNG_STEP
      READ (10,1007) RDR_ALT
      READ (10,1007) MISS_DIST
      WRITE (6,1111)
      READ (5,1100) TITLE
      WRITE (6,1112)
      READ (5,1113) ALT_DIFF
C
C     CONVERSIONS,ETC
C
      SQRT2=SQRT(2.)
      PI=4*ATAN(1.)
      PI_OVER_2=PI/2.
      DEG_TO_MR=PI/.180
      SIGN=-1.
```

```
      DO 5 I=1,40
      IF(DEL_DB(I).LT.0.) SIGN=1.
      SUM_VOLT(I)=10.**(SUM_DB(I)/20.)
      DEL_VOLT(I)=SIGN*10.**(DEL_DB(I)/20.)
      ELANG_MR(I)=ELANG_DEG(I)*DEG_TO_MR
 5    CONTINUE
C
C     MONOPULSE CALIBRATION CURVE
C
      DO 10 I=1,40
      CAL_MONO(I)=DEL_VOLT(I)/SUM_VOLT(I)
 10   CONTINUE
C
C     PREVENT CALIBRATION CURVE FROM BEING DOUBLE VALUED
C
      DO 15 I=1,39
      IF(CAL_MONO(I).LT.0.) GO TO 15
      IF(CAL_MONO(I+1).GT.CAL_MONO(I)) GO TO 15
      CAL_MONO(I+1)=CAL_MONO(I)+.0001
      WRITE(6,1001) I
 15   CONTINUE
      DO 16 I=40,2,-1
      IF(CAL_MONO(I).GT.0.) GO TO 16
      IF(CAL_MONO(I-1).LT.CAL_MONO(I)) GO TO 16
      CAL_MONO(I-1)=CAL_MONO(I)-.0001
      WRITE(6,1008) I
 16   CONTINUE
      IF(IBUG.LT.1) GO TO 25
      WRITE(7,1012)
      DO 22 I=1,40
      WRITE(7,1011) CAL_MONO(I),ELANG_MR(I)
 22   CONTINUE
 25   CONTINUE
C
C     MIDI CALIBRATION CURVE
C
      DO 20 I=1,40
      CAL_MIDI(I)=2.*ATAN(CAL_MONO(I)*SQRT2)
 20   CONTINUE
      IF(IBUG.LT.1) GO TO 24
      WRITE(7,1013)
      DO 23 I=1,40
      WRITE(7,1011) CAL_MIDI(I),ELANG_MR(I)
 23   CONTINUE
 24   CONTINUE

      NPOINTS=0
C
C     TABULAR DATA HEADERS
C
      WRITE (20,1002) TITLE
      WRITE (20,1003)
C
C     BEGIN ENORMOUS ITERATIVE LOOP
C

 30   CONTINUE
C
C     VECTOR SUMMATION OF RETURNS FROM FACETS
C
C     READ TARGET POSITION, DIRECT SIGNAL, SPECULAR RETURN
C
      READ(30,*) TGT_X,TGT_Y,TGT_Z,VEL_TGT_X,VEL_TGT_Y,VEL_TGT_Z
```

```
      WRITE(50,1200)TGT_X,TGT_Y,TGT_Z,VEL_TGT_X,VEL_TGT_Y,VEL_TGT_Z
      READ(30,*)DIR_DIR_SIG
      WRITE(50,1220)DIR_DIR_SIG
      READ(30,*) SPEC_RNG,SPEC_ANG,SPECULAR_DI,SPECULAR_II
      WRITE(50,1210)SPEC_RNG,SPEC_ANG,SPECULAR_DI,SPECULAR_II

 1200 FORMAT(1X,'TGT_X,TGT_Y,TGT_Z,VEL_TGT_X,VEL_TGT_Y,VEL_TGT_Z=',
     1       6E12.4)
 1210 FORMAT(1X,'SPEC_RNG,SPEC_ANG,SPECULAR_DI,SPECULAR_II=',
     1       6E12.4)
 1220 FORMAT(1X,'DIRECT SIGNAL VOLT=',E12.4)
      TGT_RNG(NPOINTS+2)=TGT_Y-88.
      TGT_ANG=(ALT_DIFF)*1000./TGT_RNG(NPOINTS+2)
      SPEC_ANG_ANT=-1000.*SPEC_ANG-TGT_ANG
C
      ANT_ANG_DIRECT=0.
      CALL LININT(ELANG_MR,SUM_VOLT,40,ANT_ANG_DIRECT,GAIN_SUM,
     1            IVIEWO)
      CALL LININT(ELANG_MR,DEL_VOLT,40,ANT_ANG_DIRECT,GAIN_DEL,
     1            IVIEWO)
      IF(IVIEWO. NE. 0. ) WRITE(6,1009) IVIEWO
C

      CALL LININT(ELANG_MR,SUM_VOLT,40,SPEC_ANG_ANT,VOLT_MULT_SUM,
     1            IVIEW1)
      SUM_TOTAL=SPECULAR_DI*GAIN_SUM*VOLT_MULT_SUM+SPECULAR_II
     1         *VOLT_MULT_SUM**2+SUM_SIG_DIR*DIR_DIR_SIG*GAIN_SUM**2
      CALL LININT(ELANG_MR,DEL_VOLT,40,SPEC_ANG_ANT,VOLT_MULT_DEL,
     1            IVIEW1)
      DEL_TOTAL=SPECULAR_DI*GAIN_SUM*VOLT_MULT_DEL/2.+SPECULAR_II
     1         *VOLT_MULT_SUM*VOLT_MULT_DEL+DEL_SIG_DIR*DIR_DIR_SIG
     2         *GAIN_SUM*GAIN_DEL+SPECULAR_DI*VOLT_MULT_SUM
     3         *GAIN_DEL/2.
C
C     READ DIFFUSE,WEIGHT WITH ANTENNA GAIN
C
      READ(30,*) NFACETS
      WRITE(50,1230) NFACETS
 1230 FORMAT(1X,'NFACETS= ',I5)
      DO 35 J=1,NFACETS
      READ(30,*) RNG_FAC,EL_ANG_FACET,AZ_ANG_FACET,
     1           DIFFUSE_MEAN_DI,DIFFUSE_SD_DI,
     2           DIFFUSE_MEAN_II,DIFFUSE_SD_II
      TGT_FACET_ANG EL_ANG_FACET-TGT_ANG/1000.
C
      FACET_ANG_ANT=-1000.*ACOS(COS(TGT_FACET_ANG)*COS(AZ_ANG_FACET))
      CALL LININT(ELANG_MR,SUM_VOLT,40,FACET_ANG_ANT,VOLT_MULT_SUM,
     1            IVIEW1)
      SUM_TOTAL=SUM_TOTAL+DIFFUSE_SD_DI*GAIN_SUM*VOLT_MULT_SUM
     1         +DIFFUSE_SD_II*VOLT_MULT_SUM**2
      CALL LININT(ELANG_MR,DEL_VOLT,40,FACET_ANG_ANT,VOLT_MULT_DEL,
     1            IVIEW1)
      DEL_TOTAL=DEL_TOTAL+DIFFUSE_SD_DI*GAIN_SUM*VOLT_MULT_DEL/2.
     1         +DIFFUSE_SD_II*VOLT_MULT_SUM*VOLT_MULT_DEL+
     2         DIFFUSE_SD_DI*VOLT_MULT_SUM*GAIN_DEL/2.
 35   CONTINUE
C
C     SUM_TOTAL AND DEL_TOTAL SIGNAL COMPUTATION NOW COMPLETE
C     COMPUTE IN PHASE AND QUADRATURE COMPONENTS OF
C     DEL/SUM RATIO
C
      S1 CABS(SUM_TOTAL)
      WRITE(50,1240) S1
```

```
 1240   FORMAT(1X,'S1= ',6E12.4)
        D1=CABS(DEL_TOTAL)
        R1=REAL(SUM_TOTAL*CONJG(DEL_TOTAL))
        IN_PHASE=R1/(S1**2)
        ANG=ACOS(R1/(D1*S1))
        QUAD(NPOINTS+2)= D1*SIN(ANG)/S1
        QUAD(NPOINTS+2)=QUAD(NPOINTS+2)**2
        IF(QUAD(NPOINTS+2).LT..0001) QUAD(NPOINTS+2)=.0001
        QUAD(NPOINTS+2)=10.*ALOG10(QUAD(NPOINTS+2))
C
C       MONOPULSE MEASUREMENT
C
        CALL LININT(CAL_MONO,ELANG_MR,40,IN_PHASE,
     1              ANT_TGT_ANG_MES,IVIEW3)
        TGT_ANG_MES=ANT_TGT_ANG_MES
        IF(IBUG.EQ.1) WRITE(7,1020) IN_PHASE,TGT_ANG_MES
        ERROR_MONO(NPOINTS+2)=TGT_ANG_MES
C
C       MIDI MEASUREMENT
C
        DEL_ROTATED=DEL_TOTAL/SQRT2
        CALL ROTATE(DEL_ROTATED,PI_OVER_2)
        A=SUM_TOTAL/2.+DEL_ROTATED
        B=SUM_TOTAL/2.-DEL_ROTATED
        DUM1=REAL(A*CONJG(B))
        DUM2=CABS(A)*CABS(B)
        IF(DUM1.GE.DUM2) GO TO 27
        C=-ACOS(DUM1/DUM2)
        GO TO 26
C       USE LAST VALUE OF C
 27     CONTINUE
        WRITE(6,1016) NPOINTS+1
        IF(IBUG.EQ.1) WRITE(7,1016) NPOINTS+1
 26     CALL LININT(CAL_MIDI,ELANG_MR,40,C,ANT_TGT_ANG_MES,IVIEW4)
        TGT_ANG_MES=ANT_TGT_ANG_MES-ANG_OFF_BORESIGHT
        IF((IVIEW3+IVIEW4).GT.1) WRITE(6,1081) IVIEW3,IVIEW4,NPOINTS+1
        ERROR_MIDI(NPOINTS+2)=TGT_ANG_MES
        IF(IBUG.EQ.1) WRITE(7,1021) C,TGT_ANG_MES
        NPOINTS=NPOINTS+1
        WRITE(20,1004) TGT_RNG(NPOINTS+1),TGT_ANG,
     3                                ERROR_MONO(NPOINTS+1),
     1                                ERROR_MIDI(NPOINTS+1),QUAD(NPOINTS+1),IVIEW1,
     4                                IVIEW2,
     2                                IVIEW3,IVIEW4
        IVIEW1=0
        IVIEW2=0
        IVIEW3=0
        IVIEW4=0
        READ(30,*) IFLAG
        WRITE(50,*) IFLAG
        IF(IFLAG.EQ.1) GO TO 30
        IF(NPOINTS.EQ.1) GO TO 99

C       END DO LOOP
C
        ERROR_MONO(1)=NPOINTS
        ERROR_MIDI(1)=NPOINTS
        QUAD(1)=NPOINTS
        TGT_RNG(1)=NPOINTS
C
C       PLOT RESULTS
C
        IF(IPLOT.EQ.0) GO TO 99
```

```
      CALL GRAPH1(TGT_RNG,ERROR_MIDI,LABX,LABY,TITLE,2,XMIN,XMAX,YMIN,YMAX)
      CALL GRAPH2(TGT_RNG,ERROR_MONO,TYPE_LINE,1)
      WRITE(6,1015) XMIN,XMAX,YMIN,YMAX
C
      CALL GRAPH1(TGT_RNG,QUAD,LABX,LABY1,TITLE,1,XMIN,XMAX,YMIN,YMAX)
      WRITE(6,1015) XMIN,XMAX,YMIN,YMAX
 99   CONTINUE
C
C     FORMAT STATEMENTS
C
 1000 FORMAT(1X,'MONO ERROR',I4)
 1001 FORMAT(1X,'POSITIVE MONO_CAL ERROR AT NPOINTS =',I4)
 1002 FORMAT('1',A80)
 1003 FORMAT(1X,'   TGT_RNG  TGT_ANG_MR   ERROR_MONO  ERROR_MIDI
     1    QUAD      IVIEW1     IVIEW2     IVIEW3     IVIEW4')
 1004 FORMAT(1X,4(2X,F10.2),2X,F10.5,4(3X,I4,3X))
 1005 FORMAT(2I1)
 1006 FORMAT(10F10.3)
 1007 FORMAT(F10.2)
 1008 FORMAT(1X,'NEGATIVE MONO_CAL ERROR AT NPOINTS =',I4)
 1009 FORMAT(1X,'IVIEWO ERROR',I4)
 1010 FORMAT(1X,'MIDI ERROR',I4)
 1011 FORMAT(1X,2(2X,F10.5))
 1012 FORMAT(1X,'CAL_MONO          ELANG_MR')
 1013 FORMAT(1X,'CAL_MIDI          ELANG_MR')
 1015 FORMAT(1X,'XMIN,XMAX,YMIN,YMAX',4E12.4)
 1016 FORMAT(1X,'DUM ERROR AT NPOINTS =',I4)
 1020 FORMAT(1X,'MONO IN_PHASE,TGT_ANG_MES',2(2X,E12.5))
 1021 FORMAT(1X,'                    C,TGT_ANG_MES',2(2X,E12.5))
 1023 FORMAT(1X,3(2X,E10.3))
 1070 FORMAT(1X,'VOLT ERRORS',2I4)
 1080 FORMAT(1X,'IVIEW ERRORS 1&2',3I4)
 1081 FORMAT(1X,'IVIEW ERRORS 3&4',3I4)
 1111 FORMAT(1X,'ENTER TITLE: ')
 1100 FORMAT(A80)
 1112 FORMAT(1X,'ENTER DIFFERENCE BETWEEN TARGET AND RADAR ALTITUDES
     1  (TGT_ALT-RDR_ALT)')
 1113 FORMAT(F10.2)
C
C
      STOP
      END

      SUBROUTINE ROTATE(XCOMPLEX,ANGLE)
      DIMENSION XCOMPLEX(2)
      A=XCOMPLEX(1)
      B=XCOMPLEX(2)
      C=COS(ANGLE)
      S=SIN(ANGLE)
      XCOMPLEX(1)=A*C+B*S
      XCOMPLEX(2)=-A*S+B*C
      RETURN
      END
```

```
      PROGRAM  CORRELATION DISTANCE VERSION 2
      DIMENSION DIFF(51),DEL_Y(51),MISS(51)
      CHARACTER*80  TITLE
      CHARACTER*40  LABX,LABY
      CHARACTER*6   TYPE_LINE

      DOUBLE PRECISION DIST,PATH_LENGTH_DIFF

      REAL  MISS

      LABX = 'MISS DISTANCE'
      LABY = 'DELTA -- M'

      WRITE(6,1000)
 1000 FORMAT(1X,'ENTER RDR_ALT,TGT_ALT,TGT_RNG,DEL_X',4F10.2)
      READ(5,1001)RDR_ALT,TGT_ALT,TGT_RNG,DEL_X
 1001 FORMAT(4F10.2)
      WRITE(6,1002)
 1002 FORMAT(1X,'ENTER TITLE')
      READ(5,1003) TITLE
 1003 FORMAT(A80)
      CALL DELTA(RDR_ALT,TGT_ALT,TGT_RNG,PATH_LENGTH_DIFF)
C     WRITE(6,*)PATH_LENGTH_DIFF

      DEL_Y(1) = -15.
      MISS(1) = -15.

      DO 10 I=1,30
      MISS(I+1)=MISS(I)+1
      DEL_Y(I+1)=MISS(I+1)
      RNG=TGT_RNG+DEL_X
      ALT=TGT_ALT+DEL_Y(I+1)
      CALL DELTA(RDR_ALT,ALT,RNG,DIST)
      DIFF(I+1)=DIST-PATH_LENGTH_DIFF
C     WRITE(6,*)DIFF(I+1)
   10 CONTINUE

      MISS(1)=30.
      DIFF(1)=30.

      CALL GRAPH1(MISS,DIFF,LABX,LABY,TITLE,1,XMIN,XMAX,
     2                YMIN,YMAX)

      STOP
      END

      SUBROUTINE DELTA(HR,HT,RT,DEL)
      DOUBLE PRECISION A,B,Q,R1,R2,DEL
      A = (HT + HR)**2
      B = (HT - HR)**2
      Q = RT**2
      R1 = DSQRT(A+Q)
      R2 = DSQRT(B+Q)
      DEL = R1-R2
      RETURN
      END
```

```
      PROGRAM MCORELATE
C
      DIMENSION SUM_DB(40),DEL_DB(40),ELANG_DEG(40),
     1                  CAL_MONO(40),
     2                  ELANG_MR(40),CAL_MIDI(40),
     3                  SUM_VOLT(40),DEL_VOLT(40)
      DIMENSION QUAD(200),RELATIVE_ERROR(200)
      DIMENSION ERROR_MONO(200),ERROR_MIDI(200)
      DIMENSION DEL_Y(200),DIFF(200),MISS(200)
C
      CHARACTER*80 TITLE
      CHARACTER*40 LABX
      CHARACTER*40 LABY
      CHARACTER*40 LABY1
      CHARACTER*6  TYPE_LINE
C
      COMPLEX SUM_SIG_DIR,SUM_SIG_MULT,DEL_SIG_DIR,DEL_SIG_MULT
      COMPLEX RHO_CPLX,SUM_TOTAL,DEL_TOTAL,DEL_TOTAL_TGT
      COMPLEX DEL_ROTATED,UNIT_IN,UNIT_QUAD,SUM_TOTAL_TGT
      COMPLEX SUM_SIG_MULT_TGT,DEL_SIG_MULT_TGT
C
      REAL IN_PHASE,MISS_DIST
C
      DOUBLE PRECISION DIST,PATH_LENGTH_DIFF

      WAVELENGTH=0.032
      LABX='MISS DISTANCE -- M'
      LABY='DELTA -- M'
      LABY1='RELATIVE ERROR -- MR'
C
C     INTERNAL DATA
C
      DATA SUM_SIG_DIR/(1.,0.)/
      DATA DEL_SIG_DIR/(1.,0.)/
      DATA UNIT_IN/(1.,0.)/
      DATA UNIT_QUAD/(0.,1.)/
C
C     INPUT
C
      READ (10,1005) IPLOT,IBUG
      READ (10,1006) (SUM_DB(I),I=1,40)
      READ (10,1006) (DEL_DB(I),I=1,40)
      READ (10,1006) (ELANG_DEG(I),I=1,40)
      READ (10,1007) PHASE_ANG_DEG
      READ (10,1007) RHO
      READ (10,1007) TGT_ALT
      READ (10,1007) TGT_MAX_RNG
      READ (10,1007) TGT_MIN_RNG
      READ (10,1007) RNG_STEP
      READ (10,1007) RDR_ALT
      READ (10,1007) MISS_DIST
      READ (10,1100) TITLE
C
C     CONVERSIONS,ETC
C
      SQRT2=SQRT(2.)
      PI=4*ATAN(1.)
      PI_OVER_2=PI/2.
      DEG_TO_MR=PI/.180
      SIGN=-1.
      DO 5 I=1,40
      IF(DEL_DB(I).LT.0.) SIGN=1.
      SUM_VOLT(I)=10.**(SUM_DB(I)/20.)
```

```
          DEL_VOLT(I)=SIGN*10.**(DEL_DB(I)/20.)
          ELANG_MR(I)=ELANG_DEG(I)*DEG_TO_MR
  5       CONTINUE
C
C         MONOPULSE CALIBRATION CURVE
C
          DO 10 I=1,40
          CAL_MONO(I)=DEL_VOLT(I)/SUM_VOLT(I)
  10      CONTINUE
C
C         PREVENT CALIBRATION CURVE FROM BEING DOUBLE VALUED
C
          DO 15 I=1,39
          IF(CAL_MONO(I).LT.0.) GO TO 15
          IF(CAL_MONO(I+1).GT.CAL_MONO(I)) GO TO 15
          CAL_MONO(I+1)=CAL_MONO(I)+.0001
          WRITE(6,1009) I
  15      CONTINUE
          DO 16 I=40,2,-1
          IF(CAL_MONO(I).GT.0.) GO TO 16
          IF(CAL_MONO(I-1).LT.CAL_MONO(I)) GO TO 16
          CAL_MONO(I-1)=CAL_MONO(I)-.0001
          WRITE(6,1008) I
  16      CONTINUE
          IF(IBUG.LT.1) GO TO 25
          WRITE(7,1012)
          DO 22 I=1,40
          WRITE(7,1011) CAL_MONO(I),ELANG_MR(I)
  22      CONTINUE
  25      CONTINUE
C
C         MIDI CALIBRATION CURVE
C
          DO 20 I=1,40
          CAL_MIDI(I)=2.*ATAN(CAL_MONO(I)*SQRT2)
  20      CONTINUE
          IF(IBUG.LT.1) GO TO 24
          WRITE(7,1013)
          DO 23 I=1,40
          WRITE(7,1011) CAL_MIDI(I),ELANG_MR(I)
  23      CONTINUE
  24      CONTINUE
C

          WRITE(6,1000)
C
 1000     FORMAT(1X,'ENTER RDR_ALT,TGT_ALT,TGT_RNG,DEL_X',4F10.2)
          READ(5,1001)RDR_ALT,TGT_ALT,TGT_RNG,DEL_X
 1001     FORMAT(4F10.2)
          WRITE(6,1002)
 1002     FORMAT(1X,'ENTER TITLE')
          READ(5,1003)TITLE
 1003     FORMAT(A80)
          CALL DELTA(RDR_ALT,TGT_ALT,TGT_RNG,PATH_LENGTH_DIFF)
C         WRITE(6,*)PATH_LENGTH_DIFF
          PHASE_ANG_RAD=PI+PATH_LENGTH_DIFF*2.*PI/WAVELENGTH
C
C         TARGET ANGLE ERROR,MIDI
C
          TGT_ANG_DIR=1000.*(TGT_ALT-RDR_ALT)/TGT_RNG
          TGT_ANG_MULT=-1000.*(TGT_ALT+RDR_ALT)/TGT_RNG
          ANT_ANG_MULT=TGT_ANG_MULT-TGT_ANG_DIR
          CALL LININT(ELANG_MR,SUM_VOLT,40,ANT_ANG_MULT,VOLT_MULT_SUM,
```

```
     1              IV1)
      CALL LININT(EL ANG_MR, DEL_VOLT, 40, ANT_ANG_MULT, VOLT_MULT_DEL,
     1              IV2)
      SUM_SIG_MULT_TGT=VOLT_MULT_SUM*RHO*UNIT_IN
      DEL_SIG_MULT_TGT=VOLT_MULT_DEL*RHO*UNIT_IN
      CALL ROTATE(SUM_SIG_MULT_TGT, PHASE_ANG_RAD)
      CALL ROTATE(DEL_SIG_MULT_TGT, PHASE_ANG_RAD)
      BORESIGHT_ANG=0.
      CALL LININT(EL ANG_MR, SUM_VOLT, 40, BORESIGHT_ANG, BORESIGHT_GAIN_SUM,
     1              IV3)
      CALL LININT(EL ANG_MR, DEL_VOLT, 40, BORESIGHT_ANG, BORESIGHT_GAIN_DEL,
     1              IV4)
      SUM_TOTAL_TGT=SUM_SIG_DIR*BORESIGHT_GAIN_SUM+
     1               SUM_SIG_MULT_TGT
      DEL_TOTAL_TGT=DEL_SIG_DIR*BORESIGHT_GAIN_DEL+
     1               DEL_SIG_MULT_TGT
      S1 CABS(SUM_TOTAL_TGT)
      D1 CABS(DEL_TOTAL_TGT)
      R1 REAL(SUM_TOTAL_TGT*CONJG(DEL_TOTAL_TGT))
      C R1/S1**2

      CALL LININT(CAL_MIDI, ELANG_MR, 40, C, ANT_TGT_ANG_MES,
     1              IV5)
      TGT_ERROR=ANT_TGT_ANG_MES
      WRITE(025, 1301) TGT_ERROR, C, PHASE_ANG_RAD
1301  FORMAT(1X, 'TGT_ERROR, C, PHASE_ANG_RAD=', 7F10.4)
      WRITE(025, 1302)
1302  FORMAT(1X, 'DEL_Y      ANT_ANG_DIR    GAIN_DEL
     1            C     ANT_PROJ_ANG_MILS  PHASE_ANG_RAD')
      DEL_Y(1)=-15.

      DO 30 I=1, 30
      DEL_Y(I+1)=DEL_Y(I)+1.
      RNG=TGT_RNG+DEL_X
      ALT=TGT_ALT+DEL_Y(I+1)
      CALL DELTA(RDR_ALT, ALT, RNG, DIST)
C
C     PROJECTILE ANGLE ERROR, MIDI
C
      PHASE_ANG_RAD=PI+DIST*2.*PI/WAVELENGTH
      ANG_OFF_BORESIGHT=1000.*(DEL_Y(I+1)-DEL_X*
     1                  TGT_ANG_DIR/1000.)/RNG
      PROJ_ANG_DIR=1000.*(ALT-RDR_ALT)/RNG
      PROJ_ANG_MULT=-1000.*(ALT+RDR_ALT)/RNG
      ANT_ANG_DIR=ANG_OFF_BORESIGHT
      ANT_ANG_MULT=PROJ_ANG_MULT-PROJ_ANG_DIR+ANG_OFF_BORESIGHT

      CALL LININT(ELANG_MR, SUM_VOLT, 40, ANT_ANG_MULT, VOLT_MULT_SUM,
     1              IV1)
      CALL LININT(ELANG_MR, DEL_VOLT, 40, ANT_ANG_MULT, VOLT_MULT_DEL,
     1              IV2)
      SUM_SIG_MULT=VOLT_MULT_SUM*RHO*UNIT_IN
      DEL_SIG_MULT=VOLT_MULT_DEL*RHO*UNIT_IN
      CALL ROTATE(SUM_SIG_MULT, PHASE_ANG_RAD)
      CALL ROTATE(DEL_SIG_MULT, PHASE_ANG_RAD)
      CALL LININT(ELANG_MR, SUM_VOLT, 40, ANT_ANG_DIR,
     1              GAIN_SUM, IV3)
      CALL LININT(ELANG_MR, DEL_VOLT, 40, ANT_ANG_DIR,
     1              GAIN_DEL, IV4)
      SUM_TOTAL=SUM_SIG_DIR*GAIN_SUM+SUM_SIG_MULT
      DEL_TOTAL=DEL_SIG_DIR*GAIN_DEL+DEL_SIG_MULT
      S1=CABS(SUM_TOTAL)
      D1=CABS(DEL_TOTAL)
```

```
          R1 RFAL(SUM_TOTAL*CONJG(DEL_TOTAL))
          C=R1/S1**2

          CALL LININT(CAL_MIDI,ELANG_MR,40,C,ANT_PROJ_ANG_MES,
         1                IV6)
          PROJ_ERROR=ANT_PROJ_ANG_MES-ANG_OFF_BORESIGHT
          RELATIVE_ERROR(I+1)=PROJ_ERROR-TGT_ERROR
          WRITE(025,1300) DEL_Y(I+1),ANT_ANG_DIR,GAIN_DEL,C,ANT_PROJ_ANG_MES
         1                ,PHASE_ANG_RAD
 1300     FORMAT(10F10.4)

          DIFF(I+1)=DIST-PATH_LENGTH_DIFF
C         WRITE(6,*)DIFF(I+1)
    30    CONTINUE

          DEL_Y(1)=30.
          DIFF(1)=30.
          RELATIVE_ERROR(1)=30.

          CALL GRAPH1(DEL_Y,DIFF,LABX,LABY,TITLE,1,XMIN,XMAX,
         1            YMIN,YMAX)
          CALL GRAPH1(DEL_Y,RELATIVE_ERROR,LABX,LABY1,TITLE,1,XMIN,
         1            XMAX,YMIN,YMAX)
C
C         FORMAT STATEMENTS
C
 1005     FORMAT(2I1)
 1006     FORMAT(10F10.3)
 1007     FORMAT(F10.2)
 1008     FORMAT(1X,'NEGATIVE MONO_CAL ERROR AT I=',I4)
 1009     FORMAT(1X,'POSITIVE MONO_CAL ERROR AT I=',I4)
 1011     FORMAT(1X,2(2X,F10.5))
 1012     FORMAT(1X,'CAL_MONO          ELANG_MR')
 1013     FORMAT(1X,'CAL_MIDI          ELANG_MR')
 1100     FORMAT(A80)
          STOP
          END

          SUBROUTINE DELTA(HR,HT,RT,DEL)
          DOUBLE PRECISION A,B,C,R1,R2,DEL
          A = (HT + HR)**2
          B = (HT - HR)**2
          C = RT**2
          R1 = DSQRT(A+C)
          R2 = DSQRT(B+C)
          DEL  = R1-R2
          RETURN
          END



C
          SUBROUTINE ROTATE(XCOMPLEX,ANGLE)
          DIMENSION XCOMPLEX(2)
          A=XCOMPLEX(1)
          B=XCOMPLEX(2)
          C COS(ANGLE)
          S=SIN(ANGLE)
          XCOMPLEX(1)= A*C+B*S
          XCOMPLEX(2)=-A*S+B*C
          RETURN
          END
```

```
      PROGRAM INTERFER_TO_SIG
C
C     COMPUTE CLUTTER TO TARGET AND MULTIPATH TO TARGET RATIOS
C
      DIMENSION SUM_DB(16),DEL_DB(16),ELANG_DEG(16),
     1                 ELANG_MR(16)
      DIMENSION TGT_RNG(200),MULT_TO_TGT_SUM(200),
     1          CLUT_TO_TGT_SUM(200),MULT_TO_TGT_DEL(200),
     2          CLUT_TO_TGT_DEL(200)
C
      CHARACTER*80 TITLE
      CHARACTER*40 LABX
      CHARACTER*40 LABY
      CHARACTER*40 LABY1
      CHARACTER*6  TYPE_LINE
C
      REAL MULT_TO_TGT_SUM,MISS_DIST,MULT_TO_TGT_DEL
C
C     INTERNAL DATA
C
      LABX='TARGET RANGE  -- M'
      LABY='CLUTTER TO TARGET RATIO -DB'
      LABY1='MULTIPATH TO TARGET RATIO--DB'
      TYPE_LINE='DASH'
C
C     INPUT FROM FILE
C
      READ (10,1005) IPLOT,IBUG
      READ (10,1006) (SUM_DB(I),I=1,16)
      READ (10,1006) (DEL_DB(I),I=1,16)
      READ (10,1006) (ELANG_DEG(I),I=1,16)
      READ (10,1007) PHASE_ANG_DEG
      READ (10,1007) RHO
      READ (10,1007) TGT_ALT
      READ (10,1007) TGT_MAX_RNG
      READ (10,1007) TGT_MIN_RNG
      READ (10,1007) RNG_STEP
      READ (10,1007) RDR_ALT
      READ (10,1007) MISS_DIST
C     READ (10,1100) TITLE
      WRITE(6,1000)
      READ (5,1001) TITLE
C
C     INPUT FROM TERMINAL
C
      WRITE(6,1200)
      READ(5,*)SIGMA_ZERO,SIGMA_TGT,BEAM_WIDTH,RNG_RES
 1200 FORMAT(1X,'ENTER SIGMA_ZERO--DB,SIGMA_TGT--DBSM,
     1       BEAM_WIDTH--DEG,RNG_RES--M')
      WRITE(10,*)SIGMA_ZERO,SIGMA_TGT,BEAM_WIDTH,RNG_RES
C
C     CONVERSIONS,ETC
C
      SQRT2=SQRT(2.)
      PI=4*ATAN(1.)
      PI_OVER_2=PI/2.
      DEG_TO_MR=PI/.180
      DO 5 I=1,16
      ELANG_MR(I)=ELANG_DEG(I)*DEG_TO_MR
    5 CONTINUE
C
      BEAM_WIDTH_RAD=BEAM_WIDTH*DEG_TO_MR/1000.
      NPOINTS 0
```

```
      TGT_RNG(1)=TGT_MIN_RNG-RNG_STEP
      NSTEPS=INT((TGT_MAX_RNG-TGT_MIN_RNG)/RNG_STEP)+1
      IF(IVIEWO. NE. 0. ) WRITE(6,1009) IVIEWO
C
C     BEGIN CALCULATION DO LOOP
C
      DO 30 I=1,NSTEPS
      TGT_RNG(I+1)=TGT_RNG(I)+RNG_STEP
      ANG_OFF_BORESIGHT=1000.*MISS_DIST/TGT_RNG(I+1)
      ANT_ANG_DIRECT=ANG_OFF_BORESIGHT
      CALL DQUADINT(ELANG_MR,SUM_DB,16,ANT_ANG_DIRECT,GAIN_SUM,
     1              IVIEWO)
      CALL DQUADINT(ELANG_MR,DEL_DB,16,ANT_ANG_DIRECT,GAIN_DEL,
     1              IVIEWOO)

      TGT_ANG_DIR=1000.*(TGT_ALT-RDR_ALT+MISS_DIST)/TGT_RNG(I+1)
      TGT_ANG_MULT=-1000.*(TGT_ALT+RDR_ALT+MISS_DIST)/TGT_RNG(I+1)
      ANT_ANG_MULT=TGT_ANG_MULT+ANG_OFF_BORESIGHT-TGT_ANG_DIR
      CLUT_ANG=-1000.*RDR_ALT/TGT_RNG(I+1)
      ANT_ANG_CLUT=CLUT_ANG-TGT_ANG_DIR+ANG_OFF_BORESIGHT
      CALL DQUADINT(ELANG_MR,SUM_DB,16,ANT_ANG_MULT,GAIN_MULT,
     1              IVIEW1)
      CALL DQUADINT(ELANG_MR,SUM_DB,16,ANT_ANG_CLUT,GAIN_CLUT,
     1              IVIEW2)
      SIGMA_CLUT=10.*ALOG10(TGT_RNG(I+1)*BEAM_WIDTH_RAD*RNG_RES)
     1           +SIGMA_ZERO
      CLUT_TO_TGT_SUM(I+1)=2*(GAIN_CLUT-GAIN_SUM)-SIGMA_TGT+SIGMA_CLUT
      MULT_TO_TGT_SUM(I+1)=GAIN_MULT-GAIN_SUM+20.*ALOG10(RHO)
      CALL DQUADINT(ELANG_MR,DEL_DB,16,ANT_ANG_MULT,GAIN_MULT_DEL,
     1              IVIEW3)
      CALL DQUADINT(ELANG_MR,DEL_DB,16,ANT_ANG_MULT,GAIN_CLUT_DEL,
     1              IVIEW4)
      CLUT_TO_TGT_DEL(I+1)=GAIN_CLUT_SUM+GAIN_CLUT_DEL-GAIN_DEL
     1                     -SIGMA_TGT+SIGMA_CLUT
      MULT_TO_TGT_DEL(I+1)=GAIN_MULT_DEL-GAIN_DEL+20.*ALOG10(RHO)
      WRITE(11,*)TGT_RNG(I+1),CLUT_TO_TGT_SUM(I+1),GAIN_SUM,
     1  GAIN_CLUT,SIGMA_CLUT
      NPOINTS=NPOINTS+1
 30   CONTINUE
C
C     END DO LOOP
C
      CLUT_TO_TGT_SUM(1)=NPOINTS
      MULT_TO_TGT_SUM(1)=NPOINTS
      CLUT_TO_TGT_DEL(1)=NPOINTS
      MULT_TO_TGT_DEL(1)=NPOINTS
      TGT_RNG(1)=NPOINTS
C
C     PLOT RESULTS
C
      CALL GRAPH1(TGT_RNG,CLUT_TO_TGT_SUM,LABX,LABY,TITLE,2,XMIN,XMAX,
     1            YMIN,YMAX)
      CALL GRAPH2(TGT_RNG,CLUT_TO_TGT_DEL,TYPE_LINE,1)
      CALL GRAPH1(TGT_RNG,MULT_TO_TGT_SUM,LABX,LABY1,TITLE,2,XMIN,XMAX,
     1            YMIN,YMAX)
      CALL GRAPH2(TGT_RNG,MULT_TO_TGT_DEL,TYPE_LINE,1)
      WRITE(6,1015) XMIN,XMAX,YMIN,YMAX
C
 99   CONTINUE
C
C     FORMAT STATEMENTS

1000  FORMAT(1X,'ENTER TITLE: ')
```

```
 1001   FORMAT(A80)
 1005   FORMAT(2I1)
 1006   FORMAT(8F10.3)
 1007   FORMAT(F10.2)
 1009   FORMAT(1X,'IVIEWO ERROR',I4)
 1015   FORMAT(1X,'XMIN,XMAX,YMIN,YMAX',4E12.4)
 1100   FORMAT(A80)
C
        STOP
        END
```

APPENDIX D
SECOND GENERATION MIDI
TRACKING ERRORS DUE TO LAND
CLUTTER INTERFERENCE

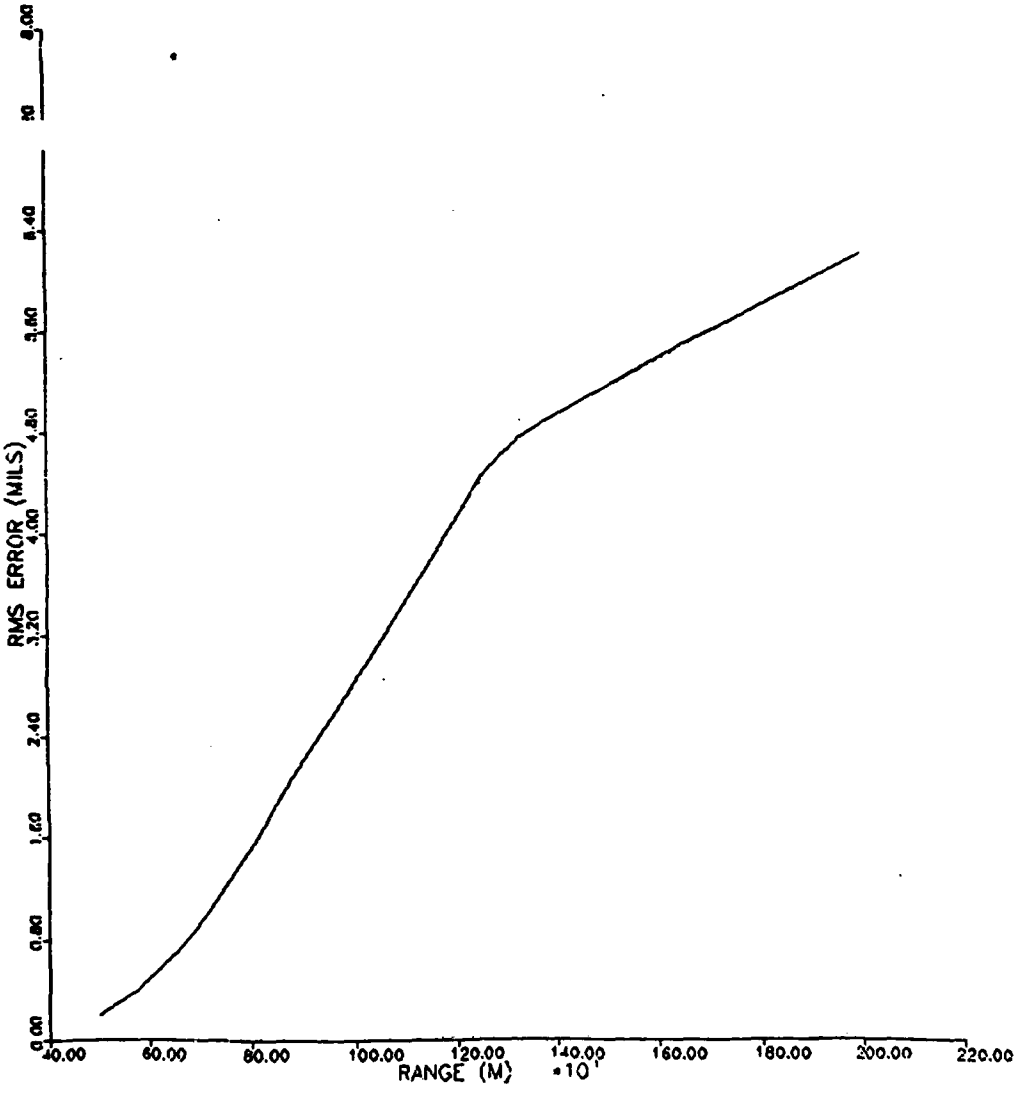

Figure D-1. MIDI tracking error: Vulcan scoring; X-band; 40dB MTI improvement factor; target height = 15 m.

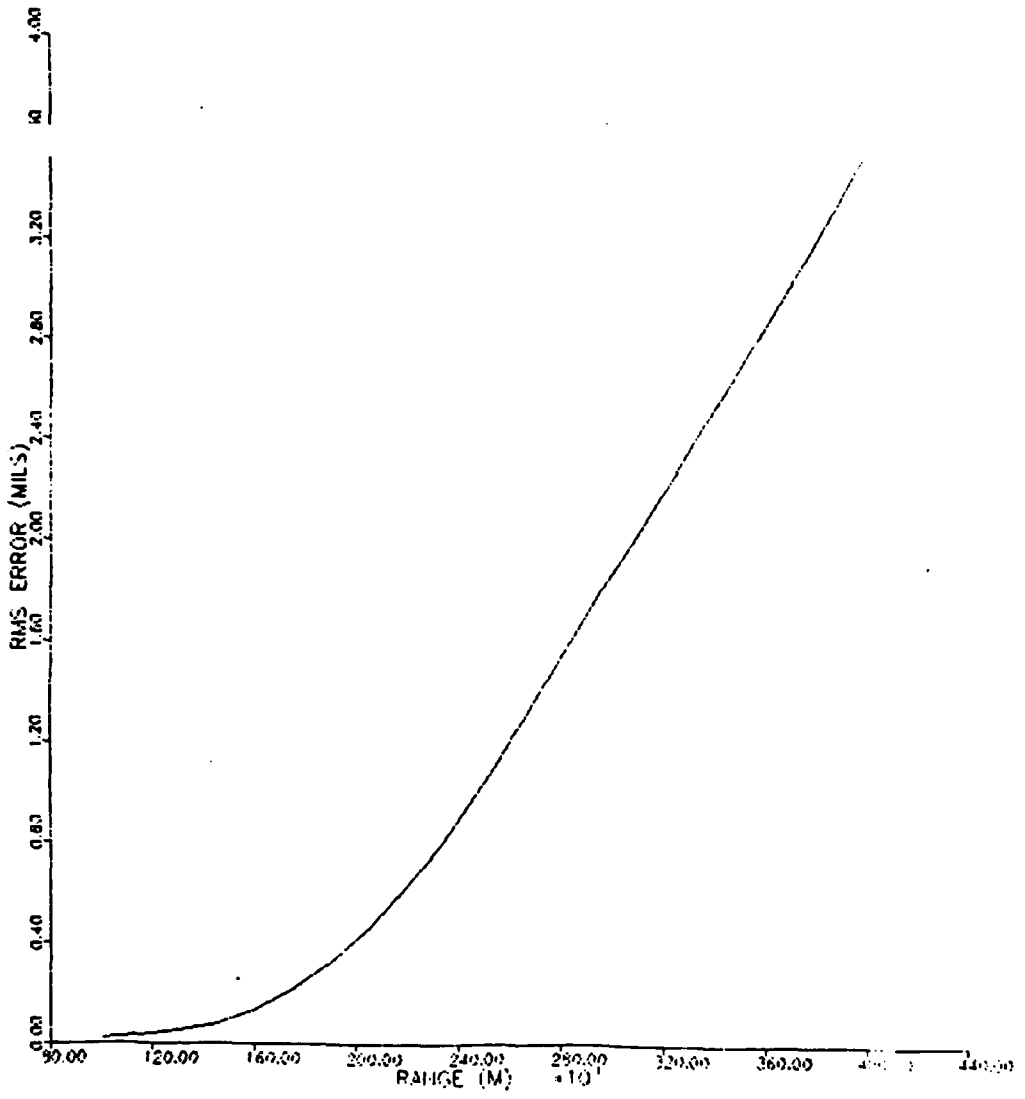

Figure D-2. MIDI tracking error: York scoring; X-band; 40dB MTI improvement factor; target height = 50 m.

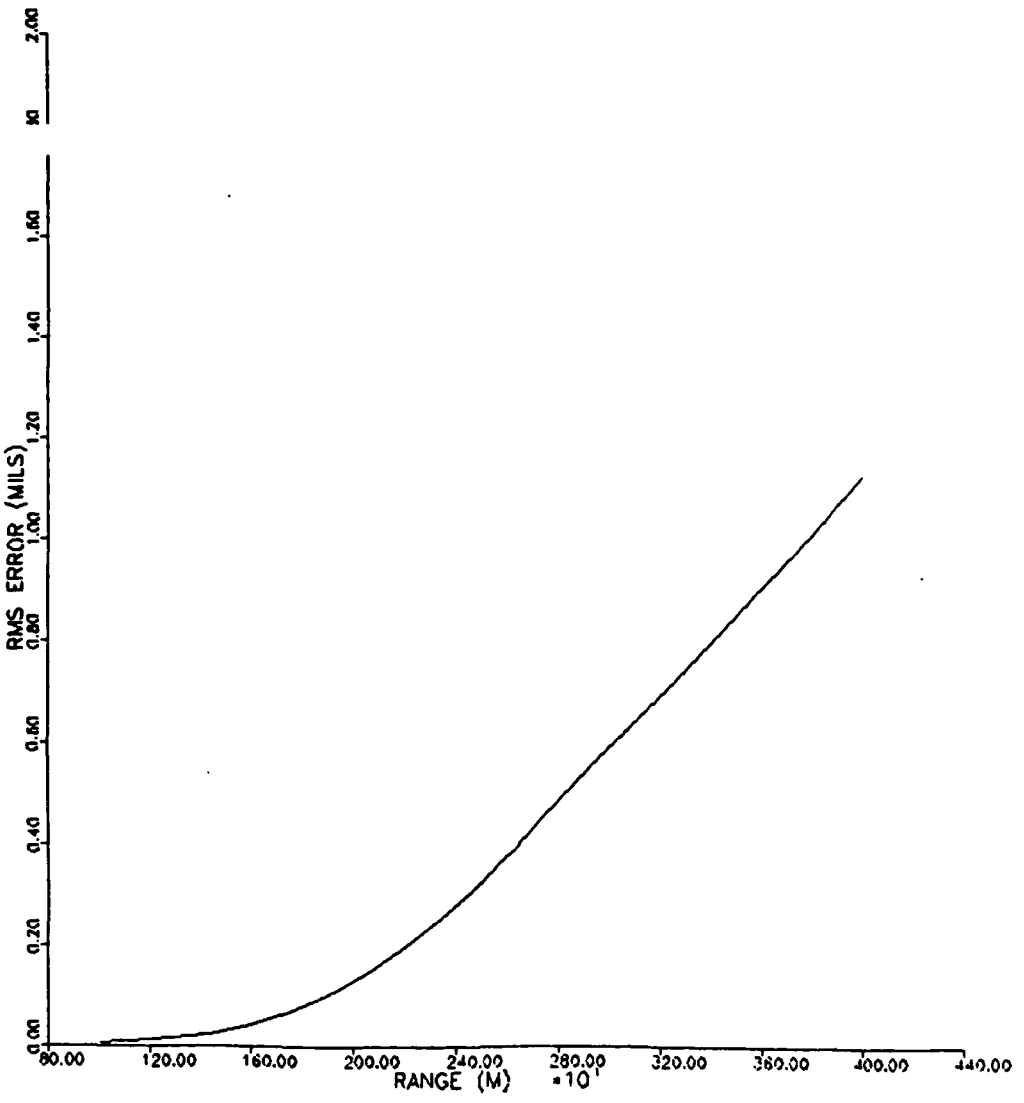

Figure D-3. MIDI tracking error: York scoring; X-band; 50dB MTI improvement factor; target height = 50 m.

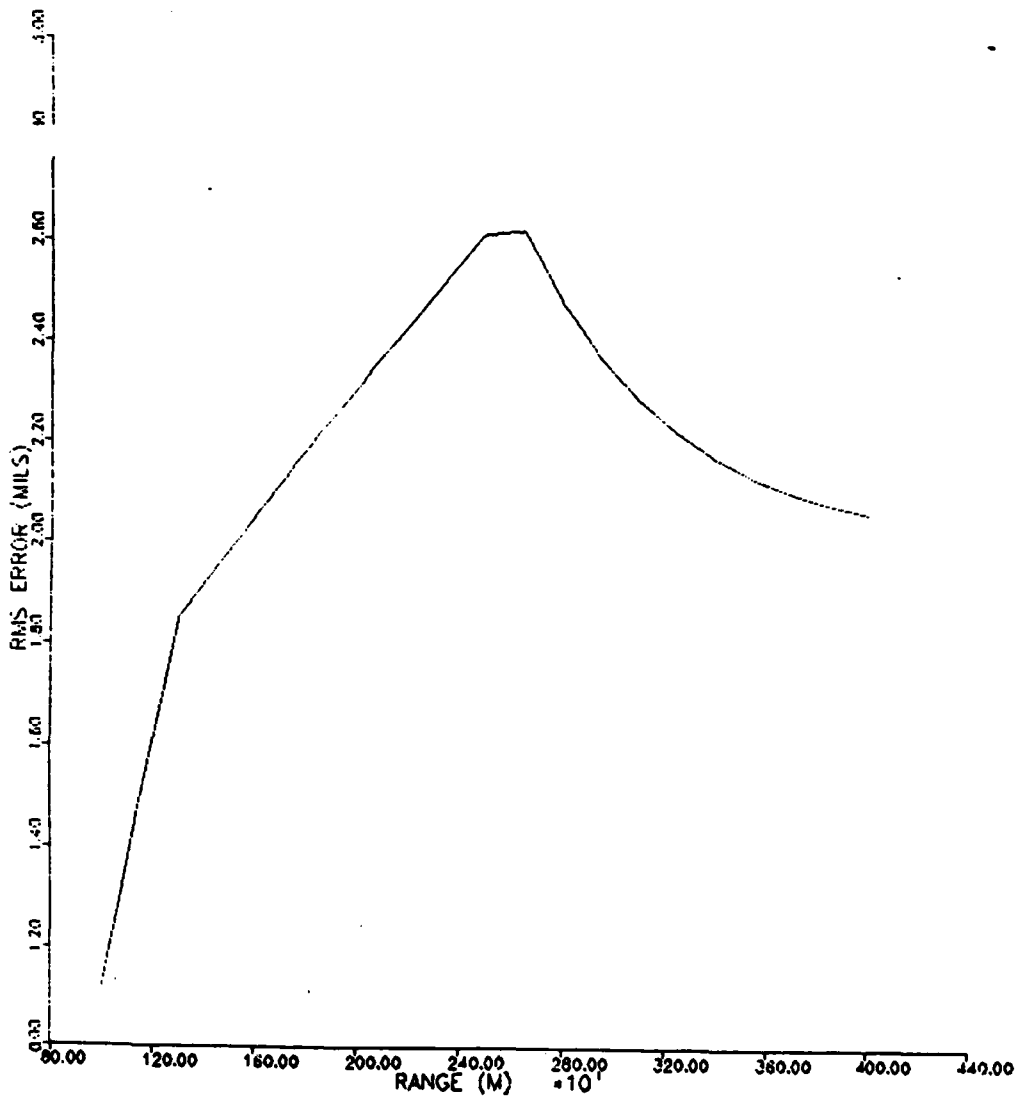

Figure D-4. MIDI tracking error: York scoring; X-band; 40dB MTI improvement factor; target height = 15 m.

AD-A148 467 METHODOLOGY IMPROVEMENT PROGRAM FOR THE SECOND GENERATION MISS DISTANCE R..(U) GEORGIA INST OF TECH ATLANTA ENGINEERING EXPERIMENT STATION 3/3

UNCLASSIFIED G V MORRIS ET AL. 30 OCT 84 F/G 17/9 NL

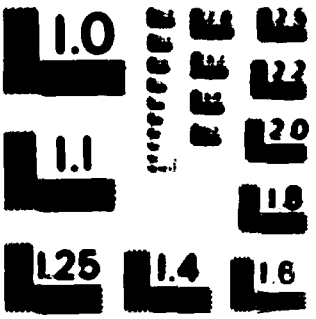
1.0
1.1
1.25
1.4
1.6
2.0
2.2

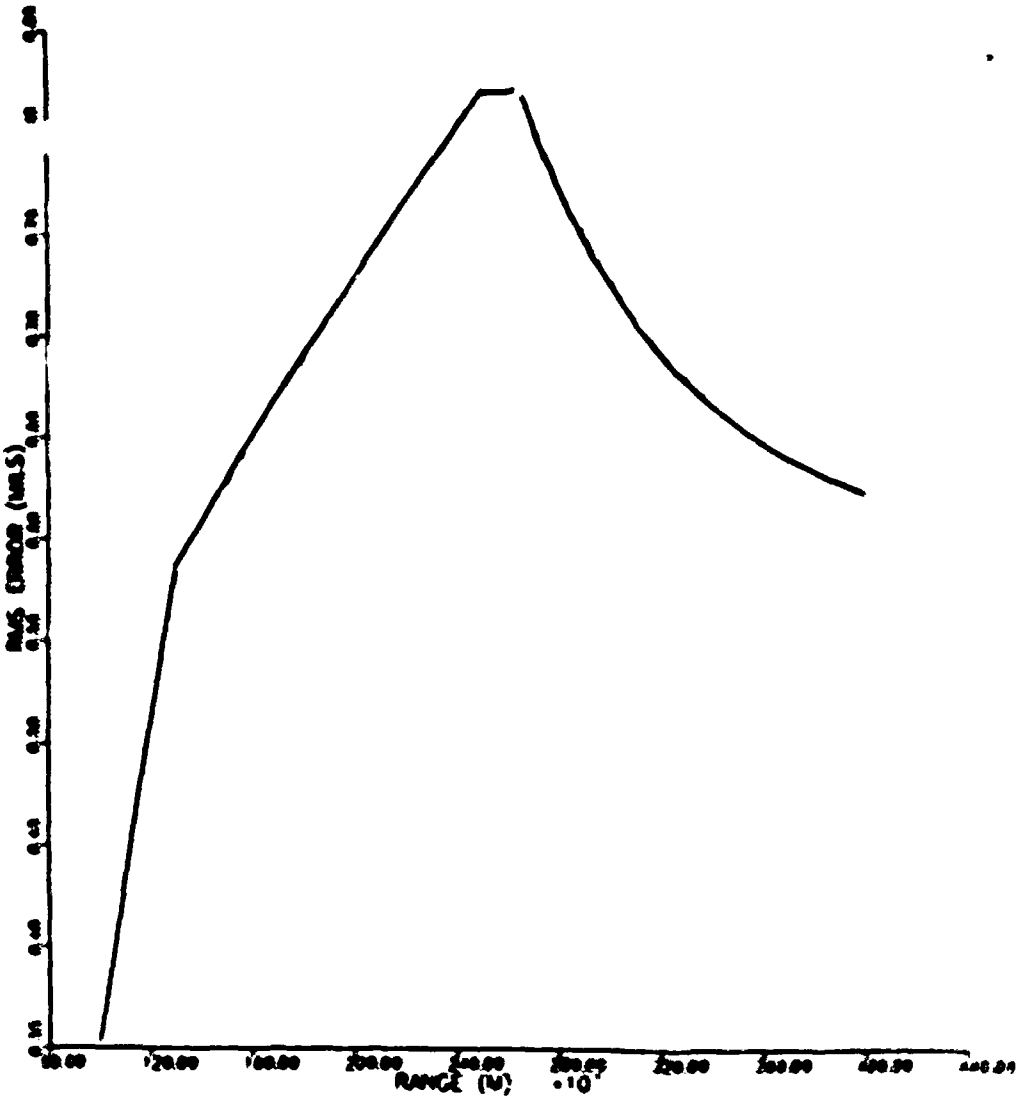

Figure D-5. MIDI tracking error: York scoring; X-band; 50dB MTI improvement factor; target height = 15 m.

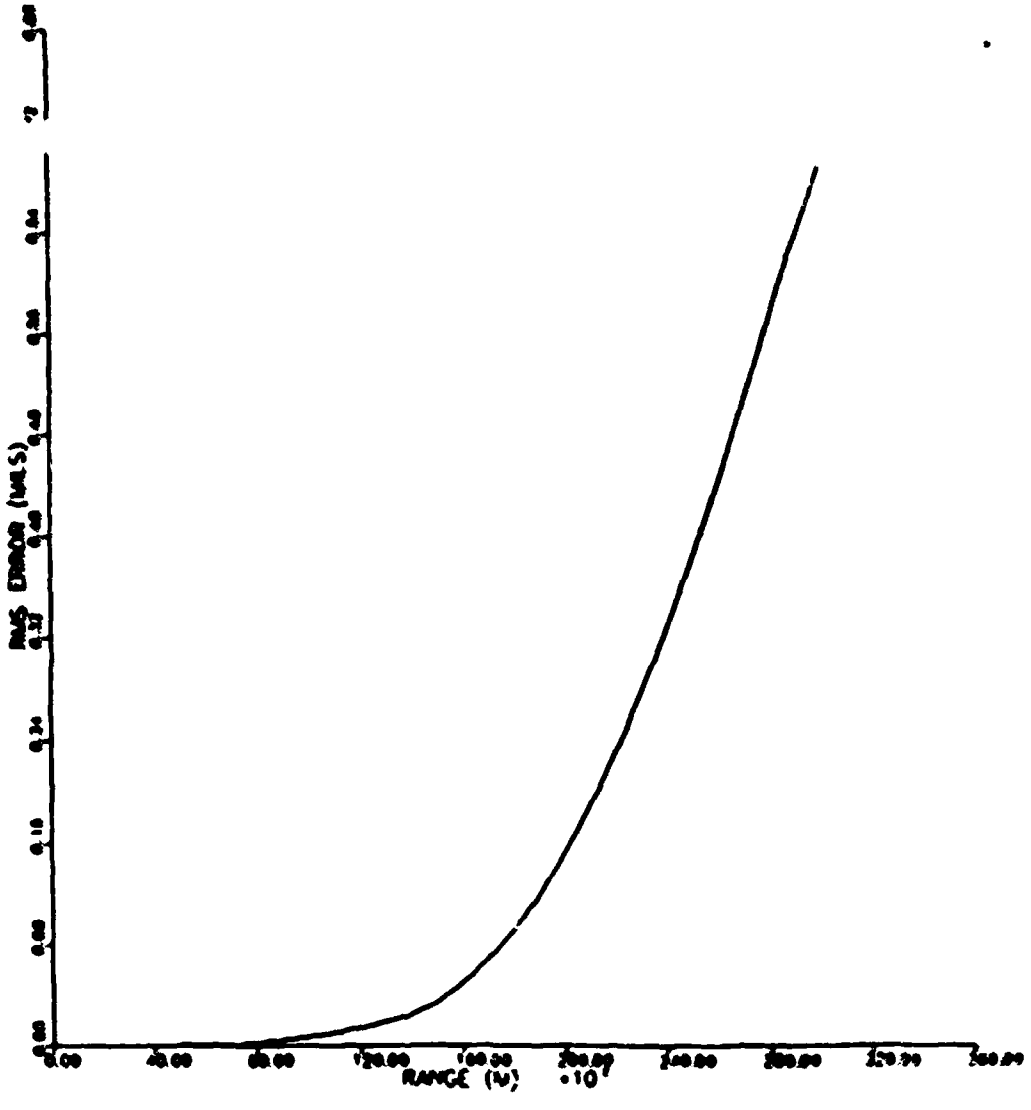

Figure D-6. MIDI tracking error: missile scoring; Ka-band; 40dB MTI improvement factor; target height = 150 m.

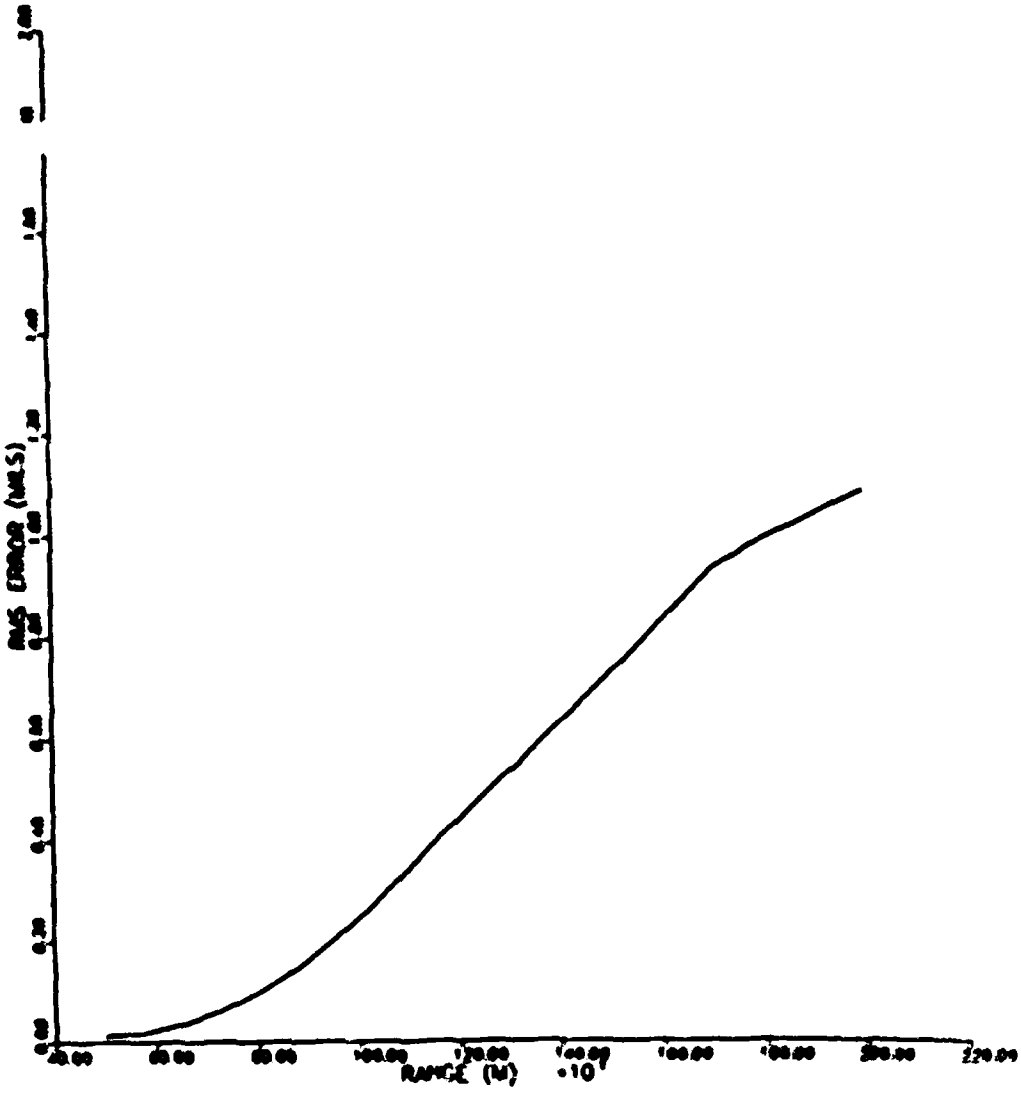

Figure D-7. MIDI tracking error: missile scoring; Ka-band; 40 dB MTI improvement factor; target height = 60 m.

END

FILMED

1-85

DTIC